# TIME-RESOLVED RATIOMETRIC DETECTION OF THE PLASMONIC COUPLING BETWEEN GOLD NANOPARTICLES: A NOVEL TECHNIQUE FOR SINGLE-MOLECULE BIOPHYSICS

by

Diane Marie Wiener

A dissertation submitted in partial fulfillment
of the requirements for the degree of
Doctor of Philosophy
(Mechanical Engineering)
in The University of Michigan
2012

Doctoral Committee:

Professor Noel C. Perkins, Co-Chair
Associate Professor Katsuo Kurabayashi, Co-Chair
Professor Nils G. Walter
Assistant Professor Anastasios John Hart

To Troy –
You and me
We're in this together now.

## ACKNOWLEDGEMENTS

I am forever grateful to my advisors, Dr. Noel Perkins and Dr. Katsuo Kurabayashi, for their unwavering support and belief in my abilities. They have set an example which I hope to be able to follow throughout my career. I thank the members of my thesis committee, Dr. Nils Walter and Dr. A. John Hart. Their interest and guidance are much appreciated. My committee's direction and assistance were instrumental towards making this work the best that it can be. I also thank Dr. Edgar Meyhöfer for his support and funding in the early phases of this work without which this work may not have been realized, and for that I will always be appreciative. I thank Dr. Troy Lionberger for his contributions to this project, vibrant discussions, and support during the most challenging phases of this work. His constant motivation and enthusiasm helped me to believe that anything is possible with enough dedication. I also thank the present and former members of the Nanomechanics Laboratory (Ming-Tse Kao, Adam Hendricks, Neha Kaul, Chang Jiang, Jenna Campbell, and Victor Ng). I am also appreciative of my discussions with Björn Reinhard. His insights and advice were invaluable. I am also grateful for the financial support provided by the National Science Foundation and the National Defense Science and Engineering Graduate Research Fellowship Programs which granted me the independence to pursue my work.

## TABLE OF CONTENTS

## LIST OF TABLES

Table

## LIST OF FIGURES

Figure

# CHAPTER 1

## Introduction

The understanding of complex biological systems has significantly benefited from the progressive ability to probe smaller and smaller biological components within a given process, ultimately reaching the level of individual biomolecules. Initially, biomolecular interactions were studied through ensemble, bulk measurements of many molecules. However, bulk measurements from ensembles of molecules in solution only describe the population average, thereby obscuring transient changes and interactions from individual molecules. Therefore, it is largely impossible to study the transient dynamics and mechanistic details underpinning biomolecular functions. Signaled by the development of single-molecule techniques to optically observe individual molecules, detailed studies of the biomolecules in enzymatic reactions make possible the fundamental understanding of cellular processes. Single-molecule techniques both to detect and to manipulate (through the application of force) individual biomolecules are playing an increasingly critical role in the analysis and characterization of biomolecular interactions [1-9]. Single-molecule observations not only provide greater insight into the stochastic and transient behaviors of individual molecules within the distribution of the population, but

also reveal specific, quantitative details of biomolecule interactions and conformations with respect to distances and displacements, and forces generated by or applied to the biomolecule with high precision. Furthermore, the distributions observed in single-molecule assays retrieve the ensemble average that bulk methods provide. Single-molecule experimental techniques have thus become essential for a deeper understanding of biological processes on the molecular to cellular scale.

Techniques to study the details of the protein and biomolecule dynamics must be of very high spatial and temporal resolution, given the small size scale and fast dynamics of biological systems of interest. Many small nanometer-scale proteins and biomolecules undergo structural rearrangements and dynamically interact with substrates on very fast timescales [10-12]. As one example, DNA molecules transiently assume noncanonical forms and structures. Transient events, such as base flip-out and base pair melting, spontaneously produce kinks and internal loops in the DNA for durations on the order of a few milliseconds [13-16]. Likewise, dynamic interactions between enzymes with a rapidly fluctuating DNA molecule require high temporal resolution. A full description of conformational changes, thus, requires time resolutions in the microsecond to millisecond range. Moreover, provided the nanometer size scale of molecules and molecular interactions of interest, sub-nanometer spatial resolution over a wide range of distances is imperative to best understand the dynamics of the system.

Single-molecule techniques have made great advancements in attaining high spatial and temporal resolution measurements. However, fundamental shortcomings in the current methodologies leave gaps in our ability to fully probe and understand biological systems. To address the need to observe single biomolecules with high spatial and temporal resolution, it was my goal to further develop and extend an emerging single-molecule technique utilizing the plasmonic coupling between gold nanoparticles as a metrology tool for high temporal resolution assays [17, 18]. Herein, conventional experimental methods for interrogating single molecules with high spatial and temporal resolution are detailed, highlighting both the advantages and limits of these approaches. Subsequently, developments utilizing gold nanoparticles as optical probes in conventional single-molecule experimental techniques are discussed, outlining many of the unique (and favorable) properties of gold nanoparticle probes. Finally, initial applications demonstrating the potential of the response from the plasmonic coupling between gold nanoparticles to resolve distances between the nanoparticle probes as a single-molecule technique are explored, emphasizing the state of the field, current obstacles, and areas where improvements may be made and pursued to advance the technique.

### *1.1 Conventional single-molecule techniques for high spatial and temporal resolution measurements*

To date, many achievements have been accomplished in improving single-molecule techniques, such that high temporal and spatial resolution

measurements on individual biomolecules are feasible. Importantly, high spatial resolution techniques must contend with the Rayleigh criterion, that is, the spatial resolution accessible by conventional microscopy techniques is diffraction-limited [19, 20]. For example, the diffraction limit for light microscopy is approximately 250 nm, or about half of the excitation wavelength. Therefore, details below this limit are obscured and not capable of discrimination. High precision spatial resolution techniques take advantage of optical probes, such as fluorescent molecules or metallic nanoparticles, to detect the nanometer-sized biomolecules of interest [1, 21-24]. Currently, the most widely used optical technique for distance measurements with resolution well below the diffraction limit of light microscopy is fluorescence resonance energy transfer (FRET).

In FRET, the energy from a donor fluorophore may be transferred to an acceptor fluorophore in a highly distance dependent manner through nonradiative dipole-dipole coupling [25-27]. Since the transfer efficiency to the acceptor fluorophores is inversely related to the sixth power of the donor-acceptor separation, the distance range is typically limited to less than 10 nm. The extreme nonlinearity of the transfer efficiency, while limited in range, however, results in the FRET technique providing a highly sensitive method for quantifying conformational changes and molecular interactions, see Figure 1, top. Single-molecule FRET has been used on a range of biological systems including, for example, previously unresolved structural rearrangements within individual protein molecules [2, 26, 28-31]. FRET has also been used to study the mechanical properties of DNA [32-36] and DNA-protein interactions [37-40].

However, despite its popularity in biological measurements, FRET suffers from the fundamental trade-off between photostability and signal strength, principally linked to the use of fluorescent dye molecules. FRET has a relatively low signal-

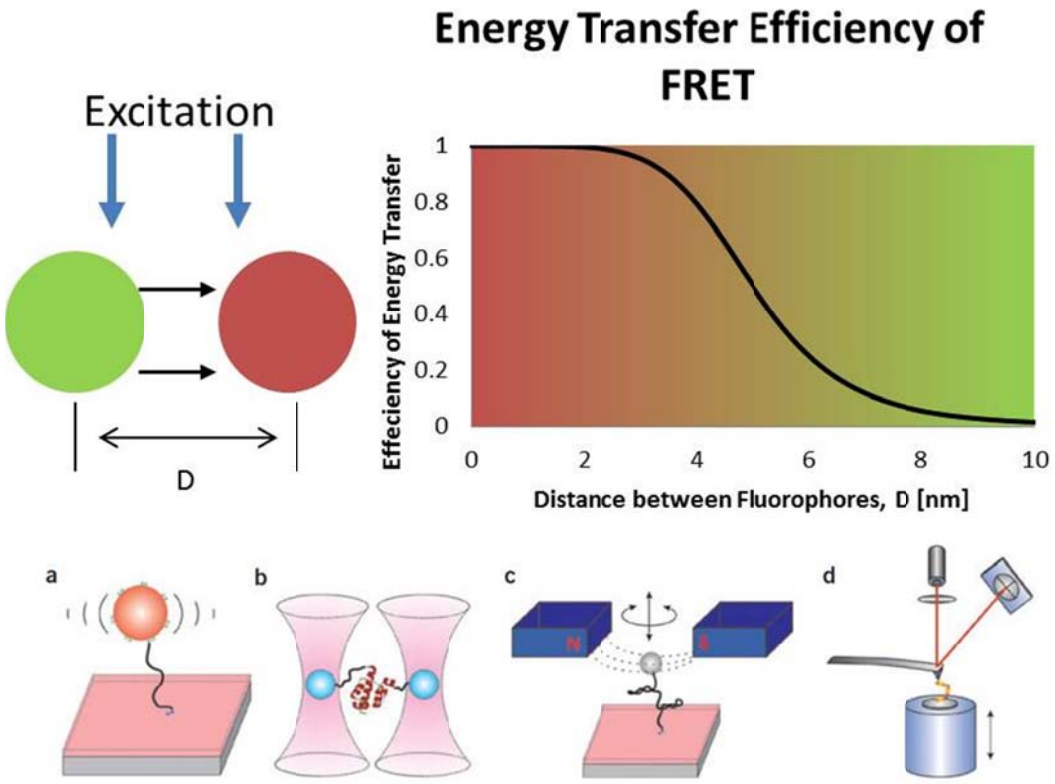


**Figure 1.** Common Single-molecule Techniques. **(Top)** Fluorescence resonance energy transfer (FRET) measures distances between two fluorescent probes in the range from 1-10 nm. **(Bottom)** Other single-molecule techniques, as described in the text, include tethered particle motion (a), optical trapping (b), magnetic trapping (c), and atomic force microscopy (d). (Bottom image reprinted by permission from Macmillan Publishers Ltd: [NATURE] Walter *et al.* [4], copyright 2008.)

to-noise ratio specifically due to the limited number of photons emitted and collected per unit of time. Further, when a strong signal is desired, the observation time for FRET is short. Fluorophores suffer from instability in their photophysical properties, that is, they photobleach rapidly within a few seconds

and exhibit dark states (blinking) due to photodamage at excitation intensities that permit millisecond measurements [41]. Most importantly, the range over which distances may be tracked through FRET is small (~1-10 nm). These limitations make FRET an inappropriate method to measure with sub-millisecond resolution over a wide distance range the transient dynamics of single biomolecules. Other single-molecule techniques exist, though not in the force-free condition afforded by small probe labeling.

Two common methods used to measure sub-nanometer distances are magnetic and optical trapping (sometimes referred to tweezers). These methods can be used to determine distance changes through the application of a force via micrometer-sized handles, typically small beads 1-2 μm in diameter, see Figure 1, bottom. Magnetic trapping experiments exert forces through a magnetic field induced on a superparamagnetic bead [42-44]. Optical trapping experiments apply a force through the radiation pressure from a highly focused, high intensity laser on a small latex bead [45]. Optical trapping has been shown to resolve single base pair (0.34 nm) translations by a polymerase molecule on a DNA substrate [46]. However, when such large probes are attached to biomolecules they will provide significant viscous fluid dampening in aqueous buffer solutions, generating resistive forces and dramatically slow motions of the molecule. Moreover, recent theoretical work provides strong evidence that the application of any small (even piconewton) force normally exerted in trapping experiments will alter the transient dynamics of DNA molecules [47]. While some other techniques, such as tethered particle measurements [48-50], or approaches not

restricted to single-molecule observations, like small angle x-ray scattering [51-53] and electron paramagnetic resonance [54, 55], do address some of the enumerated limitations, none of these techniques are capable of measuring the dynamics of biomolecular interactions where both high spatial and temporal resolution over long measurement times are simultaneously required. The general lack of a technique with the ability to monitor molecules at high spatial and temporal resolution over long time durations motivates efforts to establish alternative approaches.

### *1.2 Research Objectives*

The objective of this research is to satisfy the need to develop a single-molecule technique capable of high temporal resolution over long time scales of observation, and with the potential to measure nanometer separations over a broad distance range. It has been demonstrated, as described below, that, with distinct advantages, the plasmonic coupling between gold nanoparticles may be used to measure the distance between the particles based on the preferential scattering of the nanoparticles at specific wavelengths. Reinhard *et al.* calibrated the peak resonance wavelength spectral response with the distance between the gold nanoparticles, but with very low temporal resolution [17]. It was my goal to extend the initial work to establish plasmonic coupling between gold nanoparticles as a single-molecule technique. The current limitations in the method include increasing the temporal resolution beyond hundreds of milliseconds, and general handling and labeling of the gold nanoparticles for use

in a broad range of biological systems. The above objective will be met by completing three major research tasks. The first task, detailed in Chapter 2, is to design and implement instrumentation to create a novel excitation and detection technique. This technique will increase the temporal resolution with which the plasmonic coupling between gold nanoparticles may be observed through a ratiometric analysis technique of the scattering signal from two specific wavelengths. The next task, summarized in Chapter 3, is to widely apply gold nanoparticles to biomolecular systems. Generalized methods were developed to both stabilize the gold nanoparticles in biologically relevant solutions, and to conjugate the gold nanoparticles to many biomolecules, including DNA molecules and polymerases. The final task, discussed in Chapter 4, is to demonstrate the applicability of the developments in experimental technique and gold nanoparticle conjugation methods to biomolecular systems. This was accomplished by detecting the binding between two gold nanoparticles through their plasmonic coupling response. The sensitivity of the ratiometric analysis technique was further examined, and preliminary experiments to observe the binding of polymerases to DNA molecules were conducted, further establishing the applicability of the technique to single-molecule biophysics. A detailed summary of the previous research towards the application of gold nanoparticles and their plasmonic coupling response to single-molecule biophysics, which motivated my objectives, follows.

*1.3 The case for gold nanoparticles as novel single-molecule probes*

The drive to overcome the shortcomings of fluorophores and fluorescence has led to developments using spherical metallic nanoparticles as molecular markers. Noble metals, specifically gold and silver, have traditionally been applied in many techniques in molecular biology, ranging from electron microscopy [56] to surface plasmon resonance [57]. Spherical gold nanoparticles are in many ways ideal molecular probes, because they are photostable, can be covalently conjugated to biomolecules through gold-thiol chemistry, are biologically inert, and scatter light efficiently, especially at their resonance frequency. As such, the application of gold nanoparticles has broadened to a number of biological applications. For instance, single-molecule biophysics assays requiring precision tracking have been utilizing gold nanoparticles as labels, because of the dramatic improvements in brightness and photostability over fluorescent dyes [50, 58-63]. Specifically, gold nanoparticles scatter light approximately 1000-times better than latex beads of the same diameter [1, 64]. Indeed, the use of gold nanoparticles in the precision tracking experiments have achieved high temporal resolution experiments to as low as a few microsecond, owing largely to the high scattering efficiency at the peak resonance wavelength of the gold nanoparticle labels [63]. A host of ultra-sensitive biological detectors, sensors, and diagnostic techniques take advantage of the strong surface plasmon resonance of gold or silver thin films and nanoparticles (see, for example [65-76]).

Surface plasmon resonance is the resonant excitation of the conduction electrons at the interface of a metal and a dielectric material. Surface plasmons are excited by light (or electron) waves, where the electric field of the incident electromagnetic radiation induces an in-phase dipole of the conduction electrons. A surface restoring force created at a unique resonance frequency compensates for the dipole causing the electrons to oscillate coherently [64, 77-83]. Importantly, silver and gold nanoparticles exhibit sharp plasmon resonance peaks in the visible spectrum, ensuring enhanced light scattering at that wavelength, ideal for light microscopy techniques. The specific peak plasmon resonance wavelength response from the nanoparticle strongly depends on many factors [84-87].

Material, geometrical, and environmental conditions influence the peak resonance wavelength. First, the particle material composition (specific metal or blend of metals) generally defines the peak resonance, e.g. the peak resonance wavelength for a 30 nm diameter silver nanoparticle is near 430 nm, whereas the same sized gold nanoparticle has a peak wavelength near 530 nm [18, 64, 83, 88]. Secondly, the size of the nanoparticle shifts the peak resonance response. For example, gold nanoparticles 5 nm in diameter exhibit a peak frequency near 514 nm, lower than for the 30 nm particles previously described [89]. As the particle size increases, the peak resonance response increases (red-shifts). As may be deduced by the influence of the size of the nanoparticles, the shape of the particle also changes the peak response of the nanoparticles. Metallic particles are now synthesized in a variety of shapes from the conventional

sphere to triangles, rods, and stars [90]. Each of these shapes display an assortment of plasmonic responses. As one example, gold nanorods exhibit two resonance peaks, longitudinal and transverse modes [91-95]. The peak resonance response for the nanorods depends on the aspect ratio and size. Yu *et al.* synthesized gold nanorods with ~10 nm short axis diameter particles of three aspect ratios (1.8, 3.0, and 5.2), and measured longitudinal resonances responses of 600 nm, 710 nm, and 873 nm, respectively, whereas the transverse response was approximately 520 nm in all cases [95]. Additionally, as has been applied in biosensing assays [74, 75], the peak resonance response depends on the refractive index of the surrounding medium [96]. Raschke *et al.* evaluate the response of binding by the BSA protein molecules to a single 40 nm diameter gold nanoparticle based on the change in the peak resonance wavelength change (approximately a 1.5 nm shift), owing to the change in refractive index [74]. However, one critical influence to the peak resonance response of metallic nanoparticles, and of particular interest to this work, is the proximity of neighboring nanoparticles.

Observing the interaction between two biomolecules often requires that each molecule be specifically labeled. The dependence of the peak resonance response of the nanoparticle to proximate nanoparticles led to the development to create techniques to detect biomolecular interactions. As the distance between two particles decreases, the free conduction electrons of the nanoparticles begin to couple, which results in the peak resonance wavelength to shift to a longer wavelength (red-shift) [66, 97]. The coupling effect is observed in a range

between the particles of approximately 2.5 times the particle diameter [17, 98]. The coupling effect between gold nanoparticles can be exploited to develop a measurement technique capable of tracking transient dynamic changes in biomolecules with nanometer resolution. Preliminary efforts in this line will be described in the subsequent section; first, though, additional features of gold nanoparticles must be established.

Gold nanoparticles as outlined above have many beneficial properties, including high scattering cross-sections, which provide stable, bright optical signals, and biocompatibility. However, trade-offs with using gold nanoparticles exist. The specific nanoparticle diameter has several benefits and drawbacks. Based on Mie theory, the scattering response from the nanoparticles depends on the size of the nanoparticle, decreasing with the sixth power with particle diameter [64]. Smaller nanoparticles will scatter less than larger particles, making them difficult to detect. However, smaller diameter nanoparticles are advantageous due to their better size and shape distributions, and their peak resonance wavelength occurs in the visible spectrum [64, 99, 100]. Larger diameter gold nanoparticles have a strong scattering signal, but the peak resonance wavelength is closer to the IR in the light spectrum [64]. Additionally, the size and shape distribution is more difficult to control for larger gold nanoparticles [99-101]. In addition to selecting the size of the nanoparticle, observing and measuring the signals from the nanoparticles are varied, owing to the advantages and limits of each.

Observations of the nanoparticles, like molecules, may be conducted in bulk solution techniques or through single particle techniques. One important metric of gold nanoparticles is the determination of the peak resonance response of gold nanoparticles. Typically, spectral analysis measures the peak resonance wavelength, and may be accomplished by both bulk solutions and single particles [64, 80]. Bulk solution spectra are typically measured through UV/Vis absorption methods [66, 89, 102, 103], while single particle spectra are measured by scattering signals collected with a spectrometer [17, 18, 74, 104, 105]. Bulk spectra provide an ensemble, population average of the resonance response. Single particle spectra only provide information on an individual particle. In both cases, it is difficult to obtain either the overall aspects of the population of the gold nanoparticles because many noisy single particle spectra must be compiled, or to observe rarely occurring, or subpopulations from bulk solutions. Single particle spectra further suffer from low scattering signals from the gold nanoparticles, which require long integration times, and cause uncertainty in the signal, which makes it difficult to discriminate small shifts in the response. The spectral measurements require that the scattered light from the gold nanoparticles be separated from the illumination source, which is not trivial.

Established single-molecule light microscopy techniques are typically designed for fluorescence microscopy. The discrimination of the fluorescent signal from the illumination source is easy, based on the Stokes shift of the dye molecules. The fluorescent probes emit lower energy, longer wavelength photons after excitation. Hence, the difference in the excitation and emission wavelengths

allows for easy detection. However, gold nanoparticles are observed through their scattering response. In contrast to fluorescence, the light scattered by the particle is the same wavelength as the incident excitation source. That is, there is no Stokes shift by which to eliminate the excitation from the scattering response. Conventional microscopy techniques are not effective for experiments involving gold nanoparticles.

Alternate techniques have been developed to overcome the observation limitation, though with trade-offs of their own. Darkfield illumination rejects the excitation from the scattering signal by illuminating the particles with high numerical aperture rays. Using a low numerical aperture objective, only the scattering signal is collected [19, 20]. Traditional darkfield illumination, though, has low power densities, which limits the spatial and temporal resolution. Objective-type darkfield illumination techniques have been implemented to provide higher power densities to the sample, though these techniques are more difficult to implement, and mostly used for particle tracking [59, 63, 106]. One method that may reduce the background scattering from gold nanoparticles deep in solution is through total internal reflection. This technique has been implemented in three studies utilizing gold nanoparticles, but using white light arc lamps as the excitation sources [107-109]. Total internal reflection illumination produces an evanescent wave, which only penetrates about 100-150 nm into the sample such that only the scattering signal from proximal gold nanoparticles are observed. However, in the implementations of total internal reflection, the illumination source again limits the spatial and temporal resolution. These

techniques, though, are a facile method to create a high signal-to-noise system through prism total internal reflection, which served as inspiration in the current work.

While some drawbacks exist with gold nanoparticles, techniques have been developed such that the use of gold nanoparticles does not fundamentally limit the experiment. Gold nanoparticles may be the ideal biomolecular probe—photostable, biocompatible, and with high signal strengths. Further, initial work to establish a gold nanoparticle-based metrology technique has demonstrated the utility of gold nanoparticles for long time duration experiments with the potential for high spatial and temporal resolution.

### *1.4 Plasmonic coupling between gold nanoparticles as a distance reporting single-molecule technique*

Preliminary studies to apply the plasmonic coupling between gold and silver nanoparticles to measure distances termed the technique “molecular rulers” [17, 18]. The initial experiments relating the plasmonic coupling between the nanoparticles to distances were moderately slow and static experiments, relating the shift in the resonance wavelength of gold and silver nanoparticles to changes in the interparticle distance and plasmon coupling. For these measurements, the nanoparticles were illuminated with white light excitation from a tungsten arc lamp through a darkfield condenser, and the scattered light from the nanoparticles was collected with a microscope objective and analyzed with a spectrometer. Owing to the low scatting signal from the nanoparticles, the

scattering spectra signal from individual nanoparticles, approximately 40 nm in diameter, was recorded with one second integration time, typical for most single particle scattering spectra [17, 18, 108, 110]. In both of the preliminary experiments, gold nanoparticles, 42 nm and 87 nm in diameter, were labeled with one end of a DNA strand. By introducing another gold nanoparticle which was capable to conjugate to the other end of the DNA strand, the spectral shift of the resonance wavelength upon conjugation was correlated to the distance between the two particles. The distance was assumed to be determined by the elastic rod properties of the DNA molecules linking the gold nanoparticles, through the worm-like chain model, the most common model predicting the material properties of DNA molecules [42, 111-119]. It should be noted that the distance determined through the model may not accurately define the actual distance between the gold nanoparticles, because there is the potential of multiple DNA molecules to form many tethers between the gold nanoparticles, which decreases the distance between the gold nanoparticles. Through this technique, distance changes of 5 nm were resolved by using 10 base pair and 20 base pair DNA constructs. The measurement error is determined to range between less than 1 nm to around 20 nm, based on the ability to discriminate the peak resonance wavelength as well as standard issues with gold nanoparticle size and shape distributions. The obvious limitation of the technique is the low signal, which restricts the temporal resolution, and also introduces uncertainty in the actual peak resonance wavelength determination, lowering the spatial resolution,

both of which cast the technique to a regime of low applicability to molecular biology, and single-molecule biophysics.

The molecular ruler technique was further applied in a clever way in which the temporal resolution was increased by only measuring the total scattering intensity from the nanoparticles, and by uniquely choosing the DNA strand lengths so that the particle separations are known *a priori*, to observe the cleavage of DNA molecules conjugated to gold nanoparticles by a restriction enzyme protein. In this manner the experiment departs from measuring the spectral shift in the plasmon resonance to measure distances, but rather simply detects the intensity difference of two gold nanoparticles as compared to a single gold nanoparticle when one of the gold nanoparticles was released into solution upon cleavage of DNA by the restriction enzyme [120]. In fact, this experiment simply takes advantage of the high scattering cross-section of the gold nanoparticles, and could, in principle, be conducted with fluorescent molecules or organic dyes, if the signals were strong enough to measure the signal change before and after the restriction enzyme cleaves away the second probe. This experimental assay revealed information on irreversible events, such as restriction enzyme cleavage, or two-state phenomena where a second gold nanoparticle was either introduced or removed upon an event occurring. The temporal resolution was high by simply integrating the entire scattering signal, and was capable of observation at 240 Hz, though any distance information was inferred by the design of the assay. In a second restriction enzyme experiment, the molecular ruler technique was applied to biosensing. The surface of a single

gold nanoparticle was densely packed with DNA, and the spectrum was measured before and after cleavage [110]. The spectrum and plasmon resonance frequency changed because the surface properties of the gold nanoparticle changed when 6 to 42 base pairs of DNA is cleaved from each DNA strand. Both of these experiments made advancements to further the application of plasmonic molecular rulers to single-molecule experiments, though limitations still exist to measure distances between gold nanoparticles with high spatial and temporal resolution. Recently, the temporal resolution of the molecular ruler technique has been increased through a ratiometric analysis of the scattering signal from gold and silver nanoparticles, though with broadband excitation.

### *1.5 Ratiometric analysis of the scattering signal from plasmonic nanoparticles increases temporal bandwidth*

As has been described before, the collection of detailed spectra from single nanoparticles requires long integration times. Current research efforts have focused on increasing the temporal resolution by replacing the collection of spectra with a ratiometric analysis of the scattering signal from two wavelength bands. Broadband excitation from a tungsten arc lamp was filtered through bandpass filters centered at 530 nm and 580 nm, so that by quickly switching between the filters using a filter wheel the intensity from each band pass is independently collected. The shift in the wavelength of the scattered spectrum is then correlated to the ratios of the scattering intensity [121]. The ratiometric detection technique eliminates the need to measure the shift of the peak

resonance wavelength upon plasmon coupling between two gold nanoparticles. Detecting the peak resonance wavelength is technically limiting for two reasons: (1) it inherently requires spectral information to be collected, which necessarily requires broadband excitation and many photons over the entire spectrum of excitation, thus leading to high integration times, and (2) the peak resonance wavelength is determined by post-processing fitting routines from the spectra. These are subject to error based on the low signal strength and noise within the

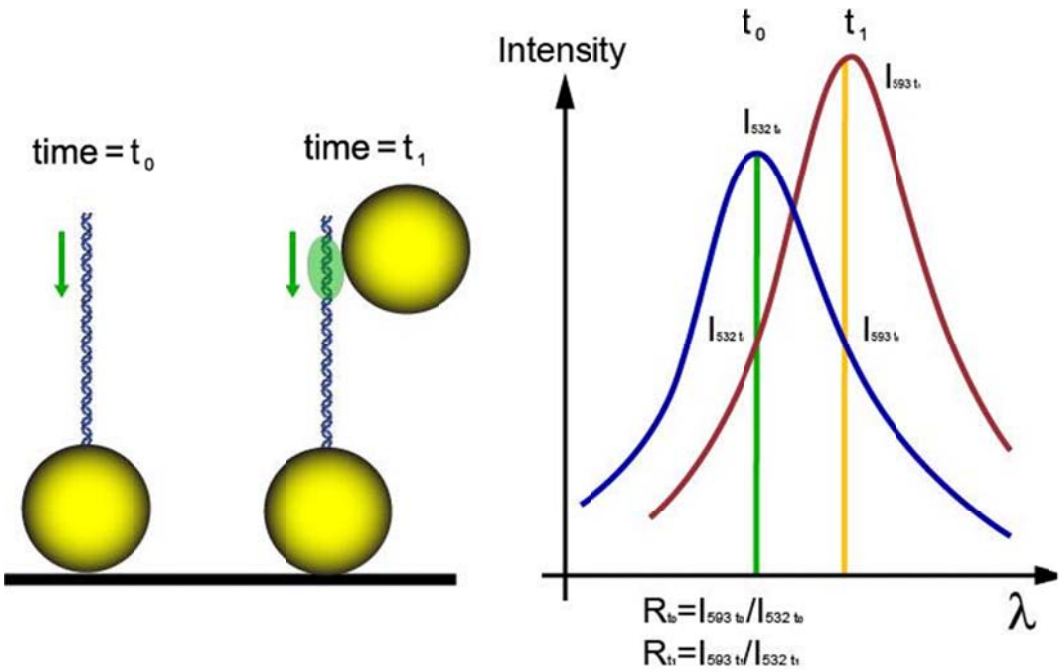


**Figure 2.** Ratiometric Analysis Compared to Spectra Collection. Consider a representative example to compare the ratiometric analysis technique to spectra collection. **(Left)** A T7 RNA polymerase and a DNA molecule are conjugated to individual gold nanoparticles. Upon binding by a T7 RNA polymerase to the DNA, the two gold nanoparticles plasmonically interact. **(Right)** This results in a shift in the peak resonance wavelength to longer wavelengths. Instead of detecting the shift in the spectral response, a ratio is measured between two representative wavelengths, 593 nm and 532 nm.

spectra. In contrast, a ratiometric detection technique can be implemented in real-time, with high scattering signals, see Figure 2. This ultimately provides accurate information regarding the spectral behavior of the gold nanoparticle

plasmonic response, and can enhance the sensitivity over spectral techniques. The ratiometric analysis allows the temporal resolution to be increased, based on the ability to increase the excitation source. Through the ratiometric analysis Rong *et al.* implemented, they were able to increase the temporal resolution to 10 Hz for gold nanoparticles [121], and 5 Hz for silver nanoparticles [88], and indicated that the temporal resolution is bounded by the use of a filter wheel to switch between the two bandpasses. Through the ratiometric analysis, distance changes of about 9 nm were resolved based on the condensation of DNA by the addition of a dendrimer [121]. In a subsequent implement implementation focusing more on polarization anisotropy aspects, compaction of DNA was also observed in a three-state system, resolving interparticle distances of 20 nm to 12 nm to 9 nm [122]. This measurement was based on refractive index changes, polarization anisotropy and total scattering intensity. Applying the ratiometric analysis technique to the plasmonic coupling of silver nanoparticles, Rong *et al.* further established that the ratiometric analysis can be sensitive for 2 nm interparticle separations [88]. However, the fundamental drawback of these experiments is the implementation of the excitation.

The ratiometric analysis technique to quantify the plasmonic coupling between metallic nanoparticles has advanced the field, though still requires further development. The present state of the field is to use white light illumination, which has lower power densities and cannot be focused to a diffraction-limited region as compared to laser excitation. Further, to accomplish specific wavelength excitation, the two bandpasses of 10 nm wavelengths are

switched through the mechanical actuation of a filter wheel to select the wavelengths. By sequentially collecting the intensity from the two wavelength bands, the overall temporal resolution is actually doubled due to the delay between the image acquisition. Additionally, dynamic fluctuations and interactions may cause the gold nanoparticles to change position or orientation between the two bandpass wavelengths, obscuring the actual ratio response. The sequential collection of images would only be sufficient in cases where either the expected biological system dynamics is slower than the overall temporal resolution, or if the switching were fast enough such that any fluctuations do not occur in the time difference between the two intensity images. Finally, the use of bandpasses as opposed to monochromatic wavelengths of excitation adds error to the ratio that is determined, as the scattering signal is collected over a range of wavelengths, obscuring the actual response from the plasmonic coupling between the gold nanoparticles. Owing to the illumination implementation, the broadband ratiometric analysis technique is limited in temporal resolution to the actuation of the filter wheel, which is 5 Hz.

The present challenge in the ratiometric analysis is with respect to instrumentation. By integrating several changes to the experimental instrument design, the ratiometric analysis technique may be further developed. In fact, in 2010, it was initially suggested in the literature, that “the use of monochromatic lasers allows significantly higher frame rates,” though current instrumentation prevented exploration of that option [88]. First, monochromatic laser excitation by two wavelengths eliminates many of the drawbacks from the broadband

implementation. Specifically, monochromatic laser illumination may be focused to attain high excitation power densities, which allow for greater temporal resolutions. Monochromatic scattering signals will not have the added uncertainty from the use of bandpasses of white light. By imaging the two intensities simultaneously from the scattering response, there is no lag, and hence no added error, in the ratio calculated from the two different scattering intensities. Through alternative designs to the excitation and detection of the scattering signal, overcoming the current barriers in the ratiometric analysis technique appears to be realizable.

The ratiometric analysis technique shows great promise for application to a variety of biological applications. In fact, the ratiometric analysis of the scattering response from gold nanoparticles has been employed in one other experimental assay, though for different goals. Grecco and Martinez measured the scattering response from gold nanoparticles for single nanoparticle tracking experiments in cells [123]. Specifically, the goal of their work is to reject spurious scattering particles from within the cell to image the gold nanoparticles of interest. In this method, the wavelengths were selected to discriminate between these two populations, resonant particles, and background scatterers. As established by Mie theory, the scattering signal is dependent to the inverse fourth power to wavelength. Based on this, nonresonant particles preferentially scatter shorter wavelengths. Hence, the ratio between 473 nm and 532 nm wavelengths was calculated so that the gold nanoparticles would easily be tracked. Grecco and Martinez did implement their technique with laser excitation, however, to

provide the excitation at the sample a beamsplitter was used such that only 70% of the excitation is provided to the sample and only 30% of the scattering signal collected by the objective reaches the detector, which ultimately reduces the signal intensities and temporal resolution. In addition, as their application only was interested in the classification of particles, the scattering signals from each wavelength were sequentially imaged. This approach establishes the ratiometric analysis of the plasmonic signal from gold nanoparticles to have broad application to molecular biophysics.

Current work presents strong evidence that this experimental approach is suitable for measuring the distance between gold nanoparticles for long durations with nanometer resolution for biophysical applications. However, the temporal resolution in the methods based on past work remains limited to the hundreds of milliseconds time domain preventing transient dynamic processes in biological systems to be observed on more biologically relevant timescales. Here, I provide the first insight into the use of monochromatic laser excitation in conjunction with ratiometric analysis to measure the plasmonic coupling between gold nanoparticles through the integration of dual-wavelength laser excitation with prism total internal reflection to simultaneously record the scattering signal from both wavelengths discriminately. Through this implementation of the experimental technique, the temporal resolution may now be further increased to more relevant timescales, and has the potential to be even further extended to even higher timescales with modifications of the detection scheme.

*1.6 Contributions and advancements*

The contributions of this work have broad applications to single-molecule biophysics, biotechnology and biosensing, and plasmonics. A novel ratiometric analysis experimental technique was developed using monochromatic laser excitation and total internal reflection-based darkfield microscopy to collect the scattered light from gold nanoparticles at two excitation wavelengths on spatially separated channels of a CCD camera array by use of a dichroic mirror. As a proof-of-principle to establish the ratiometric analysis approach, the plasmonic coupling between a surface-bound biotin-functionalized gold nanoparticle and a neutravidin-conjugated gold nanoparticle from solution, was measured upon binding. Here, the first demonstrated detection of the plasmonic coupling between the two gold nanoparticles with better than 25 Hz temporal resolution is reported. At this time resolution, the individual gold nanoparticle intensity is better than 100 times above background. The instrumentation and implementation developed here is the first to use monochromatic laser illumination for ratiometric analysis, increasing the sensitivity of the technique over the current state of the field in detection shifts in the peak resonance wavelength. The intensity ratio more than doubles upon binding by the second gold nanoparticle. The signal-to-noise ratio for the ratiometric analysis technique is 25, indicating that up to six sub-states are possible to resolve. Importantly, and in contrast with previous methods, the developed technique is fully extendable to faster timescales, limited largely by the choice of detector. Further, conjugation procedures were developed to broadly extend the plasmonic coupling technique to general

biomolecular systems. Finally, through the demonstration of the sensitivity of the technique to detect single-molecule binding with high temporal resolution, a direction is paved toward high spatial resolution metrology through future developments and calibrations.

# CHAPTER 2

## Instrumentation Design and Implementation for Ratiometric Analysis

The plasmonic coupling between gold nanoparticles offers the ability to detect binding and distance measurements owing to the peak resonance wavelength shift. Detecting the plasmonic coupling between gold nanoparticles has been applied to a limited number of single-molecule experiments, all of which involve DNA to tether two gold nanoparticles together [17, 18, 120-122]. The current state of the field collects spectra of the scattered light from the gold nanoparticles, where the particles are illuminated by white light darkfield excitation. Through analysis of the collected spectra, the peak resonance wavelength is determine and correlated to the spatial separation between the two gold nanoparticles. However, applications of this approach are hindered due to the integration time required to collect the spectra from single gold nanoparticles. Gold nanoparticles, though, are extremely photostable with the ability to be continuously observed over days. Furthermore, the gold nanoparticles scatter light efficiently. Both of these properties make them ideal single-molecule probes, if the appropriate excitation and detection techniques are employed. In general, one must improve the ability to detect the gold nanoparticles by a combination of

increasing the scattering signal from the gold nanoparticle, and increase the sensitivity of the detector used to collect the scattered light.

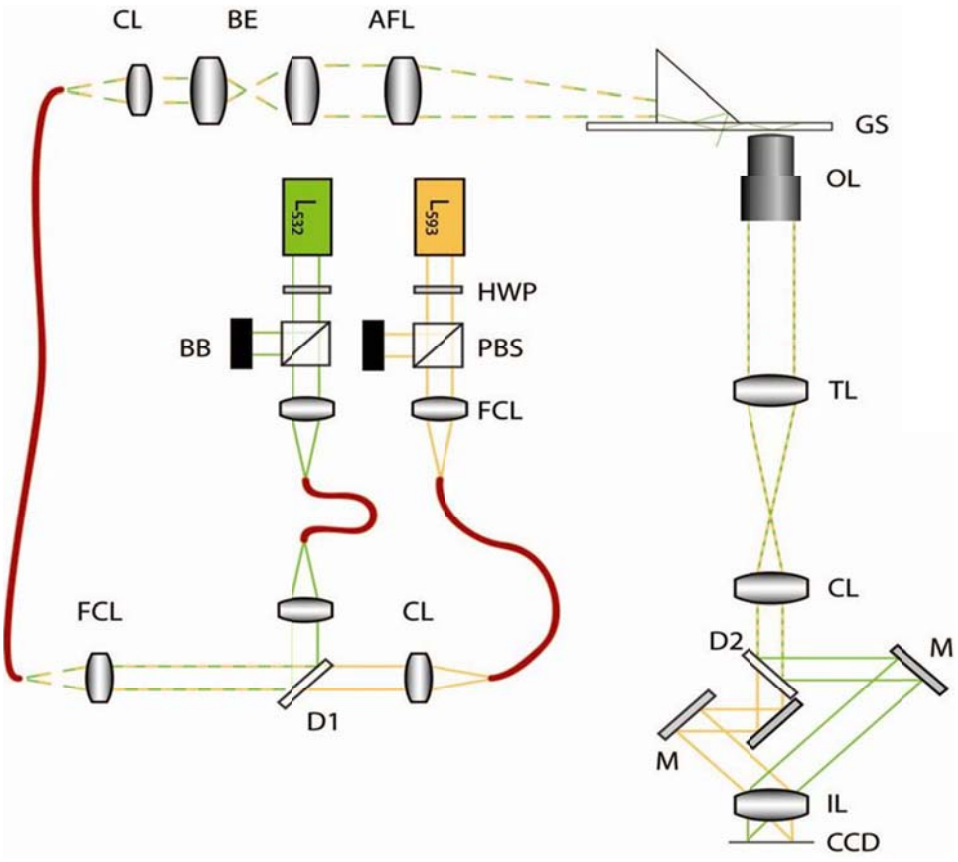


**Figure 3.** Experimental Schematic. The experimental schematic, as detailed in the text, couples the intensity from two wavelengths and combines them into a single-mode fiber. Focusing optics direct the light to a 45° prism to produce the propagating total internal reflection (TIR) wave. A particular TIR spot is selected to reject backscattered light, creating two wavelength darkfield excitation through total internal reflection. The image from the microscope objective is spatially separated with a dichroic mirror and imaged on two regions of a CCD array. Abbreviations: Collimation Lens (CL), Beam Expander (BE), Achromatic Focusing Lens (AFL), Glass Slide (GS), Objective Lens (OL), Tube Lens (TL), Dichroic Mirrors (D1, D2), Mirror (M), Imaging Lens (IL), CCD Camera (CCD), Fiber Coupling Lens (FCL), Beam Block (BB), Polarizing Beam Splitter (PBS), λ/2 Waveplate (HWP), Lasers ($L_{532}$, $L_{593}$).

The solution I implemented increases the temporal resolution by which to detect the plasmonic coupling between gold nanoparticles. The white light darkfield illumination is replaced by dual monochromatic laser excitation. The laser excitation provides much higher power densities at the sample plane, and

may be focused to a diffraction-limited region. Reduction of any background illumination is accomplished through total internal reflection darkfield microscopy. As only two wavelengths are scattered by the gold nanoparticles, spectrum collection is no longer required. Hence, simultaneous collection of the scattering signal from the two wavelengths is recorded on two spatially separated regions on a CCD camera array. Figure 3 details the experimental schematic for the designed optical system. Ratiometric analysis of the scattering signal from the two wavelengths determines the extent to which the two gold nanoparticles are interacting.

*2.1 Specific aims and research objectives*

This chapter concentrates on the design and development of the experimental instrumentation which makes possible the ability to detect the plasmonic coupling between two gold nanoparticles through a ratiometric analysis. The main objective of this work is to demonstrate through a novel experimental method that the plasmonic coupling between two gold nanoparticles may be detected with greater than 25 Hz temporal resolution. Importantly, and in contrast to the previous methods, this technique is fully extendable to faster timescale, limited largely by the choice of the detector. To achieve this aim, several objectives need to be fulfilled, including: (1) selecting the specific gold nanoparticle size and two wavelengths to optimize the ratiometric response, (2) designing a laser to fiber coupling system to independently modulate the excitation power of the two lasers sources and a

dual wavelength fiber coupling system to colocalized the wavelengths into the same single-mode fiber to deliver the light to the microscope, (3) creating a low-drift, high-precision microscope stage so that long time duration observations are possible, (4) developing a system to create a high intensity, low background darkfield illumination system through prism-based total internal reflection, (5) integrating a method for simultaneous acquisition of the two scattering signals by the gold nanoparticles from the two sampling wavelengths. The details of the instrumentation design and development objectives for the ratiometric analysis technique follow.

### *2.2 The ratiometric analysis of monochromatic scattered light detects the plasmonic coupling between gold nanoparticles*

The ratiometric analysis technique eliminates the need to measure the shift of the peak resonance wavelength upon the plasmonic coupling between two gold nanoparticles. Instead of collecting the scattered light from many wavelengths, only the scattered light from two wavelengths is collected. Therefore, increased temporal resolution in the detection of gold nanoparticle plasmonic interactions is possible. Furthermore, if the two wavelengths are chosen correctly, it is possible to enhance the sensitivity of the measurements as compared to the peak wavelength detection. Detecting the peak resonance wavelength is technically limiting, because it inherently requires spectral information to be collected, which requires many photons with broadband excitation, and hence high integration times, and the peak is determined by post-

processed fitting routines, which are susceptible to error from noisy spectra. In contrast, the ratiometric detection can be implemented in real-time and still provides accurate information about the spectral behavior of the particle scattering. The fundamental experimental condition from which all other design considerations hinge is selecting the size of the gold nanoparticles. From this selection, the two wavelengths which have the greatest sensitivity over the desired measurement range may be chosen, and the instrument developed.

Selecting the diameter of the gold nanoparticles carries many trade-offs. First, it is desirable to decrease the size of the gold nanoparticle probe to as small as possible so that the dynamics of the biomolecule of interest are not influenced by the gold nanoparticle probe. However, the distance range within which the near-field plasmonic coupling interactions between gold nanoparticles occur is within approximately 2.5 particle diameters, meaning that smaller particles have a smaller dynamic range [98]. Furthermore, the scattering signal from the gold nanoparticles is highly dependent on the particle radius. For a specific wavelength, the scattering intensity scales with the $6^{th}$ power to the particle radius [64]. As an example, Reinhard *et al.* measured spectra from both 80 nm and 40 nm diameter gold nanoparticles [17]. Based on Mie theory, the 80 nm diameter gold nanoparticles scatter 64 times the amount of light as the 40 nm diameter gold nanoparticles, which provides a signal that could vastly increase the temporal resolution. In most single-molecule assays where gold nanoparticles serve as marker probes, the particles are not smaller than 40 nm in diameter [17, 18, 50, 58-61, 63, 121]. In fact, it has been noted that particles

smaller than 30 nm in diameter are not detectable with conventional light microscopy techniques [17, 18, 101]. Taking into account all of the above considerations, 40 nm diameter gold nanoparticles were selected. The particles are smaller than typical silica beads (100-1000 nm), though on the order, though slightly larger than many fluorophores (10 nm). The particles are still detectable by standard optical microscopy techniques. And, the upper limit of the near-field for two 40 nm gold nanoparticles is approximately 100 nm, which is sufficient for many single-molecule biological applications. With the size of the gold nanoparticles determined, the excitation wavelengths used for ratiometric analysis may be chosen.

The ratiometric analysis technique increases the potential to conduct high temporal resolution experiments by replacing white light arc lamp excitation with monochromatic excitation through two laser sources. The power density from white light excitation delivered through darkfield illumination is much lower than what is possible with laser excitation. Under standard darkfield illumination with a ball darkfield condenser and excitation through a xenon arc lamp, the power of the light scattered by the 40 nm gold nanoparticle was measured to be approximately 0.2 pW. However, unlike light generated by an arc lamp, laser excitation may be tightly focused to a diffraction-limited region. As such, the power density can be increased over a range from 1 $\mu W/\mu m^2$ to 1 $mW/\mu m^2$. The obvious benefit of the increased power density is an increase in the scattering signal from the gold nanoparticles, and an increase in the temporal resolution. While laser excitation is preferred over the darkfield illumination, excluding

special exceptions, the laser wavelengths cannot be dynamically tuned for the specific gold nanoparticle pairs, or specific distance range. Therefore, the two wavelengths chosen for ratiometric analysis must be selected based on a few design factors: (1) the particular experimental conditions for measuring the plasmonic coupling between two gold nanoparticles, (2) the availability of commercially sourced lasers at particular wavelengths with sufficient output power, and (3) the cost of the lasers.

The design of the ratiometric analysis technique was based on the experimental conditions to detect distance changes between the gold nanoparticles after the particles are already in the near-field either after binding by a protein conjugated gold nanoparticle to a DNA molecule functionalized with a gold nanoparticle (see Section 4.8), or after binding by a DNA-binding protein to a DNA molecule bound at each end with a gold nanoparticle (see Section 3.5). The peak plasmon resonance wavelength of a 40 nm diameter single gold nanoparticle is near 532 nm, a commonly available laser line. However, it is difficult to generate laser emissions in the yellow-orange spectrum (570-610 nm) [124]. As the two gold nanoparticles interact, the peak plasmon resonance wavelength red-shifts and nears 593 nm, where the two particles are strongly coupled. For reference, Reinhard *et al.* expect the peak resonance wavelength to be 593 nm when there is approximately a 5 nm edge-to-edge distance between the gold nanoparticles [17]. Conveniently, the 593 nm laser line is commercially available with sufficient output powers up to 35 mW. The signal from the 532 nm scattering is optimized for long interparticle separations. Conversely, the signal

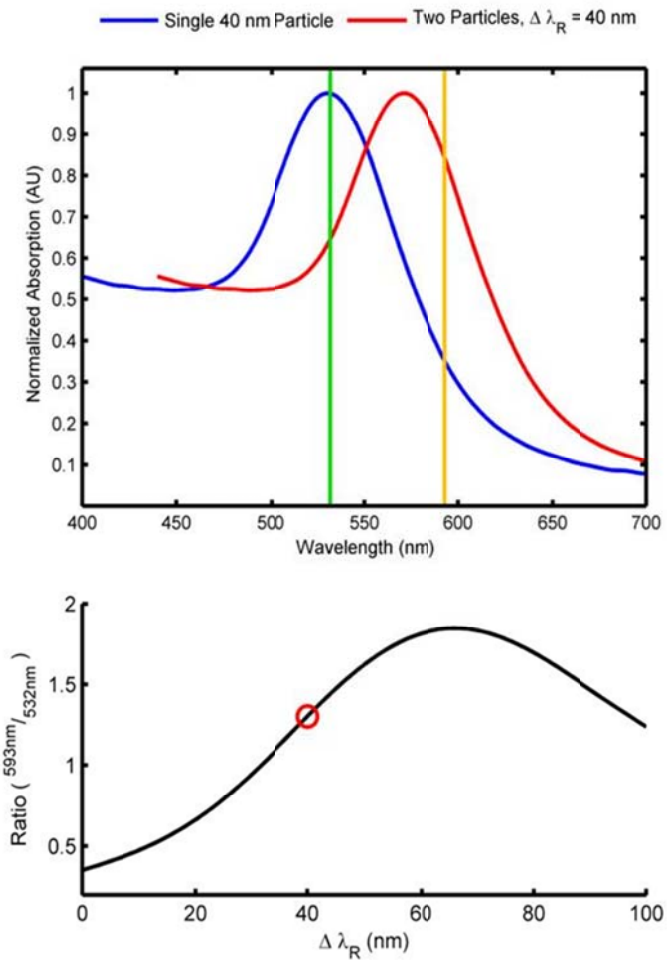


**Figure 4.** Anticipated Ratio Response. **(Top)** The absorption spectrum from a bulk solution of 40 nm gold nanoparticles was shifted such that the ratiometric response between the 593 nm and 532 nm intensities are calculated for increasing peak resonance wavelengths. The red spectrum represents the expected spectral response given that the peak resonance wavelength shifts by 40 nm. **(Bottom)** The calculated ratiometric response curve as the peak resonance wavelength increases. The red circle indicates that expected ratio provided that the peak resonance wavelength changes by 40 nm.

from the 593 nm scattering is optimized for close interparticle separations. These two wavelengths (532 nm and 593 nm) were selected for the excitation illumination.

The selection of the two wavelengths, 532 nm and 593 nm, must be verified to be sensitive to plasmonic coupling between the two gold nanoparticles. To benchmark the expected ratiometric response based on the two wavelengths, an experimentally collected absorption spectrum from 40 nm diameter gold nanoparticle bulk solutions (for reference, see Figure 10) was used to simulate the expected ratiometric response (Figure 4). As two gold nanoparticles interact, the peak resonance

wavelength shifts to longer wavelengths, as does the overall spectral response [18]. To simulate the spectral response based increases in the plasmonic coupling between the two gold nanoparticles, the experimental bulk spectrum was used to evaluate the ratiometric response between the two selected wavelengths, 532 nm and 593 nm. The gold nanoparticle bulk solution spectrum was shifted in 0.5 nm increments, and the new ratio between the two sampling wavelengths is computed, which would be simulating that two gold nanoparticles are increasingly interacting, presumably due to a decrease in the distance between the gold nanoparticles.

In this simulation, it is important to acknowledge that the known broadening of the spectrum upon the coupling between the gold nanoparticles is disregarded. Moreover, single particle scattering spectrum would better evaluate the ratiometric response, as the bulk absorption spectrum measures the average response of the full solution. The bulk spectrum does, however, represent the general shape and intensities of the scattering spectrum of the monomeric gold nanoparticles. The monomeric gold nanoparticle bulk solution spectrum was shifted in 0.5 nm increments, which shifts the peak resonance wavelength by that amount. At each new peak resonance wavelength, the ratio between the 593 nm and 532 nm intensities are calculated. When the gold nanoparticles interact, the peak resonance wavelength shifts toward the IR spectrum, and the ratio of the 593 nm to 532 nm signal increases. As illustrated in the ratio response curve, the ratio increases as the peak resonance wavelength increases until the peak resonance wavelength surpasses the 593 nm sampling wavelength. At a peak

resonance shift of approximately 69 nm, the ratio response begins to decrease owing to the subsequent decrease in both the 532 nm and 593 nm wavelengths. The uncertainty in peak ratio response is dependent on the uncertainty in the peak resonance wavelength from the bulk solution spectrum which is 7 nm. Further analysis was conducted to determine the sensitivity of the sampling wavelengths.

The capability to determine the distance between the gold nanoparticles through the ratio response technique with the selected wavelengths was compared to work by Reinhard *et al.* in which the extent that the gold nanoparticles plasmonically couple is found through post-processing the peak wavelength [17]. Based on the experimental spectra collected by Reinhard *et al.* at several interparticle separations, the peak resonance wavelength was tabulated and the intensity ratio calculated (Table 1). Importantly, an additional advantage of the ratiometric analysis technique emerges: enhanced sensitivity. The ratiometric analysis of the two selected wavelengths (532 and 593 nm) measures a 54% difference between the ratiometric response for edge-to-edge separations of 29.3 nm to 14.7 nm, while less than a 1% change arises in the

| | Monomer | 67 bp DNA tether | 20 bp DNA tether |
|---|---|---|---|
| Particle Separation | | 29.3 nm | 14.7 nm |
| Peak Wavelength [nm] | 543.5 | 563 | 567.774 |
| Ratio: 593 nm/532 nm | 0.2369 | 0.9349 | 1.437 |
| Ratio: 638 nm/532 nm | | 0.2788 | 0.7912 |

**Table 1.** Theoretical Predictions of Ratiometric Response. The ratiometric response for selected sampling wavelengths is compared to the peak resonance wavelengths. The intensity ratio was calculated based on the experimental spectra collected at several particle separations from the published by Reinhard *et al.* [17].

peak resonance wavelength (detecting less than a 5 nm peak resonance wavelength change).

The ratiometric response at the chosen wavelengths is also superior when compared with the monomeric spectra. For the two separations that were analyzed (29.3 nm and 14.7 nm), the ratiometric response has a 295% and 507% change as compared to a 3.6% and 4.5% change for the peak resonance detection, for the respective separations. For further insight into the benefits of the ratiometric analysis as compared to the peak resonance wavelength detection, consider the peak resonance wavelength measured by Reinhard *et al.* for various interparticle separations [17]. The distribution of the measured peak resonance wavelength is broad, where the same peak resonance wavelength (560 nm) can be detected in all of the interparticle separations (10-75 nm). Not only are the typical issues in the experimental measurements (refractive index, particle size and shape distributions, actual distance correlation, etc., see Chapters 3 and 4) present, but also the limited intensity from the scattering of a single gold nanoparticle make fitting to a noisy spectrum difficult and introduces further uncertainty. The ratiometric analysis of the scattering signal from gold nanoparticles at two monochromatic wavelengths, not only affords the opportunity to increase the temporal resolution of the plasmonic coupling technique, but also has the additional benefit of greater sensitivity than the peak resonance wavelength detection.

The selection of the two monochromatic wavelengths is very important for the application. As an example, a very common laser line from a helium-neon

laser, in the red spectrum was also considered. An available diode pumped solid state laser emits a frequency near the HeNe laser line, 638 nm. The hesitation in using this wavelength was the lack of spectral information for the monomer. The scattering signal response from plasmonically coupling gold nanoparticles is very low for all particle separations at 638 nm excitation, though it does increase when the particles interact. As presented in Table 1, there is a 183% change (even better than the 593 nm to 532 nm ratio) in the ratio response of the scattering signal between 638 nm and 532 nm for the two edge-to-edge separations. However, there is no spectral information for the monomer at 638 nm, and it is expected that it would be near zero. This is because given a particular particle diameter the intensity decreases with the fourth power as a function with the wavelength [64]. While it would be anticipated that 638 nm may be preferred for binding sensitivity, since signal changing from nearly zero in the unbound state to a low intensity in the bound state, due to the lack of spectral information, the 638 nm line was not initially selected. However, it should be noted that the dual wavelength fiber laser coupling system was designed so that it may be expanded to incorporate more than just two wavelengths.

One limitation of the ratiometric analysis of two monochromatic wavelengths must be noted. The sensitivity of the ratio entirely depends upon the particle size. The choice of the wavelengths for peak sensitivity varies for different gold nanoparticle diameters. The 532 nm wavelength is essentially the peak resonance for a 40 nm diameter gold nanoparticle. However, when smaller or larger gold nanoparticles are used, the 532 nm and 593 nm wavelengths

would no longer be straddling the peak resonance wavelength, and ratio would no longer simply increase as the gold nanoparticles become closer or decrease when the particles are farther apart, but would be more complex to interpret. For example, the peak resonance wavelength for a 25 nm diameter gold nanoparticle, the peak resonance wavelength is ~514-520 nm. Therefore, as the two particles interact, both the 532 nm scattering intensity and the 593 nm scattering intensity will increase. This limitation could be overcome by two methods: (1) a tunable laser, such as an argon ion laser which produces particular wavelengths between 488 nm and 528 nm, and/or (2) incorporating several laser lines as was made possible in the design for the laser coupling. In this way, the particular wavelengths are then selected based on the specific assay conditions.

The ratiometric analysis technique proves to be better than the peak resonance wavelength fitting. It affords the ability to increase the temporal resolution with the use of monochromatic laser illumination, which may be increased by using higher output power lasers, and/or by highly focusing the monochromatic light to a diffraction-limited region. Moreover, I have demonstrated that the ratiometric technique is more sensitive than the peak resonance wavelength detection for distance determination. With the sampling wavelengths chosen, the mechanical and optical design may be developed and implemented.

*2.3 Dual wavelength laser coupling colocalizes two wavelengths*

The ratiometric analysis of monochromatic wavelengths of laser illumination requires that the two wavelengths be colocalized to the same region within the field of view of the assay chamber to simultaneously illuminate the gold nanoparticles with the two wavelengths. A dual laser fiber coupling system was developed so that precise, stable, and reliable colocalization of the two wavelengths into the excitation region in the image plane of the microscope is accomplished. (Detailed drawings of all of the mechanical parts are provided in the Appendix.) First, the two lasers were designed to be coupled into individual single mode fibers. Then, the two lasers are combined into the same single mode fiber with the use of a dichroic mirror. Once the two lasers are combined into the same single mode fiber, the two monochromatic sources may be directed into the microscope system.

The two lasers were selected for their stability and output power. The diode-pumped solid state lasers were supplied by CrystaLaser (GCl-532-L, 532 nm, and GCL-593-L, 593 nm, 25 mW and 35 mW, respectively). The diode-pumped solid state lasers provide a single longitudinal mode and single $TEM_{00}$ mode (a Gaussian beam profile) with extremely low noise and high stability in a compact design. These features allow the lasers to be coupled into a single mode fiber, which permits ease in interfacing with downstream optical components and the microscope. Further, single-mode fibers spatially filter the exiting illumination to a Gaussian $TEM_{00}$ mode. Each laser was coupled into a single-mode fiber, after including optics to independently control the power at

each wavelength. To control the power that is coupled into the fiber, the laser emission is passed through a λ/2 waveplate, which changes the orientation of the linear polarization axis by rotation of the waveplate. The light is then directed into a polarizing beamsplitter cube just prior to coupling the light into the single-mode fibers. The λ/2 waveplate specifies the polarization of the laser illumination. Subsequently, the polarizing beamsplitter controls the transmitted intensity of the light by splitting the light based on the polarization state specified by the λ/2 waveplate. One important design feature introduced into the final application, is two opposed two degree rotations of the λ/2 waveplate and the polarizing beamsplitter. The two-two degree wedge angles were incorporated to prevent backreflection and interference due to the parallel optical surfaces of the λ/2 waveplate and the polarizing beamsplitter. The backreflection and interference caused intensity instability, and difficulty in coupling the excitation into the single-mode fiber. The two opposed two degree wedge angles does not translate the principle beam, however the reflected beam will focus to a different location than the primary beam, eliminating the backreflections and interference. After the beam is transmitted through the polarizing beamsplitter, the light is coupled into the single-mode fiber.

A fiber coupling assembly was created to interface with fiber coupling optics provided by Oz Optics so that better than 80% of the transmitted laser illumination is coupled into the single-mode fiber (3.5 μm diameter, 0.11 numerical aperture). Specifically, the Oz Optics fiber coupler includes a focusing lens to focus the laser beam to a diameter smaller than the single-mode fiber

diameter and with a numerical aperture that does not exceed the numerical aperture of the fiber. These design features are described by two equations to calculate the focused laser beam waist diameter (w) and the numerical aperture (NA) of the rays, given the laser beam diameter ($w_o$), focusing lens focal length (f), wavelength (λ), and refractive index (n):

$$w = \frac{\lambda f}{\pi w_0} \quad \text{(Eq. 1)}$$

$$NA = n \sin\left(\tan^{-1}\left(\frac{w_0}{2f}\right)\right) \quad \text{(Eq. 2)}$$

From the two equations, the available focal length lenses and single-mode fibers are selected to optimize the coupling efficiency into the fiber. Additionally, two other features were included to achieve the highest coupling efficiency possible: (1) angle polished ends of the fiber, and (2) adjustable fiber focusing. The fiber ends are often polished with an angle of 8°. This angle, like the wedge angle incorporated in the previous optical elements, prevents any reflections from being coupled into the fiber, which reduces backreflections, and improves the stability of the excitation. The adjustable fiber focus feature on each end of the single-mode fibers is very important for two reasons. The first is that the ability to adjust the focus of the fiber end, that is translating the fiber end with respect to the location of the focusing lens, allows the maximal coupling of the transmitted laser illumination into the single-mode fiber, nearly 80% for the individual laser to fiber coupling. The adjustable focus feature compensates for any aberrations in the specific position of the fiber coupler so that the beam waist of the focused laser illumination is located at the fiber end. Second, the ability to adjust the

focus allows one of the laser beams to be defocused prior to coupling into the same single-mode fiber so that maximal coupling is achieved for both wavelengths. The focal length for the focusing lens which focuses the two wavelengths onto the same single-mode fiber is slightly different for both wavelengths, requiring that the one beam be slightly defocused [20]. Upon coupling the laser illumination into the single-mode fibers, the two beams are directed to be coupled together.

The two beams are collimated with collimating lenses that are essentially the reverse implementation of the fiber couplers and collimate the beams to a 2 mm diameter so that the damage threshold of the dichroic mirror is not exceeded. Equations 1 and 2 are used again to select the focal lengths of the collimating lenses. Once the two beams are collimated they are colocalized with a dichroic mirror (Chroma, T585LP) in which the shorter wavelength (532 nm) is reflected and the longer wavelength (593 nm) is transmitted. The two collimation optical assemblies (Oz Optics) are arranged perpendicularly to each other (Figure 5). Once the two collimated beams are colocalized, they are then coupled again into one single-mode fiber, again to spatially filter the beam to a Gaussian profile, and allow ease of interfacing with the microscope. As indicated previously, to best couple the two wavelengths into the same single-mode fiber, one of the fibers must be slightly defocused with respect to the other, which is easily accomplished with the adjustable fiber focus feature. The designed dual wavelength fiber coupling system achieves approximately 25% coupling for each wavelength of the initial laser output power from the exit of the single-mode fiber

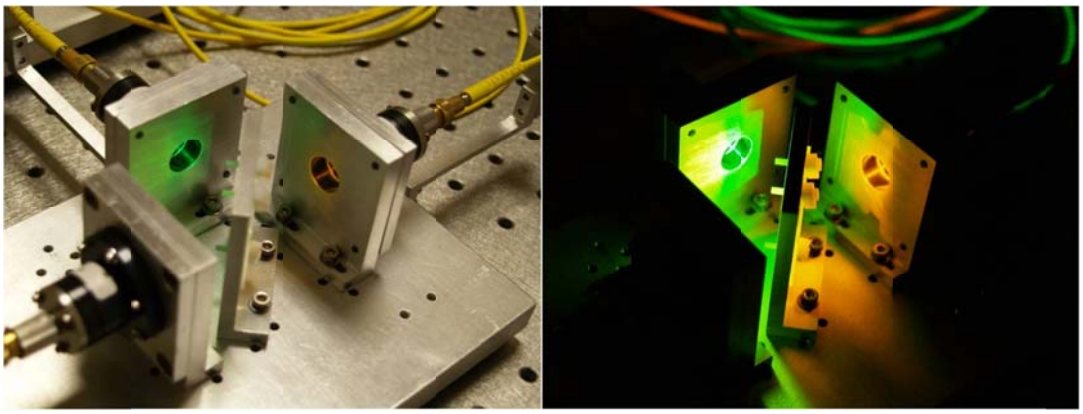

**Figure 5.** Dichroic Fiber Coupling. The two wavelengths of excitation are combined with a dichroic mirror in which the shorter wavelength (532 nm) is reflected and the longer wavelength (593 nm) is transmitted.

which transmits the two colocalized beams. It should be noted that prior to coupling the light into the final single-mode fiber, should additional wavelengths of monochromatic laser illumination were desired to be incorporated, additional dichroic mirrors may be included. The design requires that the two longest wavelengths are combined with a specific dichroic mirror in which the shorter of the two is reflected. Subsequently, the two longest, combined wavelengths are then transmitted through the second dichroic mirror, and the shorter wavelength is reflected. Again, in this arrangement, the shorter wavelength's collimation assemblies are perpendicular to the transmitted laser illumination. The developed dual wavelength fiber coupling system has been demonstrated to produce two collinear laser beams of different wavelength and with a Gaussian profile, to allow independent control of the individual laser's output power, to couple ~50% of the initial excitation power, and can be expanded to include additional wavelengths of excitation.

*2.4 Development of a high-precision, low-drift microscope stage*

One of the advantages of using gold nanoparticles as probes in single-molecule experiments is the ability to collect with very high temporal resolution scattering signals over days of constant excitation. However, a critical design consideration to be able to conduct long time-duration single-molecule experiments is the stability of the microscope both for the stage in the image plane and also in the focal position of the objective. Furthermore, should incredibly high temporal resolution experiments (on the order of microsecond resolution) utilizing avalanche photodiodes be desired, then precise positioning of a specific gold nanoparticle must be made possible, which requires that the stage maintain nanometer stability over the entire extent of the experiment.

During an experiment, thermal and mechanical drift can cause undesirable effects: the sample may no longer be in the field of view, and the sample may drift out of focus. To compensate for these effects, a precision stage was engineered which incorporates a commercially available piezoelectric stage (Physik Instrumente, P-541.2CD) and integrated with a custom-designed low-drift stage for the microscope. The piezoelectric stage provides precise nanometer translation (300 μm travel with ±0.4 nm resolution. However, the electrical interface to the piezo stacks did not allow independent control of the x and y displacements. The electrical connection was replaced to allow each direction to be specifically addressed. Furthermore, a precision voltage controller was designed which independently adjusts the x and y displacements by changing the voltage applied to the piezo stacks. (See the Appendix for a detailed

electrical schematic.) The addition of a custom-built stage provides the capability to displace the stage for large travel (50 mm travel with ±0.7 μm sensitivity). The custom-built stage was designed specifically to reduce drift and give high stability in the x-, y-, and z- directions.

To confirm that the custom stage system has the necessary stability, the drift of the stage was recorded over several hours. Images were captured from fixed fluorescent beads in the field of view. From the images, the change in the position and the focus of the bead were measured. The designed custom stage has less than 200 nm of drift in the x and y directions during the first hour of the observation and no detectable drift in the z (objective focus) position. The majority of the drift is accounted due to thermal expansion of the microscope stage, because over the following hour period the total drift was unchanged, and the position remained stable after 16 hours of observation. It should be noted that any drift in the field of view can be further reduced by modifying the voltage controller for the piezo-nanopositiong stage to include feedback control. The custom-built stage has proven to be capable of high precision, low-drift observations, a necessary experimental feature for most single-molecule experiments.

### *2.5 Prism-based total internal reflection darkfield microscopy illuminates the gold nanoparticles*

Critical to measuring the plasmonic coupling between gold nanoparticles, is the method of illuminating the gold nanoparticles to collect the scattered light

from them. Importantly, it should again be impressed upon the reader that the scattering signal from a particle (whether gold, or polystyrene and silica beads) illuminated by monochromatic light is the same wavelength as the excitation light [64]. In contrast to fluorescent techniques, which take advantage of the Stokes' shift between the excitation and emission to filter away the excitation from the image, the scattering signal must be discriminated from the excitation as they are of the same wavelength. Owing to this requirement that the scattering signal must be collected above the excitation, most typical illumination methods are inappropriate where the scattered light cannot be detected above background.

The common method to reject the excitation illumination from the scattering signal is through darkfield microscopy. Spencer outlines darkfield microscopy as rejecting the zero-order contribution to the image so that the background is dark [19]. The standard implementation of darkfield microscopy directs the illumination from a 100 W tungsten white light arc lamp through a darkfield condenser creating a darkfield image in the field of view of the microscope. Previous single-molecule experiments incorporating the plasmonic coupling of gold nanoparticles have limited temporal resolution, which depending on the assay ranges from to 200 milliseconds to the typical resolution of several seconds due to the use of darkfield microscopy and the chosen detection techniques [17, 18, 110, 121, 122, 125]. The temporal resolution may be increased through several enhancements, including changing the method of excitation of the gold nanoparticles. For example, preliminary measurements of the scattered light from single gold nanoparticles under darkfield illumination with

an 85 W xenon arc lamp (capable of delivering more power in the visible spectrum over tungsten arc lamps) found that the power of the light scattered by a 40 nm gold nanoparticles is less than 0.2 pW, distributed over all wavelengths of excitation. The maximal power density in the sample plane with the darkfield illumination was measured to be is 0.05 $\mu W/\mu m^2$, whereas monochromatic illumination is capable of power densities from 1 $\mu W/\mu m^2$ to 1 $mW/\mu m^2$ by focusing the light to a diffraction-limited region. This suggests that the scattering signal from the gold nanoparticles will be in excess of 4 nW, and at a particular wavelength. Given the anticipated scattering response under monochromatic excitation, the initial design constraints were to achieve microsecond time resolution and nanometer resolution, which requires advancements in the excitation and detection.

Alternative darkfield microscopy methods using either total internal reflection illumination, or objective-type darkfield are the current state-of-the-art methods in which the excitation may be increased at the sample plane, while not sacrificing the extremely low background afforded by darkfield illumination. There have been few applications of total internal reflection illumination specifically to measure the plasmonic coupling between gold nanoparticles, owing largely to the need to use white light excitation for measuring spectra, which is the limiting factor to the temporal resolution [107-109]. These implementations still require long integration times on the order of seconds. However, recent experimental techniques have been devised to use gold nanoparticles for single-molecule particle tracking with high temporal and spatial resolution by measuring the

scattering signal from the particles, capable of up to microsecond temporal resolution [59, 63, 106, 123]. All of these particle tracking techniques use objective-based darkfield microscopy to illuminate the gold nanoparticles. In this method, a converging laser beam reflects on a small mirror to direct it to be focused in the back focal plane of the objective, which results in collimated laser light exiting the microscope at an extreme angle. Backreflections are eliminated by placing a field iris slightly below the conjugated image plane, which removes all light not scattered by the gold nanoparticles. There are several drawbacks to this implementation though. First, the optical path for the collected scattered light is partially blocked by the optics used to reflect the excitation beam into the back focal plane of the objective. Second, the laser beam must be collimated to a very small diameter to integrate the optics well with the microscope. This requires very small optics with high damage thresholds. Moreover, the space limitations make integrating any mechanical and optical components difficult. The best aspects of total internal reflection illumination and objective-based darkfield microscopy were combined to create prism-based total internal reflection darkfield microscopy.

Total internal reflection is a standard illumination technique utilized in single-molecule microscopy [126, 127]. Total internal reflection (TIR) occurs when a propagating light beam interacts at an interface of two mediums of different indices of refraction in which the second index of refraction is lower than the first. Specifically, for single-molecule microscopy, the light beam propagates through a glass medium of high index of refraction to a water or air medium of

low index of refraction. The light undergoes TIR when the beam is incident at a very high angle, measured from the surface normal, greater than the critical angle for TIR [20, 126, 128]. In this case, the light does not refract, but rather totally internally reflects. The critical angle ($\theta_c$) is determined by the equation given the refractive index of the two media (n):

$$\theta_c = \sin^{-1}\left(\frac{n_2}{n_1}\right) \quad \text{(Eq. 3)}$$

When the angle of incidence is greater than (or equal to) the critical angle, an evanescent wave is created in the liquid (air) that exponentially decays in intensity with respect to the penetration distance from the surface, typically less than 200 nm, Figure 6. The penetration depth (d) and intensity (I) are given by the following two equations, given the wavelength (λ), angle of incidence (θ), and refractive index of the two mediums (n):

$$I(z) = I_0 e^{\left(\frac{-z}{d}\right)} \quad \text{(Eq. 4)}$$

$$d = \frac{\lambda}{4\pi}\left(n_1^2(\sin\theta)^2 - n_2^2\right)^{-\frac{1}{2}} \quad \text{(Eq. 5)}$$

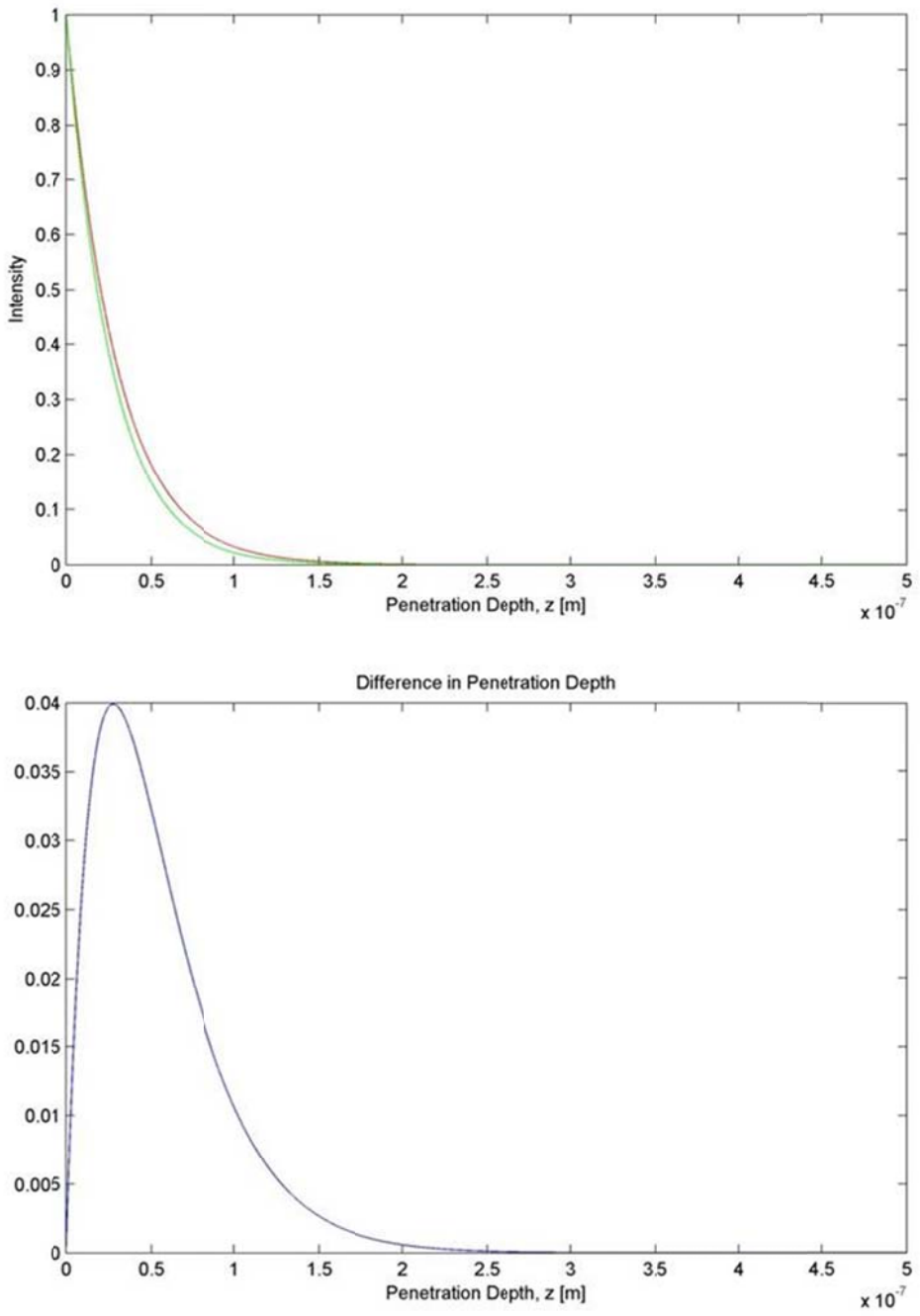


**Figure 6.** Evanescent Wave Penetration Depth. **(Top)** The exponential decay of the evanescent wave created through total internal reflection for both the 532 nm (green) and 593 nm (red) wavelengths is plotted with the penetration depth into solution. **(Bottom)** Based on the calculated penetration depths, the difference in the two intensities is determined to be less than 4%.

The evanescent wave is of the same wavelength as the incident beam, and travels parallel to the interface surface. Importantly, as depicted in Figure 6, the intensity and penetration depth are dependent on the wavelength. As the desired application requires two different wavelengths to illuminate the gold nanoparticles, the difference in the intensity must be quantified. Based on the implemented design and equations 4 and 5, the difference in the intensity is less than 4% between the two wavelengths. The maximal difference, though, is deeper in solution, where the intensity is already near negligible. The distinct advantage of TIR is the evanescent wave, which only excites the gold nanoparticles within the <200 nm region from the glass surface. Since gold nanoparticles are excellent scatterers, it is imperative to eliminate the scattering from the free gold nanoparticles in solution, which TIR provides.

Prism-based TIR darkfield illumination additionally eliminates the need for complicated designs to interface with the microscope, as are necessary in objective-type darkfield illumination. The prism-based TIR creates darkfield illumination, because, as previously described, the excitation is rejected and only the scattered light from the particles in the sample is collected without the use of filters [20, 106]. The specific design (see Appendix for detailed drawings) integrates a 10 mm right angle glass prism on the top surface of the glass slide defining the assay chamber. The two monochromatic beams of laser excitation exiting from the single-mode fiber are focused through an achromatic focusing lens (75 mm focal length) such that the light is focused in the image plane of the sample. The achromatic focusing lens is necessary so that the two wavelengths

are focused to the same location within the image plane. The focusing rays enter the glass prism and propagate into the glass slide. As discussed, the backreflected light must be rejected to easily observe the scattered light from the gold nanoparticles. In the initial integration of prism TIR, backreflections from the glass surfaces of the prism were coupled into the objective, making the darkfield image of very low signal quality, Figure 7 (top, left). However, as the light propagates through the glass slide it undergoes total internal reflection at the glass-air interface (top surface) and the glass-water interface (sample region), Figure 7 (top, right). When a downstream TIR location at the glass-water interface is selected, the backreflections are eliminated, producing a high quality TIR darkfield illumination, for examples see Figures 16, 17, and 18. The prism-based TIR darkfield illumination has other advantages over standard darkfield illumination with white light excitation through a darkfield condenser.

Traditional darkfield illumination with a darkfield condenser introduces an annulus of light of a specific numerical aperture [19, 20, 129], usually between 1.2-1.4. A lower numerical aperture objective (typically 0.7-1 NA) is combined with the darkfield condenser such that the high numerical aperture rays are not collected, and only the scattered light from the sample is imaged. Owing to this illumination scheme a particular range of polar angles are illuminated in the sample plane. As will be discussed in great detail in Section 4.5, the plasmonic coupling between the gold nanoparticles is maximized when the polarization of the excitation light is in line with the interparticle axis. Coupled gold nanoparticles aligned with the polarizations available from darkfield

illumination will be excited. However, when the interparticle axis is not aligned within this range of angles, uncertainty is introduced into the polarization orientation, and it is not possible to fully determine the orientation of the gold nanoparticle pair [129].

Conversely, the prism-based TIR darkfield illumination scheme does not suffer from this fundamental limitation. All polarizations are possible to illuminate, if two orthogonally propagating TIR waves are introduced. Without two orthogonally propagating TIR waves, then all polarizations within one plane is

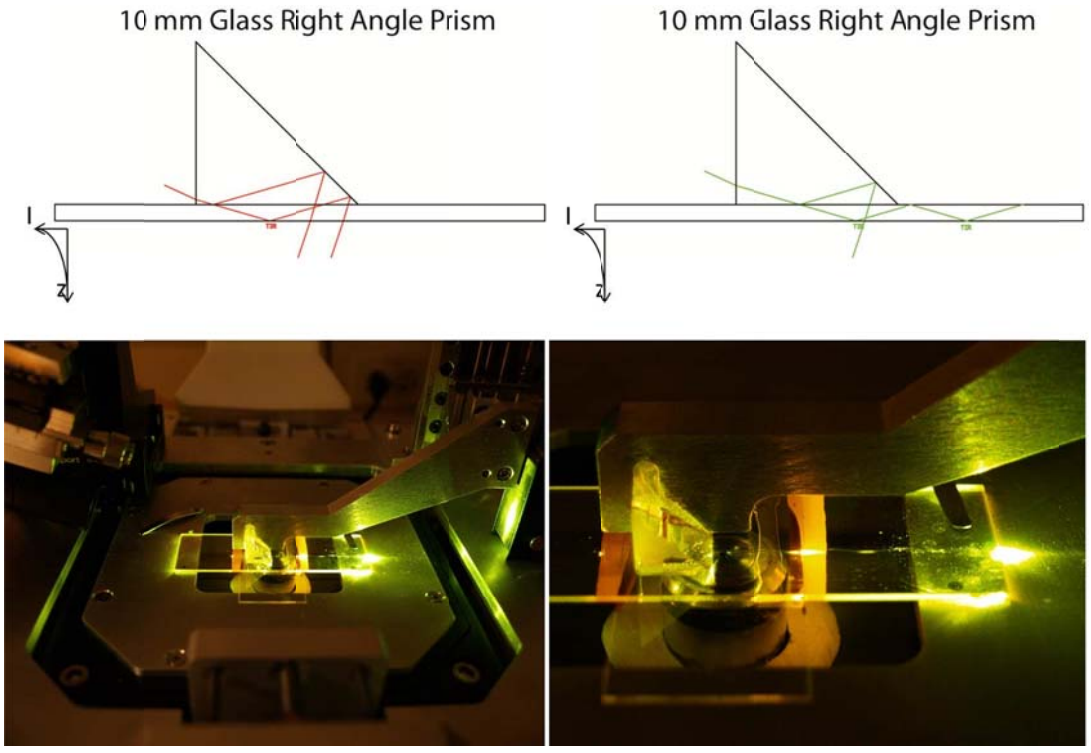


**Figure 7.** Prism-Based Total Internal Reflection Schematic. Propagating the TIR wave through the glass slide eliminates any backscattering from the excitation by selecting a TIR location far from the prism. **(Top, Left)** The initial implementation of prism TIR found that backreflections were directed into the objective of the microscope. **(Top, Right)** However, by selecting a TIR location far from the prism, the backreflections no longer interfere. (**Bottom)** The two images are the actual implementation in the microscope system. It is possible to see the locations of total internal reflection in the right image.

possible (see Figures 20, and 23, as well as Chapter 4 text). Furthermore, traditional darkfield illumination uses an unpolarized white light excitation source, which is additionally detrimental with respect to orientation determination and plasmonic coupling between the gold nanoparticles. Unpolarized white light introduces all polarizations within the specific polar angles described by the numerical aperture of the darkfield condenser. This inherently means that the scattering signal derived from the plasmonic coupling between two gold nanoaprticles will be averaged from all of the polarizations which are aligned with the interparticle axis (maximizing the signal) and also not aligned with the gold nanoparticle axis (reducing the signal). This makes correlating the ratio response at specific wavelengths of excitation to the monochromatic laser-based excitation through TIR illumination difficult. Also, as described previously, white light sources distribute the power over a range of wavelengths, which reduces the power at specific wavelengths. In opposition, monochromatic laser illumination concentrates the intensity to a single wavelength. The laser excitation is also capable of being focused to a diffraction-limited region, concentrating the power further, which is not possible with illumination by an arc lamp source.

Additionally, darkfield microscopy requires the use of low numerical aperture objectives so that the excitation is rejected from the scattered light. However, low numerical aperture objectives collect less of the scattered light from the gold nanoparticles. Under the TIR darkfield illumination, a higher numerical aperture objective may be used, which increases the collected scattering signal. The objective used in this work is a Zeiss Achroplan 100x

variable aperture, oil objective (NA 0.7-1.25, in which NA 1.25 was used). Prism-based total internal reflection darkfield microscopy has been demonstrated to be a superior excitation technique for application to the plasmonic coupling between gold nanoparticles.

### *2.6 A dual view imaging system detects the scattering signal from the gold nanoparticles at each wavelength simultaneously*

The final design element is the choice of the detection scheme. There are several options to collect the scattering signal from the gold nanoparticles. All detection schemes must be able to simultaneously collect the scattering intensity from the two wavelengths of excitation independently. In addition, the detector must be capable of high temporal resolution, fundamental to the design of the instrument. The potential detectors include high speed CCD camera arrays, including EMCCD cameras and CMOS CCD arrays, photodiodes, and photomultiplier tubes [130]. Based on the sensitivity of the detector and the spatial resolution (depending on the binning of pixels in the CCD arrays), the CCD arrays from cameras are capable of several microscecond time resolution [63]. Avalanche photodiodes have high quantum efficiency and are capable of 1 μs exposure times. Quadrant photodiodes were implemented in the objective-darkfield design by Nan *et al.*, which were shown to operate with 25 microsecond time resolution [59]. Each choice of detector has trade-offs. CCD camera arrays make possible the multiplexing of experimental interrogation. That is, many surface-bound gold nanoparticles may be observed in parallel. However,

multiplexed detection requires use of the majority of the CCD array, which slows the time resolution. Photodiodes may be driven with extremely low exposure time on the order of microseconds, and further have high quantum efficiency which makes possible detection of a weak scattering response from the gold nanoparticles at such high temporal resolutions. However, for photodiodes to achieve such high sensitivity, the region of collection from the image plane is limited to a single gold nanoparticle pair. This is specifically due to the size of the photodiode, and the fact that photodiodes are equivalent to a single pixel element. While it would be ideal to be able to have both the functionality of high parallelizability and ultra-temporal resolution, one specific detection scheme must be selected for the initial proof-of-principle application.

Given the lack of experimental information with respect to ratiometric analysis of the plasmonic coupling between gold nanoparticles, the ability to monitor many surface-bound gold nanoparticles within the field of view was considered to be imperative. As such, it was determined that the use of an EMCCD (Photometrics, Cascade 512F) camera would be an ideal detector to integrated into the microscope system. An EMCCD camera is easily incorporated in the optical path of the microscope and has commercially available software to drive the camera, whereas photodiodes would require custom electronic circuitry and software to control them and would only be capable of probing one gold nanoparticle pair. With the selected EMCCD camera, it was possible to measure the scattering signal from individual gold nanoparticles with 5-38 ms exposure times without the need of any gain. The maximum power exiting the fiber was

measured to be approximately 6 mW for each wavelength, though the actual power used to collect the images was modulated so that the pixels would not saturate. For example, with less than 2 mW exiting the fiber from each wavelength, 5 ms exposure images are possible of the gold nanoparticle monomers without the need of camera gain. Another advantageous feature of the use of an EMCCD camera is the facile ability to spatially segregate the two individual wavelengths to independently collect the scattering intensities [130].

Commercially available dual view imaging systems (Photometrics DV2) mount between the microscope and the EMCCD camera and use a dichroic mirror to split the two wavelengths and simultaneously acquire both, Figure 3 (bottom right). Importantly, it should be made clear that the use of a dual view imaging system allows simultaneous intensity collection. The two previous applications of ratiometric analysis to detect the plasmonic coupling between gold nanoparticles alternated the excitation and collected the intensity from the two bandpasses of scattering wavelengths in sequential images [88, 121]. This will influence the measured ratio. The time between images, due to the use of a filter wheel to switch between the two bandpasses from a white light arc lamp, is at best 5 Hz, or 200 ms between images. The particle dimer axis will diffuse over the time of collection, which means that the polarization effects of the orientation of the dimer axis will influence the scattering signal from the two sequential images. If very fast temporal switching of the excitation were possible then the sequential imaging would become negligible. However, as it currently stands, the alternating wavelength collection increases the uncertainty in the previously

implemented ratiometric analysis. The selected dual view imaging system splits the light with a Chroma 565dcxr dichroic mirror. This dichroic mirror splits light with 50% of transmission at 565 nm, a wavelength between the scattering signal wavelengths (532 nm and 593 nm). Specifically, less than 0.5% of the light from the 532 nm channel is transmitted, while better than 97% of the light from the 593 nm channel is transmitted. The dual view imaging system has been shown to collect the scattering signals simultaneously well with high signal-to-noise ratios, for representative examples see Figures 16, 17, and 18.

The signal-to-noise ratio was calculated for single gold nanoparticles adsorbed onto the surface of a glass assay chamber. Images were collected with 38 ms and 5 ms exposure times with the dual view imaging system and EMCCD camera. The signal-to-noise ratio is calculated based on the intensity from a single gold nanoparticle from the channel with the lowest intensity as compared to the background intensity. The dark current, that is the intensity collected when no light is incident on the CCD array, is subtracted from all intensity values. The scattering signal is background corrected by subtracting the background signal from the scattering intensity. The ratio of the signal to the background is then calculated. Specifically, with 38 ms exposure times, the signal-to-noise ratio is better than 100. Smaller region of interest images were collected with 5 ms exposure time under reduced power excitation (1.7 mW exiting the fiber). This was because pixels would saturate after the two gold nanoparticles coupled. Under the above signal-to-noise definition, the ratio is better than 20 from the 5 ms exposure time images. The designed detection scheme proves to be possible

to make initial proof-of-principle measurements to validate the ratiometric analysis technique. This technique should be capable of achieving the microsecond time resolution commensurate to the work demonstrating in the objective-based darkfield schemes using detectors with higher temporal resolution [59, 63]. The technique is fully extendable to faster time resolutions through the use of the alternate detectors described above. If the scattering signal from the gold nanoparticles is limited under the current excitation, the laser illumination may be further focused to diffraction-limited regions, higher power lasers may be used, and high quantum efficiency detectors could be integrated. Fundamentally, the excitation and detection make possible high temporal resolution experiments for single-molecule applications of gold nanoparticles.

### *2.7 Discussion and conclusions*

The main objective of this work is to develop a single-molecule experimental technique capable of high temporal resolution assay detecting the plasmonic coupling between two gold nanoparticles. A ratiometric analysis technique was created such that laser-based excitation provides a scheme to increase the scattering signal from the gold nanoparticles, and thus increase the temporal resolution. To accomplish this goal, instrumentation design and construction were necessary. The two sampling wavelengths were selected to maximize the intensity ratio response from the chosen 40 nm diameter gold nanoparticles. The two laser sources were fiber coupled to easily deliver the light to the microscope and to spatially filter the excitation to a Gaussian beam

distribution. Moreover, a design was engineered to couple the two wavelengths into the same single-mode fiber to colocalized the two sources into the same region of interest. An inverted microscope was modified such that a custom, high-precision, low-drift stage was incorporated to provide the ability to monitor the sample over long time durations, and specifically locate particular gold nanoparticles within the regions of interest. A novel implementation of prism-based total internal reflection through a 45° right angle prism was designed to create an evanescent darkfield illumination source to detect the scattering signal from gold nanoparticles while eliminate backreflections. Finally, a commercially-available detection scheme was integrated to spatially separate the scattering response from the two wavelengths, such that they are recorded simultaneously on a CCD array.

Taken together, this technique has diverse application to many single-molecule experiments. The prism-based TIR darkfield illumination scheme simplifies the illumination necessary for gold nanoparticle tracking, having all of the advantages of objective-based darkfield illumination, while not reducing the image quality. This technique, specifically designed for detection of the plasmonic coupling between gold nanoparticles, has proven to be superior to any other excitation and detection technique applied in the field. This is the first implementation of monochromatic illumination through laser excitation to observe the plasmon coupling between two gold nanoparticles, and has been shown to detect the plasmonic coupling between two gold nanoparticles with >25 Hz time resolution (38 millisecond exposure time) with a signal-to-noise ratio better than

100 from a monomeric gold nanoparticle. Further, the developed instrumentation, unlike the previous techniques, is capable of being built upon to extend the range to even high temporal resolution by increasing the power of the laser sources, or selecting alternate detectors to collected the scattering signal.

# CHAPTER 3

## Gold Nanoparticle Synthesis and Conjugation

Gold and silver nanoparticles are ideal candidates for single-molecule biophysics applications. Their peak resonance wavelength occurs within the visible spectrum, and they are biocompatible and photostable [17, 18, 64, 78, 81, 83, 85, 89, 104, 131, 132]. The application of gold nanoparticle plasmonic coupling to single-molecule biophysics necessitates the functionality to independently label and control the gold nanoparticles with biomolecules. Applications with gold nanoparticles, as opposed to silver, dominate as they have increased stability in high ionic strength solutions, do not oxidize or corrode, and conjugate better to biomolecules with covalent thiol bonding, and amines, although efforts are underway to increase the utility of silver nanoparticles [18, 133-135]. While gold nanoparticles are more stable than silver particles, stability and conjugation remain current challenges to overcome. Another, more detrimental and prominent problem with the metal nanoparticles are the size and shape distributions (heterogeneity), where the inability to synthesize highly monodisperse spherical nanoparticles has great consequences [17, 131, 136]. All of these factors (stability, heterogeneity, and bio-conjugation) influence the plasmonic response of the gold nanoparticles and their applicability to single-

molecule experiments [64, 83, 84, 102, 104, 108, 131, 137, 138]. Great efforts have been made to synthesize, stabilize, and conjugate the gold nanoparticles to DNA molecules [103, 120, 135, 139-146].

### *3.1 Specific aims and research objectives*

This chapter specifically focuses on the use of gold nanoparticles as probes in biological systems. The main goal of this research aims to generalize methods such that gold nanoparticles are easily integrated into biomolecular experiments. Significantly, the gold nanoparticle size and shape distributions dominate the characteristics of the detected plasmonic response. As such, I sought to synthesize gold nanoparticles with narrow size and shape distributions. Additionally, gold nanoparticles are highly sensitive to biological buffers; the particles aggregate in these solutions. I developed methods to stabilize the gold nanoparticles for use in high ionic strength solutions. Furthermore, conjugation methods were developed so that the gold nanoparticles may be attached to a wide range of biomolecules of interest, not just DNA molecules, which were used to demonstrate the application of plasmonic coupling to single-molecule biophysics. Specifically, I employed several labeling and conjugation methods to create gold nanoparticle conjugates suitable for single-molecule bioassays by conjugation through covalent thiol bonding, and specific biotin-neutravidin to DNA molecules and proteins. To accomplish this task, methods were also developed to biotinylate biomolecules for purification, and conjugation to neutravidin gold nanoparticles. Finally, alternative research efforts are summarized to fully

understand the current limitations in the application of gold nanoparticles and areas where further work is required. The details of gold nanoparticle handling and conjugation are explained below.

*3.2 Gold nanoparticle synthesis through citrate reduction*

Controlled gold nanoparticle synthesis was established by Frens in which tri-sodium citrate reduces chlorauric acid to produce gold nanoparticles in the range from 12 nm to 150 nm in diameter [99, 100]. Gold nanoparticles 15 nm, 25 nm, and 40 nm in diameter were synthesized using this method. An aqueous solution containing 0.01% $HAuCl_4$ was heated and reduced with the addition of 1% $Na_3$-citrate solution. The volume of the 1% tri-sodium citrate solution specifies the final gold nanoparticle diameter [100]. Smaller gold nanoparticles (5 and 10 nm diameter) were synthesized through a similar method in which tannic acid serves as an additional reducing agent [147]. In what I consider a visually stunning reaction, upon addition of the tri-sodium citrate, to the acid the solution changes color from a yellow-clear to blue. This marks the reduction and nucleation phase of the reaction. The tri-sodium citrate not only reduces the chlorauric acid, but also further serves to stabilize the gold nanoparticles. As such, when the volume of the $Na_3$-citrate solution is reduced, the gold nanoparticle diameter size increases. After approximately one minute, the solution rapidly changes from a faint blue to deep blue/purple to a wine-colored red, which is indicative of the completion of the chemical reaction, and the stable formation of the gold nanoparticles. The gold nanoparticles that were synthesized

have peak resonance wavelengths in the green spectrum (514-540 nm). However, the solution appears red. This effect is due to the strong absorption by the gold nanoparticles at the peak resonance wavelength, which results in the transmitted light being the complementary color to the absorbed color.

Rayleigh scattering and Mie theory well describe the scattering of light by spherical particles [64, 77, 78, 85, 86, 89]. Rayleigh scattering is limited to particles much less than the wavelength of light, though Yguerabide and Yguerabide note that the theoretical results described by Rayleigh scattering correspond well with Mie theory for gold nanoparticles with diameters of 40 nm or less [64]. Importantly, from Rayleigh theory two relations apply: (1) the intensity of a particular wavelength of the scattered light depends to the sixth power on the diameter of the gold nanoparticles, and (2) the intensity is inversely related to the wavelength with the fourth power [64, 77]. These relations indicate that there is a trade-off with choosing the particle diameter: reducing the size of the nanoprobe to limit the influence its effects on the biomolecule of interest, and the scattering signal. I chose the gold

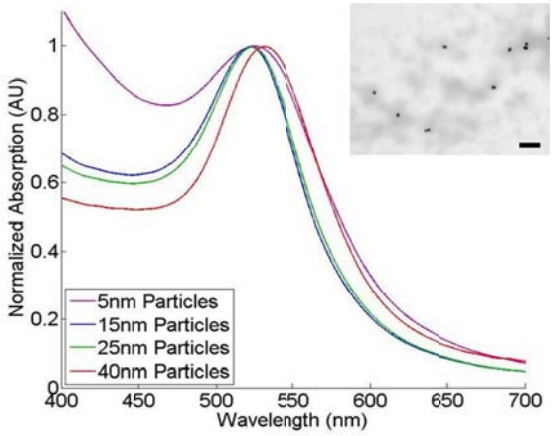


**Figure 8.** Bulk Spectra of Gold Nanoparticles. UV/Vis spectra of gold nanoparticles directly after synthesis, diluted in DI-$H_2O$. Notice that as the particle size increases, the peak resonance wavelength increases. **(Inset)** A TEM image of synthesized 40 nm gold nanoparticles adsorbed onto a grid, scale bar: 250 nm.

nanoparticles within the range of 5-40 nm for both conjugation ease and experimental implementation for single particle observation.

After synthesis of the gold colloid solution, the particles were analyzed with transmission electron micrographs and bulk UV/VIS absorption spectroscopy (Figure 8). From the UV/Vis spectra, the characteristic dependence of the peak resonance wavelength with the nanoparticle diameter is clear; as the gold nanoparticle size increases, the peak resonance wavelength increases. The 15 nm diameter gold nanoparticles, based on TEM micrographs were fairly monodisperse and spherical. Conversely, the TEM images of the 40 nm gold nanoparticles synthesized in-house, show that the gold nanoparticles are neither monodisperse nor are many of the particles spherical (Figure 8, inset). The gold

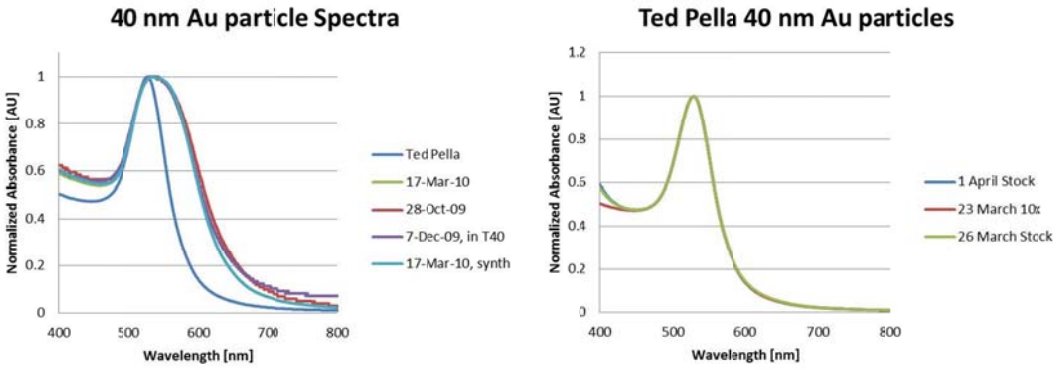


**Figure 9.** Comparison of Commercial and Custom Synthesis. **(Left)** UV/Vis spectra of in-house, custom synthesized gold nanoparticles indicate that the size and shape distributions are greater than the commercially available Ted Pella British Biocell gold nanoparticles. **(Right)** Additionally, the commercial particles are stable for several months, as indicated by no change in the spectra.

nanoparticles were compared to commercially available gold nanoparticles of the same diameter (40 nm, Ted Pella British Biocell), which have been implemented in several experimental applications, and have been suggested to be of suitable

quality [17, 18, 120, 132]. Additionally, many varied applications utilize gold nanoparticles purchased through commercial suppliers [17, 18, 58, 76, 110, 120, 148-151]. UV/Vis absorption spectra from the in-house synthesized gold nanoparticles are much broader than the spectrum from the commercial particles (Figure 9, left). It became evident that commercially supplied gold nanoparticles must be used. Furthermore, analysis proved that the externally supplied gold nanoparticles were stable for many months, since the UV/VIS spectra were unchanged (Figure 9, right). However, subsequent TEM analysis these gold nanoparticles have raised doubts to their monodispersity and homogeneity [17].

Indeed, independent bulk UV/VIS absorbance analysis compared to the

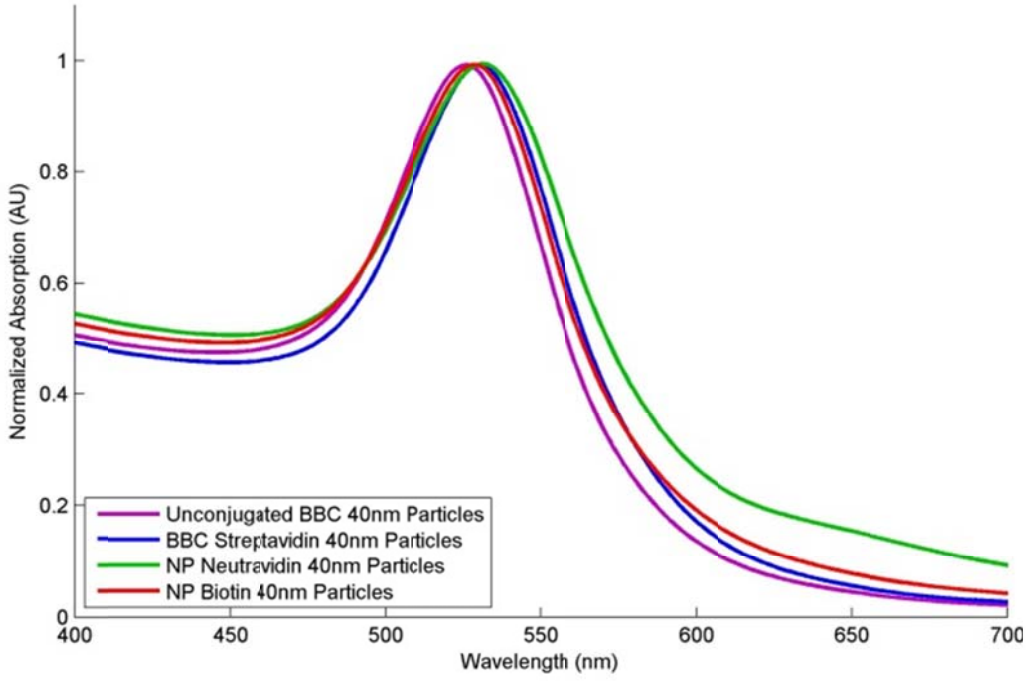


**Figure 10.** Spectra of Commercial Gold Nanoparticles. UV/Vis spectra compare the size and shape distributions of commercially available gold nanoparticles from Ted Pella British Biocell (BBC) and NanoPartz (NP) that are unconjugated, or functionalized with a biotin, or streptavidin (neutravidin).

supplier specifications unearths discrepancies indicative of broader size and shape distributions (Figure 10). Table 2 compiles the peak resonance wavelength and full width half maximum for each of the four commercially sourced gold nanoparticles: Ted Pella British Biocell unconjugated 40 nm gold nanoparticles, Ted Pella British Biocell 40 nm streptavidin-conjugated gold nanoparticles, NanoPartz 40 nm neutravidin-functionalized gold nanoparticles, and NanoPartz 40 nm biotin-conjugated gold nanoparticles.

| | British Biocell Unconjugated | British Biocell Streptavidin | NanoPartz Neutravidin | NanoPartz Biotin |
|---|---|---|---|---|
| Peak Resonance Wavelength [nm] | 526.25 | 530.75 | 531.5 | 529 |
| FWHM [nm] | 86.5 | 84 | 122.5 | 100 |

**Table 2.** Peak Resonance Wavelengths of Commercial Gold Nanoparticles. The peak resonance wavelength and the full width half maximum (FWHM) are calculated for the 4 externally sourced gold nanoparticles, as determined by the UV/Vis spectra in Figure 10.

Ted Pella British Biocell do not publish TEM or spectral information for their supplied gold nanoparticles, although Reinhard *et al.* have characterized the size and shape distributions for these gold nanoparticles, and found their diameter to be 41.7 ± 3.1 nm, the particles to be ellipsoidal, and that 10% of the gold nanoparticles are triangular or pentameric [17]. Importantly, as will be extensively discussed in Chapter 4, the size and shape distributions influence the not only the peak resonance wavelength for an individual nanoparticle, but also the plasmonic coupling response between two gold nanoparticles. The commercial source NanoPartz supplies individual specifications for the peak resonance wavelength and a bulk UV/VIS spectrum for their gold nanoparticles.

These specifications prescribe the peak resonance wavelength of the biotin gold nanoparticles to be 530 nm, and 536 nm for the neutravidin gold nanoparticles. Further, the full width half maximum determined from spectra in the certificates of analysis is approximately 100 nm for each conjugate of gold nanoparticle. When comparing the results, the NanoPartz biotin-functionalized gold nanoparticles are nearly consistent, while the NanoPartz neutravidin-conjugated gold nanoparticles are much broader. The implications of these results are detrimental (see Chapter 4) in the gold nanoparticle applications to metrology through plasmonic coupling, which introduces uncertainty into the absolute distances.

Application of the gold nanoparticles to bioassays requires their stability in biologically relevant buffers, i.e. solutions of high ionic strength. When the gold nanoparticles are simply stabilized by the citrate ions, gold nanoparticles are incredibly sensitive to the ionic strength of the solution [102, 145, 146, 151, 152]. The 40 nm citrate-stabilized gold nanoparticles are only stable in approximately 40 mM NaCl. (The stability of the gold nanoparticles with ionic strength depends on the size of the gold nanoparticle, with smaller gold nanoparticles more stable in higher ionic strength solutions.) Many methods exist to further stabilize the gold nanoparticles to higher ionic strength solutions. Gold nanoparticles may be stabilized through the nonspecific surface adsorption of proteins or biomolecules, such as BSA, casein, and streptavidin / neutravidin, or through specific, covalent gold-thiol chemistry with thiolated DNA molecules [17, 18, 74, 102, 142, 143, 148, 153]. Alternatively, small chain hydrocarbons, such as polyethylene glycol, have been utilized to not only stabilize the gold nanoparticles to high ionic

strength solutions, but also to limit the number of biomolecules conjugated to the gold nanoparticles [120-122, 146, 151, 154]. Finally, the commercial supplier NanoPartz stabilizes their available gold nanoparticles with a polymer shell, which not only reduces nonspecific binding but also increases the stability of the gold nanoparticles in up to 1 M NaCl solutions. Maximal stability were not specifically conducted for the neutravidin and biotin gold nanoparticles, though the gold nanoparticles remained stable in 100 mM NaCl solutions. Similar work in adding a polymeric shell to the gold nanoparticles has found that the gold nanoparticles are suitably stabilized to high ionic strength solutions [155, 156]. An important consequence of stabilizing the gold nanoparticles is that the particles may be further purified through electrophoresis [120, 142, 153], chromatography [141], or salt precipitation [152] prior to their final biological applications.

### *3.3 Gold nanoparticle conjugation to biotin and avidin variants*

Many standard single-molecule biophysics experiments utilize the strong bonding between biotin and avidin [118, 157-160]. As detailed in Section 4.3, biotin-avidin bonds are highly specific interactions, which make facile conjugation schemes. Avidin and its derivatives, streptavidin and neutravidin, monomers all bind up to four biotin molecules each, with $10^{15}$ $M^{-1}$ affinity [161-163]. Biotin and avidin allow conjugations to a wide range of proteins or DNA molecules though the integration of a biotin molecule to the biomolecule. As a precursor to

subsequent conjugation through the biotin-avidin bond, gold nanoparticles were conjugated to streptavidin.

Experiments utilizing streptavidin gold nanoparticles include applications to plasmonic coupling, myosin kinetics, and biosensing [17, 18, 58, 65, 74-76, 164]. Functionalizing gold nanoparticles with streptavidin gold nanoparticles is through a nonspecific adsorption. The method employed borrowed from the labeling work of Dunn *et al.* for 60 nm gold nanoparticles [58] and Reinhard *et al.* for 40 nm gold nanoparticles [17]. This method, as compared to either independent labeling reaction, was found to most efficiently complex the 40 nm gold nanoparticles to streptavidin. Specifically, 40 nm gold nanoparticles purchased from Ted Pella British Biocell were concentrated ten-fold through a fast centrifugation at low centrifugal force meant to gently pellet the gold nanoparticles, though not irreversibly aggregate the particles. The gold nanoparticles were resuspended in a buffer containing a very low ionic strength (2 mM Tris·HCl, pH 8.0, an equivalent ionic strength as 2 mM NaCl). Streptavidin conjugated to tetramethylrhodamine (TMR) was selected for adsorption to the gold nanoparticles such that control assays verify the success of the reaction. TMR, a fluorescent dye, can be stimulated by laser illumination at 532 nm and then emits photons of longer wavelengths with a maximum at 580 nm. The TMR-streptavidin was added to the concentrated gold nanoparticles with a final concentration of 2 mg/ml, and incubated for 10 to 20 minutes at 4°C. Subsequently, the gold nanoparticles were incubated overnight at 4°C with 0.1% polyethylene glycol with a molecular weight of 6000 (PEG 6000). PEG 6000

stabilizes the gold nanoparticles and enhances the ability to centrifuge the gold nanoparticles to dilute and remove the free TMR-streptavidin from the solution. After the overnight incubation, excess TMR-streptavidin was eliminated through repeated centrifugation and resuspension in fresh 2 mM Tris·HCl. The functionalization of the gold nanoparticles with the TMR-streptavidin was verified using the prism-based TIR microscopy.

The experimental apparatus excites the sample with 532 nm and/or 593 nm laser illumination, and collects in spatially separated regions on a CCD camera array the shorter and longer wavelengths, split at 565 nm based on the dichroic mirror. To verify the conjugation of the TMR-streptavidin to the gold nanoparticles, the gold nanoparticles were nonspecifically adsorbed on the

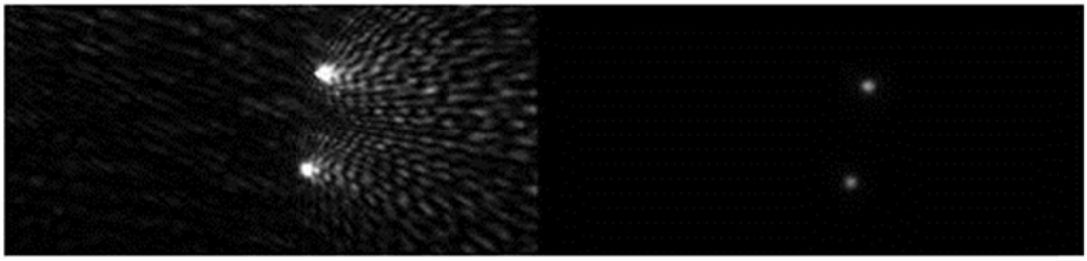

**Figure 11.** Verification of Streptavidin-Conjugated Gold Nanoparticles. 40 nm gold nanoparticles conjugated with TMR-streptavidin are excited by 532 nm laser illumination. Through the prism-based TIR darkfield illumination, both the scattering signal from the gold nanoparticles and the fluorescent emission from the TMR dye are detected by the CCD camera with the dual-view system. This representative image proves that the gold nanoparticles are labeled with streptavidin molecules.

surface of a glass assay chamber. A solution of anti-photobleaching agents (glucose, glucose oxidase, and catalase) was added to prevent the TMR fluorescent dye from photobleaching under the laser excitation. The gold nanoparticles and the TMR were excited with only 532 nm laser illumination. The

532 nm laser illumination was set to 6 mW and the exposure of the CCD camera was 25 milliseconds. In this manner, the scattering from the gold nanoparticles at 532 nm is collected on the short wavelength channel, while the fluorescent emission from the TMR-streptavidin is detected on the long wavelength channel of the CCD array. Figure 11 presents the colocalization of the TMR dye with the scattering signal from the gold nanoparticles. These results indicate that the gold nanoparticles are successfully conjugated with the TMR-streptavidin.

Although the gold nanoparticles were conjugated with streptavidin, the concentration and stability of the gold nanoparticles were difficult to control. Given the specifications from commercially available sources NanoPartz and Ted Pella British Biocell, it was determined that the commercially supplied gold nanoparticles preconjugated with neutravidin or streptavidin had preferential distributions, conjugations, and stability. Furthermore, the gold nanoparticles supplied by NanoPartz limited the number of neutravidin monomers to 30 per gold nanoparticle, as compared to the approximately 200 neutravidin monomers expected through the outlined methods. NanoPartz covalently conjugate and stabilize the gold nanoparticles through a polymeric shell in which the polymer is terminated with the neutravidin monomer. The NanoPartz gold nanoparticles are supplied at high concentrations, approximately 20 nM, owing to the polymeric shell. The polymeric shell additionally provides stability in high ionic strength solution. NanoPartz indicates that the polymeric cage on the gold nanoparticles is of such a low molecular weight that the thickness is within the coefficient of variance of the gold nanoparticles, incapable of detection in the TEM images.

Finally, the polymeric coat is not expected to influence the peak resonance wavelength, where by NanoPartz determined that the peak resonance wavelength varies at most by 1 nm.

As a proof-of-principle assay for the ratiometric analysis of monochromatic laser illumination, the binding between gold nanoparticles was observe through plasmonic coupling. The most basic binding assay was through the specific interaction between a biotin and neutravidin (see Section 4.3). This binding assay was made amenable through biotin conjugated gold nanoparticles supplied through NanoPartz. Like the neutravidin-functionalized gold nanoparticles, the biotin-conjugated gold nanoparticles are specified to have 30 active sites per gold nanoparticles. The NanoPartz biotin gold nanoparticles also have the similar properties as the neutravidin gold nanoparticles, that is, high concentrations and stability, and little to no influence of the polymeric coat to the size of the gold nanoparticle and peak resonance wavelength. Moreover, Figure 10 and Table 2 indicate that the biotin gold nanoparticles have more narrow size and shape distributions with peak resonance wavelengths nearer to unconjugated gold nanoparticles. These results are both favorable and negative. The higher monodispersity of the biotin gold nanoparticles reduces the uncertainty in the biotin-neutravidin gold nanoparticle binding assay. However, the neutravidin gold nanoparticles have higher utility in conjugation to single biomolecules. The broader distribution in the neutravidin gold nanoparticles increases the uncertainty of the results.

*3.4 Gold nanoparticle conjugation through covalent thiol bonding*

Bioconjugation of gold nanoparticles may be achieved through several methods: (1) surface adsorption, (2) biotin-streptavidin (neutravidin), (3) antibody-antigen, and most importantly (4) gold-thiol bonding. While bonding through biotin-avidin is highly specific and strong, the bond between gold and thiol is covalent and stronger than the other linkages, though little is known regarding the specific interaction [153, 165-167]. The bond energy of a gold-thiol bond is high, measured to be 40-45 kcal/mol [168]. Conjugation of DNA through a single gold-thiol bond was found to have varying success to gold nanoparticles larger than 30 nm in diameter. Further development of conjugation schemes yielded a trithiolated anchor, which stabilizes particles up to 100 nm in diameter for robust conjugation to the DNA molecule [143].

Gold nanoparticle stability in high ionic strength solutions is paramount for successful DNA and protein conjugation, e.g. DNA requires higher ionic strength solutions to remain double-stranded [111-113, 169]. Two developments have been created which best screen the particles from flocculation (aggregation) due to the high ionic strength. First, through an exchange reaction, phosphine replaces the citrate as the stabilizing agent for the gold nanoparticles [120]. The reaction between bis(*p*-sulphonatophenyl)phenylphosphine dipotassium salt ($K_2$BSPP) and the gold nanoparticles enables both centrifugation of the gold nanoparticles and stability in high salt solutions necessary for single-stranded DNA conjugation [102, 152, 170]. Centrifugation is essential to achieve sufficiently high concentrations of gold nanoparticles, which are required for both

DNA labeling and biologically relevant concentrations for experimental conditions. The $K_2$BSPP ligand is incubated at a concentration of 1 mg/ml of the gold nanoparticles overnight. After the ligand exchange to $K_2$BSPP, the gold nanoparticles are sufficiently stabilized for further complexation. The second advancement that enables successful conjugation of gold nanoparticles to biomolecules is a subsequent exchange of the surface passivation agent to a short, monodisperse low molecular weight (~450 Dalton) polyethylene glycol (mPEG) [144]. Ligand exchange with the mPEG occurs after bioconjugation. Typically the mPEG is thiolated and carboxy terminated. The mPEG incubates with the gold nanoparticles at a ratio of 1:100,000 again overnight. Upon protection by the mPEG, the gold nanoparticles are stable in buffers with 500 mM NaCl for many days [120, 144]. Both of these stabilizing ligands provide the ability for successful conjugation of the gold nanoparticles to single-stranded DNA and hybridization to the complementary DNA strand.

### *3.5 Complexation of gold nanoparticles with DNA oligomers*

Conjugation of DNA molecules to gold nanoparticles has been most successful through three methods. The first single-molecule plasmonic coupling experiments, in which DNA tethered two gold nanoparticles, utilized each of these three conjugation schemes: biotin-neutravidin, antibody-antigen, and gold-thiol [17, 18]. Given the covalent strength of the gold-thiol bond, DNA functionalization was approached by this method. Agarose gel electrophoresis of the labeled species is a common experimental technique to assay for successful

conjugation, and this analysis method was used to verify that labeling was accomplished [105, 120, 142, 153, 171]. Zanchet *et al.* specify the ease of DNA conjugation and electrophoresis to 12 nm gold nanoparticles [142]. Therefore, as a proof-of-principle, DNA labeling to 12 nm was initially pursued.

The 12 nm gold nanoparticles were synthesized in-house, and following the stability analysis results outlined in Section 3.4, were protected with $K_2$BSPP. Subsequently, the 12 nm gold nanoparticles were then concentrated to 30 nM. Complementary single-stranded DNA oligonucleotides labeled with a single thiol group on the 5'-end of the DNA strand were purchased. The single-stranded DNA molecules were 100 bases in length. The DNA-gold nanoparticle labeling reactions were conducted separately for both of the complementary single-stranded DNAs in parallel. Prior to incubation with the gold nanoparticles, the thiol group at the 5'-end of the DNA was reduced using tris(2-carboxyethyl) phosphine, a reducing agent which does not require removal after the reduction as it does not contain sulfide groups [172-174]. Immediately after thiol reduction, the single-stranded DNA was mixed with stoichiometric amounts of gold nanoparticles. The DNA to gold nanoparticle labeling ratios were varied from 5:1 to 0.25:1, which allows comparative analysis upon agarose gel electrophoresis.

Following the labeling methods of Reinhard *et al.* for thiol-modified DNA, the gold nanoparticle solution was exchanged to 10 mM Tris buffer supplemented with 40 mM NaCl (T40 buffer) [120]. The use of T40 buffer promotes the stability of the DNA on the gold nanoparticle surface. The thiolated single-stranded DNA oligonucleotides were incubated with the gold nanoparticles

for approximately 12 hours. After conjugation, the single-stranded DNA-gold nanoparticle conjugates were purified by removing the free DNA through two centrifugation and resuspension steps. Owing to the substantial molecular weight difference between the gold nanoparticles and the single-stranded DNA, the single-stranded DNA-gold nanoparticle conjugates settle in the pellet, while the free DNA remains in the supernatant. Following the single-stranded DNA-gold nanoparticle labeling, the two complementary DNA-gold nanoparticle conjugates were hybridized. Equal volumes of the two species were combined and incubated for 12 hours. The complementary DNA anneals during this time, creating dual gold nanoparticle conjugates tethered by double-stranded DNA. The successful labeling and hybridization of the gold nanoparticle-DNA-gold nanoparticle assemblies were verified through agarose gel electrophoresis. As demonstrated in Figure 12, the gel electrophoresis results confirm that the assemblies are reproducibly generated to tether two 12 nm diameter gold nanoparticles with a single double-stranded DNA molecule. Based on the

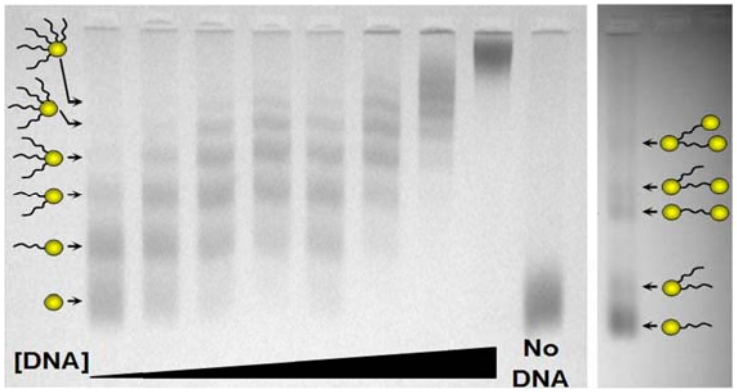


**Figure 12.** Agarose Gel Analysis of DNA Conjugation to Gold Nanoparticles. Using agarose gel electrophoresis it is possible to resolve the conjugation stoichiometry. **(Left)** Agarose gel electrophoresis compares the mobility of 12 nm gold nanoparticles after labeling with varying concentrations (0.25:1 to 5:1 DNA:gold) in an electrif field. **(Right)** Subsequent hybridization of complementary single-stranded DNA are indicated by the appearance of new populations within the gel.

success of the complexation of a double-stranded DNA molecule to two gold nanoparticles, the methods were applied to 40 nm diameter gold nanoparticles.

DNA molecules were designed for several experimental applications, including control sequences for distance calibration, DNA binding by the loop repressor protein *lac* repressor, and transcription by T7 RNA polymerase. For these various applications, the single-stranded DNA oligomers varied in length between 50 bases and 100 bases and were modified with a single thiol group at the 5' end of the DNA strand. Repeated labeling reactions to 40 nm diameter gold nanoparticles following the developed methods for labeling reactions with 12 nm diameter gold nanoparticles, however, were unsuccessful. Based on the agarose gel electrophoresis results, the 40 nm gold nanoparticles were not stable in the T40 buffer necessary for the DNA conjugation and hybridization. Several adaptations of the DNA conjugation methods were attempted. First, after the single-stranded DNA-gold nanoparticle labeling reaction, the DNA-gold nanoparticles were incubated with thiolated mPEG molecules (see Section 3.4) to provide greater stability in high ionic strength solutions. The thiolated mPEG molecules have been used in subsequent applications of the single-molecule plasmonic coupling between gold nanoparticle dimers to obtain homogeneous, and stable gold nanoparticles [120, 121]. Additionally, the DNA oligomers were redesigned to include modifications capable of creating multiple thiol bonds to the gold nanoparticle. The preliminary conjugations utilized single-stranded DNA oligonucleotides labeled with a thiol group on the 5'-end of the strand and covalently attached the thiol to the gold nanoparticle. It has been postulated that

the free rotation of the linker arm between the gold nanoparticle and the DNA molecule can dominate the observed Brownian dynamics of short DNA molecules [175]. Further, multiple thiol anchors were found to better functionalize to gold nanoparticles with diameters of 30 to 100 nm [143]. As such, oligonucleotides labeled with a tri-thiol group on the 5'end and a single thiol group on the 3'-end were expected to result in successful labeling. Using these DNA constructs, each gold nanoparticle will have four covalent bonds to the double-stranded DNA molecule (three from the 5'-end of one strand and one from the 3' end of the other strand), which serves as a stronger anchor to limit the free rotation of the linker arm, and increases the bonding energy [143, 168]. While these methodologies have been successfully employed by the Reinhard group [120-122], none of these revisions provided the desired DNA-gold nanoparticle conjugates.

The unsuccessful covalent conjugation of DNA to the 40 nm gold nanoparticles through gold-thiol bonding led to the redesign of experimental assays to test the capabilities of the developed plasmonic coupling technique. As an alternative to covalent bonding through gold-thiol conjugation, complexation of double-stranded DNA through biotin-neutravidin interactions was pursued. The biotin-neutravidin bonding methods outlined in Reinhard *et al.* were adapted for the T7 RNAP binding experiments (see Section 4.8) [17]. The conjugation of double-stranded DNA to a single gold nanoparticle was conducted through a sequential directed build-up assembly within the experimental assay chamber, in contrast to the *a priori* functionalization attempted in the covalent conjugation

schemes. Gold nanoparticles supplied by Ted Pella British Biocell were either conjugated with TMR-streptavidin, or already labeled with streptavidin. The particular method to functionalize the gold nanoparticles with DNA begins by non-specifically adsorbing 6 pM of streptavidin gold nanoparticles to the glass surface within the assay chamber. (The TMR-streptavidin gold nanoparticles served as a control for the adsorption of streptavidin gold nanoparticles to the surface of the assay chamber.) The gold nanoparticles, diluted with T40 buffer to promote surface adsorption, were flowed into the assay chamber and allowed to incubate for 2 minutes. Subsequently, any remaining gold nanoparticles freely diffusing in solution were flushed out of the chamber. To limit the number of DNA molecules which might nonspecifically bind to the gold nanoparticles and the glass surface, passivating proteins (casein and BSA) were incubated for 15 minutes. Finally, a 75 base pair, double-stranded DNA molecule modified with a biotin on the 5' end of one of the DNA strands was introduced into the assay chamber and allowed to incubate for 30 minutes. Through the strong affinity of the biotin-streptavidin bond, the DNA binds to the gold nanoparticle. Any DNA that is freely diffusing in the chamber, is washed away prior to the addition of the T7 RNA polymerase-gold nanoparticle conjugates. Through the use of TMR-streptavidin control assay outlined in Section 3.3, the DNA-gold nanoparticle labeling was verified through the binding of a T7 RNAP to the DNA promoter site (see Section 3.6 and Figure 15). Many methods exist to conjugate gold nanoparticles with DNA. Section 3.7 presents limitations and additional guidelines for more successful methods for gold nanoparticle conjugation.

*3.6 Extension of gold nanoparticle conjugation to biotinylated biomolecules*

One current limitation of the application of the plasmonic coupling of gold nanoparticles to single-molecule biophysics experiments is the lack of independent control of the interacting gold nanoparticle species. That is, all previous experiments have only analyzed gold nanoparticles functionalized with DNA [17, 18, 88, 120-122, 151, 176]. However, dynamic interactions of proteins with DNA are of great interest. Given this deficiency in the field, fundamental approaches were established to extend the plasmonic coupling technique to include functionalization of gold nanoparticles with biomolecules.

Enzymes and proteins probed through single-molecule experiments typically require bioconjugation either to fluorescent probes, silica or latex beads, or glass surfaces [1, 4, 26]. Many methods non-specifically bind proteins to the surfaces of the probe, while others specifically bind through the thiol from the side chain of a cysteine residue. It is sometimes possible to introduce a biotin group at the C-terminus of a protein for which a streptavidin-biotin conjugation is made available, however with the trade-off of introducing a bulky (~20,000 Dalton) subunit to the protein [177, 178]. A novel biotinylation method biotinylates a specific lysine residue in a consensus sequence, in which only thirteen amino acids needs to be added to the protein amino acid sequence [179]. As a general overview, the process of this biotinylation method involves molecular cloning of the specific consensus sequence into the gene of the protein of interest. Next, the protein is co-expressed with a vector that includes biotin ligase, a protein

which biotinylates the lysine residue within the protein of interest. Subsequently, the biotinylated protein is purified through highly specific protein purification techniques which take advantage of the added biotin label.

This method was employed to biotinylated a model protein, T7 RNA polymerase, with which a gold nanoparticle is conjugated through the biotin-streptavidin bonding for application to single-molecule plasmonic coupling experiments. T7 RNA polymerase (T7 RNAP) is a robust protein which synthesizes RNA from a DNA substrate. Thomen *et al.* previously introduced and applied this biotinylation method to T7 RNAP for single-molecule optical trapping experiments [180, 181]. Following their methods, biotinylated T7 RNAP polymerase was expressed, purified, analyzed for activity, and labeled with streptavidin gold nanoparticles. Specifically, through standard molecular cloning techniques nineteen amino acids were introduced at the N-terminus of the T7 RNAP gene (MAGGLNDIFEAQ**K**MEWRLE), including the consensus sequence (underlined sequence) for which the coexpressed biotin ligase protein biotinylates the lysine residue (in bold). The plasmid, which includes the entire T7 RNAP gene with the N-terminus modification, was then transformed into AVB101 *E. coli* cells. The AVB101 cells, supplied through Avidity, were selected because this strain of cells includes the plasmid pBirAcm, a vector which encodes the gene for the biotin ligase protein, induced through IPTG addition. Subsequent purification of the biotinylated T7 RNAP protein is simplified because the protein has the biotin tag, which can be used to specifically interact with an avidin resin. The avidin resin is advantageous because it uses monomeric avidin, which

maintains high affinity for biotin, though reversibly releases the bound biotinylated T7 RNAP under mild elution conditions which include free biotin in solution to compete for avidin binding. Filtration is used to remove the free biotin from the eluted protein solution, yielding pure biotinylated T7 RNAP protein.

Particular expression and purification methods were created for the biotinylated T7 RNA polymerase. The T7 RNAP gene is promoted by the *lac* UV5 promoter, which is known to have a low level of expression, approximately 11 times lower than the *tac* promoter used to express the biotin ligase protein [182]. It was found that due to the low expression levels for the T7 RNAP protein, the volume of wet cells grown for expression and purification needed to be increased so that a suitable concentration and amount of purified biotinyated T7 RNAP was produced. In a particular expression, two liters of culture were grown with the transformed AVB101 cells. At mid-log growth, the cells are induced to express the T7 RNAP and biotin ligase with 1.5 mM IPTG and supplemented with 50 μM D-biotin supplied by Research Organics. (Research Organics D-biotin was found to work best for this application). The cells grow for an additional three hours. The wet cells are pelleted through centrifugation, collected, and frozen at -80°C for future purification.

Purification was conducted through Softlink Avidin resin, supplied by Promega, with which the maximal purification and recovery is 4 mg of biotinylated protein per milliliter of avidin resin. The most effective method for purification was through batch procedures with the avidin resin. The frozen cells containing the expressed biotinylated protein are thawed on ice and resuspended

in a lysis buffer containing 50 mM Tris·HCl, 2 mM EDTA, and 100 mM NaCl, pH 8.0. The cells are fully resuspended by quickly vortexing and mechanically stirring the solution with a three-fold excess of lysis buffer to protein. After resuspension, the cells are incubated with lysozyme and protease inhibitors for 20 minutes on ice. The cells are then transferred to a glass beaker and sonicated to break the cells. A standard sonication procedure is employed in which a 50% duty cycle is used for 4 cycles of 30 second pulses followed by 30 seconds rest on ice. The lysed cells are centrifuged to separate the pelleted cellular debris from the supernatant containing the expressed protein. The cell lysate is subsequently incubated with the avidin resin to promote binding of the biotinylated T7 RNAP to the avidin resin. Typically, the supernatant from 10-15 g of wet cells is incubated with 250 µl of avidin resin. The solution is stirred at 4°C for 5 hours to ensure maximal biotinylated T7 RNAP recovery. The resin material, which now is bound by the biotinylated T7 RNAP, is washed by successive centrifugation and resuspension steps. The resin material is pelleted through centrifugation, while any unbound proteins which would contaminate the purified protein stay suspended in the supernatant solution. The supernatant is removed and replaced by fresh buffer. The washes are repeated six times so that only the bound biotinylated T7 RNAP protein remains. The biotinylated T7 RNAP is eluted by adding 5 mM free biotin to the solution and incubating overnight at 4°C. The resin is again centrifuged to pellet it, but now the unbound biotinylated T7 RNAP is suspended in the supernatant. The supernatant is collected, and a

second elution in 5 mM free biotin for 3 hours at 4°C is conducted to enhance the recovery of biotinylated T7 RNAP.

The recovered biotinylated T7 RNAP after the elution is contaminated with 5 mM free biotin, which must be removed so that the biotinylated protein may bind to the streptavidin gold nanoparticles. This is performed through diafiltration with a centrifugal filter specifying to have a molecular weight cut-off of 50,000 Dalton. The biotinylated T7 RNAP, a 100,000 Dalton protein remains on the filter while the small biotin molecule (~250 Da) passes through the filter. Diafiltration is repeated until the biotin concentration is calculated to be less than 1 pM. The diafiltration serves an additional, significant purpose to concentration the biotinylated protein. After the diafiltration, the biotinylated T7 RNAP is flash frozen with liquid nitrogen, and stored at -80°C. Furthermore, standard SDS-polyacrylamide gel electrophoresis techniques verify the purity of the biotinylated T7 RNAP, and estimate the concentration. Figure 13 presents the SDS-PAGE analysis of the purification. The biotinylated T7 RNAP is found to be pure and concentrated to approximately

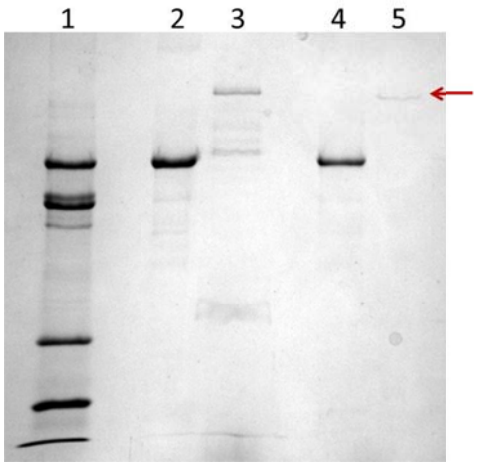


**Figure 13.** Gel Analysis of Biotinylated T7 RNAP Purification. SDS-polyacrylamide gel electrophoresis indicate the purity and concentration after purification of biotinylated T7 RNA polymerase. Lane 1 is a molecular weight ladder, the highest band corresponding to BSA (MW 66.5 kDa). Lanes 2 and 4 are purified biotinylated BSA, serving as a positive control for the purification procedure. Lane 3 is the purified biotinylated T7 RNA polymerase. Lane 5 is pure T7 RNA polymerase from New England Biolabs.

6 μM. Upon obtaining pure, biotinylated protein, the protein must be confirmed to be enzymatically active.

In the particular purification of the chosen model system, biotinylated T7 RNA polymerase, enzymatic activity was assayed by challenging the polymerase to transcribe DNA. A bulk transcription technique was performed, in which the biotinylated T7 RNA polymerases must transcribe a small 100 base pair DNA minicircle [183]. The RNA strand produced through transcription is detected through hybridization to a molecular beacon sequence. Molecular beacons are single-stranded oligonucleotides, in which a hairpin forms between the two ends, creating a stem-loop structure. The molecular beacon sequence is labeled on one end with a fluorophore, and on the other end with a quencher. When the loop region hybridizes with the RNA product, the two ends separate and hybridize with the RNA in a more thermodynamically favorable conformation. Importantly, upon hybridization with the RNA, the two ends of the molecular beacon are spatially separated. Prior to hybridization, the two ends of the molecular beacon are near, as when in the stem-loop conformation, the quencher prevents a fluorescent signal from being emitted. However, after hybridization, the two ends are far away, which allows fluorescence from the fluorophore.

To assay for transcription, the DNA, biotinylated T7 RNAP, and three of the four nucleotides (ATP, CTP, and GTP) are incubated together. The T7 RNAP is allowed to reach a stable elongation complex, but then stalled at a particular site in which a UTP must be added to the elongating RNA strand. At this point, heparin is added into the solution. Heparin is a known inhibitor of T7 RNA

polymerase, in which unbound T7 RNAP molecules are incapable of binding and transcription DNA. [184]. The assay is designed such that the biotinylated T7 RNAP bind to a minicircle DNA molecule, reaching stable elongation, and stalling at a site such that all of the DNA molecules are loaded with one T7 RNAP, however the excess T7 RNAP are inhibited from binding. Transcription is allowed to proceed by the addition of UTP. After the transcription concludes, the T7 RNAP releases the RNA transcript, and is inhibited by the heparin in solution. The RNA transcripts hybridize with the molecular beacons, producing a fluorescent response. In this manner, the fluorescent signal has a baseline prior to addition of UTP. Once UTP is included, transcription proceeds, indicative that the biotinylated T7 RNAP is active, see Figure 14. With active biotinylated protein, conjugation to gold nanoparticles may be pursued.

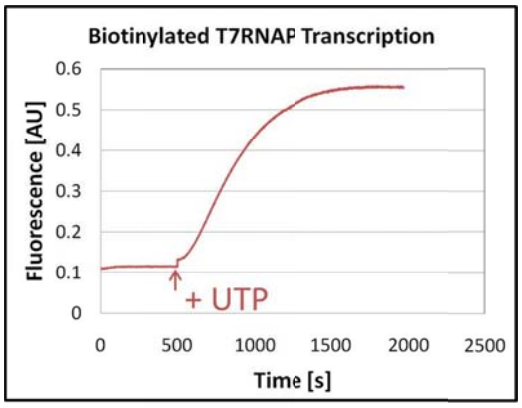


**Figure 14.** Molecular Beacon Transcription Assay. The fluorescent response from the molecular beacon transcription assay indicates the activity of the biotinylated T7 RNA polymerase. Upon the addition of UTP, stalled biotinylated T7 RNA polymerases transcribe a DNA template. The increase in fluorescence indicates that the biotinylated T7 RNA polymerase is active.

The conjugation of biotinylated proteins to gold nanoparticles through a biotin-streptavidin bond is similar to the scheme used with biotinylated DNA molecules (see Section 3.5). There are some distinctions between the conjugations, though, based on the experimental conditions for the chosen assays. In the model system binding assays, the biotinylated T7 RNAP is free in

solution and allowed to bind to DNA linked to surface-bound gold nanoparticles. As such, the labeling is not conducted through a build-up assembly, but rather through an incubation of the biotinylated protein and the gold nanoparticles. The streptavidin gold nanoparticles were incubated with the biotinylated T7 RNAP at a stoichiometric ratio of 38 T7 RNAP polymerases per gold nanoparticle. The gold nanoparticle stability limits how high it can be concentrated, which dictates the reaction conditions. However, given the high concentration of the biotinylated T7 RNAP, an extremely low volume of the protein may be introduced into the gold nanoparticle solution, which effectively maintains the gold nanoparticle initial concentration. The streptavidin gold nanoparticle concentration is maintained at 1.5 nM, while the final concentration of the biotinylated T7 RNAP is 50 nM, where the stock ranges from 1-6 μM. In typical polymerase binding and transcription assays, high ionic strength solutions are required, e.g. transcription is mediated with two magnesium ions [180, 185]. Owing to the high ionic strength solutions, the gold nanoparticles must be stabilized.

It was found that the passivating proteins casein and BSA that are used to passivate the glass chamber surface were the best to passivate the freely diffusing gold nanoparticles as well. When the freely diffusing streptavidin gold nanoparticles were passivated with 0.1 mg/ml of casein and BSA, the gold nanoparticles continued to remain in solution over several (>3) days of observation. To control whether the conjugation to the protein was successful, the biotinylated protein was conjugated to TMR-streptavidin conjugated gold nanoparticles. The standard binding experiment was conducted (see Section

4.8), however both the surface-bound and the freely diffusing gold nanoparticles were labeled in-house with TMR-streptavidin.

Observing only the fluorescent signal from the TMR, gold nanoparticles on the surface are localized. The biotinylated DNA molecules bind to the TMR-streptavidin functionalized gold nanoparticles. Under high excitation by the 532 nm laser, the TMR dye on the surface-bound gold nanoparticles photobleaches.

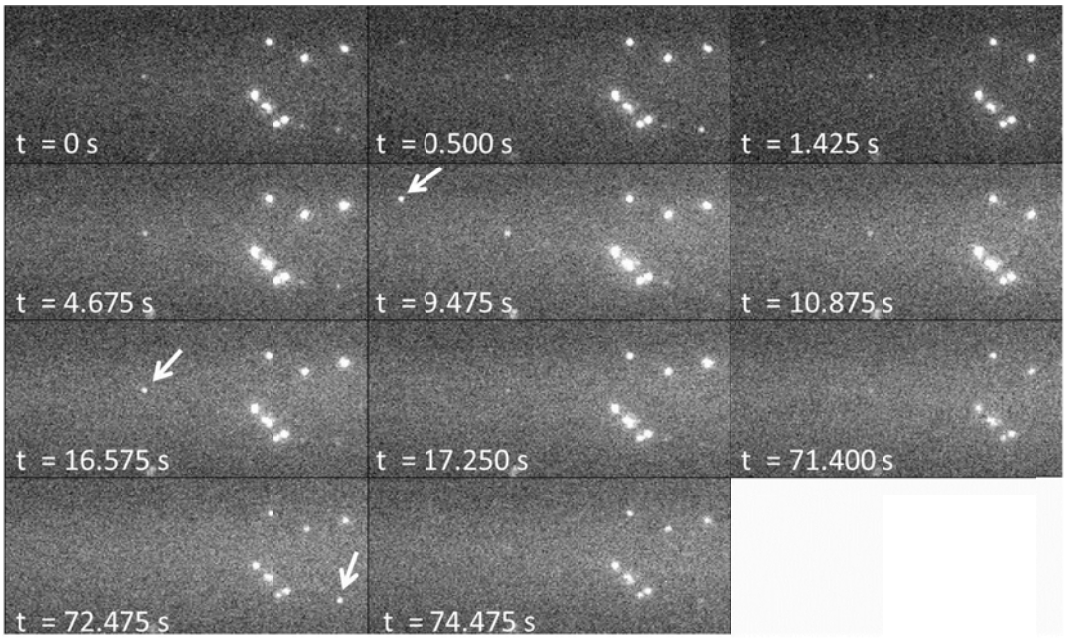


**Figure 15.** A Time-Series Montage of T7 RNA Polymerase Binding. The fluorescence response from TMR dye under 532 nm laser excitation reveals interactions between the T7 RNA polymerase and DNA. The gold nanoparticles are labeled with TMR-streptavidin, which allows only a fluorescent signal to be detected from the gold nanoparticles. Surface-bound gold nanoparticles are located in the field of view based on the fluorescent signal, which subsequently photobleaches. DNA molecules are bound to the surface-bound gold nanoparticles, which serves as a binding substrate for biotinylated T7 RNA polymerase conjugated to a TMR-streptavidin functionalized gold nanoparticles. As evidenced in the montage, three distinct binding events are observed at 9.475, 16.575, and 72.475 seconds.

Subsequently, the biotinylated T7 RNA polymerases conjugated to the TMR-streptavidin functionalized gold nanoparticles are flowed into the assay chamber.

Increases in fluorescence intensity at locations where surface-bound gold nanoparticles are, indicate that the T7 RNA polymerase binds to the DNA molecule, Figure 15. The control experiment provides further evidence that the gold nanoparticles are successfully conjugated with biotinylated proteins and DNA.

### *3.7 Limitations and outlook of gold nanoparticle synthesis and conjugation*

The surface plasmonic coupling technique hinges on the ability to reliably synthesize monodisperse gold nanoparticle solutions, and conjugate the gold nanoparticles to the proteins of interest for study. Advances have been made in both of these pursuits. The monodispersity of the gold nanoparticles is paramount in application of plasmonic coupling for distance detection and binding. As discussed in detail in Chapter 4, the size and shape of the gold nanoparticles significantly influences the extent to which the gold nanoparticles interact, and the scattering signal response. In this work, it was found that commercially available gold nanoparticles, which are widely available and used, provided better size and shape distributions than in-house synthesis through the citrate reduction method. However, the commercially available size distributions are still broad and there are many asymmetric particles of several shapes (ellipsoidal, triangular, and pentameric) [17, 150]. Great research efforts are underway by many groups to better control the size and shape distributions of the gold nanoparticles through several techniques [90, 186-188]. Gold nanoparticle distributions have been controlled by: (1) alternative synthesis

methods utilizing inorganic methods, such as CTAB reduction [189] and dimethylformamide [190], (2) reduction methods with sodium borohydride [191], (3) through size sorting through salt precipitation [152]. While these methods may better the size and shape distributions, their applications to biologically relevant systems require further processing that exchanges the solution within which the particles are dispersed into solutions mimicking cellular conditions and maintain stability of these particles in the solutions.

Stability of the gold nanoparticles is an additional research area of interest for applications of gold nanoparticles to biotechnology. Unconjugated gold nanoparticles aggregate in solutions of low ionic strength. Additionally, the general handing of unconjugated gold nanoparticles is very sensitive to temperature, pH, and centrifugation. Several methods have been found to increase the stability of the gold nanoparticles. In this work, a phosphine or polymeric shell, and a simple protein passivation techniques with casein and BSA were determined to stabilize the gold nanoparticles such that the particles were able to remain dispersed in high ionic strength solutions up to 150 mM NaCl and 25 mM $MgCl_2$. Alternative passivation methods have utilized a two-fold surface ligand exchange method, which stabilized the gold nanoparticles first with a phosphine shell and then thiolated polyethylene glycol molecules [120, 151]. The PEG capping method provides great stability over several months. Additionally, the number of DNA molecules per gold nanoparticle can be controlled through reaction conditions and agarose gel purification. However, the gold-thiol bonding is challenging. The gold-thiol bond is slow to react and hard to

control in bulk labeling. Additionally, each of the ligand exchanges requires overnight incubations. The difficulty of passivating the gold nanoparticles limits the versatility and application [192].

As an example, the gold nanoparticle dimer conjugation through DNA is sensitive to the DNA sequence and length. Most DNA molecule conjugations to gold through a thiol bond require a specialized sequence to enhance the ability to create the bond, typically a sequence of ten adenosine bases are incorporated at the 5' end with the thiol group [148, 151]. Bioconjugation methods pursued in this work were not limited by the sequence of the DNA, specifically because the bonding was facilitated through the biotin-streptavidin bond. In addition, through the use of biotin-streptavidin conjugation method, the conjugation to biotinylated proteins was made possible, extending the application of techniques utilizing functionalized gold nanoparticle with biomolecules. The biotin-streptavidin conjugation scheme, though, cannot control the number of DNA molecules or proteins bound to the gold nanoparticle. NanoPartz specifies the number of neutravidin molecules per gold nanoparticle, but most suppliers do not control the number of molecules per gold nanoparticle. Furthermore, purification through typical methods to specify the number of DNA molecules or proteins per gold nanoparticle is not possible. Each of the passivation and conjugation methods have benefits and drawbacks, requiring further development in bioconjugation techniques for gold nanoparticles so that gold nanoparticle applications are more widely used.

The application of gold nanoparticles to single-molecule biophysics is still in its infancy. Bioconjugation and stability of the gold nanoparticles in biologically relevant buffers are still challenging, limiting many implementations. Specific to applications which measure the plasmonic coupling response between two gold nanoparticles, the monodispersity of the gold nanoparticles also must be improved. While much more effort and research are still required to make gold nanoparticle plasmonic coupling a standard technique, the work here provides an initial foundation for further pursuits.

### *3.8 Discussion and conclusions*

Presented here are methods to integrate the plasmonic coupling experimental technique into a wide range of biophysical assays. It was determined that commercially available gold nanoparticles provide better size and shape distributions over in-house synthesis methods. Techniques were created to stabilize the commercially available gold nanoparticles in the high ionic strength solutions required for biological experiments. The gold nanoparticles were passivated through a common single-molecule passivation method in which globular proteins adsorb onto the gold nanoparticles surface, which provides stability in solutions with up to 150 mM NaCl and 25 mM $MgCl_2$. Conjugation methods were created to functionalize DNA molecules and proteins with gold nanoparticles. Many methods were explored to conjugate the gold nanoparticles through gold-thiol covalent bonding, and through the biotin-streptavidin bond. It was found that conjugation mediated through the biotin-streptavidin bond makes

the best trade-offs between specificity and number of molecules per gold nanoparticle, time for conjugation, ease of handling, and broad application to biomolecules. Furthermore, methods were created to biotinylate proteins of interest with a small biotin linkage. The biotinylation expression and purification schemes produce a high yield of biotinylated protein, which makes possible conjugation to the gold nanoparticles. These methodological developments extend the range of applicability of gold nanoparticles and the plasmonic coupling between gold nanoparticles beyond DNA assays to include general biomolecular systems.

# CHAPTER 4

## Gold Nanoparticle Binding Assays

Following the development and implementation of the instrumentation and ratiometric analysis, detailed characterization of the system is required. The major goal of this work is to create a technique, which detects the plasmonic coupling of gold nanoparticles with significantly higher temporal resolution than has been previously achieved for applications to single-molecule biological systems. All experimental configurations to date have illuminated the gold nanoparticles with white light directed to the sample with a darkfield condenser [17, 18, 88, 120-122]. Subsequently, detection of the plasmonic coupling between gold nanoparticles has been through a CCD camera or a spectrometer. Owing to the implementation of these experimental schemes, the temporal resolution has reached 10 Hz with no ability to increase temporal resolution due to the low efficiency to collect and measure the scattered light from the gold nanoparticles. The monochromatic ratio detection technique has the capability to greatly increase this temporal resolution. To benchmark the technique, I chose to measure the binding of single gold nanoparticles. The binding of two gold nanoparticles, creating a dimer, would maximize the plasmonic coupling signal expected to be detected. It is also possible to monitor the dynamics of the

binding event, thus determining the temporal sensitivity of the experimental system. The plasmonic coupling response between the gold nanoparticle pair is dependent upon the orientation of the dimer axis with the polarization of the excitation source [88, 97, 98, 109, 122, 136, 138, 193]. Analysis of the polarization sensitivity of the monochromatic ratiometric technique further advances the understanding of the developed plasmonic coupling technique. Through the polarized ratiometric analysis, dimer orientation can be established. The signal response from the gold nanoparticle pair could then be optimized based on the orientation of the polarized light with the dimer axis. The following study focuses on the application of the ratiometric analysis technique to the plasmonic coupling response of two gold nanoparticles under several binding conditions.

### *4.1 Specific aims and research objectives*

The specific goals discussed in this chapter are to demonstrate the capabilities of developed experimental technique. First, single gold nanoparticles are observed with the prism-based total internal reflection illumination and dual view detection technique. The monomeric gold nanoparticle intensity ratio is measured and compared to spectra from single gold nanoparticles. Next, to determine the maximum expected ratio signal change, the binding between two gold nanoparticles is detected through a change in the intensity ratio due to the plasmonic coupling between the two gold nanoparticles. The two gold nanoparticles are functionalized with biotin or neutravidin, which mediates the

binding of two gold nanoparticles. Further, the temporal resolution of the implemented monochromatic ratiometric experimental technique is quantified through the time-resolved binding of a neutravidin gold nanoparticle free in solution to a biotin gold nanoparticle bound on the glass slide surface. The sensitivity of the ratiometric analysis technique to the polarization state of the incident illumination was examined through the designed binding assay when polarization optics that specifically define the polarization are incorporated. The results from the binding experiments are compared with published theoretical analysis, and a model is developed to further extract information from the collected scattering intensities and their ratio. The final demonstration of the experimental technique to single-molecule biophysics culminates in a binding assay in which a polymerase functionalized with a gold nanoparticle is monitored while freely diffusing until binding to its promoter DNA sequence. The DNA is conjugated to a surface-bound gold nanoparticle. This preliminary single-molecule binding experimental establishes the applicability of the technique to single-molecule biophysics experiments.

### *4.2 Monomeric gold nanoparticles are distinguished with the ratiometric detection technique*

The first characterization of the experimental technique is to determine the signal response of monomeric gold nanoparticles under the excitation and detection. This establishes the expected starting ratio of the scattered light from the two monochromatic wavelengths, 593 nm and 532 nm. Additionally, the

signal-to-noise ratio from a single gold nanoparticle determines the sensitivity of the system for temporal and spatial resolution. As previously discussed, several gold nanoparticle conjugates were created or purchased. Gold nanoparticle monomers conjugated with biotin or neutravidin were analyzed with the ratiometric analysis experimental technique. The general approach used to measure the initial ratio for a single gold nanoparticle begins by adsorbing a particular conjugated gold nanoparticle to the glass surface of an assay chamber. The standard passivation scheme using the proteins casein and BSA is performed to ensure that the local refractive index of the medium is identical to the real biological assay. Images of the surface-bound gold nanoparticles are collected from many fields of view in the assay chamber. The images record the intensity of the scattered light from both of the two excitation wavelengths. The scattering signal from each wavelength is spatially separated into two channels on a CCD array. The ratios of the scattering response from the 593 nm wavelength to the scattering response from the 532 nm wavelength are calculated from the intensity. By collecting many fields of view of assay chambers, a large number of gold nanoparticles may be analyzed, and a distribution of the ratios created.

Figure 16 displays typical images from surface-bound 40 nm biotin and neutravidin conjugated gold nanoparticles from which the ratio distributions for both were calculated. The mean and standard deviation of the ratio is a function of the size and shape of the gold nanoparticles (the particle monodispersity) [83, 88] and the local refractive index. As previously discussed, the gold nanoparticle

distributions of the size and shape are difficult to control (see Section 3.2) with the best distributions in the size and shape found from commercial suppliers. However, the bulk absorbance spectra (see Figure 10) reveal that the particles are not as monodisperse as is suggested by gold nanoparticle suppliers. Additionally, Reinhard *et al.* explored through TEM imaging the size and shape of 40 nm gold nanoparticles from commercial sources [17]. The TEM imaging

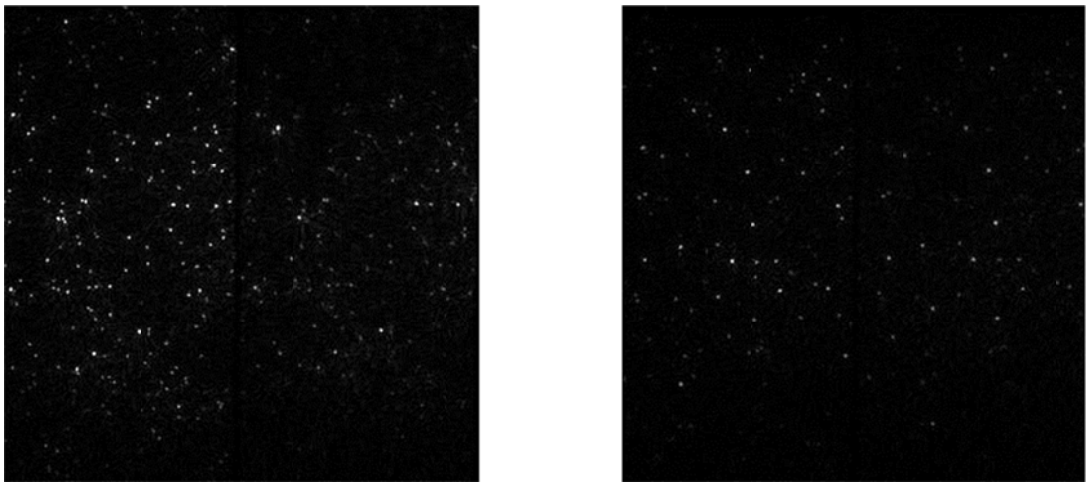

**Figure 16.** Gold Nanoparticle Scattering Under Dual Wavelength Excitation. The scattering signal is collected from the two wavelengths of excitation (532 nm and 593 nm) in the same image. **(Left)** Biotin gold nanoparticles are imaged with the dual-view imaging system under dual wavelength excitation. The left side of the image is the 532 nm scattering response, while the right side is the 593 nm scattering signal. **(Right)** Neutravidin gold nanoparticles are likewise imaged.

reveals that the majority of the particles are ellipsoidal, the absolute diameter is not 40 nm, and that pentagonal and triangular particles occur often. Indeed, the specifications for the NanoPartz gold nanoparticles state that both the biotin and neutravidin gold nanoparticles have a 7% coefficient of variance, the neutravidin gold nanoparticle average diameter is 41 nm, and the biotin gold nanoparticle average diameter is 37 nm. The anisotropy of the gold nanoparticles will,

therefore, have a large influence in the overall peak resonance wavelength and plasmonic coupling between the gold nanoparticle pairs.

The peak resonance wavelength also has a strong dependence on the local refractive index, as evidenced in many applications [74, 75, 194]. The local refractive index for each particle is dependent on the surface coverage of the neutravidin or biotin on each particle and the surface passivation scheme that is employed [17, 74, 88, 122, 195, 196]. The gold nanoparticles, supplied by NanoPartz, are coated with a polymer cage to stabilize the particles in high ionic strength solutions, and allow high concentrations of gold nanoparticles. The peak plasmon resonance wavelength due to the polymeric shell, as specified by NanoPartz is measured to change by at most 1 nm. Based on the specifications of the gold nanoparticle source, the number of active sites per particle is limited to 30. Additionally, the same concentrations of passivating proteins are used both for the surface passivation, and in passivating the gold nanoparticles that are used to freely diffuse in solution. As a result, the refractive index of the medium will be standardized in the assays employed, $n_E$ = 1.5-1.6 [197, 198]. The greatest variability in the ratio distributions for the performed assays will thus be from the monodispersity of the gold nanoparticle solutions. However, it should be noted that correlating published single particle spectra with the monochromatic intensity ratios depends on the local environment within which the experiments were performed.

Previous surface plasmon resonance and coupling responses from gold nanoparticles were measured with bulk absorbance spectra [66, 76, 103]. The

absorbance spectrum from gold nanoparticles correlates with the scattering spectrum [82]. From the bulk absorbance spectra measured for the 40 nm gold nanoparticle solutions used in the single-particle experiments (see Figure 10), the anticipated intensity ratio ranges from 0.17 for unconjugated gold nanoparticles to 0.30 for neutravidin-functionalized gold nanoparticles. It is important to establish that the observed spectrum from the bulk solution is an ensemble average over all of the particles in solution, including dimers and multimers, monomers of larger and smaller diameter, and monomers of varying aspect ratios. As such, the bulk solution spectra cannot provide great insight into the mean and variance in the scattering intensity ratio measured in the developed experimental technique. At best it provides an ensemble average ratio, but contains no information as to the variance of the intensities at specific wavelengths.

Single particle scattering spectra may benchmark the expected intensity ratio in the designed experimental technique, provided the same particle size distributions and refractive index are similar. These spectra provide the scattering intensity for a single gold nanoparticle over a range of wavelengths, which then can be used to calculate intensity ratios at particular wavelengths for an individual particle. Single particle spectra typically suffer from low signal strength, which will introduce additional error into the resulting ratio. Many single particle spectra must also be collected to directly correlate the expected mean intensity ratio and standard deviation. Specifically, one single particle spectrum from the work by Reinhard *et al.*, and another single particle spectrum from Raschke *et*

*al.*, corresponds well to the biological buffers and conditions we would expect [17, 74]. Based on these two spectra, the intensity ratio for single gold nanoparticles is expected to be between 0.24 and 0.54, respectively. However, based on the simulation spectrum for a 42 nm gold monomer included in Reinhard et al., the intensity ratio is 0.71. To add further difficulty to establishing *a priori* the anticipated initial intensity ratio, Jain *et al.* calculate the expected absorption and scattering spectra for single 40 nm gold nanoparticles from which the intensity ratio is 0.24 [82]. The theoretical absorption spectra for a 50 nm gold nanoparticle predicts the intensity ratio should be 0.3 [89]. Due to the limited number of published spectra of single gold nanoparticles for comparison, it is not possible to characterize the distribution of the intensity ratio for individual gold nanoparticles. In the first ratiometric analysis with unpolarized white light illumination, explained in detail in Section 1.5, Rong *et al.* measure an intensity ratio of 0.45 for a 40 nm monomeric gold nanoparticle, differing from preliminary benchmarks [121].

We find that the measured mean ratio from 417 biotin-functionalized NanoPartz 40 nm diameter gold nanoparticles is 0.9695 ± 0.1803. Likewise, the measured mean ratio from 637 neutravidin-functionalized NanoPartz 40 nm diameter gold nanoparticles is 1.0002 ± 0.3565. All of the gold nanoparticles within each field of view were analyzed, and their intensity ratio was calculated. The resulting distribution of the intensity ratio, thus, includes intensity ratios of spherical monomers, ellipsoidal monomers, dimers, and multimers (aggregates

of gold nanoparticles), which is the major source of difference between the theoretical expectations and the experimentally measured intensity ratio.

In the current arrangement of the experimental assays, it is possible to reject surface-bound gold nanoparticles from further monitoring and analysis by measuring the initial intensity ratio. Based on both the total intensity and the ratio, it is possible to discern spherical monomers from larger aggregates or anisotropic particles. It should be made clear that while it is possible to limit the specific surface-bound gold nanoparticles to observe and analyze, there is no control over the second gold nanoparticle with which plasmonic coupling interactions occur. The gold nanoparticles allowed to interact with the surface-bound gold nanoparticles freely diffuse in solution, which inherently means that the average gold nanoparticle that interacts is from the entire size and shape distributions of the gold nanoparticles. The particle size and shape distributions are currently a fundamental limitation of all single particle surface plasmonic coupling experiments [17, 18, 75, 83, 88, 137]. While this may limit the immediate applicability to certain biophysical measurements, it does not diminish the ability of the ratiometric analysis of monochromatic scattering signals technique to detect the plasmonic coupling between gold nanoparticles.

### *4.3 Biotin-neutravidin gold nanoparticle binding interactions are detected through plasmonic coupling*

In order to test the experimental approach for detecting dynamic plasmonic coupling interactions in a biologically relevant experiment, the change

in the intensity ratio upon binding of freely diffusing neutravidin gold nanoparticles to surface-bound biotin gold nanoparticles were analyzed. The biotin-streptavidin bond is one of the most robust and strongest biological bonds. The affinity for the interaction is $10^{15}$ $M^{-1}$ [161-163]. Neutravidin is an analogue of streptavidin with a near neutral isoelectric point, which limits nonspecific binding, and has the highest specificity for biotin. Streptavidin and neutravidin can bind up to four biotin molecules at a time. In the introductory biophysical plasmonic coupling experiments, multiple linkages between the two gold nanoparticles, which obfuscates the actual distance between the gold nanoparticles, could not be excluded [17, 18]. While the potential for multiple linkages between the biotin-neutravidin gold nanoparticles are possible, as there are on average 30 active sites per gold nanoparticle, two factors must be considered: (1) based on the surface density, there is one biotin/neutravidin per 168 $nm^2$, which precludes a 20 $nm^2$ neutravidin [199, 200] from binding multiple biotin molecules, and (2) regardless of the number of linkages, the minimum distance will always be the distance of a biotin-neutravidin bond.

The gold nanoparticle binding experiment not only quantifies the temporal resolution of the experimental technique, but also measures the maximal signal ratio response that is expected, given that the distance between the two gold nanoparticles is, at minimum, the distance between a single biotin-neutravidin bond, which separates the two gold nanoparticles by 4 nm [17, 74, 76, 199, 200]. As discussed in Chapter 3, the stability of the gold nanoparticles in physiologically relevant (high ionic strength) solutions requires the gold

nanoparticles to be passivated with proteins or small carbon chain molecules, which add a layer to the diameter of the gold nanoparticle, and limit the minimum distance between the gold nanoparticles. Furthermore, it is expected that in biophysical applications the gold nanoparticles will always be separated by a certain distance, due to necessary requirement that the gold nanoparticles be conjugated to the biomolecules of interest. Often these conjugates are mediated through the biotin-neutravidin bond; as such the biotin-neutravidin gold nanoparticle binding assay is an excellent model system to derive the maximal expected signal.

As a first application, the binding of the neutravidin gold nanoparticles to surface-bound biotin gold nanoparticles were observed over increasing incubation times and compared to images of the surface-bound biotin gold nanoparticles prior to the introduction of the freely diffusion neutravidin gold nanoparticles. From the before and after images, it is possible to observe simply by an increase in the intensity that a binding event has occurred, Figure 17. Within 5 minutes, binding events always occur, but often the gold nanoparticles bind sooner, as will be discussed. Figure 17 also reveals two other features from the incubation time series images: (1) not all surface-bound gold nanoparticles in the field of view are bound by neutravidin gold nanoparticles, and (2) the gold nanoparticle binding reaction saturates after an incubation of between 15-20 minutes, as evidenced in three separate assay chambers. Importantly, since not all of the surface-bound gold nanoparticles in the field of view exhibit binding events, the non-reactive gold nanoparticles serve as internal controls within all of

the binding assays that the experimental assay conditions are not adversely affecting the intensity ratios.

The mean intensity ratiometric of all of the particles in the three fields of view, 67 particles, is 0.8300 ± 0.1556. This suggests that the majority of the particles in the field of view are monomers. After the 20 minute incubation, the mean intensity ratio and standard deviation increases to 0.9559 ± 0.3340. Again,

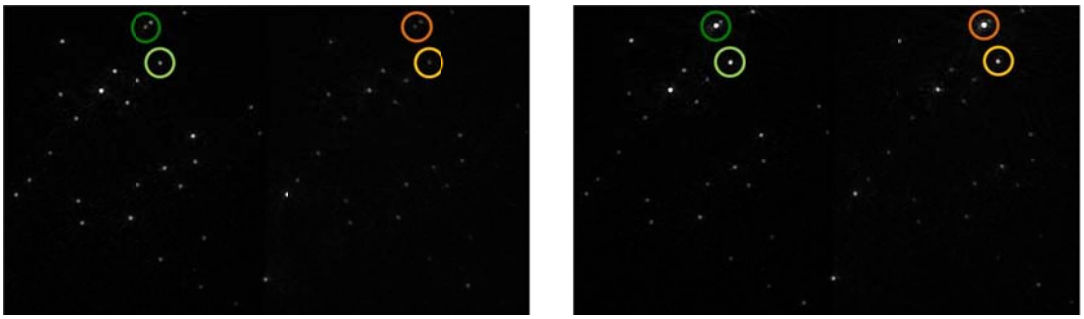

**Figure 17.** Gold Nanoparticles Binding Through Biotin-Neutravidin. **(Left)** Surface-bound biotin gold nanoparticles before incubation are imaged with the dual-view imaging system under dual wavelength excitation. The left side of the image is the 532 nm scattering response, while the right side is the 593 nm scattering signal. **(Right)** The same field of view is imaged after a 5 minute incubation with neutravidin gold nanoparticles. Binding between the two gold nanoparticles are clearly observed by an intensity increase for the two gold nanoparticle pairs indicated in the images.

all of the particles within the field of view, whether a binding event occurred with an individual particle, are analyzed. As such, the mean and standard deviation depends on the number of binding events within the three assay chamber. The observed increase in the mean and the near doubling of the standard deviation provide evidence that binding events occur. Applying nonparametric Kolmogorov-Smirnov statistical analysis with a 95% confidence, the two distributions are different with a p-value of $1.73 \times 10^{-4}$. When we select specific surface-bound gold nanoparticles in which the intensity ratios are 0.6-0.7, indicative of spherical

monomers, and binding events occur, the intensity ratio increases to a range of 1.17-1.30. However, even a surface-bound gold nanoparticle scattering a total intensity expected for a monomer but with an intensity ratio of 1.49 before incubation (indicative of a larger, possibly anisotropic particle), are still sensitive to the ratiometric analysis. Upon incubation and binding by a second gold nanoparticle, the ratio increases to 2.94. It is again important to discuss the contributing factors to the range in the distribution of the intensity ratios. As detailed in Section 4.2, the monodispersity of the gold nanoparticles complicates the interpretation of the ratios after binding. There is no control over the second particle which binds to the surface-bound gold nanoparticles. Additionally, as will be detailed in Section 4.5, the dimer orientation with the polarization of the excitation light influences the plasmonic coupling between the two gold nanoparticles [17, 88, 122, 136, 138]. When the particle pair dimer axis is aligned with the polarization of the light, the plasmonic coupling is maximized, and the intensity ratio is maximized. Conversely, when the dimer axis is oriented 180° from the polarization of the light, the intensity ratio is minimized. In the experiments detailed in Figure 17, the polarization state of the light was not specifically defined, including polarization components in both the optical axis and slide plane.

Control experiments confirm the specificity of the interaction, that is, the binding of a biotin gold nanoparticle and neutravidin gold nanoparticle. The first negative control assays whether any binding interactions occur when the freely diffusing gold nanoparticles are biotin conjugated. It is expected that there should

be no interactions between the surface-bound biotin gold nanoparticles and the freely diffusing biotin functionalized gold nanoparticles. Likewise, given the strong affinity of biotin for neutravidin, neutravidin gold nanoparticles preincubated with a ~$9.35x10^4$ excess of free biotin molecules to biotin binding sites should not interact with biotin gold nanoparticles. Under similar conditions in which free biotin is in solution to compete with biotin bound to a gold surface for the binding

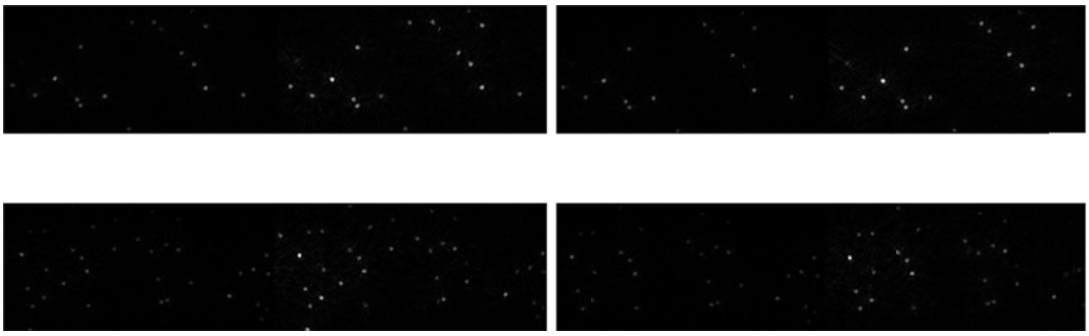

**Figure 18.** Control Experiments for Specificity of Biotin-Neutravidin. Negative controls ensure the specificity of the biotin-neutravidin interaction. Surface bound biotin gold nanoparticles before incubation **(Left)** and after a 30 minute incubation **(Right)** with freely diffusing biotin gold nanoparticles **(Top)** and freely diffusing neutravidin gold nanoparticles preincubated with an excess of biotin **(Bottom)**. No binding interactions were observed in either control experiment.

of neutravidin, Jung *et al.* measure a long off-rate of $t_{1/2}$=~3 hours [164]. As verified in the binding experiment, binding interactions are observed within 5 minutes and saturate within 15-20 minutes. The freely diffusing gold nanoparticles in the negative control assays were incubated for 30 minutes, which is sufficiently long to ensure that any potential interactions are captured. Images were collected of the surface-bound biotin gold nanoparticles before incubation and 30 minutes after incubation with the free gold nanoparticles from both the negative control experiments (Figure 18). Intensity and intensity ratios analysis of images in the control experiments are unchanged after the prolonged

incubations. For both of the negative control experiments, the two distributions of the intensity ratios before and after incubation with the freely diffusing gold nanoparticles are indistinguishable based on Kolmogorov-Smirnov statistical analysis with 95% confidence. The binding interactions that were observed through the ratiometric analysis in Figure 17 must be specific.

### *4.4 Time-resolved biotin-neutravidin gold nanoparticle binding interactions are detected through plasmonic coupling with unparalleled resolution >25 Hz*

Many biomolecular interactions occur on the millisecond timescale, requiring sub-millisecond temporal resolution to study the details within the processes. The biotin-neutravidin gold nanoparticle binding assay lends itself well to establishing the temporal resolution of the monochromatic intensity ratiometric analysis technique. Given the strong photostability of gold nanoparticles, the gold nanoparticles are capable of continuous excitation and observation. The use of a CCD array is advantageous as many surface-bound gold nanoparticles may be viewed simultaneously. Prior to the introduction of the freely diffusing gold nanoparticles, the surface-bound gold nanoparticles are monitored to ensure that the intensity ratio indicates the particle is monomeric, spherical, and stably bound to the glass surface. Subsequently, image series are recorded while the neutravidin gold nanoparticles diffuse into the field of view. The ratiometric analysis technique is challenged to detect the dynamic binding of the neutravidin gold nanoparticles to the surface-bound biotin gold nanoparticles through the plasmonic coupling signal.

The exposure time of the collected image series from the CCD camera determines the temporal resolution of the experimental technique. This serves as an intermediate limit on the intensity ratiometric analysis. The exposure time of the image series is set by two competing factors: (1) the intensity of the gold nanoparticles, both monomeric and interacting dimers, and (2) the ability of the camera to maintain the prescribed exposure time during the collection of an image series. When the scattering signal from the gold nanoparticles saturates the camera, the laser illumination intensity and/or exposure time must be decreased. However, the CCD camera cannot maintain the intended exposure time below certain limits, which are dependent on the region of interest of the camera that is used. In this application, with the dual wavelength scattering signals collected on spatially separated regions on the CCD array, the region of interest is either the full chip (512 rows x 512 columns), or a region of interest that collects fewer rows of the image. When full chip images are recorded, the camera collects images with 50 ms exposures. Smaller regions of interest, (300 rows x 512 columns), the maximum exposure with which camera collects images is 38 ms, better than 25 Hz. As further detailed in Section 5.2., the established ratiometric analysis technique is limited in the choice of detector. In fact, due to the limitations of the CCD camera, the excitation illumination was reduced to try to prevent saturation of the images, upon binding by the complementary gold nanoparticle, though in some binding events, the image would still saturate some pixels on the CCD array. However, the >25 Hz temporal resolution is unmatched

as compared to the state of the field for detecting the plasmonic coupling between gold nanoparticles [17, 18, 88, 121].

Image series of the time-resolved binding events were collected upon the introduction of the neutravidin-functionalized gold nanoparticles. The gold nanoparticle solution was introduced through capillary action, as opposed to wicking the solution into the chamber. This prevents losing the focus of the microscope because of changes in the chamber volume. Again, the CCD camera introduces some complications into the experiment. At the exposure time used in the experiment, only two minute image series can be collected and stored in the camera buffer. Due to this limitation, instead of continuous collection of image series records, an image series prior to the introduction of the gold nanoparticle solution is recorded to determine which surface-bound gold nanoparticles should be monitored. Then, the same field of view is observed, though the images are not collected, as the solution of the freely diffusing gold nanoparticles is deposited at the entrance of the assay chamber. As soon as the neutravidin gold nanoparticles are seen to be diffusing into the field of view, a two-minute image series with 38 ms exposure is recorded. In most of the assay chambers, binding events are observed within the record. A second record is typically collected, regardless of whether a binding event occurred, to observe additional binding events. Subsequent image series of the same field of view may be collected, depending on the binding results.

In the time-resolved image series, many binding events were captured in many different assay chambers. The increase in the intensity from both wavelengths indicates that a second scattering particle is within the diffraction-limited region. The increase in the scattering intensity ratio reveals that the

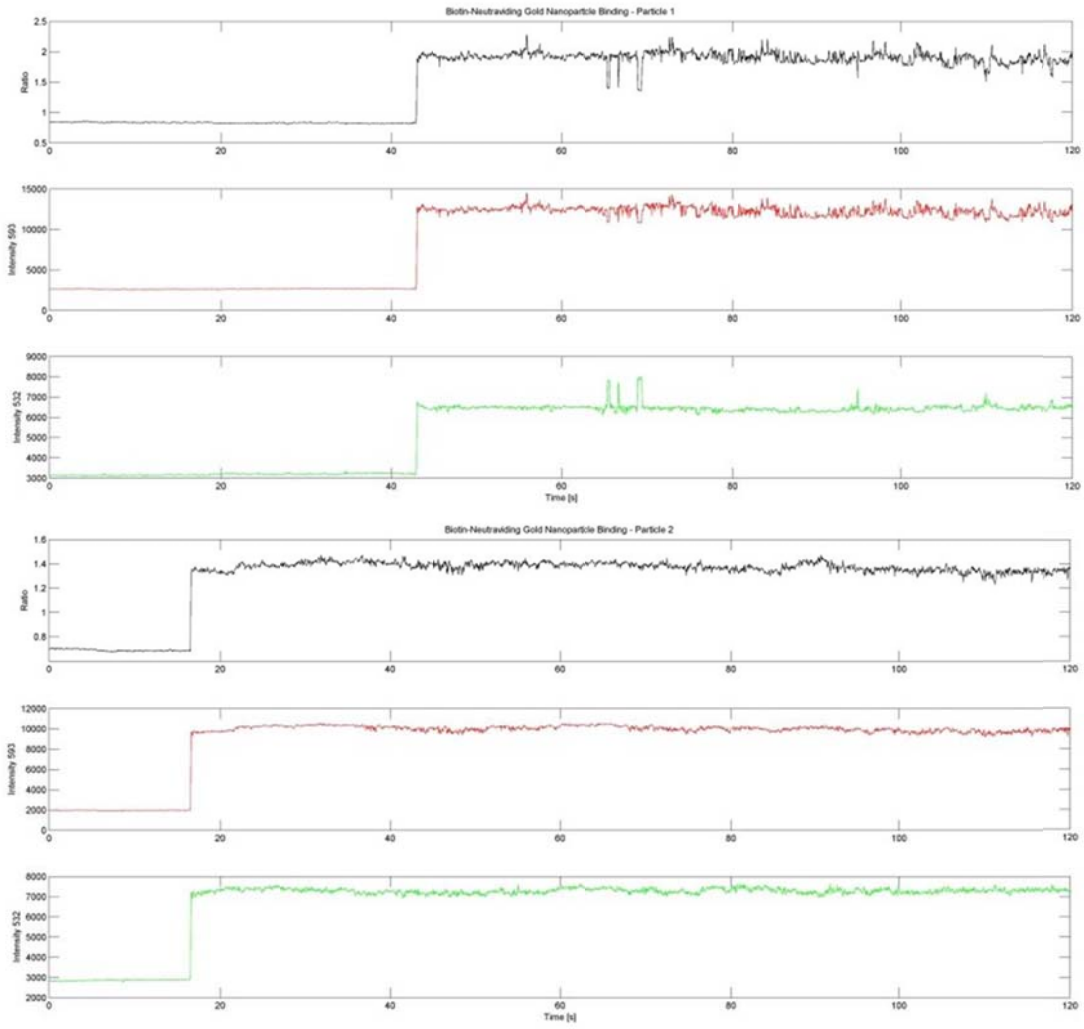


**Figure 19.** Time-Resolved Binding Between Gold Nanoparticles. Time-resolved binding events between a freely diffusing neutravidin gold nanoparticle and a surface-bound biotin gold nanoparticle are recorded with 38 ms time exposure (26 Hz). Binding interactions were observed from many assay chambers. Four representative binding observations are shown. The time records present the ratio change between the two monochromatic wavelengths (black trace) and the individual scattering intensities from each channel (red trace, 593 nm, green trace, 532 nm). The figure is continued on the next page.

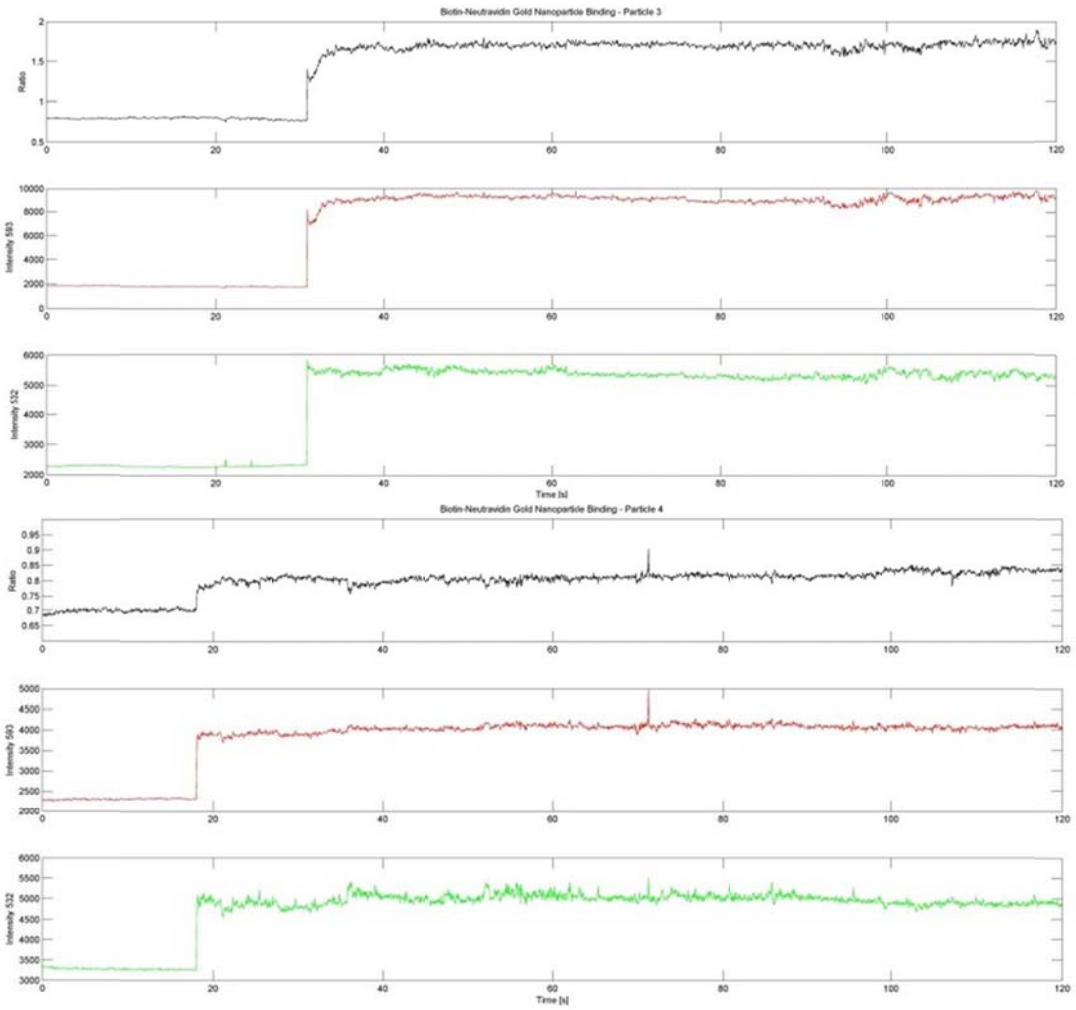


**Figure 19, continued.**

interaction is a plasmonic coupling event. Since the ratio does not change after the initial increase, the event must be a stable binding event. The initial ratio from the surface-bound gold nanoparticles again ranges from 0.55-2.25 with an average ratio of 0.77. When binding events from particles with initial scattering intensities and ratios indicative of single gold nanoparticles are analyzed, the ratio increases to a range from 0.8-2 (Figure 19).

The distribution in the ratio increase, again, is a function of the polarization of the excitation source, and the monodispersity of both the biotin and neutravidin

conjugated gold nanoparticles. As in the initial proof-of-principle binding assay, the polarization state of the monochromatic illumination includes polarization components in both the optical axis of the microscope and in the slide plane. In this polarization case, particle pairs resonate with the polarization component that is aligned with the dimer axis formed upon binding. This causes some particle pairs to be weakly resonant, while others maximally resonant. From these time-resolved binding experiments, the ratiometric analysis technique demonstrates the ability to detect the plasmonic coupling between gold nanoparticles upon binding with, as implemented, time resolution of 38 ms (>25 Hz) with a signal-to-noise ratio better than 100, which is further extendable to faster timescales. As described in Section 2.6, single gold nanoparticles, when excited with the reduced power density used in the time-resolved binding experiments, are detected with a signal-to-noise ratio >20 from images recorded with 5 ms exposure time.

Furthermore, the signal-to-noise ratio in the ratiometric analysis technique may be calculated. The application of gold nanoparticle plasmonic coupling to metrology has been demonstrated in the field through peak wavelength detection [17, 151]. The signal-to-noise ratio in the ratiometric analysis technique is important for future applications of the technique to metrology. The signal-to-noise ratio is defined as in Ueno *et al.* [63]. Specifically, given the average monomer ratio ($\mu_m$), average ratio after binding ($\mu_b$), and their variances ($\sigma^2$), the signal-to-noise is:

$$SNR = \frac{(\mu_b - \mu_m)}{\sqrt{(\sigma_b^2 + \sigma_m^2)}} \quad \text{(Eq. 6)}$$

Based on this definition, the signal-to-noise ratio of the ratiometric analysis technique is 25. We may understand the signal-to-noise ratio for the ratiometric analysis technique as the ability to discriminate sub-states or steps from the noise in the signal. From the work of Wallin *et al*., the number of data points collected per unit time necessary to detect steps is proportional to $SNR^{-2}$ [201]. Moreover, a signal-to-noise ratio of 4 is adequate to detect steps, based on simulation results of varying dwell times and number of steps with ±10% precision [201, 202]. The signal-to-noise ratio of the ratiometric analysis technique should, therefore, be capable of discriminating 6 sub-states or sub-steps within an interaction. These results indicate that the ratiometric analysis technique is better than simply a sensitive binding detection method, but may be used to detect sub-states.

### *4.5 The polarization sensitivity of the biotin-neutravidin gold nanoparticle binding interactions is detected through plasmonic coupling ratiometric analysis*

The polarization state of the illumination source influences the extent to which two gold nanoparticles resonate through plasmonic coupling [82, 91, 97, 98, 136, 203-205]. The alignment of the dimer axis of the two gold nanoparticles with the polarization state of the light maximizes the resonance and enhances scattering. When the polarization is orthogonal to the dimer axis, there is nearly no enhancement in the scattering signal. Typical experimental instrumentation utilizes unpolarized white light illumination directed to the sample through a

darkfield condenser [17, 18, 88, 120-122]. Conventional darkfield illumination introduces the excitation light as a conus of light specified by a specific range of rays of high numerical aperture [19]. The three-dimensional orientation of the gold nanoparticle pairs are only possible to be determined when the dimer axis is within the angular range of these excitation rays [129]. Any gold nanoparticle dimer axes outside of this range are not capable to be specifically aligned to a polarization. Additionally, when polarizers are not used the overall scattering signal is an average over all polarizations, which reduces the scattering response from the particles. The prism-based total internal reflection (TIR) does not have this limitation. In the initial proof-of-principle gold nanoparticle binding experiments, the polarization state of the laser excitation was not specifically defined, but rather included components in both the optical axis and slide plane. It was observed in these binding experiments that the final intensity ratios after binding varied, partially due to the polarization effects. The polarization sensitivity of the gold nanoparticle pair was explored to further understand the capabilities of the developed experimental technique.

The prism-based TIR illumination, as implemented, propagates the excitation wave along the glass slide of the sample. The orientation of the generated evanescent electric field in the assay chamber is perpendicular to the direction of propagation of the light. With the current optical arrangement, the polarization may be specified to a particular orientation through the use of a polarizing beamsplitter. Time-resolved binding experiments were conducted under two orthogonal polarizations—polarization in the slide plane, and

polarization in the optical axis. Polarization aligned with the slide plane enhances the plasmonic coupling scattering response of gold nanoparticle dimer axes aligned with the electric field oriented in the slide plane and orthogonal to the direction of propagation (Figure 20). Conversely, polarization aligned with the optical axis excites gold nanoparticle pairs with dimer axes aligned with the optical axis of the microscope. The polarizing beamsplitter has an extinction ratio greater than 10000:1 for the transmitted beam, ensuring that the polarization state is well defined. The excitation from each of the lasers was modulated to ensure that the power of the transmitted beams through the polarizing beamsplitter were equivalent to the extent that it could be controlled.

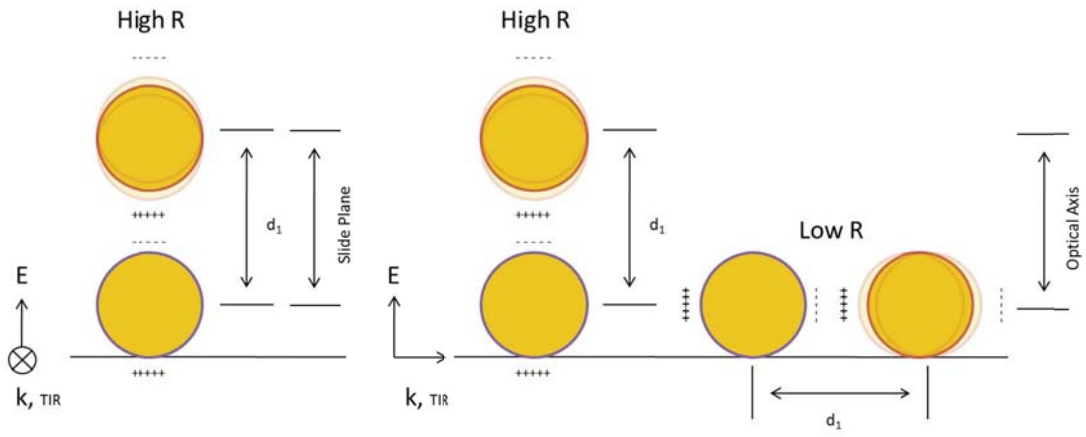


**Figure 20.** Alignment of Gold Nanoparticle Dimer Axis with Polarization. When the polarization of the light is aligned with the dimer axis, the plasmonic coupling between the gold nanoparticles is maximized. Two orthogonal views of the assay (side view facing the direction of propagation and the front view in line with the optical axis of the microscope) demonstrate the orientation of the dimer axis which maximizes the resonance response.

Under the assay conditions specified in Section 4.4, time-resolved polarized binding assays were conducted. It is anticipated that the ratio response

for some gold nanoparticle pairs upon binding will exhibit marginal increases, while other gold nanoparticle pairs will have ratios that greatly increase, depending on the orientation of the dimer axis. Indeed, it is possible to observe gold nanoparticles with scattering intensities indicative of monomers, and with

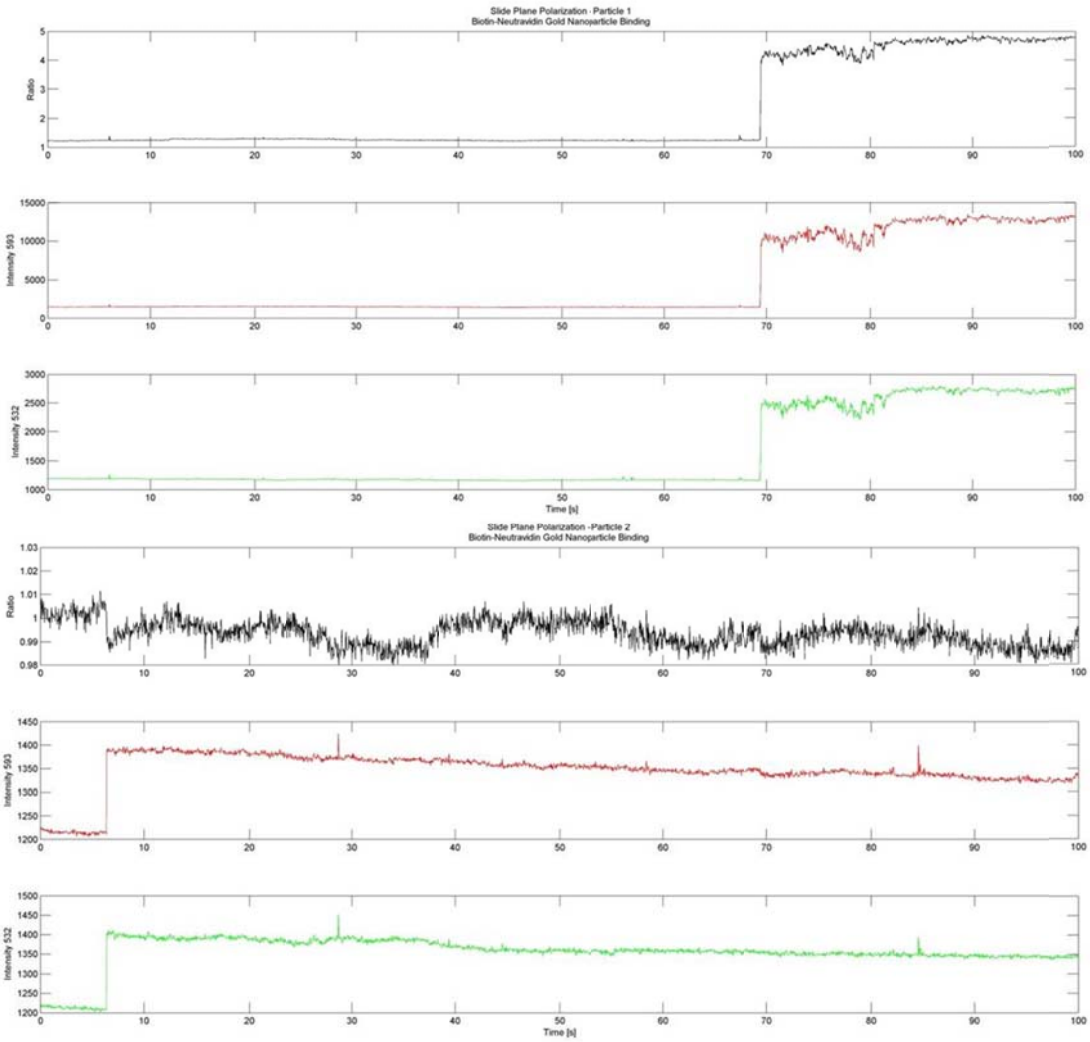


**Figure 21.** Time-Resolved Binding with Polarized Light in the Slide-Plane Orientation. Time-resolved binding events between a freely diffusing neutravidin gold nanoparticle and a surface-bound biotin gold nanoparticle are recorded with 38 ms time exposure (26 Hz). Binding interactions were observed from many assay chambers under excitation conditions of polarized light oriented with the slide plate (see Figure 20). Six representative binding observations are shown. The time records present the ratio change between the two monochromatic wavelengths (black trace) and the individual scattering intensities from each channel (red trace, 593 nm, green trace, 532 nm). The figure is continued on the next pages.

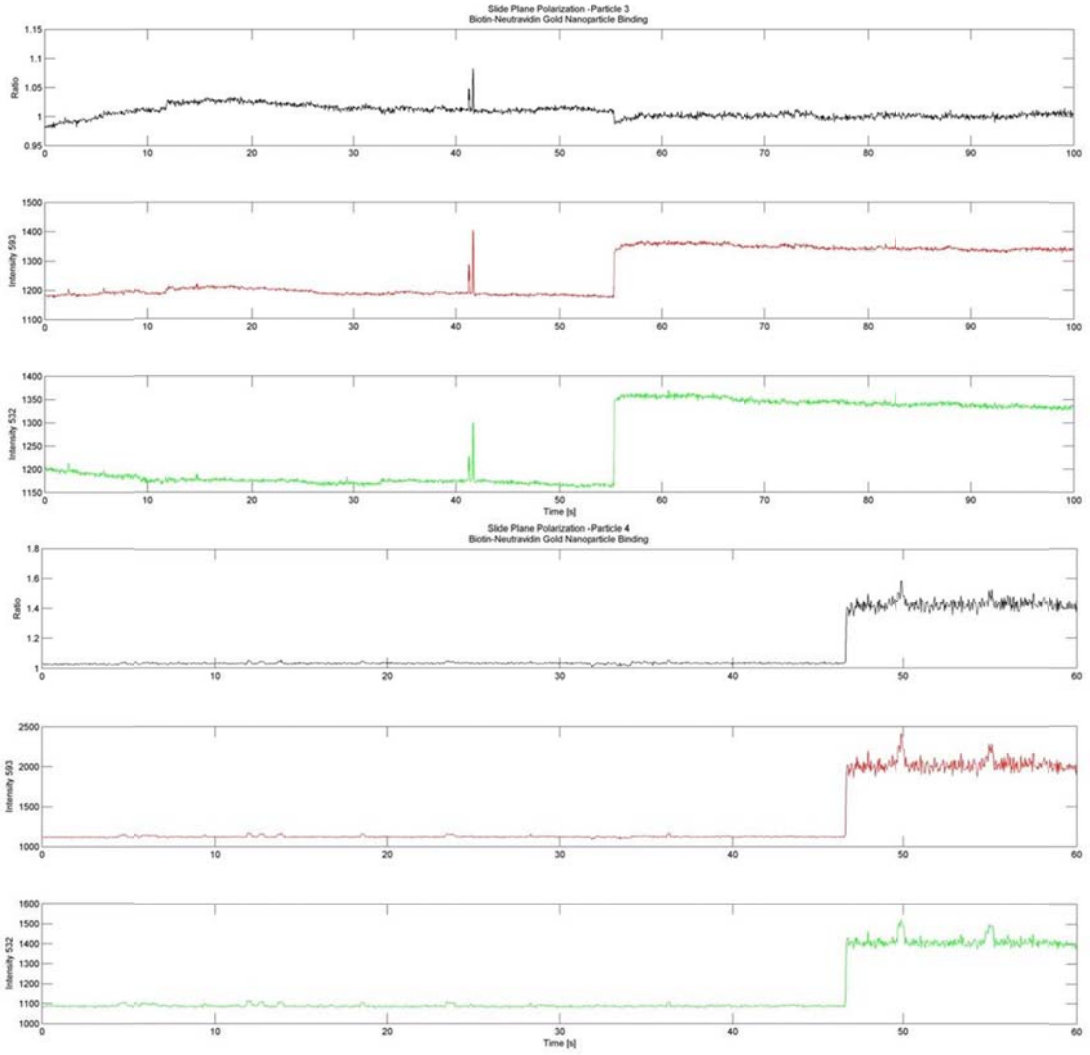


**Figure 21, continued.**

equivalent initial ratios before binding, respond quite differently after binding. Figure 21 presents binding events under polarization with the slide plane. Figure 22 shows events under polarization with the optical axis. The majority of the surface-bound gold nanoparticle ratios initially begin at 1. This was specifically prescribed to ensure that sufficient power from the 593 nm laser was directed into the sample, and approximately equivalent to the 532 nm excitation. Since the

monomeric resonance peak is near 532 nm, the initial ratio for a single monomer is skewed under these conditions. However, when a second gold nanoparticle binds, the 593 nm excitation is sufficient to observe any scattering enhancement through the ratio change. In both polarization orientations, it is possible to observe ratio changes that range from a nominal increase to nearly 5, while observing many with marginal increases to around 1.5.

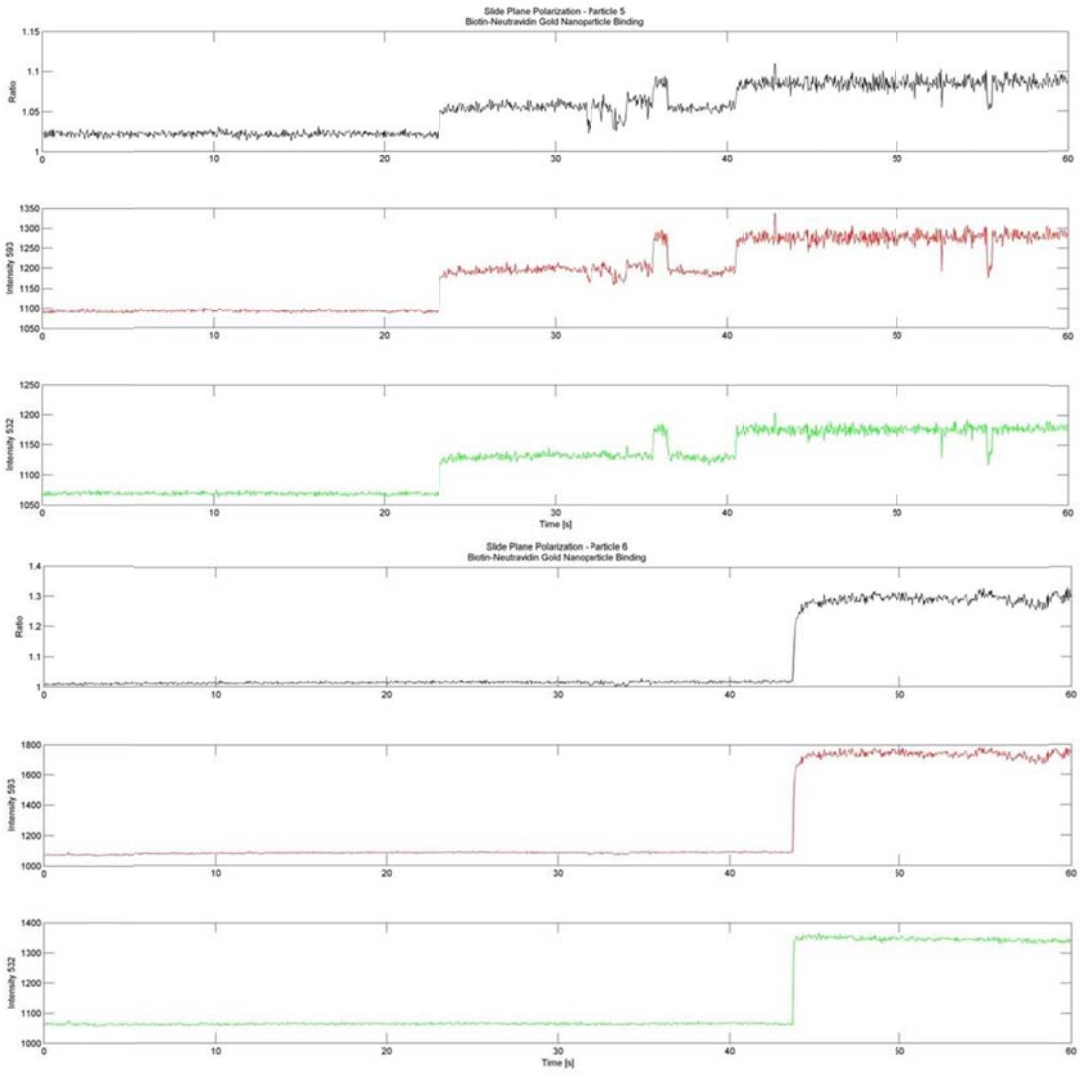


**Figure 21, concluded.**

In several of the polarization binding records, the intensity ratio does not increase upon binding, or slightly drifts. When the orientation of the gold nanoparticle dimer axis is misaligned with the electric field of the incident light, the ratio response is low. Owing to the limited plasmonic coupling, the ratio will not increase, even though the total intensity increases due to the fact that a second scattering gold nanoparticle is within the diffraction-limited region. The drift in the ratio is largely related to orientation effects of the gold nanoparticles. First, the gold nanoparticles may have several bonds between them through many biotin-neutravidin conjugations. When an additional bond between the two gold nanoparticles is formed, a step change in the ratio is expected, because the gold nanoparticles are expected to change orientation. Second, the shape distribution of both the surface-bound biotin gold nanoparticle and the neutravidin gold nanoparticle that binds influences the extent to which the polarization of the incident light affects the plasmonic coupling response. Any anisotropy in the particle shape causes changes in the plasmonic response with respect to the polarization of the incident light. Moreover, when an anisotropic nanoparticle interacts with a second anisotropic nanoparticle, the alignment of the nanoparticles' dimer axis with the incident electric field is sensitive to any diffusion of the tethered nanoparticle. Thus, the ratio may drift in response to these effects.

These results demonstrate that the ratiometric analysis experimental technique is sensitive to the orientation of the gold nanoparticle pairs, and that the polarization of the incident illumination is an important aspect to consider in

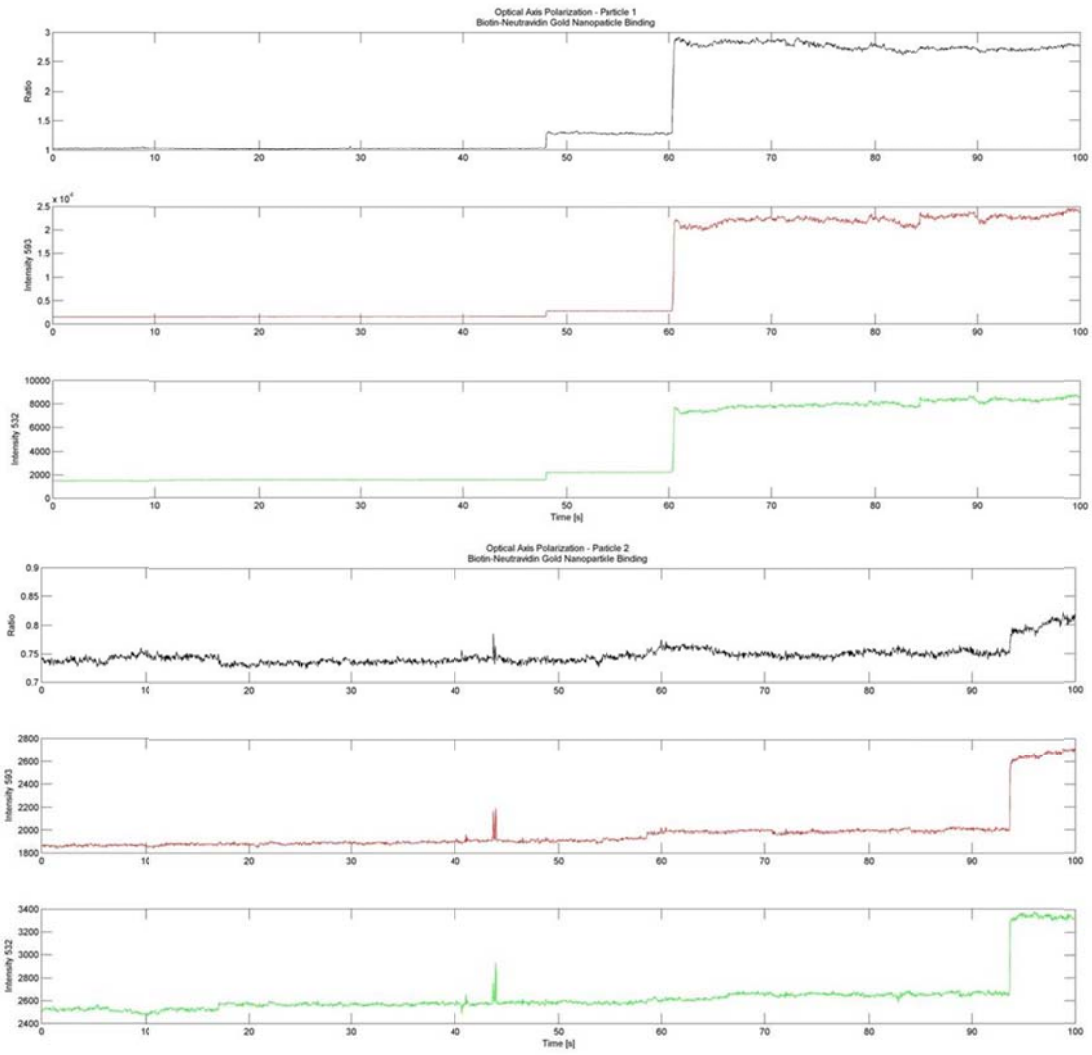


**Figure 22.** Time-Resolved Binding with Polarized Light in the Optical Axis Orientation. Time-resolved binding events between a freely diffusing neutravidin gold nanoparticle and a surface-bound biotin gold nanoparticle are recorded with 38 ms time exposure (26 Hz). Binding interactions were observed from many assay chambers under excitation conditions of polarized light oriented with the optical axis (see Figure 20). Four representative binding observations are shown. The time records present the ratio change between the two monochromatic wavelengths (black trace) and the individual scattering intensities from each channel (red trace, 593 nm, green trace, 532 nm). The figure is continued on the next page.

the experimental assays. The time-resolved binding events provide insight into the polarization effects on the plasmonic coupling between gold nanoparticles upon binding, but the time-resolved binding assays were not arranged in such a manner to analyze individual particle pairs at multiple polarization orientations.

To best establish the polarization sensitivity of the gold nanoparticle dimer pairs, intensity ratios of same gold nanoparticle pairs under different polarization

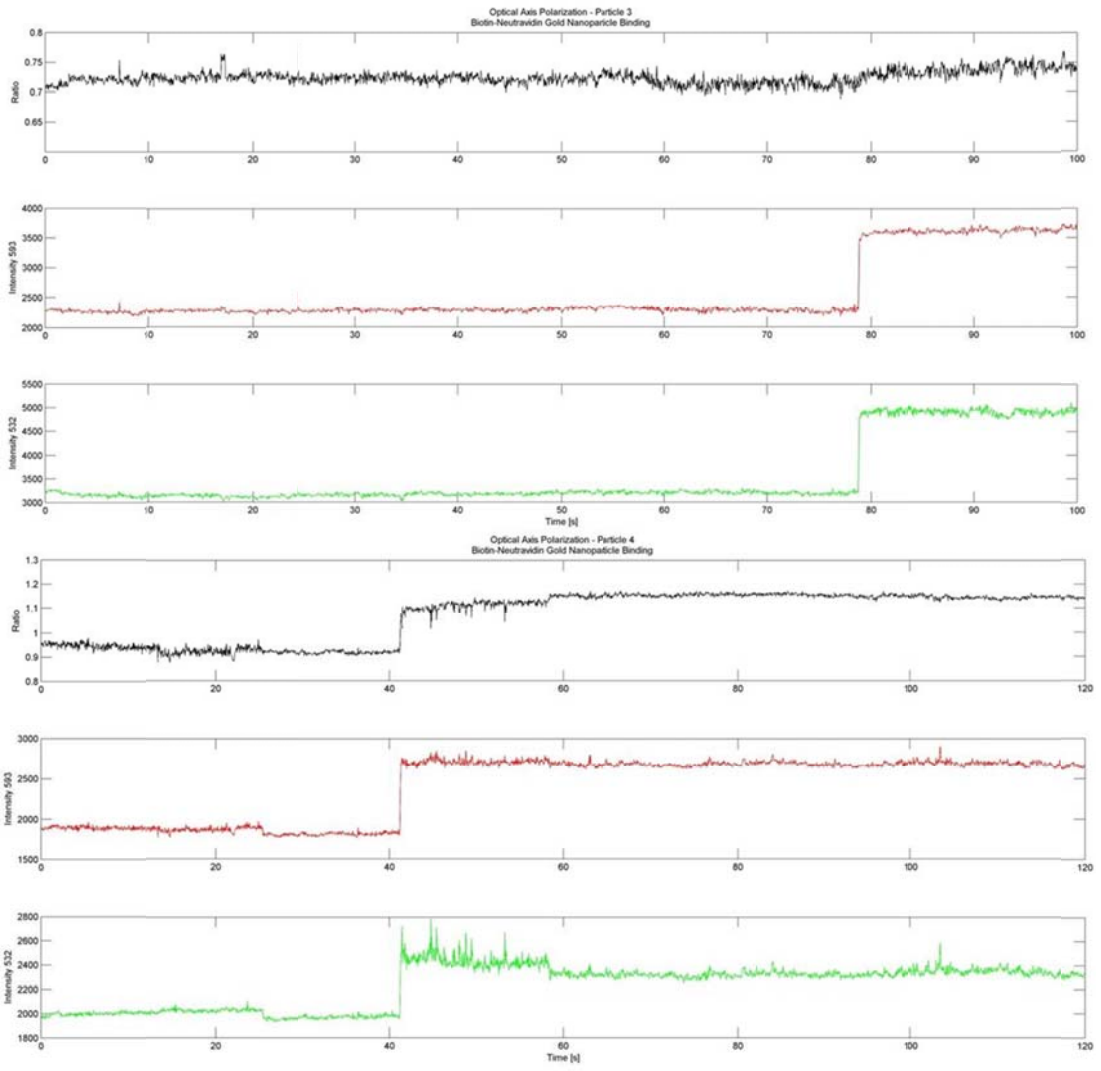


**Figure 22, continued.**

states must be correlated. The easiest method to vary the polarization of the incident excitation with equal intensity at all polarization angles is to polarize the two wavelengths by transmitting the beam through a polarization beamsplitter, and then adjust the polarization with an achromatic zero-order λ/2 waveplate. As the waveplate rotates through 180°, the polarization is likewise rotated through the 180° defined by polarization aligned with the slide plane, the orthogonal polarization aligned with the optical axis, and further rotation to polarization again aligned with the slide plane. Thus, all polarization angles are explored except for insensitivity in the direction of propagation and the azimuthal angle direction (Figure 23).

Unfortunately, the mechanical and optical configuration of the excitation precluded the use of a λ/2 waveplate. As such, implementing a method to correlate the same field of view with equal excitation power at different polarizations was limited. Given the polarization of the two excitation wavelengths prior to transmission through the polarizing beamsplitter, there are two orthogonal

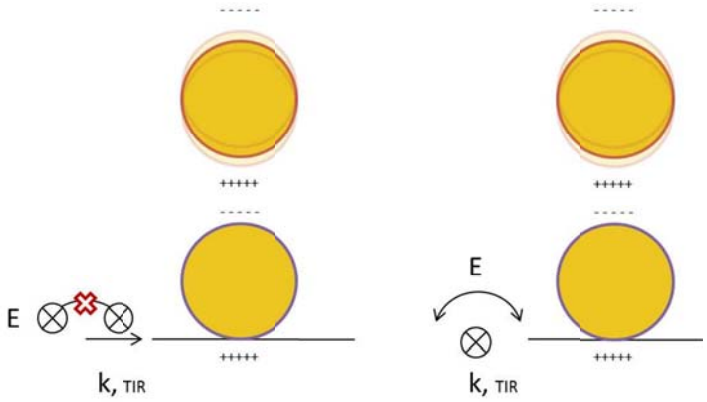


**Figure 23.** Half-Wave Retardation Plate Polarization Configuration. A λ/2 retardation waveplate allows all polarization states in a plane orthogonal to the direction of propagation to be explored, as indicated in the side view facing the direction of propagation **(Right)**. Without a second orthogonal direction of propagation, the polarization states in the azimuthal direction are not detected, as indicated in the front view in line with the optical axis of the microscope **(Left)**.

polarization states where the two wavelengths transmit equal power. These two polarizations are approximately 45° between the slide plane and optical axis polarizations. However, owing to the extinction ratio of the polarizing beamsplitter, the power is different between the +45° (1.7 mW transmitted for each wavelength) and -45° (0.65 mW) orientations. Unlike the time-resolved experiments, in which a single polarization state was explored and the intensity was modulated specifically to ensure equal transmission for that particular polarization, in the correlated images the intensities of the two lasers are not modulated between the polarization states. For reference, images were also collected at the slide plane orientation and the optical axis orientation, albeit under unequal excitation intensities for the individual wavelengths. Under these conditions, the 593 nm laser is only 20% of the intensity of the 532 nm laser when the light is polarized in the slide plane, and it is 3 times the intensity of the 593 nm laser when the light is polarized in the optical axis. These variations in the excitation limit the ability to correlate more than the two equal power polarization states.

Biotin-neutravidin gold nanoparticles binding assays were conducted in similar conditions as those in Section 4.3. Specifically to the polarization interrogation, images of the biotin gold nanoparticles within a particular field of view were collected at four polarization states (slide plane, -45°, optical axis, +45°) before the introduction of the neutravidin gold nanoparticles. The neutravidin gold nanoparticle solution was deposited at the entrance of the assay flow chamber, and the field of view was monitored at one particular polarization

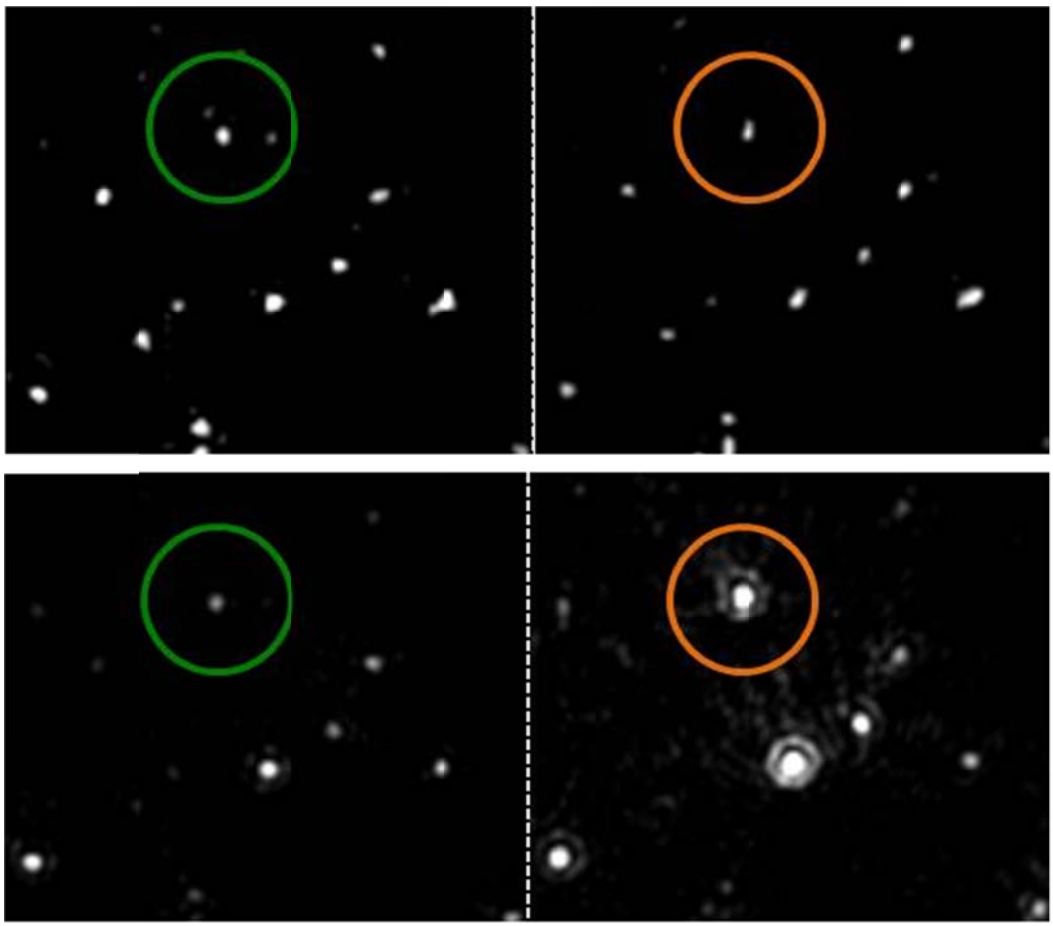

**Figure 24.** Polarization Sensitivity of the Plasmonic Coupling. Images were collected from the same field of view under two orthogonal polarization states, both before and after a 15 minute incubation with neutravidin gold nanoparticles. The figure is continued on the next page. (**Top)** Before incubation with the neutravidin gold nanoparticles, the surface-bound biotin gold nanoparticles are observed under two orthogonal polarization states: -45° (this page), and +45° (next page), as measured from the optical axis. **(Bottom)** After a 15 minute incubation with neutravidin gold nanoparticles, images were again collected from the same field of view under the same polarization states. The polarization sensitivity is clearly demonstrated in the same field of view based on the indicated particle.

for 15 minutes to ensure that binding events occurred. Subsequently, images were recorded of the field of view at each of the four polarization states. Figure 24 presents correlated polarization images before and after binding. The boxed gold nanoparticles dimer pair is representative of the polarization sensitivity of the ratiometric analysis technique.

The ratio for the surface-bound gold nanoparticle before binding at both the -45° and +45° polarization orientation is 0.94. Interestingly, after binding by a

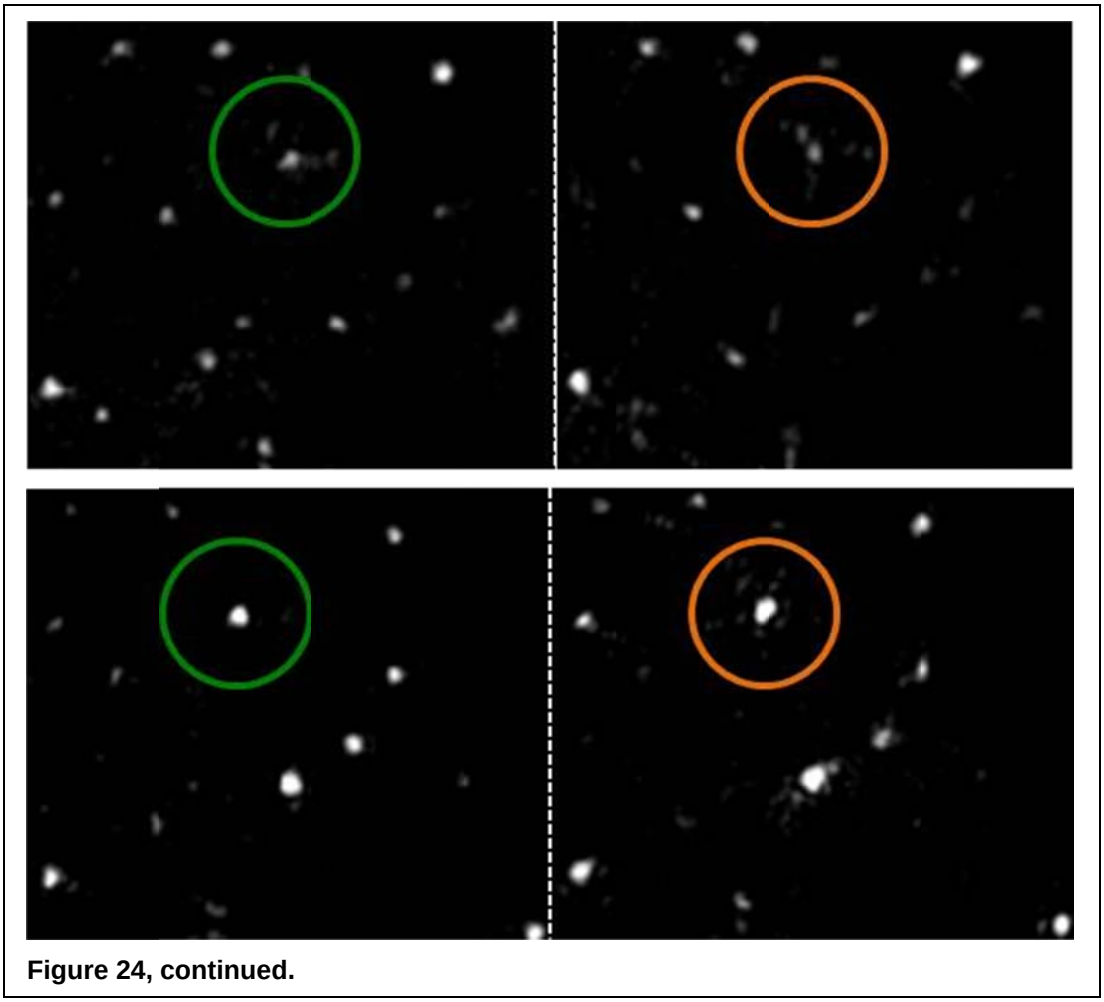

**Figure 24, continued.**

neutravidin gold nanoparticle, the ratio increases to 1.51 in the polarization direction of +45°, but to 4.17 in the -45° polarization direction. It should be noted that the slide plane and optical axis polarization images also show ratio increases, but the surface-bound gold nanoparticle ratio is not the same for either of the polarization states, even including normalization schemes, rendering those results incapable of interpretation. Further interpretation of many correlated gold nanoparticle pairs in several assay flow chambers from both the -45° and +45° polarization orientations exhibit the same trend as in Figure 24. The surface-bound biotin gold nanoparticles prior to incubation with the neutravidin gold

nanoparticle conjugates all have the same ratio at both polarizations ranging from 0.85 to 1.1. Then, after the incubation when binding occurs, the ratio increases, but by varying amounts for each polarization. The ratio increase upon binding varies from 1.12 to 3.45 for the additional particles that were analyzed. The difference in the ratio increase between the two orthogonal polarization orientations ranges between 0.1 and 2.7. It is apparent that, given that the appropriate polarization optics are installed, the ratiometric analysis of the scattering response from plasmonically coupled gold nanoparticles from dual monochromatic excitation is sensitive to the polarization anisotropy of the dimer, and it is possible to define the orientation of the gold nanoparticle dimer pair.

### *4.6 A plasmonic coupling model based on the correlation between the scattering intensities from the two monochromatic wavelengths*

The power of the application of plasmonic coupling between gold nanoparticles to single-molecule biophysics experiments is the potential to detect with high temporal resolution nanometer distances over the range a long distance range (100 nm). Previous plasmonic coupling experiments either conjugated the gold nanoparticles through a DNA spacer *a priori*, or collected slow spectra responses to study the peak resonance wavelength [17, 18, 88, 120-122], both of which prevented analysis of the initial interactions between the gold nanoparticles, and limited the applicability of the technique. When the gold nanoparticles are already tethered together, during the entire interaction the gold nanoparticles are within the near-field in which plasmonic coupling between the

gold nanoparticles already occurs. While it is possible to monitor the peak resonance wavelength to detail the dynamics of the gold nanoparticle interaction, the system temporal resolution limited its implementation. Further information of the interaction between plasmonically coupled gold nanoparticles is extracted through correlation analysis of the two individual scattering intensities.

As evidence for the gold nanoparticle binding interactions (see Figures 19, 21, and 22), and the ratiometric response exploited to detect plasmonic coupling, the change in the 532 nm scattering intensity and the 593 nm scattering intensities are different upon binding by a second gold nanoparticle due to

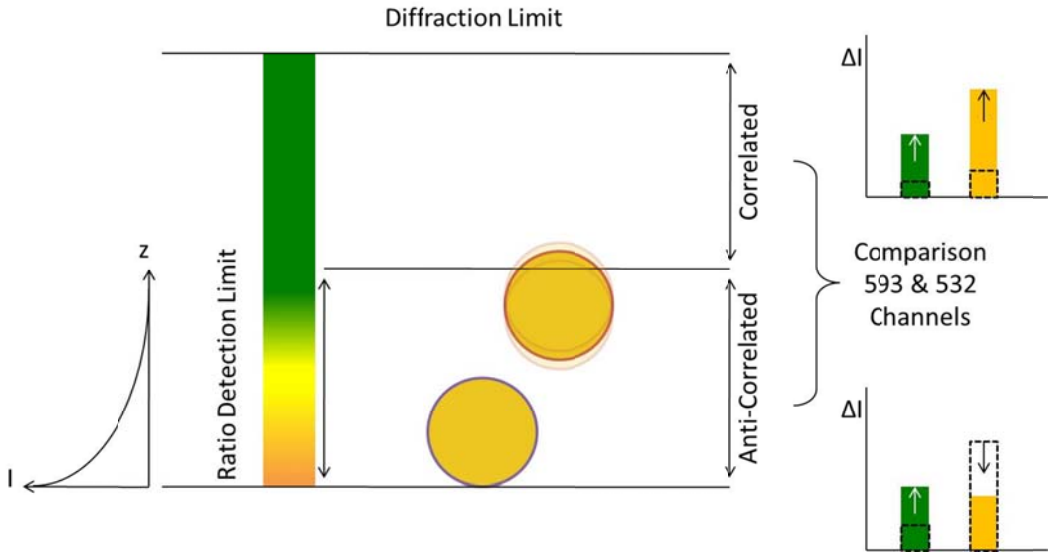


**Figure 25.** Intensity Correlation Model. The correlation between the scattering intensities from the two monochromatic wavelengths is a model to extract further information about the gold nanoparticle interactions. Refer to Section 4.6 text for a detailed description of the model.

plasmonic coupling. By conducting correlation analysis of the scattering intensities, additional details of the distance between the gold nanoparticles and the interaction are found. Figure 25 is a useful guide to the correlation analysis

model described below. Several factors influence the observed scattering response from the diffraction-limited region of interest. First, an object with dimensions below the diffraction resolution limit (approximately 250 nm, or half of the excitation wavelength), such as a gold nanoparticle, when observed in a conventional microscope, is seen as an object of the size of the diffraction limit [19, 20]. That is, a 40 nm spherical gold nanoparticle will have the same diameter when measured as two colocalized 40 nm gold nanoparticles. Second, the total internal reflection darkfield excitation produces an evanescent wave into the solution. The evanescent wave intensity exponentially decays into the solution, penetrating approximately 150 nm, see Section 2.5. The exponential decay in intensity is equivalent for both wavelengths with less than 4% deviation. Finally, the plasmonic coupling between two gold nanoparticles occurs within 2.5 particle diameters [17, 18, 66, 98], which creates a near-field region of 100 nm for the 40 nm gold nanoparticles used in this study. Based on these factors, intensity correlation analysis gives additional insight into the interactions.

Details of the gold nanoparticle interactions are explained through the correlation analysis. When a second scattering particle enters the diffraction-limited region, the total intensity increases, owing to the scattering response from the second particle. When the second particle only diffuses into the diffraction-limited region, but not within the near-field where the gold nanoparticles plasmonically couple, the scattering intensity increases in both the 532 nm and 593 nm channels. In this case, the intensity ratio is unchanged, but the correlation coefficient of the intensities will be positive; the event is positively

correlated. Alternatively, whenever the second particle diffuses farther into the near-field, there is an intensity ratio change as the peak resonance wavelength shifts due to the plasmonic coupling. The intensities are anti-correlated, indicated by a negative correlation coefficient. Anti-correlated events are always near-field, plasmonic coupling effects with which a ratio change must occur. Correlated events occur when particles diffuse within the diffraction-limited, evanescent excitation region. A ratio change will only occur in this case if the particle diffuses into the near-field and the gold nanoparticle pair dimer axis is oriented with the polarization of the excitation.

The time-resolved biotin-neutravidin gold nanoparticle binding interactions (Figures 19, 21, and 22) all display positive correlations of the two intensities with intensity ratio changes after binding by the second gold nanoparticle. However, the binding assay is not well suited in observing additional dynamics between the gold nanoparticles, because after binding the reaction is static. The correlation analysis will be further studied in the preliminary biological applications of the ratiometric plasmonic technique detailed in Section 4.8.

*4.7 Ratiometric predictions based on theoretical analysis*

The ratiometric analysis technique has the potential to be superior to other plasmonic coupling techniques in determining the distance between the gold nanoparticles. While correlation of the distance between the gold nanoparticles, and the intensity ratio response is beyond the scope of the experimental work conducted, some baseline information may be determined through theoretical

analysis. Two theoretical analyses were performed to calibrate the ratio response to distance.

The first analysis is based upon the theoretical and experimental spectra published by Reinhard *et al*. in which two gold nanoparticles were separated by defined distances through a DNA linkage and subsequent spectra were recorded [17]. From their published experimental and theoretical spectra of 42 nm gold monomers and gold nanoparticle dimers of prescribed separations, the normalized intensities at 532 nm and 593 allow the estimation of the intensity ratios for various distances. The expected ratio for 42 nm gold monomers based on the experimental spectra is 0.24, and 0.71 from the theoretical simulations. When the gold nanoparticles are separated by 67 bps of DNA and an additional 8 nm protein layer (29.3 nm total separation, edge-to-edge), the anticipated intensity ratio is 0.93, based on the experimental results. The theoretical simulations at this interparticle separation, though, anticipate a ratio response of 0.83. Finally, when the gold nanoparticles are separated by 20 bps of DNA (14.7 nm total distance) the intensity ratio is calculated to be 1.44, based on the experimentally collected spectrum. Again, the expected ratio from the theoretical simulations differs from the experimental result, predicting 1.06. These reference points indicate that the ratio responses observed in this work are consistent, but detailed correlations are difficult to establish.

Determining the expected ratios by this analysis suffers from several limitations. First, only a single spectrum at each particle separation is presented in the published work, which means that we are blind to the variance in the

expected ratio. Many spectra would need to be analyzed to quantify the variance. Furthermore, the experimental results reported in Figure 2b of Reinhard *et al*., again shed further light into the present fundamental limitation of distance detection through plasmonic coupling: the monodispersity of the gold nanoparticles. Figure 2b reports the measured peak resonance wavelength for the several gold nanoparticle dimer separations. The distributions in the peak resonance wavelength at each separation are rather broad. In fact, the same peak resonance wavelength (~560 nm) is within the distributions for dimers 250 bp apart and 10 bp apart. Finally, the authors note that the theoretical analysis performed through discrete dipole approximation and the T-matrix method, did well in matching the overall shape of the distribution, but not as much in determining the peak wavelength. They ascribed the differences between the experimental and theoretical spectra to the uncertainty in the actual distance between the gold nanoparticles from multiple DNA molecules tethering the gold nanoparticles, the size and shape distributions of the gold nanoparticles, the refractive index change owing to the adsorbed proteins on the gold nanoparticles, and the ionic strength of the buffers in the solution [17]. These enumerated limitations obviously introduce uncertainty in the expected intensity ratios.

The second method to theoretically benchmark the anticipated intensity ratio change upon binding by a second gold nanoparticle is based on the plasmon ruler equation defined by Jain *et al.* [136]. The plasmon ruler equation calculates the fractional plasmon shift (the ratio of the change in the peak

resonance wavelength to the absolute monomeric particle peak resonance wavelength) with respect to the edge-to-edge separation of the particles and the diameter of the nanoparticle, according to the relationship:

$$\frac{\Delta\lambda}{\lambda_0} \approx 0.18e^{\left(\frac{-(s/D)}{0.23}\right)} \quad \text{(Eq. 7)}$$

The equation was derived through discrete dipole simulations. Interestingly, the scaling behavior was found to be universal for particles irrespective of the gold nanoparticle size, shape, composition, and dielectric constant of the medium. The authors note that the above factors only influence the magnitude of the fractional shift. Although, they describe their model as qualitative because of exclusion of electromagnetic retardation and multipolar interactions, which are increasingly important as the edge-to-edge distance decreases to nearly touching particles [136, 206]. Applying the plasmon ruler equation to the diameter of the gold nanoparticles and the interparticle separations in the biotin-neutravidin binding experiments predicts the expected change in the peak resonance wavelength. The change in the peak resonance wavelength was calculated for two interparticle separations (4 nm and 0 nm), three particle diameters (37 nm, 40 nm, and 41 nm), and five monomeric peak resonance wavelengths (527 nm, 530 nm, 532 nm, 536 nm, and 537 nm). The interparticle separations were selected assuming that upon binding there was no separation between the gold nanoparticles, or that the particle separation is the thickness of a biotin-neutravidin monolayer [199, 200]. The three particle diameters were chosen based on the specifications by the supplier for the biotin

(37 nm) and neutravidin (41 nm) gold nanoparticles, and the nominal diameter of 40 nm. Finally, the monomeric peak resonance wavelengths were based on the unconjugated gold nanoparticle resonance wavelength (527 nm), the specifications by the supplier for the biotin (530 nm) and neutravidin (536 nm) gold nanoparticles, a nominal peak resonance wavelength (532 nm), and published experimental results (537 nm) from Rong *et al.* and Reinhard *et al.* [17, 121].

The major challenge of the theoretical analysis is correlating the shift in the peak resonance wavelength to intensity values at both 532 nm and 593 nm. There is a dearth of spectra from gold nanoparticles of a given diameter, separated by a specific amount, and with the appropriate surrounding medium refractive index, theoretical or analytical, to base the intensities at the specific wavelengths. As a first order approximation, the spectral response from a gold nanorod of the approximate dimensions of the two coupling nanoparticles (40 x 80 nm) was considered to benchmark the maximal ratio signal. However, Marhaba *et al.*, show that the spectral response from a gold nanorod is quite different from two gold nanoparticles nearly touching [150]. Two methods were employed to overcome this obstacle and approximate the anticipated ratio change. The first assumes that the overall size and shape of the spectra is unchanged and simply shifts the spectra by the change to determine the new intensity values. However, it is known that the spectra broadens upon plasmonic coupling [17, 18], introducing error into the calculated ratio. In the second method, spectra from 88 nm gold nanoparticle dimers separated by 29.3 nm

reported by Reinhard *et al*. [17] and spectra of 88 nm gold nanodisks separated by 2 nm, 7 nm, and 8 nm gaps published by Jain *et al.* [136] were used to specify the intensities at the individual wavelengths. These spectra were selected since the peak resonance wavelength corresponded with the peak resonance wavelength calculated by the plasmon ruler equation. Table 3 displays the results. Again, this method matches the peak resonances and disregards spectrum shape differences.

| | | Plasmonic Coupling Resonace Wavelength [nm] | | | | | |
|---|---|---|---|---|---|---|---|
| | | 4 nm Separation | | | 0 m, Separation | | |
| Diameter [nm] | | 37 | 40 | 41 | 37 | 40 | 41 |
| Monomer Resonance Wavelength [nm] | 527 | 586.29 | 588.41 | 589.07 | 621.86 | 621.86 | 621.86 |
| | 530 | 589.62 | 591.76 | 592.42 | 625.40 | 625.40 | 625.40 |
| | 532 | 591.85 | 594.00 | 594.66 | 627.76 | 627.76 | 627.76 |
| | 536 | 596.30 | 598.46 | 599.13 | 632.48 | 632.48 | 632.48 |
| | 537 | 597.41 | 599.58 | 600.25 | 633.66 | 633.66 | 633.66 |

**Table 3.** Plasmon Ruler Equation Predictions. The peak resonance wavelength is theoretically determined by the plasmon ruler equation.

The change in the peak resonance wavelength ranges from 59 nm to 63 nm when the gold nanoparticles are separated by 4 nm, varying with the monomeric peak resonance wavelength and the particle diameter. By shifting the spectra, the expected intensity ratio varies from 1.841 to 1.855, respectively. From the published spectra, the ratio ranges from 2 (Jain *et al*.) to 4.45 (Reinhard *et al*.). When there is no separation between the gold nanoparticles, the diameter has no influence on the resulting peak resonance change. Hence, only the monomeric particle peak resonance wavelength was explored. The change in the peak resonance wavelength ranges from 95 nm to 97 nm. The method of shifting

the spectrum is no longer valid for such a change in the peak resonance wavelength, because shifting the initial spectrum by that extent causes spectral data where the plasmon resonance effect no longer dominates the scattering signal. Published spectral data predicts that the intensity ratio will increase, ranging from 2.25-4.33. The analysis, though limited by the lack of suitable scattering intensity data, is consistent with the results that were measured. However, no further insight is possible without more accurate intensity information from theory.

### *4.8 T7 RNA Polymerase binding to DNA: a preliminary single-molecule application of the plasmonic coupling between gold nanoparticles technique*

The penultimate application of the ratiometric analysis of monochromatic scattering intensities to detect the plasmonic coupling of gold nanoparticles is to measure with high spatial resolution (nanometer) interactions between single biomolecules with the versatility of high temporal resolution (sub-millisecond or better) over long time durations (days). As a first preliminary application to single-molecule biophysics, the binding of T7 RNA polymerase to the promoter sequence in DNA was assayed with the developed technique to lay a foundation for future work. T7 RNA polymerase (T7 RNAP) preferentially binds to a specific promoter sequence of DNA during the initial phase of transcription [10, 11, 207]. The experiment observes the binding of a biotin-functionalized T7 RNAP conjugated to a streptavidin gold nanoparticle (for details see Section 3.6) to DNA, which is also conjugated through a biotin-streptavidin bond to a surface-

bound streptavidin gold nanoparticle (see Section 3.5). It is anticipated that the binding of the T7 RNAP will be determined by an increase in the scattering intensity ratio due to the plasmonic coupling between the two gold nanoparticles, as outlined in Figure 26.

Following the sequential build-up assay conditions outlined in Reinhard *et al*., British Biocell streptavidin gold nanoparticles were non-specifically adsorbed onto the glass surface of the assay chamber at a concentration of 6 pM [17]. A biotinylated dsDNA 75 bp (25.5 nm) in length was incubated in the chamber to

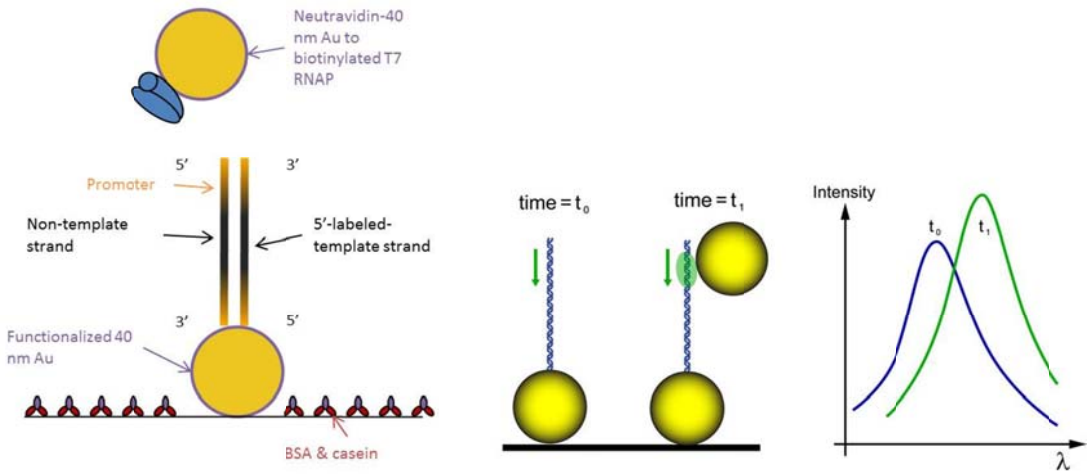


**Figure 26.** Experimental Schematic of T7 RNA Polymerase Binding Assay. Upon binding of the polymerase to the DNA promoter sequence, the peak resonance wavelength red-shifts due to the plasmonic coupling between the two gold nanoparticles. The plasmonic coupling is determined through the ratiometric analysis of the dual monochromatic excitation wavelengths.

bind to the streptavidin gold nanoparticle at a concentration of 40 nM. As described in Section 3.3, the expected surface coverage of streptavidin is 200 per gold particle. The stoichiometric ratio of the DNA to the surface-bound gold nanoparticles is 667, although there are potentially 3 DNA molecules available to bind each streptavidin. Concurrently, biotinylated T7 RNAP at an approximate

final concentration of 50 nM incubates with 1.5 nM of streptavidin gold nanoparticles. Based on this stoichiometry, there are 38 polymerases per gold nanoparticle, which again are conjugated with 200 streptavidin molecules. After an incubation period sufficient to allow the DNA to bind, the gold-conjugated T7 RNAP was introduced into the assay chamber. The experiment was conducted in the absence of free nucleotides. In the absence of free nucleotides, the polymerase may bind to the promoter binding site, but cannot transcribe the DNA sequence [208, 209]. Based on the previous binding experiments between biotin and neutravidin gold nanoparticles, the ratiometric analysis technique should detect the binding of the polymerase to the DNA.

Preliminary time-resolved binding results between the polymerase and the DNA are presented in Figure 27 for two binding events on different DNA gold nanoparticle conjugates. As an internal control, a particle in which no interactions occur in the assay chamber is also monitored throughout the duration of the interaction. The binding results are clearly different than those observed between the static binding of a neutravidin functionalized gold nanoparticle to the surface-bound biotin gold nanoparticle (compare Figure 27 to Figures 19, 21, and 22). Further histograms reveal that two-states are clearly defined in one of the binding events (Figure 27, top) while three states are defined in the other (Figure 27 bottom). The interpretation of these results is difficult for several reasons.

First, the experiments were conducted in the case where the polarization state of the laser excitation was not controlled. The idealized method to conduct

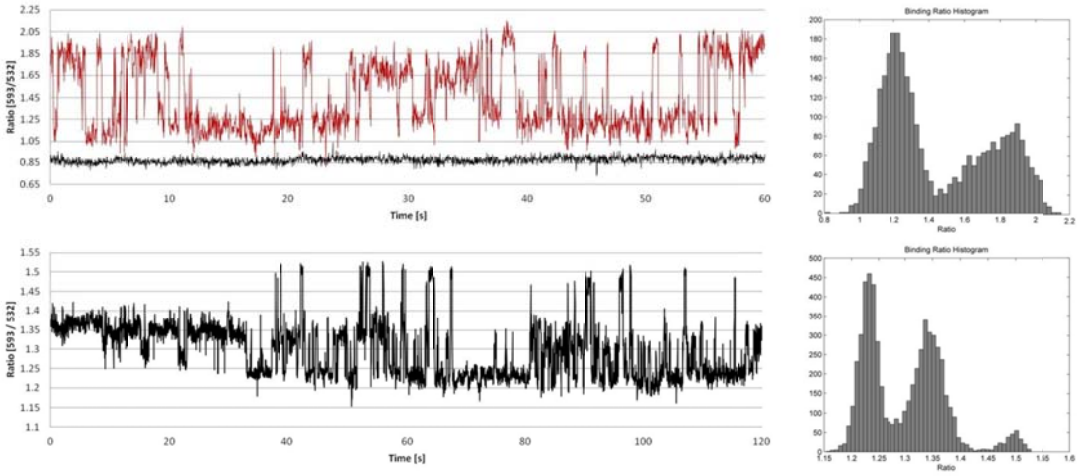


**Figure 27.** T7 RNA Polymerase Binding Detected by Plasmonic Coupling. Two separate binding events of a T7 RNA polymerase to DNA are detected through plasmonic coupling. A gold nanoparticle in which no interactions are occurring within the same field of view serves as an internal control (black trace in top record). Histograms of the ratios reveal that there are two and three states defined in the binding results.

the experiments would be to stall the polymerase at the promoter site, and then determine the polarization state where the intensity is maximized (see Section 5.2). However, given the mechanical and optical constraints of the experimental apparatus, this was not possible. Additionally, as a preliminary implementation, the number of DNAs per gold nanoparticle and the number of polymerases per gold nanoparticle were intentionally maximized so that detection of binding is kinetically possible to observe on the order minute timescale. These stoichiometries complicate the interpretation of the results. The orientation of the DNA to the gold nanoparticle is unknown, and as there are many DNAs per gold nanoparticle, there are many different orientations with which the polymerase may bind. Therefore, the gold nanoparticle dimer axis alignment with the

polarization of the laser illumination is undetermined. Furthermore, the high stoichiometry also allows multiple linkages between the gold nanoparticles to occur through several binding interactions of individual polymerases and DNA molecules. The potential ability to tether the two gold nanoparticles by many polymerase-DNA bound complexes influences the intensity ratio response in two ways: (1) the orientation of the gold nanoparticle dimer axis may change, and (2) the distance between the gold nanoparticles may change.

For additional interpretation of the T7 RNAP binding experiments, the time-resolved binding records were analyzed, based on the method outlined in

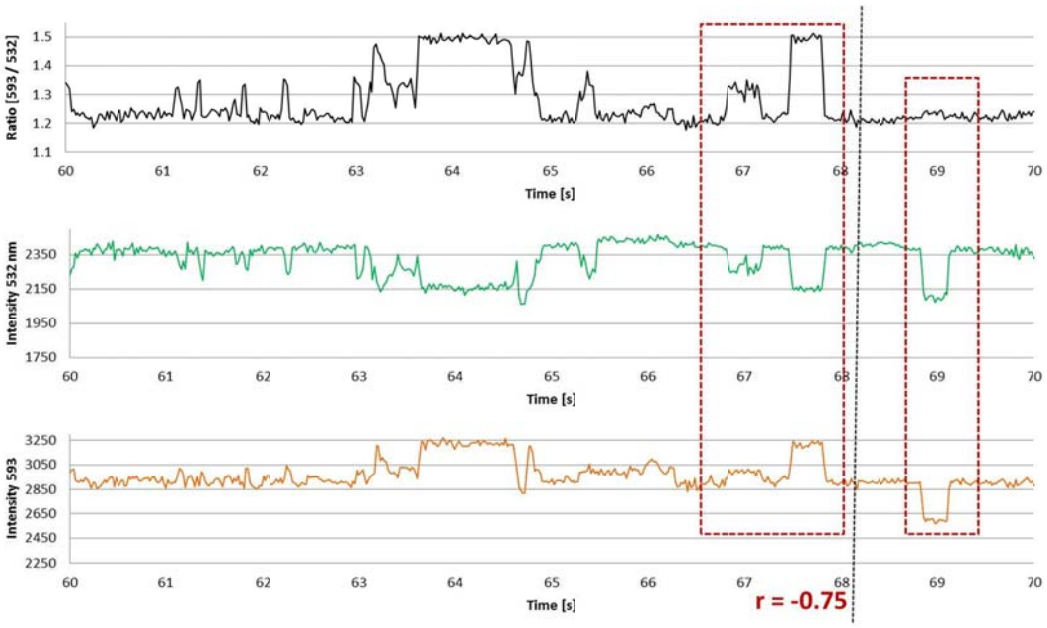


**Figure 28.** Scattering Intensity Correlation Analysis of T7 RNA Polymerase Binding. Scattering intensity correlation analysis for the T7 RNA polymerase binding record detailed in Figure 27, bottom reveal both correlated (second red boxed region) and anti-correlated (first red boxed region) intensity events. Correlation analysis determines the record is highly anti-correlated from the time range of 60-68 seconds (r = -0.75).

Section 4.6. Figure 28 details the individual scattering channel intensities for a section of the binding record in Figure 27, bottom. From the individual channel

intensities, it is apparent that the ratio change is a plasmonic interaction between two gold nanoparticles, because as we observe in the first boxed region from 66.5-68 s, as the 532 nm scattering decreases, the 593 nm scattering increases. Additionally, the correlation coefficient for the two scattering intensities is highly anti-correlated in the range from 60-68 seconds with a value of -0.75. The first boxed region in the record highlights two anti-correlated events in which the intensity ratio changes by different amounts. This may be interpreted as either an orientational change of the polymerase-functionalized gold nanoparticle with respect to the surface-bound gold nanoparticle, causing an enhancement in the plasmonic coupling, or a decrease in the distance between the gold nanoparticles due to multiple tethering. Interestingly, in the second boxed region the intensity ratio is unchanged, though the correlation coefficient of the individual channel intensities reveals a highly correlated drop in intensity. This is interpreted as an unbinding event by the polymerase followed by a rebinding.

The preliminary biological application of the time-resolved ratiometric detection technique was applied to observe with high temporal resolution the binding of a T7 RNA polymerase to a promoter recognition sequence in a DNA molecule. It is clear that the binding results are highly dynamic, as opposed to the biotin-neutravidin binding events assayed. While the details of the interaction are difficult to resolve through this preliminary experiment, fundamental experimental efforts have been established to expand the application of the plasmonic coupling between gold nanoparticles to single-molecule biophysics. The gold nanoparticles are independently labeled, and allowed to dynamically

interact without the requirement of tethering the gold nanoparticles before analysis, as conducted in previous experiments. Additionally, the ratiometric analysis and the scattering intensity correlation analysis lay a pathway to observe high temporal resolution single-molecule binding events. Through further development and calibration, the technique holds the potential for high spatial resolution metrology.

### *4.9 Discussion and conclusions*

The aim of this work is to clearly challenge the ratiometric analysis of the scattering signal from coupled gold nanoparticles experimental technique and highlight its benefits. As a proof-of-principle demonstration, the binding between two gold nanoparticles through a biotin-neutravidin interaction is observed, determining the maximum expected signal change. Through this experimental assay, significant advancements to the plasmonic field are established. Here, the first detection of the plasmonic coupling between two gold nanoparticles with better than 25 Hz time resolution is presented. At this time resolution, the signal-to-noise ratio of a single gold nanoparticle above background is more than 100. The mean intensity of the monomeric gold nanoparticle scattering intensity ratio was found to be consistent with theoretical simulations. Moreover, the intensity ratio after binding by a second gold nanoparticle more than doubles owing to the shift in the peak resonance frequency from near-field effects. The signal-to-noise ratio for the ratiometric analysis technique is 25, which according to Wallin *et al.*, allows for up to 6 sub-states to be distinguished [201]. This indicates that the

ratiometric analysis technique has the potential to be better than a binding detection method, and may be applied for distance measurements.

While the ratiometric analysis technique improves upon the previous applications of gold nanoparticle plasmonic coupling, limitations still exist. The experimental results are influenced by the size and shape distributions of the gold nanoparticles and the refractive index of the surrounding solution. All of these factors influence the exact peak resonance wavelength for each gold nanoparticle, which ultimately is reflected in the scattering intensity ratio and the range in the measured values.

In addition, the alignment of the gold nanoparticle pair with the polarization of the excitation influences the resulting ratio response. The impact of the polarization state of the incident excitation on the intensity ratio was explored. When the gold nanoparticle dimer axis aligns with the polarization, the intensity ratio is maximized. Correlated images of identical particle pairs before and after two gold nanoparticles bind reveal that the difference in the ratio response ranges from 0.1 to 2.7 in orthogonal polarization states. The specific orientation of a gold nanoparticle pair may be determined by including polarization optics, providing further details of the biomolecular interactions of interest.

Finally, first applications of the ratiometric analysis technique to general biomolecular binding experiments were performed to demonstrate extent to which the technique may be used in single-molecule biophysics assays. Binding experiments were performed in which a RNA polymerase labeled to a gold nanoparticle binds to a specific DNA promoter sequence engineering into a DNA

molecule bound to another gold nanoparticle. When a freely diffusing polymerase binds to the DNA sequence, the two gold nanoparticles interact, which provides the ratio change signal that indicates that binding has occurred. This preliminary experiment provides initial insights into broad application of the technique to single-molecule biophysics.

# CHAPTER 5

## Summary and Conclusions

The broad aim of this work was to establish a single-molecule technique with high spatial and temporal resolution over a wide range in both the distances capable of measurement and duration of observation for application to molecular biophysics. The plasmonic coupling between gold nanoparticles has been shown previously to be capable of high spatial resolution up to 1 nm, over a greater distance range as compared to alternate techniques, up to approximately 2.5 nanoparticle diameters [17, 18]. Moreover, the extreme photostability of the gold nanoparticle probes makes possible long time duration experiments lasting up to days. These positive aspects of the plasmonic coupling between gold nanoparticles make the system ideal for application to single-molecule biophysics. From the preliminary work towards applying the plasmonic coupling between gold nanoparticles to single-molecule biophysics, the present limitations are in the temporal resolution, the stability of the gold nanoparticles in biologically relevant buffers, and wide applicability to many biological systems [17, 18, 120-122, 151]. In order to advance the preliminary methods for general application to molecular biophysics, I sought to: (1) implement a novel experimental approach based on the plasmonic coupling between gold nanoparticles capable of high

spatial and temporal resolution for single-molecule experiments, (2) create methods to better stabilize and conjugate the gold nanoparticle probes to biomolecules, and (3) challenge these techniques in order to detect the plasmonic coupling between gold nanoparticles upon binding with high temporal resolution.

Generally to accomplish the first goal, a ratiometric analysis scheme from the scattering of two monochromatic wavelengths by gold nanoparticles to detect the plasmonic coupling response was integrated with a unique darkfield illumination approach to increase the temporal resolution. The power density at the sample from conventional darkfield microscopy is low. As such, a ratiometric analysis of the scattering response from two monochromatic sources was designed to maximize the ratio response upon plasmonic coupling between gold nanoparticles. In fact, it was determined that the ratiometric analysis technique is more sensitive than the conventional method of peak plasmon resonance wavelength detection. Two laser sources from different wavelengths (593 nm and 532 nm) were selected to increase the power density, which increases the scattering signal from the gold nanoparticles. To integrate the laser-based excitation, a novel prism-based total internal reflection darkfield microscopy technique was designed and developed. This method is capable of achieving a signal-to-noise ratio from a single gold nanoparticle better than 100 with 38 ms time resolution, and under reduced power densities, better than 20 with 5 ms time resolution. The time resolution is not limited by the scattering response from the gold nanoparticles, but rather in the choice of the CCD array detector. The

instrumentation development further extends the ratiometric analysis technique by simultaneously collecting the scattering signals from each wavelength on spatially segregated regions on the CCD array. Previous applications of a ratiometric analysis have switched between wavelengths and sequentially acquire the scattering signals to the detriment of the temporal resolution and the actual ratio response from the gold nanoparticle system [88, 121, 122]. The developed experimental system was designed in such a way that it is easily possible to integrate additional or alternate components to further extend the technique to even faster time resolutions, or to measure different wavelengths to allow the ratiometric analysis technique to be applied to a variety of systems involving gold nanoparticles.

It was sought to broadly apply the plasmonic coupling between gold nanoparticles to many biological systems. To date, the only applications of plasmonic coupling of metallic nanoparticles have required tethering between two nanoparticles through DNA molecules [17, 18, 88, 120-122, 151]. Expanding the range of the plasmonic coupling technique requires that the gold nanoparticles are monodisperse, stable, and capable of being conjugated to a variety of biological molecules. One of the fundamental limitations of gold nanoparticles is the size and shape distributions, both of which influence the plasmonic response from the gold nanoparticles. It was found that commercial supplies of gold nanoparticles had superior size and shape distributions over in-house synthesis techniques. While efforts are underway to synthesize nanoparticles with tighter size and shape distributions, these approaches may not be easily amenable to

the majority of single-molecule researchers. The availability of commercial sources with suitable distributions allows access of gold nanoparticles to the research community. The commercial gold nanoparticles, though, are normally supplied unstabilized. Unstabilized gold nanoparticles aggregate when exposed to even moderate ionic strength solutions [145, 146, 152]. However, biological buffer solutions are typically high in ionic strength, which required that stabilization and passivation schemes be created so that the gold nanoparticles are stable. A sequential ligand exchange method has been applied previously, but the scheme requires several overnight incubations and processing of the gold nanoparticles, which are challenging to conduct [120, 151]. Here, passivation through the use of the passivating proteins casein and BSA was used to stabilize the gold nanoparticles. After a short incubation with the proteins (15 minutes), which nonspecifically adsorb to the surface of the gold nanoparticles, the nanoparticles remain diffusive in ionic strength solutions comparable to standard biological buffers—150 mM NaCl and 25 mM $MgCl_2$. With the ease in the stabilization scheme for the gold nanoparticles determined, the conjugation of gold nanoparticles was pursued.

Gold nanoparticles have several advantageous conjugation methods to bind to biomolecules. DNA is the most common biomolecule conjugated to gold nanoparticles, given its applicability not only to molecular biology research, but also to a vast range of nanotechnology research directions [50, 90, 120, 210]. However, few single-molecule applications have conjugated gold nanoparticles to biomolecules, mostly motor proteins such as kinesin, myosin, and the rotary

motor $F_1$ATPase [56, 58, 63]. Two common conjugation methods to molecular biology can be applied to gold nanoparticles: (1) covalent conjugation through a thiol bond, and (2) conjugation through the strong biotin-streptavidin bond. Covalent conjugation through gold-thiol bonding creates a very strong bond. Furthermore, DNA may be synthesized with a single or multiple thiol group(s) at its ends and obtained through commercial sources. However, it was determined that the conditions for conjugation through gold-thiol bonding are extremely sensitive to temperature, incubation time, DNA sequence, pH, and ionic strength, and require several overnight incubations, and difficult sample handling. These challenges make the utility of the gold-thiol bond low. Conjugation through biotin-streptavidin, while not as strong as the covalent bond, is able to mediate the binding of proteins to gold nanoparticles. The biotin-streptavidin conjugation scheme has been used with both DNA and motor proteins [17, 18, 58, 63]. Biotinylated proteins and DNA were conjugated to neutravidin or streptavidin gold nanoparticles both with ease and short incubation times. The advantages of this conjugation scheme, though, are only widely applicable to many biological systems, so long as the biomolecules of interest are biotinylated. Towards this goal, I applied an *in vivo* biotinylation expression and purification method to purify with high yield a biotinylated polymerase for use in preliminary experiments using the signal from the plasmonic coupling between two gold nanoparticles to detect the binding of the gold nanoparticle conjugated polymerase to DNA labeled gold nanoparticle. Through these methodological developments, the range with which the plasmonic coupling between gold nanoparticles has been extended beyond

the previous assays of DNA mechanics and molecular rulers to a general biomolecular system. With the advancements that have been made, the entire experimental technique must be verified.

Experimental assays were created to challenge the ratiometric analysis scheme for detecting the plasmonic coupling between gold nanoparticles method. As a proof-of-principle experiment, the binding of gold nanoparticles was observed. The binding experiment characterizes the maximal increase in the ratio response from the plasmonic coupling between two gold nanoparticles, an important quantity to specify for future assays in which subtle changes in the ratio may be used for distance detection. Two gold nanoparticle solutions were functionalized with either biotin or neutravidin. The biotin gold nanoparticles were bound to the assay chamber surface, and freely diffusing neutravidin gold nanoparticles were introduced into the chamber. The binding was observed through the dual wavelength prism-based total internal reflection excitation, and dual imaging detection system with 38 ms time resolution, the fastest resolution used to date to detect the plasmonic coupling between gold nanoparticles. Control experiments were conducted such that the binding of the gold nanoparticles was determined to be a specific interaction between the biotin and neutravidin. First, the freely diffusing gold nanoparticles were replaced with biotin gold nanoparticles. Second, the neutravidin gold nanoparticles were incubated with free biotin prior to introduction into the assay chamber. In both cases, there were no binding events that were observed, even after incubation times of the freely diffusing gold nanoparticles twice as long as the time to saturate the

binding reaction in the positive assay. Therefore, the binding must be specific. Provided the anticipated outcomes of the control experiments, the specific binding results may further be analyzed with the ratiometric technique.

The intensity ratios from the scattering response of the gold nanoparticles were calculated for the bound biotin gold nanoparticle monomers before incubation with the neutravidin gold nanoparticles. Subsequently, after binding by the neutravidin gold nanoparticles the ratios were again measured. The intensity ratios are defined as the scattering signal from the 593 nm wavelength to the scattering signal from the 532 nm wavelength. The mean intensity ratio of the surface-bound biotin gold nanoparticle monomers prior to binding was 0.8300 ± 0.1556. The mean ratio is consistent with the ratio calculated from theoretical simulation spectra, 0.7102, determined by Reinhard *et al.*, in a system that parallels the experiments conducted here [17]. However, it should be noted that the spectra from the experimental results collected by Reinhard *et al.* predicted a ratio of 0.2369 [17]. Moreover, in subsequent ratiometric analysis Rong *et al*. experimentally measure a ratio of 0.45 [121]. The ratio collected by Rong *et al.* is 580 nm to 530 nm with bandpasses of unpolarized white light excitation, similar to the ratio measurements in this work. The differences between the theoretical and experimental results are due to many factors. The most influential factors are the nanoparticle size and shape distributions, the refractive index of the solution around the nanoparticles, and the methods used to detect and collect the scattered light from the gold nanoparticles. In the theoretical experiments, the particles are assumed to be perfectly spherical and of an exact particle diameter.

But, as has been established in the literature, the nanoparticles are not perfectly spherical and the particle diameter varies, all of which influence the peak plasmon resonance wavelength, and therefore the ratio response [17, 18, 75, 83, 88, 137]. Furthermore, it is difficult to specifically determine the refractive index of the environment around the gold nanoparticles, as the number and type of adsorbed proteins, polymeric shells, and the biological buffers all will have various contributions to the effective refractive index, and may be different for each individual gold nanoparticle. The theoretical simulations must estimate the refractive index, and as such may be inconsistent with the real environment surrounding each specific gold nanoparticle observed. Finally, the excitation and detection will have great influence on the spectral results from the experiments. The simulations specify that the excitation is polarized with the dimer axis of the gold nanoparticle pairs, however, darkfield illumination with unpolarized light was used to collect the spectra of monomers. The darkfield illumination introduces a conus of excitation light at extreme incident angles, and collects the scattering signal from a lower numerical aperture. Under darkfield illumination only gold nanoparticle pairs with orientations aligned with the specific polar angles defined by the darkfield condenser will display the plasmonic coupling response, and so the spectra collected are influenced by the excitation technique [129]. Owing to the differences in the experimental and theoretical arrangements, the spectral responses may not truly reflect the actual results. Despite some technical differences, the theoretical simulations more closely mimic the prism-based total internal reflection with monochromatic excitation, and the ratio results have close

agreement. The monomeric gold nanoparticle ratios are consistent with theoretical results, which lead to interpreting the ratio response upon binding by the second gold nanoparticle.

The binding between the biotin gold nanoparticles and neutravidin gold nanoparticles was detected through the plasmonic coupling response. The resulting intensity ratio is expected to increase, since the closer the gold nanoparticles are the more they plasmonically couple, and the peak resonance wavelength shifts to longer wavelengths. The gold nanoparticle ratio ranges from monomers to an interparticle separation of approximately 4 nm, the distance of the biotin-neutravidin bond, and the expected minimum separation in typical biomolecular assays. The scattering intensity ratio was determined to increase upon binding. Interestingly, the ratio response ranges from 1.1 to 3 after binding. Based on the time-resolved binding records, the maximal signal change, and the signal-to-noise ratio in the ratiometric technique are calculated. The signal-to-noise ratio in the ratiometric technique establishes the ability discriminate sub-states within a given interaction, which will be necessary for future implementations to measure distances. The signal-to-noise ratio in the ratiometric technique is 25, which based on the work by Wallin *et al.*, makes possible the distinction of 6 sub-states [201]. Therefore, this technique has the potential to be more than just a binding detection method.

The range in the ratio response may have several reasons. First, the same influences to the plasmonic response for the monomers also impact the plasmonic coupling between the two gold nanoparticles. The size and shape

distribution of the second gold nanoparticle that binds are not controlled, which means that any anisotropy in the second particle will greatly affect the plasmonic response. Additionally, the alignment of the dimer axis with the polarization state of the incident illumination affects the extent to which the gold nanoparticles plasmonically couple. There is limited independent research to benchmark the ratiometric response from the plasmonic coupling between the two gold nanoparticles, especially under similar experimental conditions and particle separations. Reinhard *et al.* recorded experimental spectra and also simulated the expected spectral response from two gold nanoparticles tethered by 20 base pairs of DNA, which under their experimental conditions, the interparticle separation is expected to approximately be 15 nm. From their work, the experimental ratio response is calculated to be 1.437, and the theoretical simulation ratio response is 1.0562 [17]. Rong *et al.* experimentally measure the an average ratio response of 1.37 after compaction by a dendrimer of DNA-tethered gold nanoparticles, which separates the particles by approximately 6 nm [121]. The range in the ratios collected by Rong *et al.* is from 0.8 to 2, similar to the results from the biotin-neutravidin binding assay. Again the differences in the implementation of the excitation and detection influence the actual results, though the results are consistent. The range in the ratio results from the plasmonic coupling called for further exploration.

One contributing factor to the range in the ratio response is the polarization sensitivity of the gold nanoparticle pair. The extent by which the two particles plasmonically couple is determined by the alignment of the gold

nanoparticle dimer axis with the polarization state of the incident light. When the dimer axis is oriented with the polarization of the light, the ratio is maximized, since the plasmonic coupling is stimulated; whereas when the particle pair dimer axis is oriented 180° from the polarization of the light, the intensity ratio is minimized [17, 88, 122, 136, 138]. The polarization sensitivity makes it possible to detect the orientation of the particle pair through the maximization of the ratio response, and provides insight into the range in the ratio response. Towards assaying the effects of the polarization of the incident illumination on the ratiometric response, correlated images of the same gold nanoparticle pairs were collected with two orthogonal polarization states. The ratio response was calculated for the two polarization states both of the gold nanoparticle monomers before, and after binding by the freely diffusing neutravidin gold nanoparticles. It is expected that isotropic, perfectly spherical gold nanoparticles would have no polarization sensitivity. Indeed, the monomeric gold nanoparticles maintained the same intensity ratio between the orthogonal polarization states consistent with the monomeric ratio observed previously. Once the two gold nanoparticles interact though, the particle dimer becomes anisotropic, and highly influenced by the polarization state of the excitation illumination. In one exemplary case examined, the monomeric ratio was 0.9400. Following incubation and binding by a neutravidin gold nanoparticle, the ratio increased for both polarization orientations, but to different extents. In one orientation the ratio increased to 1.51, though in the orthogonal orientation it increased to 4.17. Clearly the orthogonal polarization is more aligned with the dimer axis. It was found that for

the particles analyzed, the difference in the ratios from the two orthogonal polarizations ranged from 0.1 to 2.7. When additional polarization optics are included, it is possible to determine the orientation of the gold nanoparticle pairs, and further maximize the ratio response from the dimer pair, providing even more details of the biomolecular interactions of interest.

### *5.1 Overall research contributions*

Overall, this work advances the application of gold nanoparticles to single-molecule techniques with high temporal resolution. Specifically, this work has established a prism-based total internal reflection darkfield illumination technique with diverse use in systems involving gold nanoparticles. These applications include single particle tracking with ratiometric discrimination of specific probes from nonplasmonic scattering particles, similar to Grecco and Martinez [123], traditional high spatial and temporal resolution single particle tracking for molecular motors [58, 59, 63], highly sensitive biomolecular binding similar to Nusz *et al*. [75], plasmonic nanostructures [90, 148, 210], and especially extending the plasmonic coupling technique between gold nanoparticles [17, 18, 88, 120-122, 151] for high spatial and temporal resolution measurements for both long time durations and a wide distance range. This work as a whole marks a significant advance to the plasmonic field in demonstrating the first detection of the plasmonic coupling between two gold nanoparticles through the binding interaction by biotin and neutravidin with time resolution better than 25 Hz. Further, methods were created to apply the plasmonic coupling between gold

nanoparticles technique beyond DNA experiments to those involving general biomolecules, and first applications were conducted to preliminary single-molecule binding experiments between an independently functionalized T7 RNA polymerase with a gold nanoparticle and a DNA molecule with a gold nanoparticle. The freely diffusing T7 RNA polymerase was allowed to dynamically interact such that the plasmonic response between the gold nanoparticles were observed without the prerequisite of tethering the gold nanoparticles between DNA.

The novel implementation of the ratiometric analysis technique is the first to use monochromatic illumination from laser sources, and increases the sensitivity to detection of peak resonance wavelength shifts, by eliminating the need to measure subtle shifts in the peak. The ratiometric analysis technique through the prism-based total internal reflection darkfield excitation and simultaneous dual wavelength observation is superior to any other excitation and detection technique applied to experiments utilizing plasmonic nanoparticles to date. Not only does it eliminate problems with uncertainty in the measurement, but it also is extendable to faster time resolutions, not possible with conventional techniques. Through minor instrumentation changes, time resolutions in the microsecond range are possible. The excitation power density may be increased by using higher power lasers, and also by focusing the light to a diffraction-limited region. Additionally, exchanging the detectors from a CCD array to avalanche photodiodes or photomultiplier tubes increases the sensitivity to detect the scattering signal from a single scattering gold nanoparticle and further increases

the temporal resolution. Finally, the ratiometric analysis with the developed technique has demonstrated its profound ability to detect single-molecule binding events with high temporal resolution, but it also lays a pathway toward high spatial resolution metrology when calibration experiments are conducted. Given the advancements made in this work, the plasmonic coupling between gold nanoparticles as a high temporal resolution technique has been established; it will now be of critical importance to further develop the technique to integrate high spatial resolution.

### *5.2 Future directions*

The work described here has demonstrated, as a proof-of-principle, the utility of the ratiometric analysis to detect the plasmonic coupling between gold nanoparticles as a high temporal resolution technique for applications to molecular biophysics, biosensing, and nanotechnology. This foundational effort provides a framework with which further instrumentation development may continue to advance the method to bring the technique to its full potential. Here, future developments and applications are outlined:

(1) *Integration of alternative polarization optics for detailed polarization analysis.* Preliminary polarization sensitivity assays have revealed that, while the ratiometric technique is sensitive to binding regardless of the dimer axis orientation of the gold nanoparticles, the intensity ratios are most sensitive when aligned with the polarization of the incident illumination. Because changes in orientation or in distance will change the

detected ratio, in any further extension of the plasmonic coupling technique, polarization discrimination will be necessary to accurately correlate the plasmonic coupling between the gold nanoparticles to distances and orientation [17, 88, 121, 122, 129]. One simple extension of the experimental technique developed here is the addition of an achromatic λ/2 waveplate after a polarizing beamsplitter. This implementation would allow all polarization angles within the orthogonal plane to the direction of propagation to be explored such that the maximal ratio may be found. The polarization state must be sampled at a frequency fast enough to detect the fluctuations of the gold nanoparticle dimer. In an application to gold nanorods, Xiao *et al.* detail a more complicated polarization scheme that would more fully analyze the polarization contributions to the plasmonic coupling [129]. In their work, two orthogonal directions of illumination excite the sample such that a full three-dimensional description of the orientation is measured. The two directions of illumination would need to be separated, requiring additional optics within the detection scheme. This can be accomplished with birefringent materials to spatially separate polarizations, or through a quad view detector, which would separate the light based on both wavelength and polarization. Once the modifications to the optical system are completed, the ratiometric analysis technique may be tested, and the maximal intensity ratios quantified through the binding assays conducted here to fully characterize the polarization sensitivity.

(2) *Further the scope of the molecular ruler metrology technique through correlation of distances to the intensity ratio response.* The ultimate development for the experimental technique is the incorporation of high spatial resolution distance measurements for real-time applications to molecular biophysics and nanotechnology. Presently, single-molecule molecular biophysics techniques need high spatial resolution distance measurements over a larger distance range than what is currently capable (1-10 nm). Gold nanoparticle plasmonic coupling has the potential to deliver on this need, as demonstrated in the preliminary molecular ruler experiment in which distances were correlated to peak resonance wavelengths [17]. The ratiometric analysis technique has the temporal resolution for biologically relevant experiments in the millisecond time range. If additional signal is required, though, readily available methods are possible to increase both the excitation and the detection. First, the laser intensity can be increased through higher power lasers, and focusing of the laser intensity to smaller regions within the field of view, reaching the point of a diffraction-limited region. This is, of course, at the expense of highly parallelized observations. Second, detectors may be exchanged such that the scattering signals are recorded with high quantum efficiency, high temporal resolution avalanche photodiodes. As outlined in the first improvement, to high spatial resolution, it will be necessary to discriminate both polarization and wavelength to correlate the ratiometric scattering response and the interparticle separation. Therefore, any changes to the

detectors will require methods to both separate the signal based on wavelength and polarization. This is possible through both dichroic mirrors and polarizing beamsplitters being added into the detection optical path. Once the additional developments to the instrumentation are complete, correlation experiments between the interparticle distance and the ratio response may be conducted.

Several methods exist to relate the ratio response to distances, specifically, a few experimental assays are: (1) DNA dimer conjugates, similar to Reinhard *et al.* [17], (2) a T7 RNA polymerase stalling assay, (3) gold nanoparticle fiber assay, similar to Olk *et al.* [193], and (4) a microtubule-kinesin translocation assay. With all of the above distance correlation techniques, the interparticle spacing may be independently verified through FIONA style methods [22]. To accomplish the first method, DNA dimers have been constructed through antibody-antigen and biotin-streptavidin reactions with varying lengths of DNA separating the gold nanoparticles. These constructs may be used to tether the gold nanoparticles with known spacing. The scattering ratios can be measured and associated to the distance between the particles.

The second distance correlation experiment was pursued as the DNA constructs were designed such that T7 RNA polymerase would stall anytime it needed to incorporate a UTP in the RNA strand. By specifically engineering the sites where the polymerase stalls, specific distances between the gold nanoparticles and the scattering ratios may be

connected. In such an experiment, the assay conditions similar to those used in the preliminary T7 RNA polymerase work conducted here provide initial methods. The polymerase binds to the DNA, serving as an initial distance signal. Transcription is allowed to begin such that a stable elongation complex is created. Through specific DNA constructs, different stall sites at varying locations determine the distance between the gold nanoparticles and the intensity ratio response.

Olk *et al.* attached an 80 nm gold nanoparticle to a fiber probe, and adsorbed 80 nm gold nanoparticles to a substrate to measure the spectral response to varying distances between the gold nanoparticles [193]. In an assay akin to this work, 40 nm gold nanoparticles may be adsorbed in an assay chamber, similar to the typical methods. Then, a second 40 nm gold nanoparticle bound to a fiber probe is introduced to the sample. Through precise control of the fiber position, the distance between the gold nanoparticles and the intensity ratio response can be determined.

As a final example of experiments to correlate the distance between gold nanoparticles and the intensity ratio, may be conducted with the precision 8 nm stepping of the motor protein kinesin on microtubules. In this experiment, microtubules would be decorated with gold nanoparticles by biotinylating the microtubule. Kinesin are labeled with gold nanoparticles as well through a terminal biotin group. By starving the kinesin of its energy source ATP, the kinesin will slowly translocate on the microtubule allowing correlating the distance between the gold nanoparticle on the

microtubule and the gold nanoparticle on the kinesin. This experiment will especially benefit from FIONA style determination of the distances between the gold nanoparticles.

Importantly, with all of these experiments the polarization orientation must be explored such that the highest signal is obtained. This is trivial for the DNA tethering and the fiber probe experiments, as these experiments are rather static. Specifically, for the T7 RNA polymerase assay, this may be accomplished by stalling the polymerase at the promoter binding site, finding the maximum scattering signal with respect to the polarization, and finally introduce the nucleotides to allow transcription to proceed. The polarization may be maximized in the kinesin-microtubule experiment through the limiting of ATP to reduce the rate of translocation by the kinesin. The polarization maximum may be determined within the first steps of the molecule, and the remaining distances used to correlated between the gold nanoparticles.

Accomplishing this goal to create a high spatial resolution technique over a wide distance range is of great importance for many nanoscale applications. The plasmonic coupling between gold nanoparticles is a robust method, which has the potential to achieve this with the added features of high temporal resolution and long time duration observation. This study will be of high impact to nanotechnology and molecular biophysics.

(3) *Alternative wavelengths for ratiometric analysis and the signal response from varying gold nanoparticle sizes.* In this work, gold nanoparticles 40 nm in diameter were used, as a good trade-off of signal strength, probe size, and the distance range of the near-field within which plasmonic coupling between gold nanoparticles occurs. However, gold nanoparticles of many diameters exist, all which have various advantages, such as small particles having less influence on the dynamics of the biomolecule, or large particles having a wider distance range within which plasmonic coupling occurs. Importantly, when designing specific single-molecule experiments using gold nanoparticles, the size of the probe must be selected based on several factors, (1) the necessary distance range (plasmonic coupling occurs within two particle diameters [17, 98]), (2) the temporal resolution (the scattering signal is highly dependent on the particle diameter, $I \sim D^6$ [64]), and (3) the influence of the gold nanoparticle on the diffusional characteristics of the molecule of interest [1]. Further study into the ratiometric analysis technique for various gold nanoparticle sizes adds versatility to the plasmonic coupling single-molecule technique. Smaller gold nanoparticles may be used for a smaller distance range, though higher in sensitivity, while larger particles may be used for very high temporal resolution measurements with less spatial resolution. The specific wavelengths for analysis to maximize the sensitivity of the ratiometric response, though, are different based on the size of the gold nanoparticles. The experimental excitation and detection may be modified

such that preliminary experiments, both binding and distance correlation, are conducted to quantify the ratiometric response from various gold nanoparticle diameters. Alternative laser lines may be easily coupled into the designed excitation system, such that the peak resonance wavelength for the specific monomeric gold nanoparticle is used for a scattering signal in the ratiometric analysis. The detection system must have an appropriate dichroic such that the short and long wavelengths are still separated. One method in which many laser lines may be included is through a source such as a tunable argon ion laser, which emits wavelengths ranging from 488 nm to 514 nm, or an argon-krypton mixed laser source with wavelengths ranging from 457 nm to 647 nm. After other wavelengths are included in the excitation, the sensitivity of the distance ranges and binding may be analyzed.

As preliminary effort to specify particular sampling wavelengths, based on desired distance ranges, Equation 7 was applied to determine the change in peak resonance wavelength for various interparticle separations for 40 nm diameter gold nanoparticles. After calculating the new peak resonance wavelength, the theoretical simulation spectra published by Reinhard *et al.* was shifted, similar to the method used in Section 4.7 [17]. Ratios of several sampling wavelengths (based on commercially available laser lines) were calculated. From this preliminary work, several trends emerge. First, the initial peak resonance wavelength and the final peak resonance wavelength after the two particles couple within the desired distance range

should be matched as closely as possible with the two sampling wavelengths to reduce misinterpretation of the ratio. Importantly, if the longer sampling wavelength is exceeded by the final peak resonance wavelength, then the ratio begins to decrease, instead of monotonically increasing. This limitation may be overcome by utilizing the two directions of propagation illumination scheme outlined in the first future direction, or if sensitive enough, by the overall intensity. The TIR excitation wave exponentially decreases into solution, such that when the second gold nanoparticle is closer to the surface the scattering intensity is greater than when the second gold nanoparticle is farther in solution. Provided the detector is sensitive enough to differentiate the intensity change, then the total intensity from both wavelengths along with the ratio may be used to specify the distance. Another trend that appears in the analysis is that the sampling wavelengths are most sensitive and produce the greatest changes when they correspond to the initial and final peak resonance wavelengths. For example, the intensity ratios are more sensitive at far interparticle separations when short wavelengths, such as 514 nm and 488 nm, are one of the sampling wavelengths. However, the intensity ratios are more sensitive for close interparticle separations when long wavelengths, such as 593 nm and 638 nm, are used. Again, these estimates suffer from limited experimental and theoretical information to truly define the ratio response. Moreover, the actual experimental ratios are highly dependent on the specific gold nanoparticle pair.

(4) *Applications of the ratiometric analysis to biomolecular systems and biotechnology.* There are many biological systems for which the plasmonic coupling between gold nanoparticles ratiometric analysis technique may provide additional insights, a few of which are outlined here. First, simplified binding assays similar to the T7 RNA polymerase to DNA molecules may be conducted. A gold nanoparticle conjugated to DNA molecules through the techniques developed here reports the binding by a gold nanoparticle functionalized repressor protein, *lac* repressor. Various concentrations of *lac* repressor and DNA sequences would provide insight into the specificity and dynamics of the repressor protein to the DNA molecule. Furthermore, should DNA tethers between two gold nanoparticles be successfully designed and calibrated, distances and orientations of the looping by an unlabeled *lac* repressor may be observed in real time. Second, with developments in distance calibration, temporal resolution, and successful DNA tethering by two gold nanoparticles, the fast time-scale dynamics of DNA fluctuations may be monitored. In these experiments base pair flipping and enhanced flexibility would be capable of detection with the plasmonic coupling response. As outlined in the previous future direction, T7 RNA polymerase may be used to calibrate the ratiometric response based on distance. Once a calibration is created, a similar assay may be used to directly understand the binding and initiation of T7 RNA polymerase at the single-molecule level, as yet unachievable through current single-molecule techniques owing to limited

spatial and temporal resolution. Finally, again as outlined in the previous future direction, kinesin motor proteins were suggested to be used in an assay to correlate the distance between gold nanoparticles with the plasmonic response under limited ATP concentrations. Open questions remain regarding the kinetic cycle of kinesin. Through clever labeling schemes, either one head of the kinesin molecule and the microtubule, or both heads of the kinesin motor protein are labeled. Subsequently, the kinetic cycle of the kinesin molecule may be observed under physiological conditions, and make possible the ability to resolve the specifics of the stepping dynamics of the molecule.

Nanotechnology and biotechnology also benefit from the ratiometric analysis technique for detection of plasmonic signals from metallic nanoparticles. As a specific example, biosensing research strives to detect incredibly low concentrations of analyte, often exploiting the plasmonic resonance of metallic nanoparticles [74-76, 110]. Nunz *et al.* state that the goal of observing the real-time dynamics of single-molecule binding is still unattained [75]. The ratiometric analysis technique may enhance the sensitivity of plasmonic biosensing. A proof-of-principle comparison with the work of Liu *et al.* would test this hypothesis [110]. Specifically, a very high density of DNA molecules is adsorbed onto the surface of a single gold nanoparticle, which causes the peak resonance wavelength of the nanoparticle to shift, based on a change in the local refractive index. Upon cleavage of some of the bases pairs from the DNA molecules by a

restriction enzyme, the refractive index changes, and the peak resonance wavelength blue shifts closer to the unconjugated gold nanoparticle. The ratiometric analysis technique can monitor the plasmonic response with higher temporal resolution, and further, as evidenced with the binding results, may be more sensitive. The ratiometric analysis technique has many benefits over the standard spectrum collection and analysis, in direct parallel with the reasons it enhances the sensitivity to detect plasmonic coupling, which could enhance the detection sensitivity for biosensors.

## APPENDIX

## Materials and Methods

*1. Electrical Schematic*

The electrical schematic for the precision voltage controller is provided. The voltage controller drives the piezostage in the x an y directions independently.

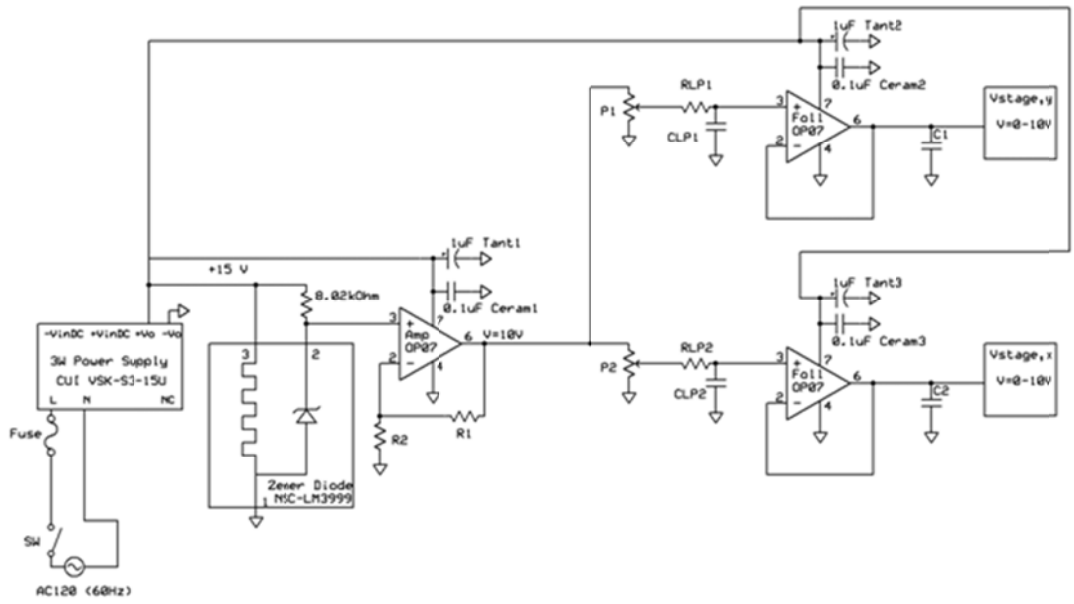


**Precision Voltage Controller.**

*2. Detailed Drawings*

Detailed drawings are provided for the laser to fiber coupling systems, dichroic fiber coupling system, and various other mechanical parts.

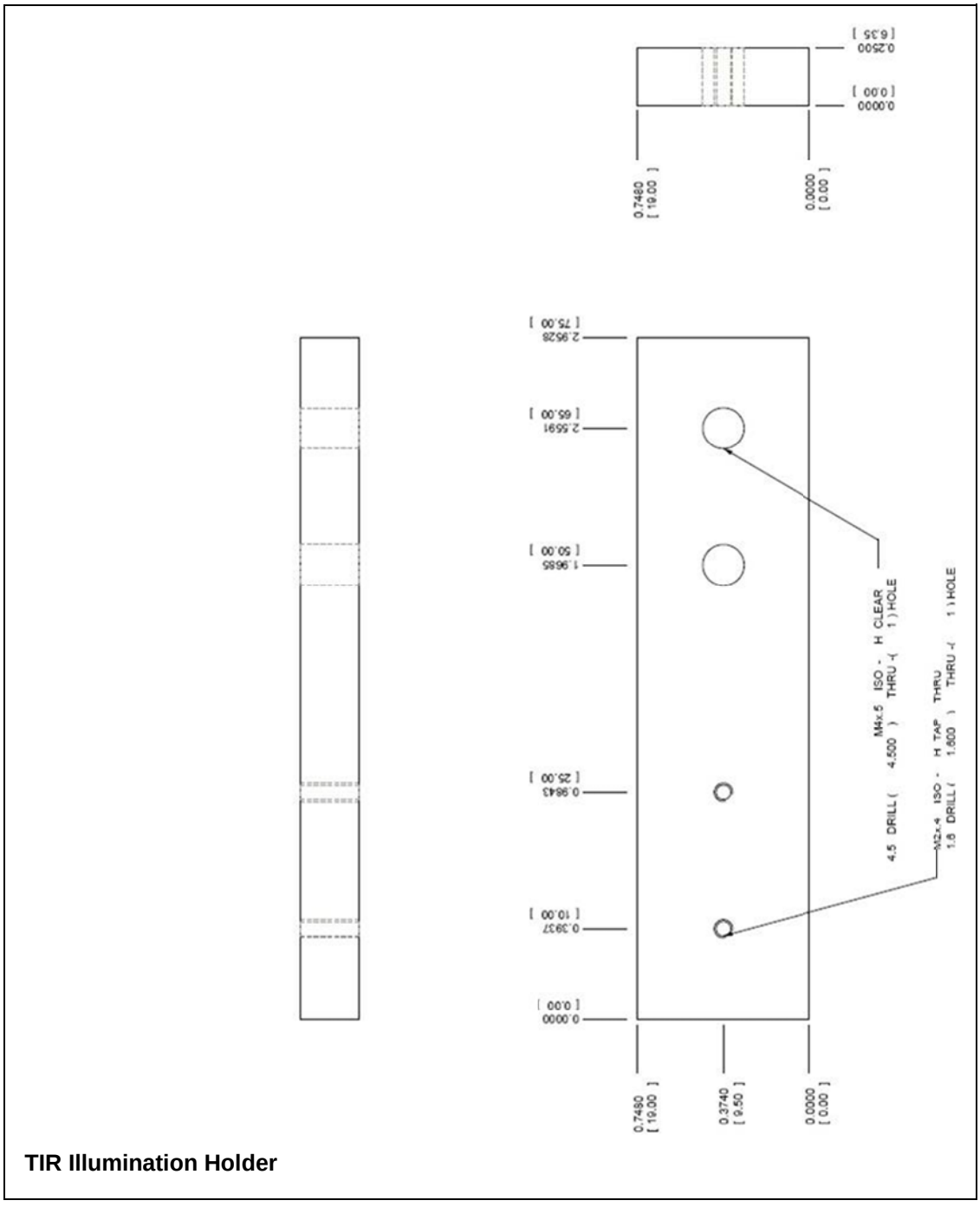


**TIR Illumination Holder**

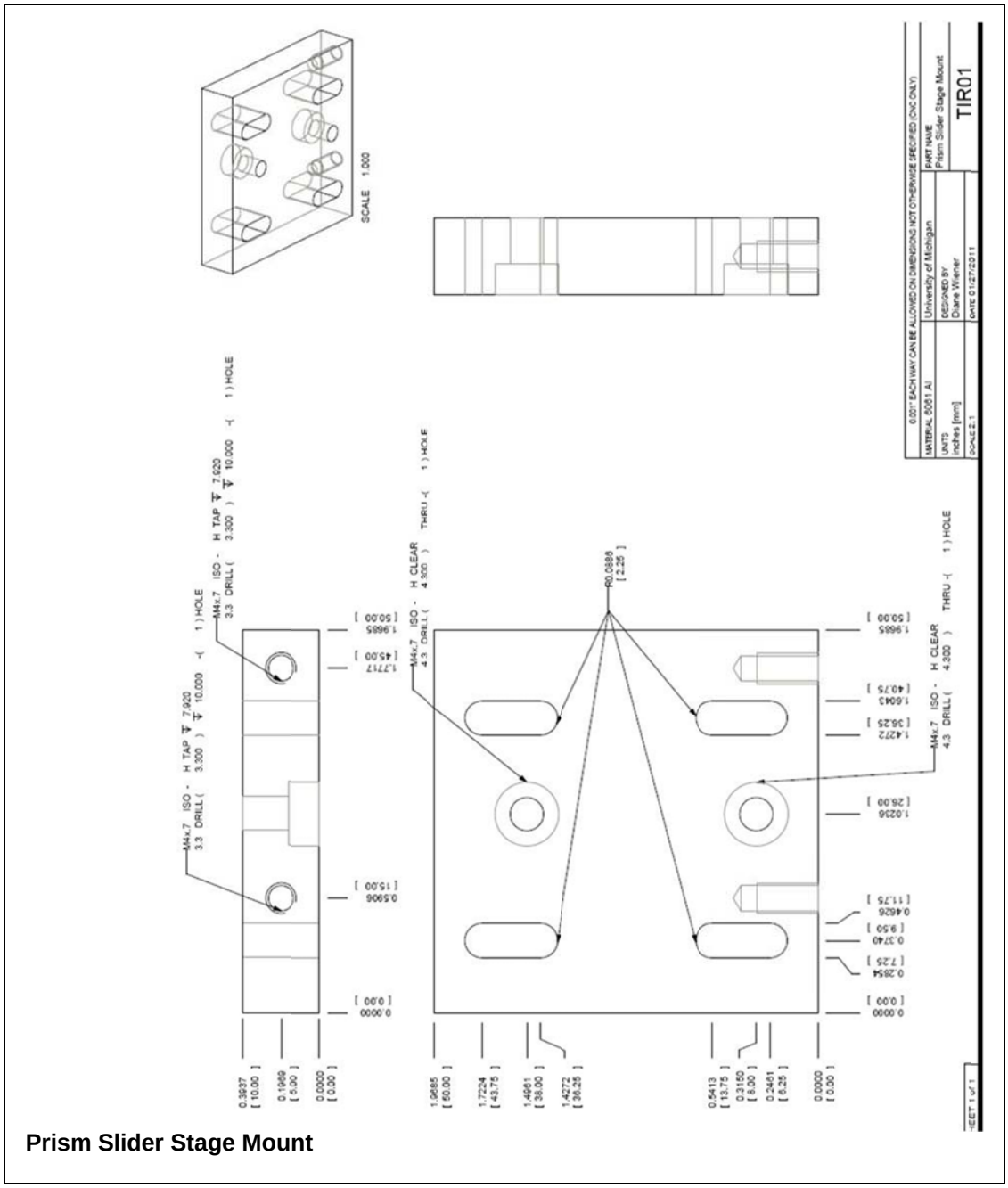


**Prism Slider Stage Mount**

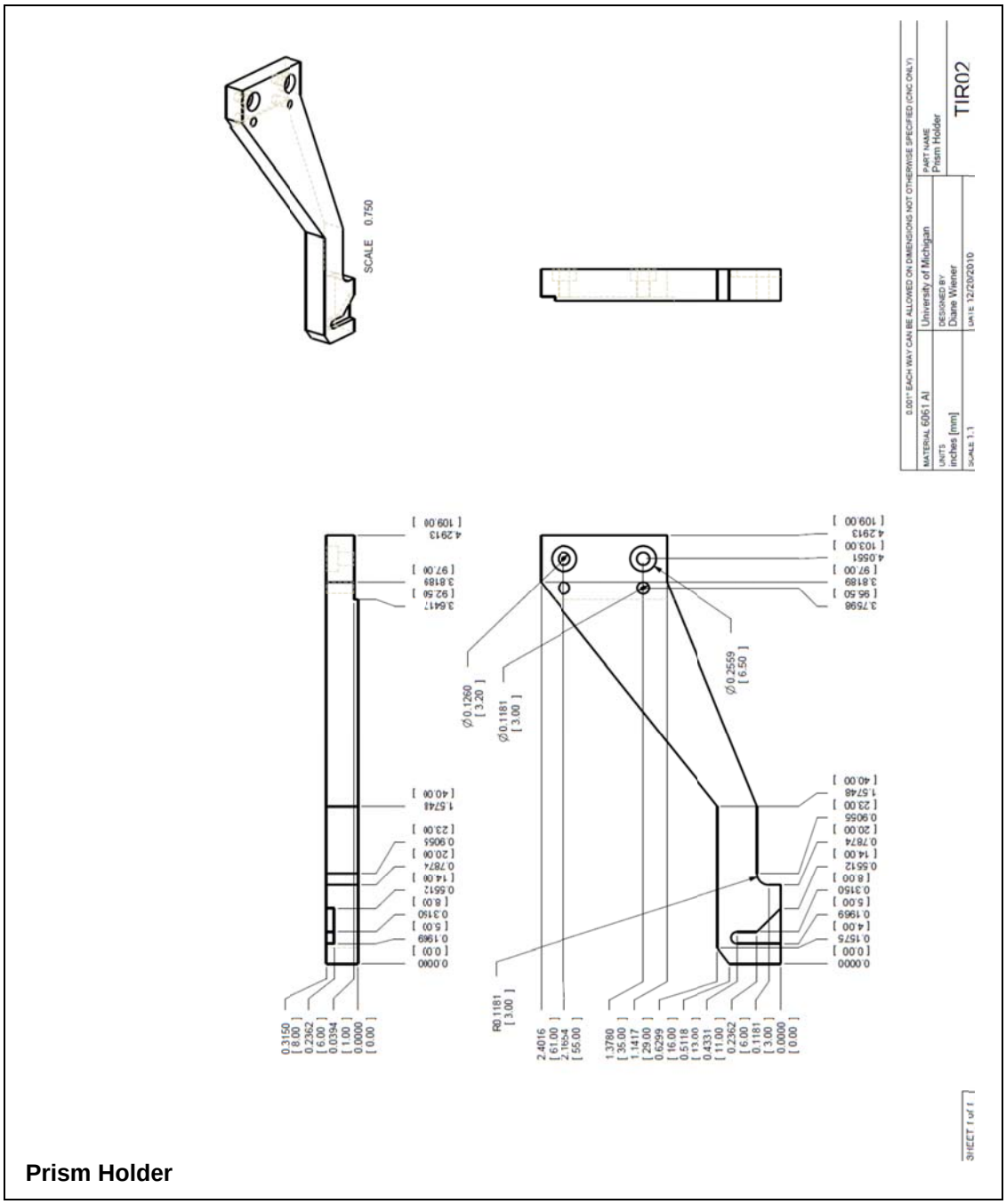


**Prism Holder**

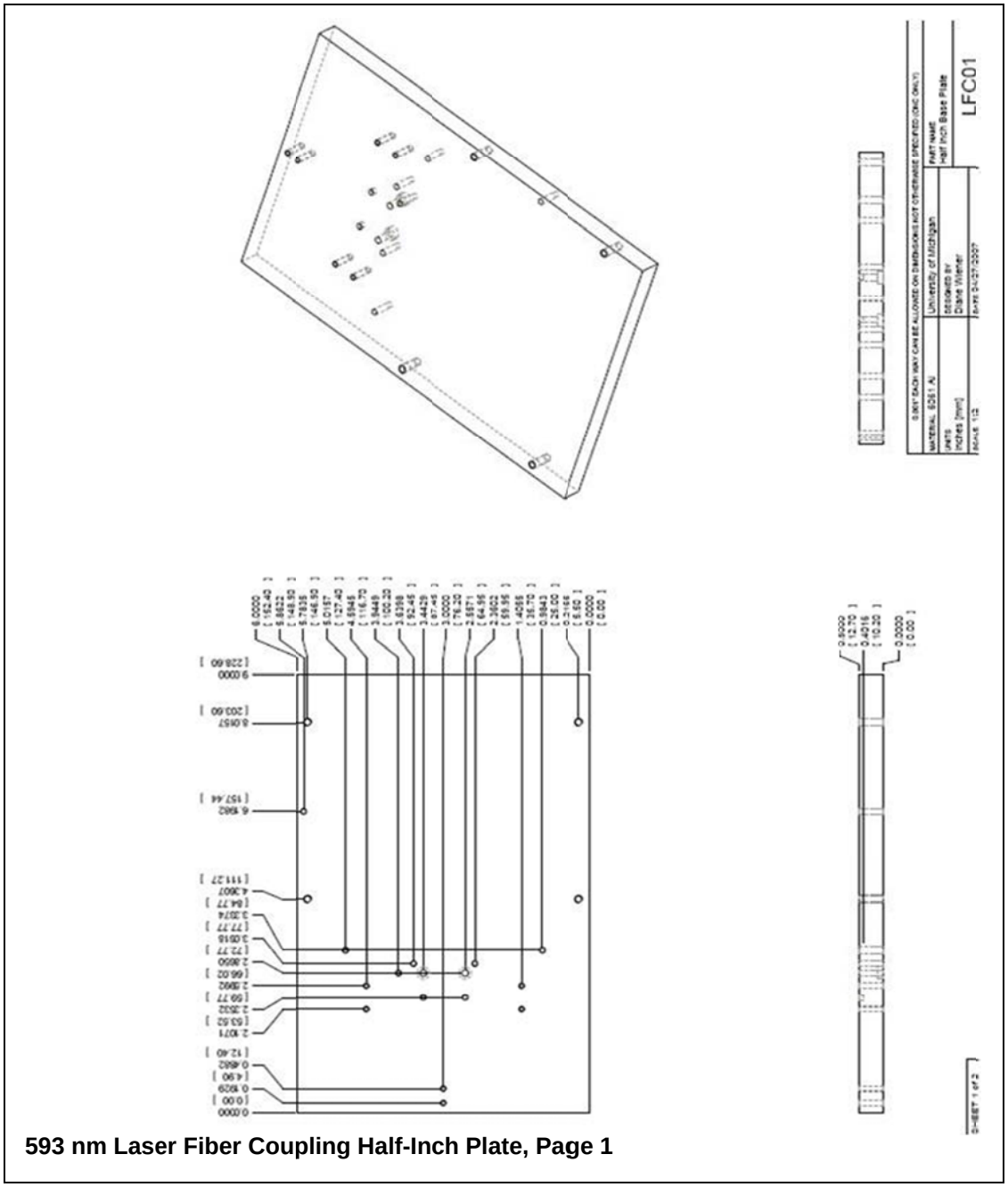


**593 nm Laser Fiber Coupling Half-Inch Plate, Page 1**

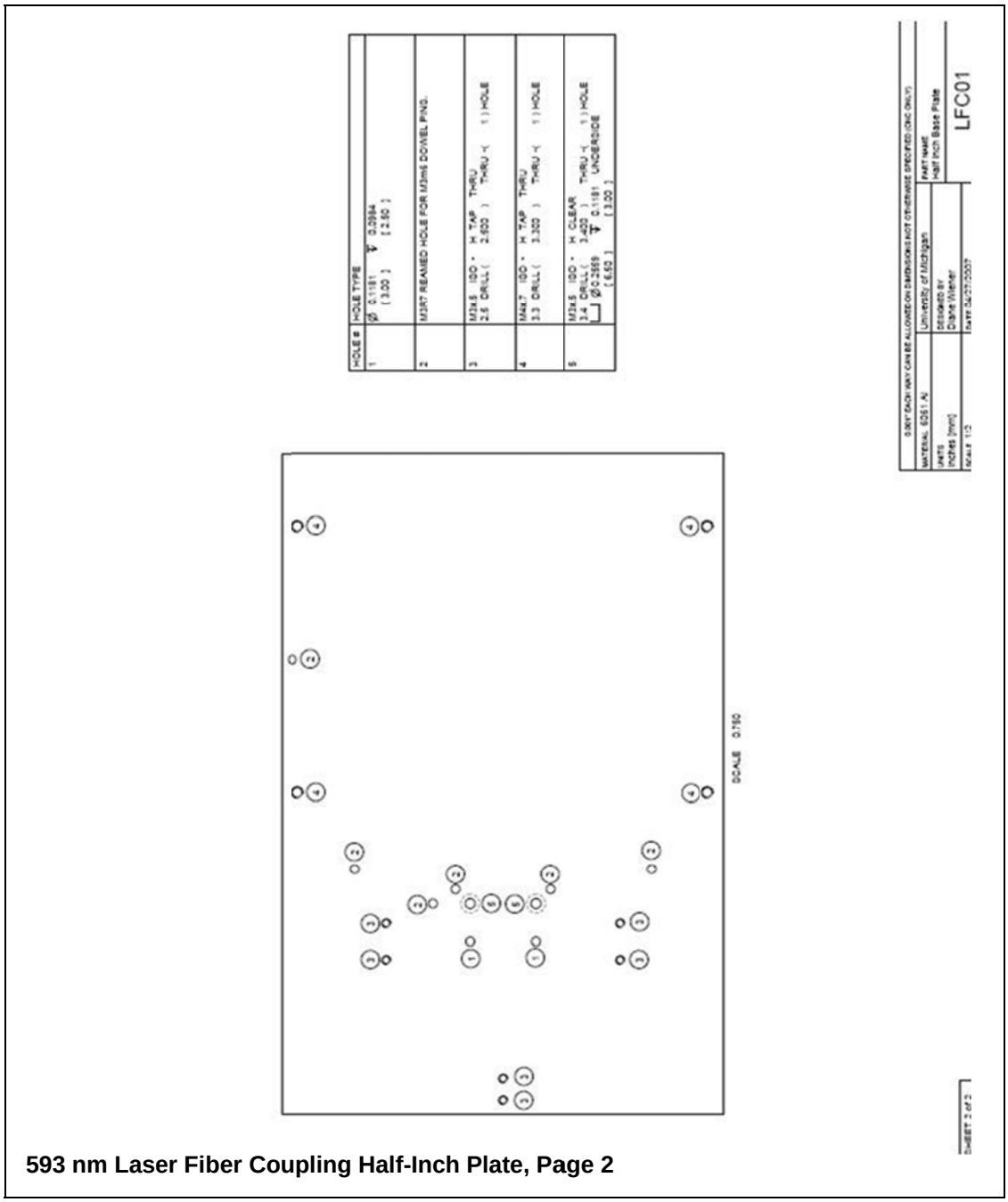


**593 nm Laser Fiber Coupling Half-Inch Plate, Page 2**

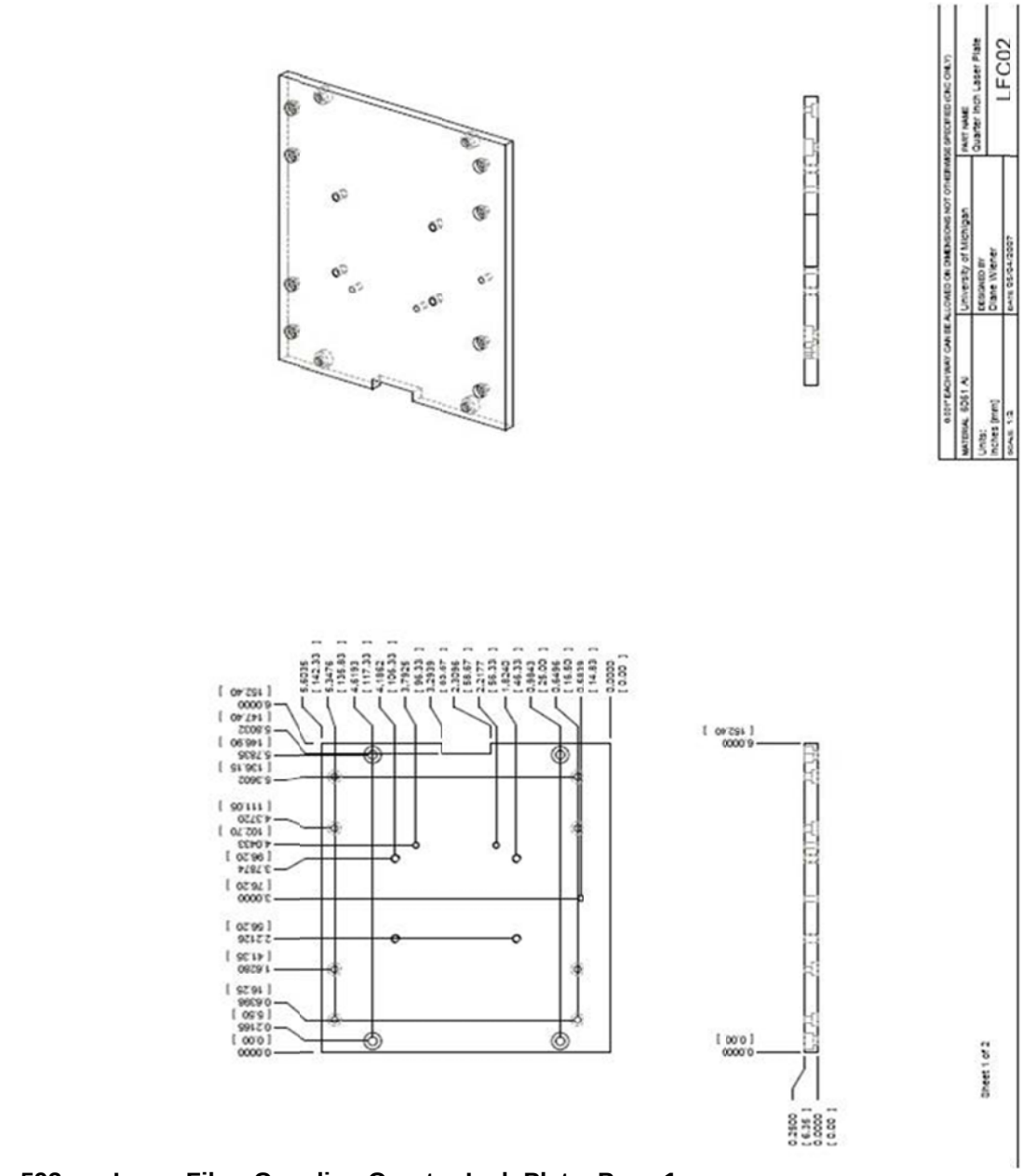


**593 nm Laser Fiber Coupling Quarter-Inch Plate, Page 1**

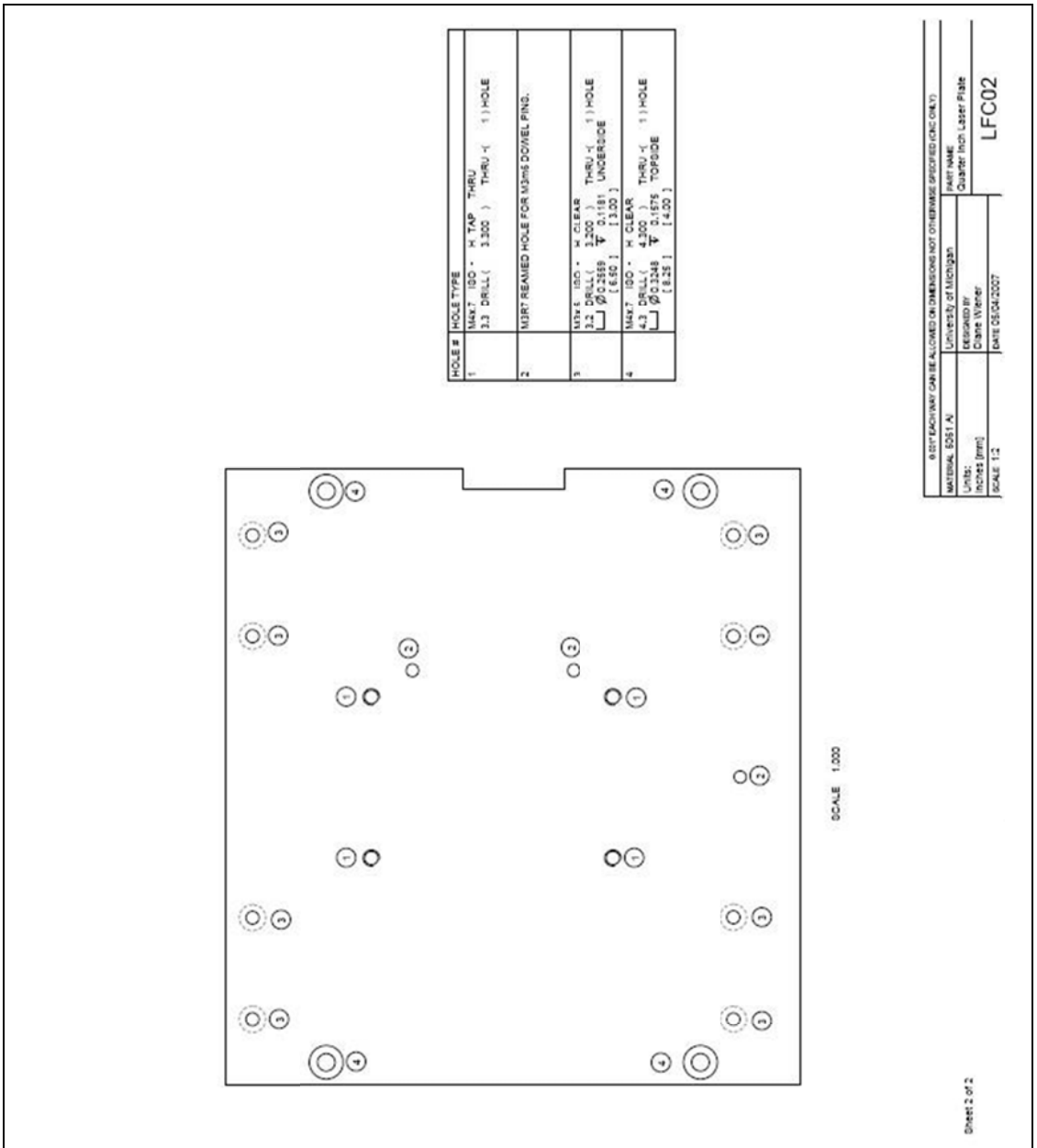


**593 nm Laser Fiber Coupling Quarter-Inch Plate, Page 2**

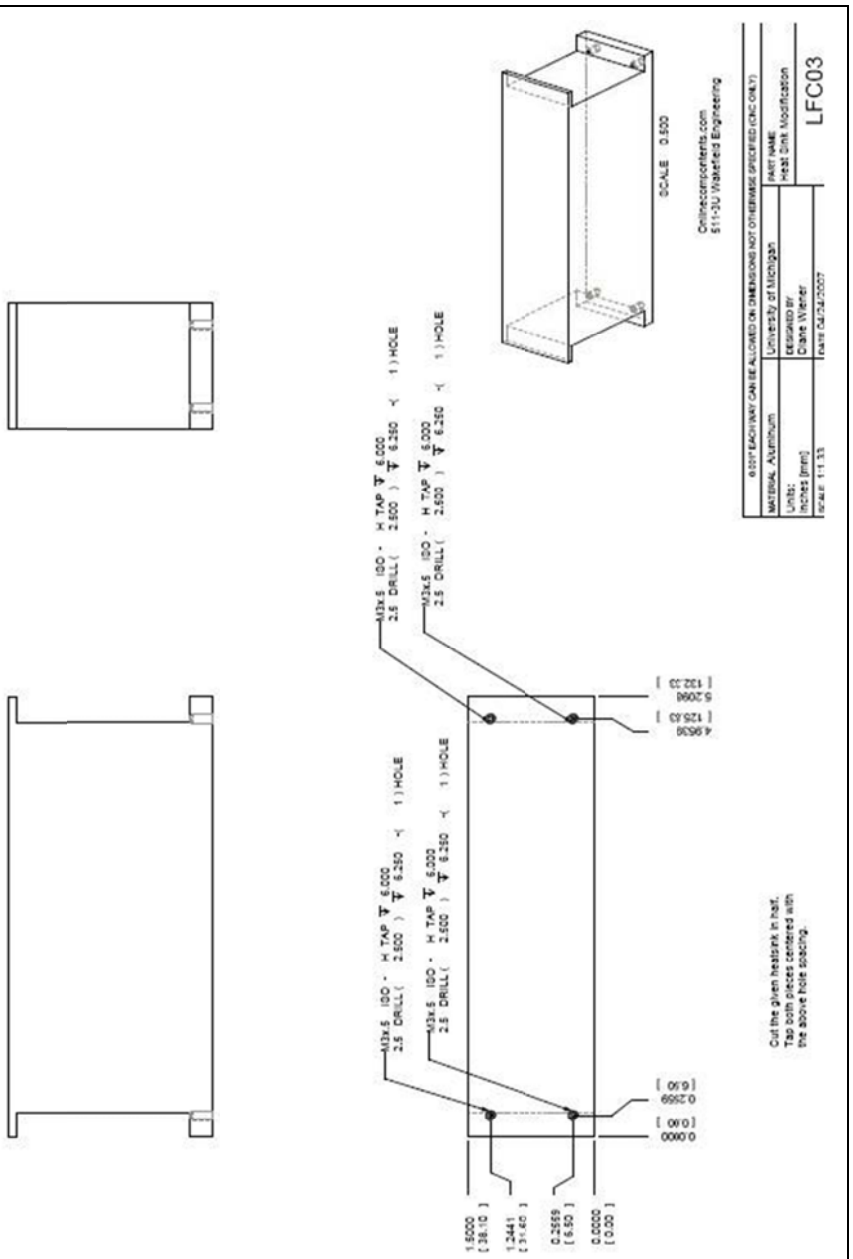


**Laser Fiber Coupling Heat Sink**

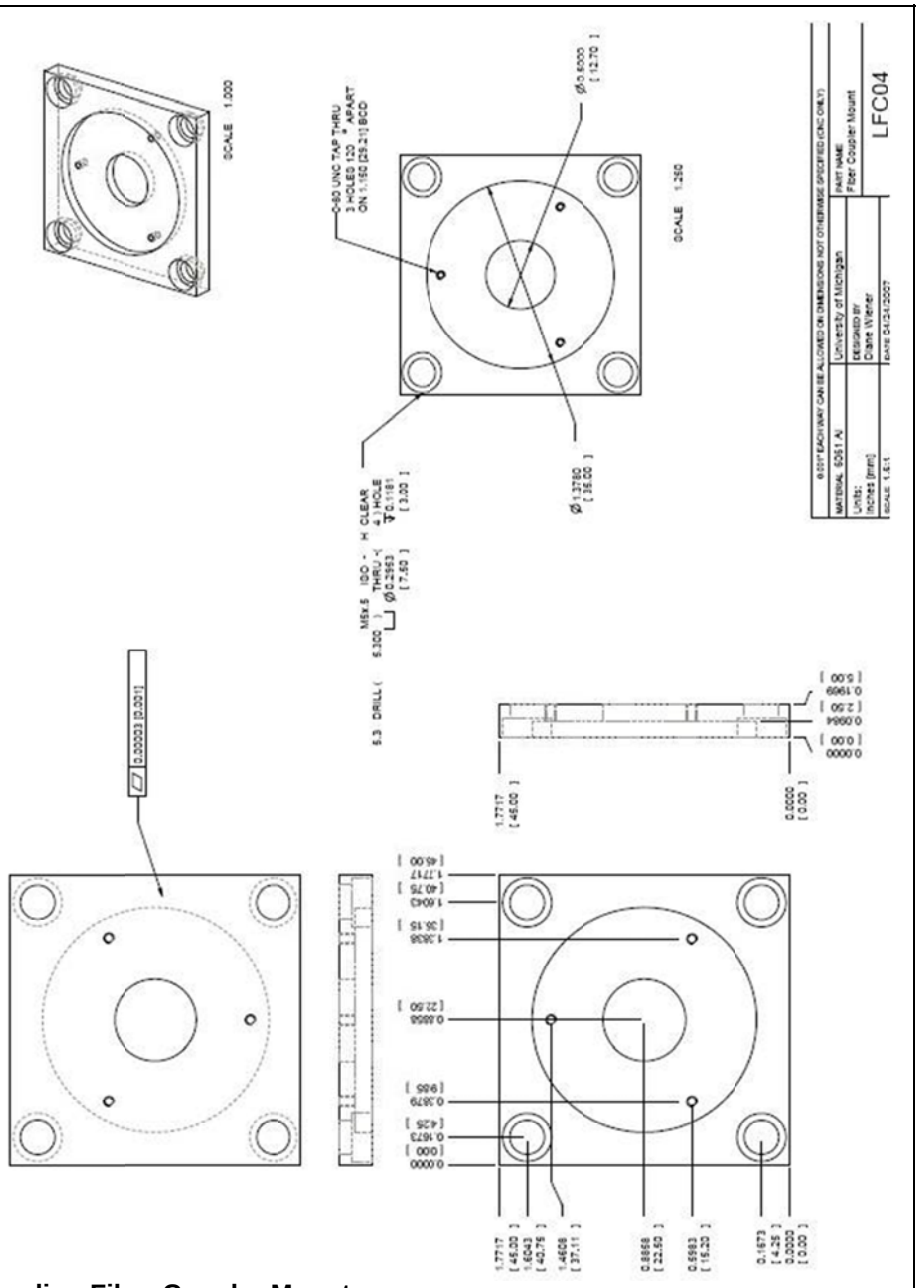


**Laser Fiber Coupling Fiber Coupler Mount**

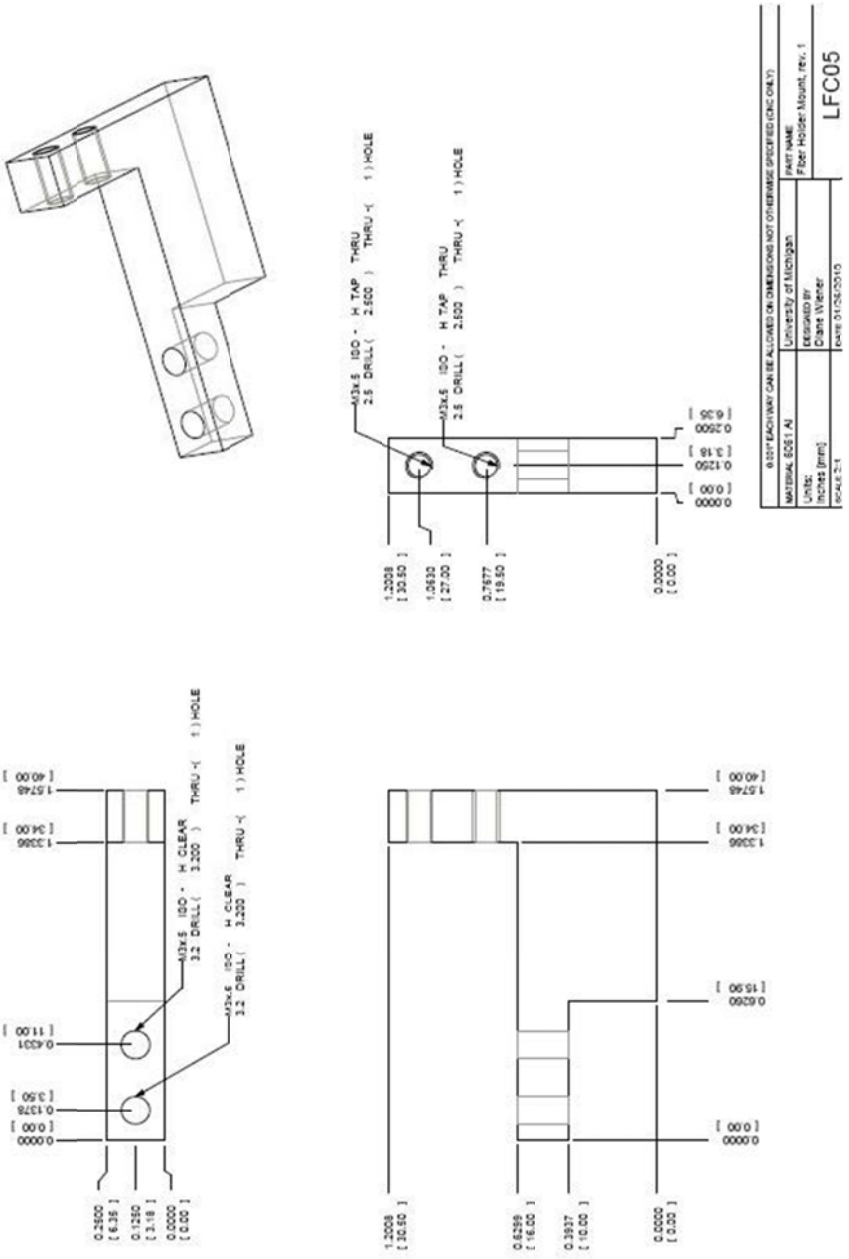


**Laser Fiber Coupling Fiber Holder Mount**

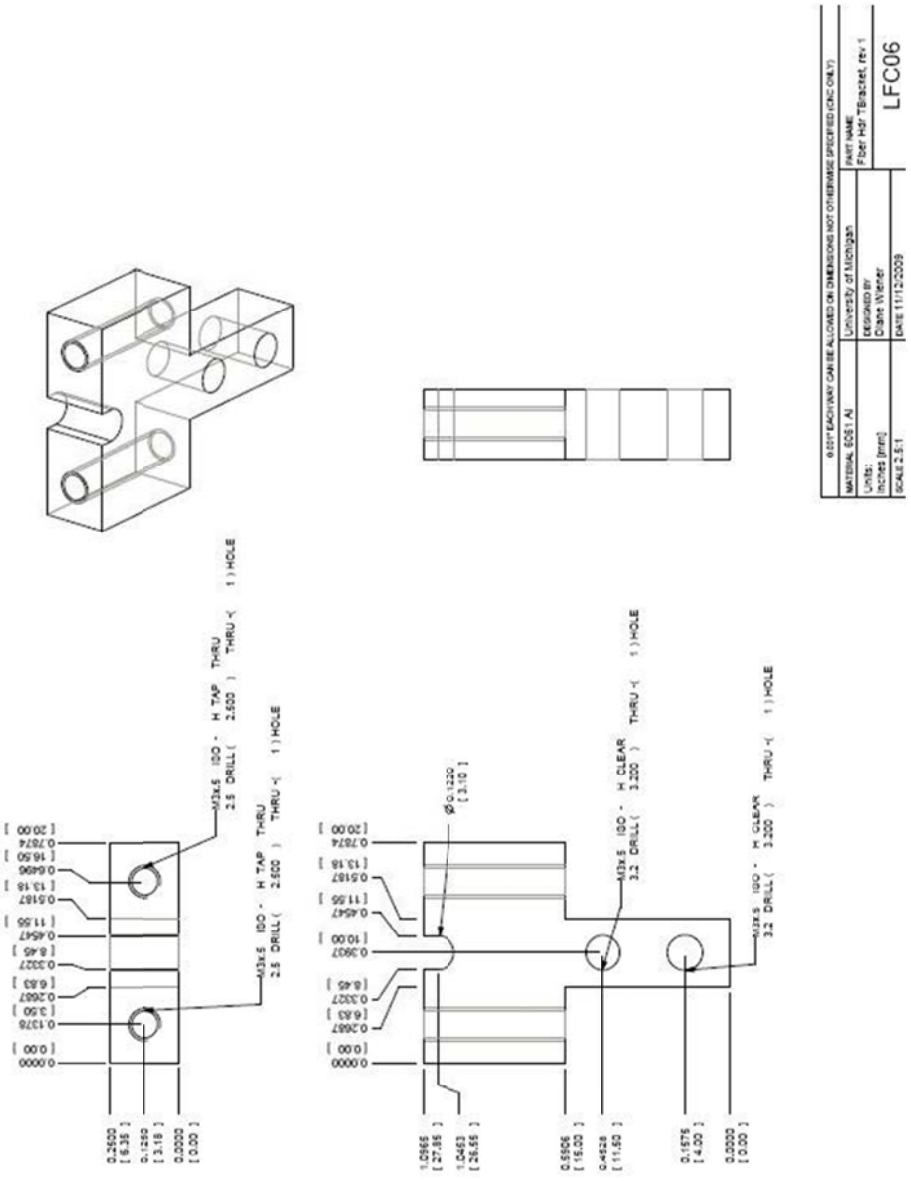
LFC06
Laser Fiber Coupling Fiber Holder T-Bracket

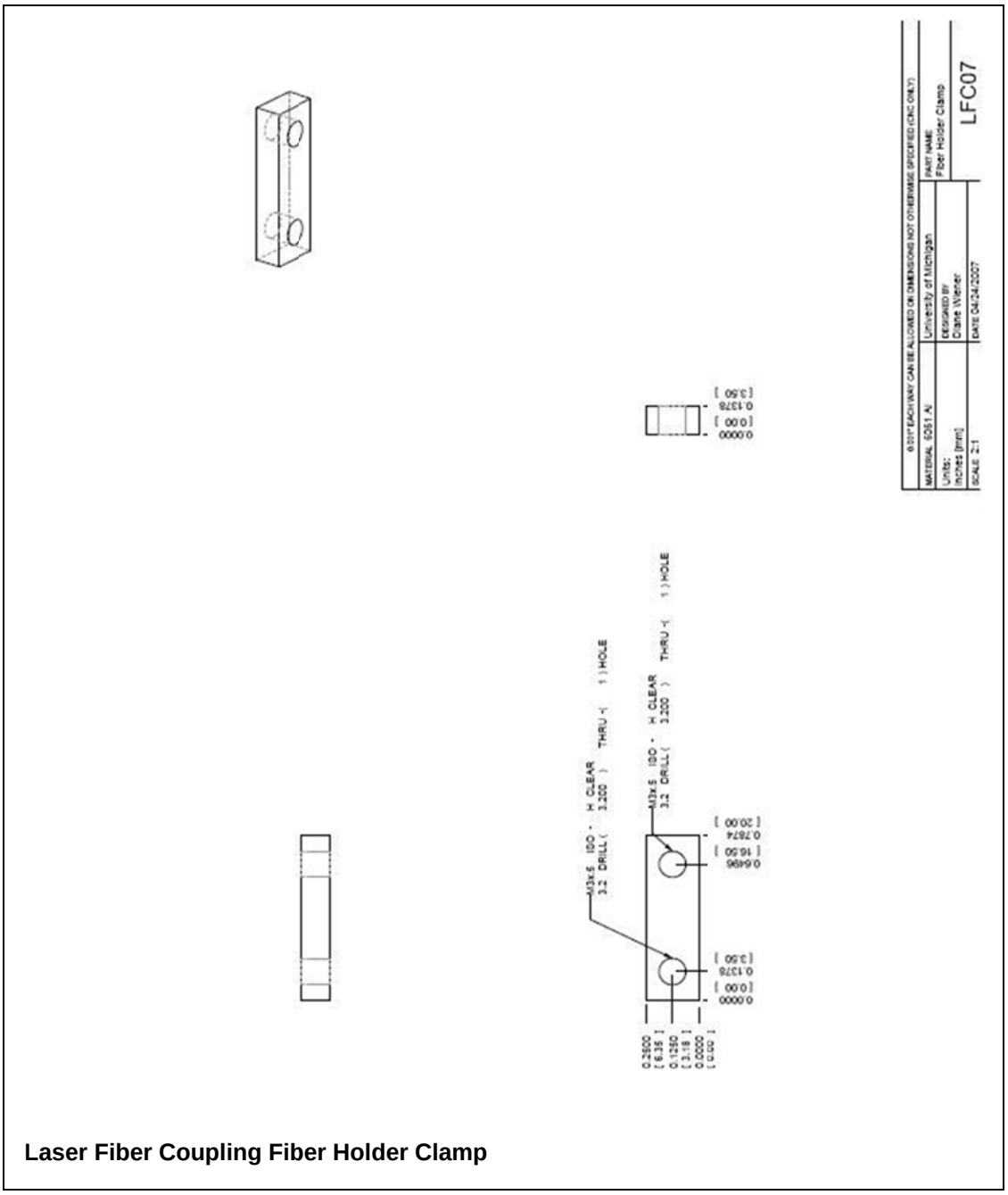


**Laser Fiber Coupling Fiber Holder Clamp**

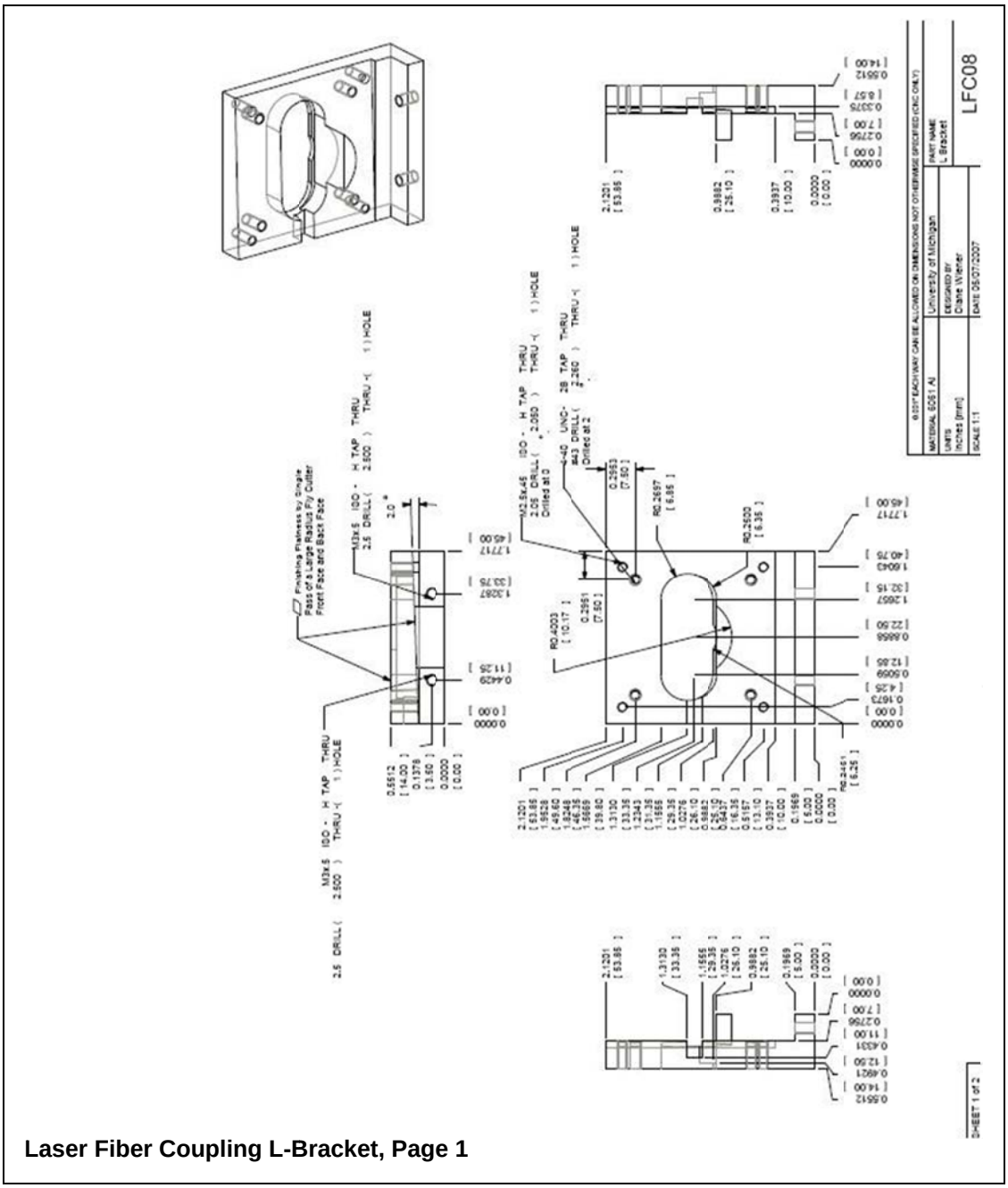


**Laser Fiber Coupling L-Bracket, Page 1**

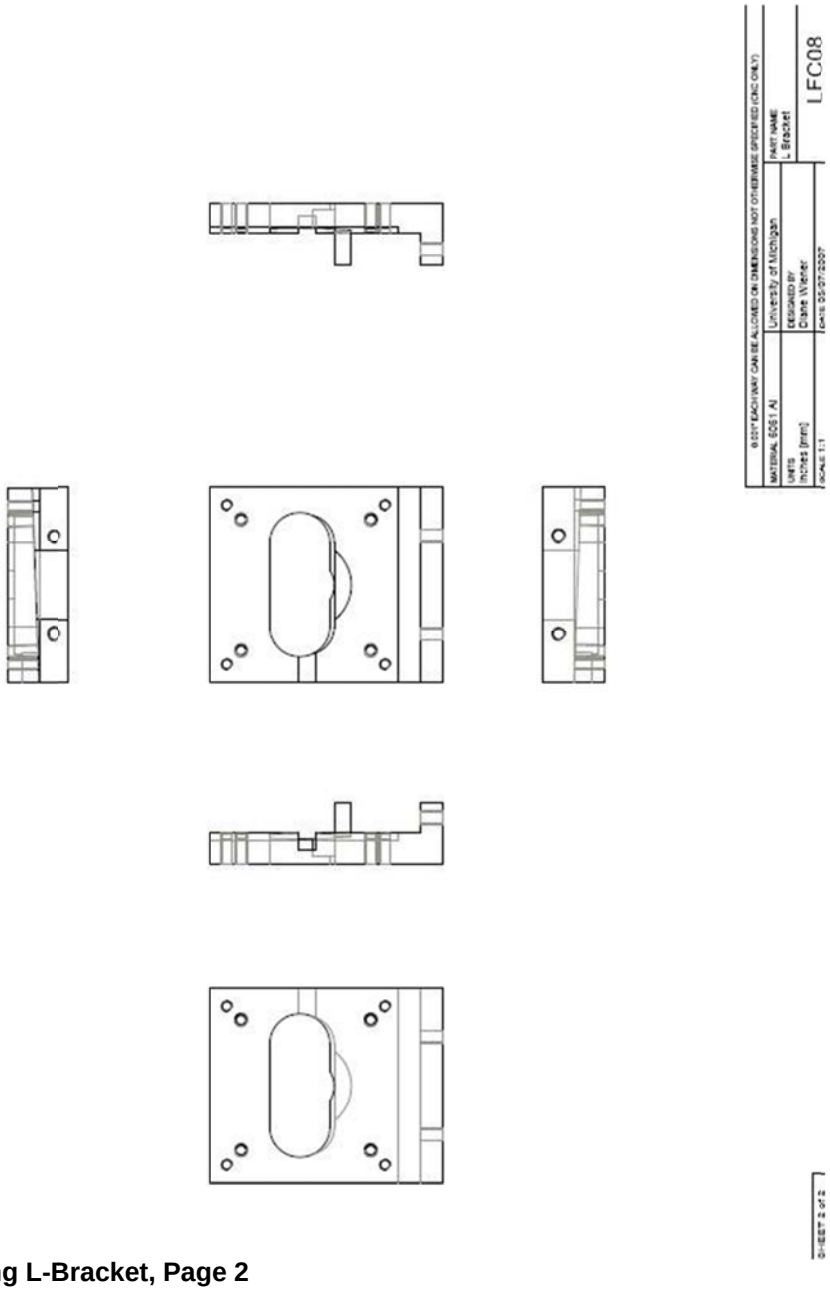


**Laser Fiber Coupling L-Bracket, Page 2**

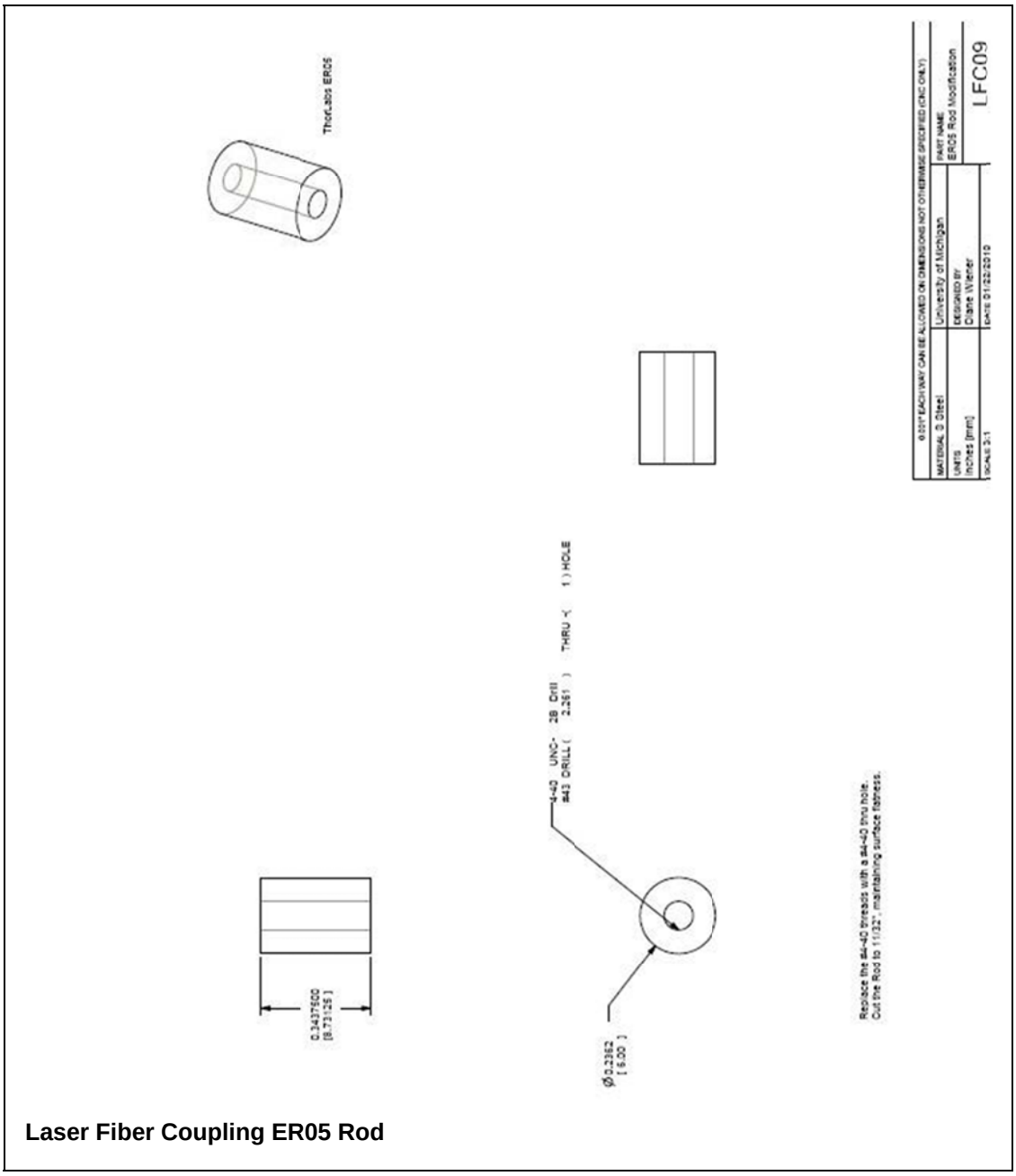


**Laser Fiber Coupling ER05 Rod**

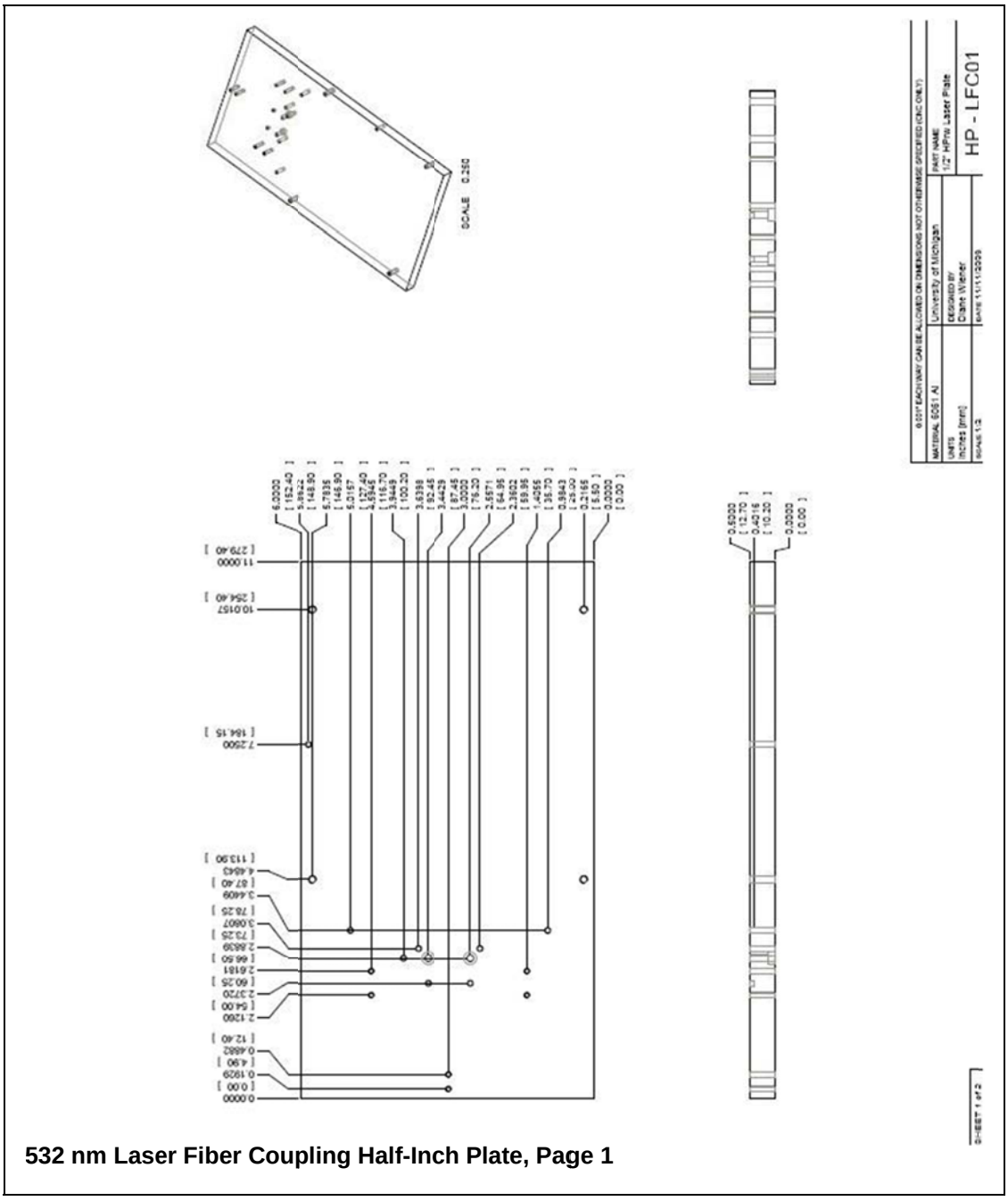


**532 nm Laser Fiber Coupling Half-Inch Plate, Page 1**

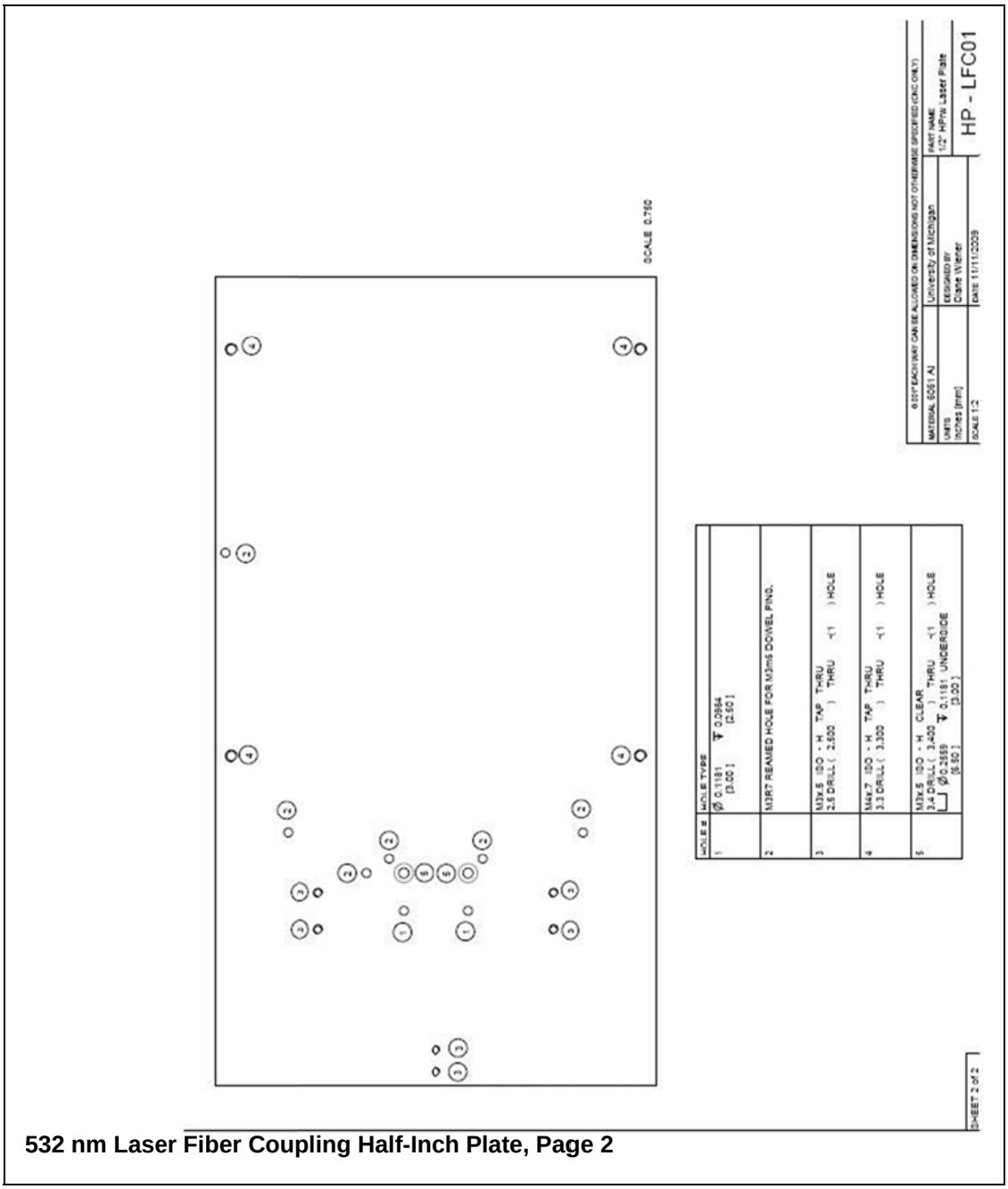


**532 nm Laser Fiber Coupling Half-Inch Plate, Page 2**

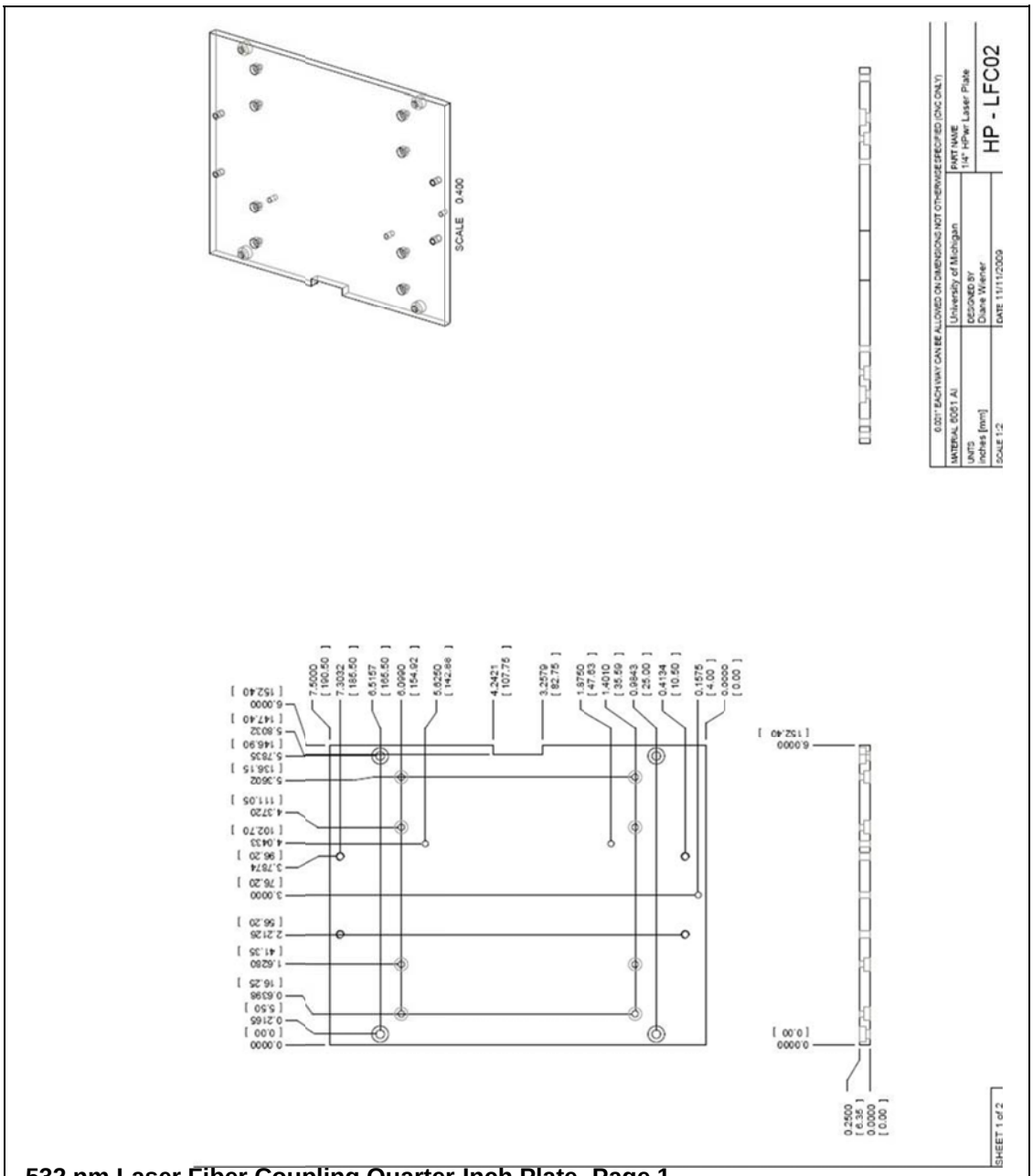


**532 nm Laser Fiber Coupling Quarter-Inch Plate, Page 1**

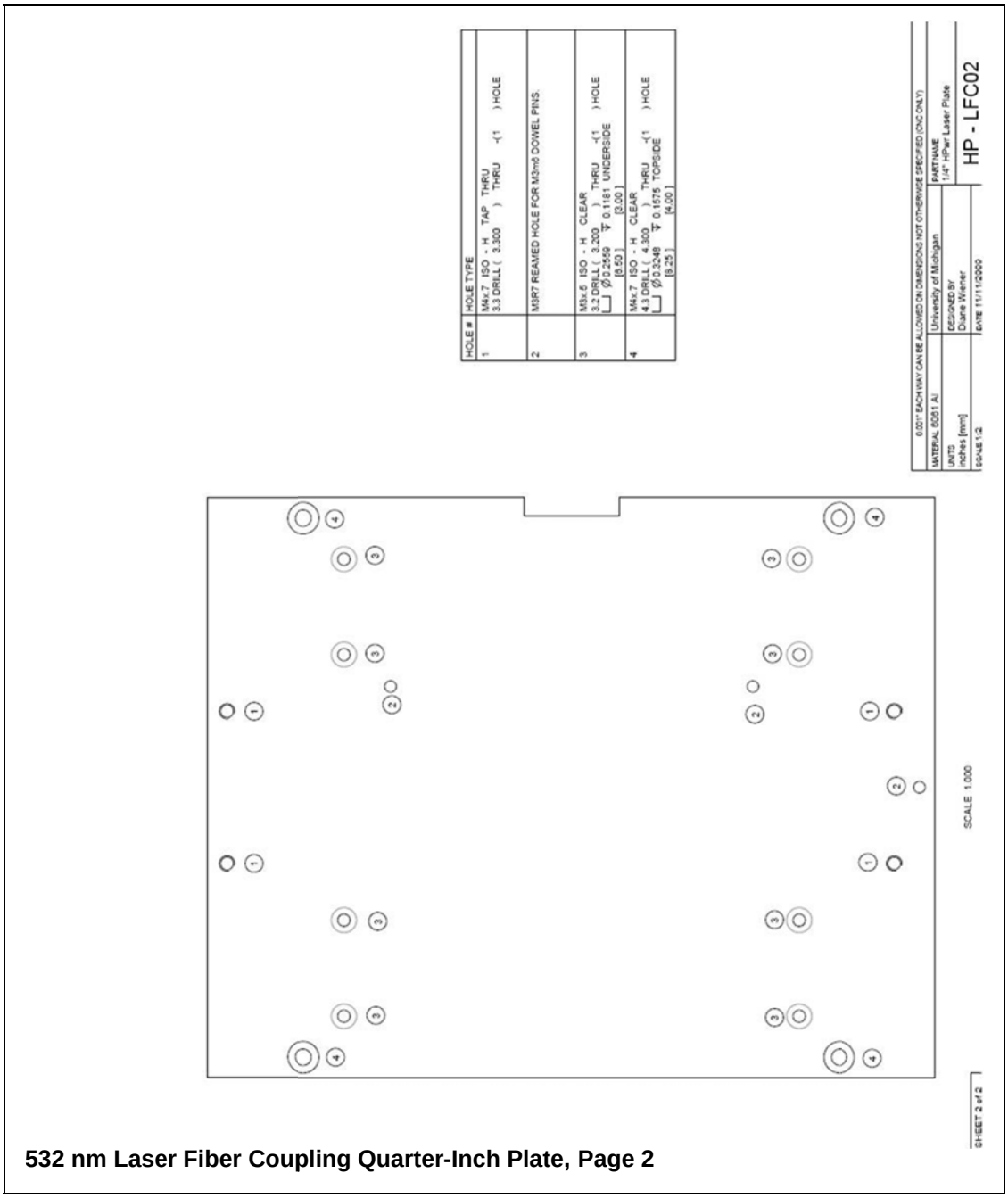


**532 nm Laser Fiber Coupling Quarter-Inch Plate, Page 2**

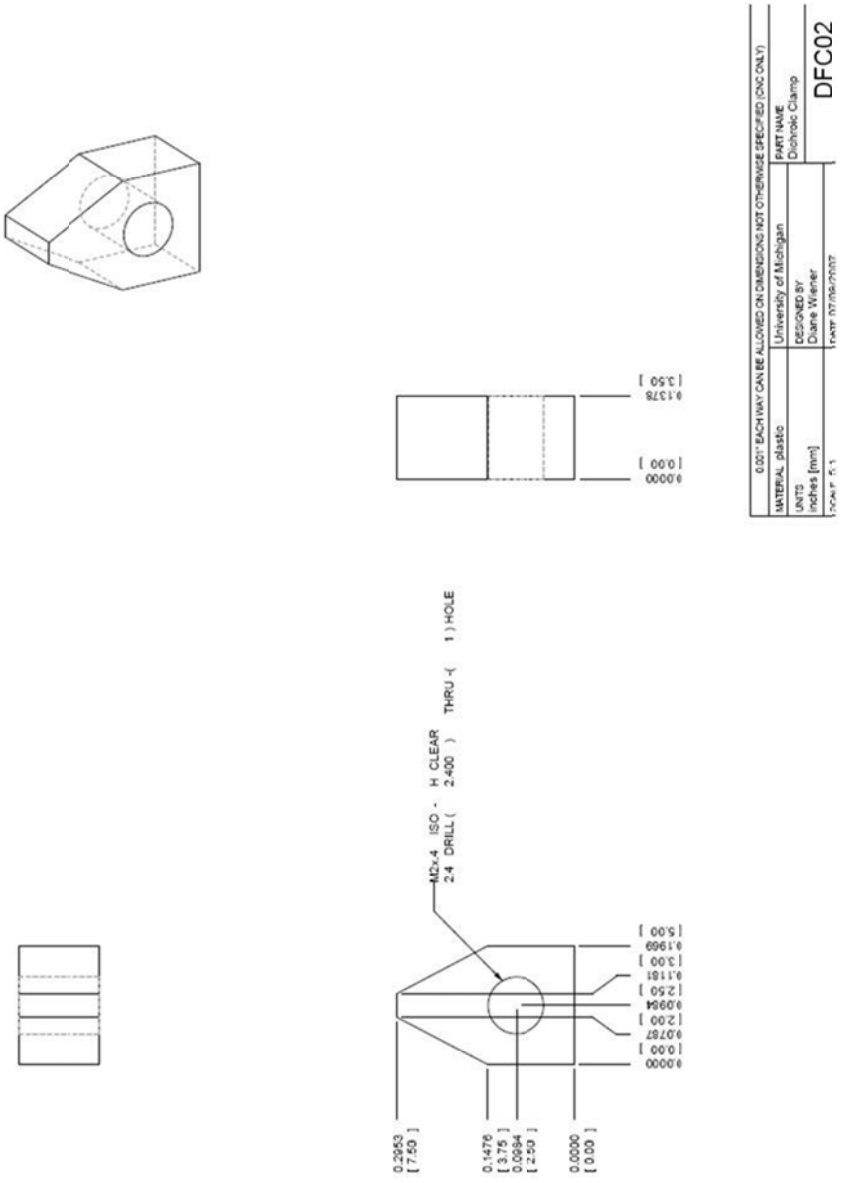


**Dichroic Fiber Coupling Dichroic Clamp**

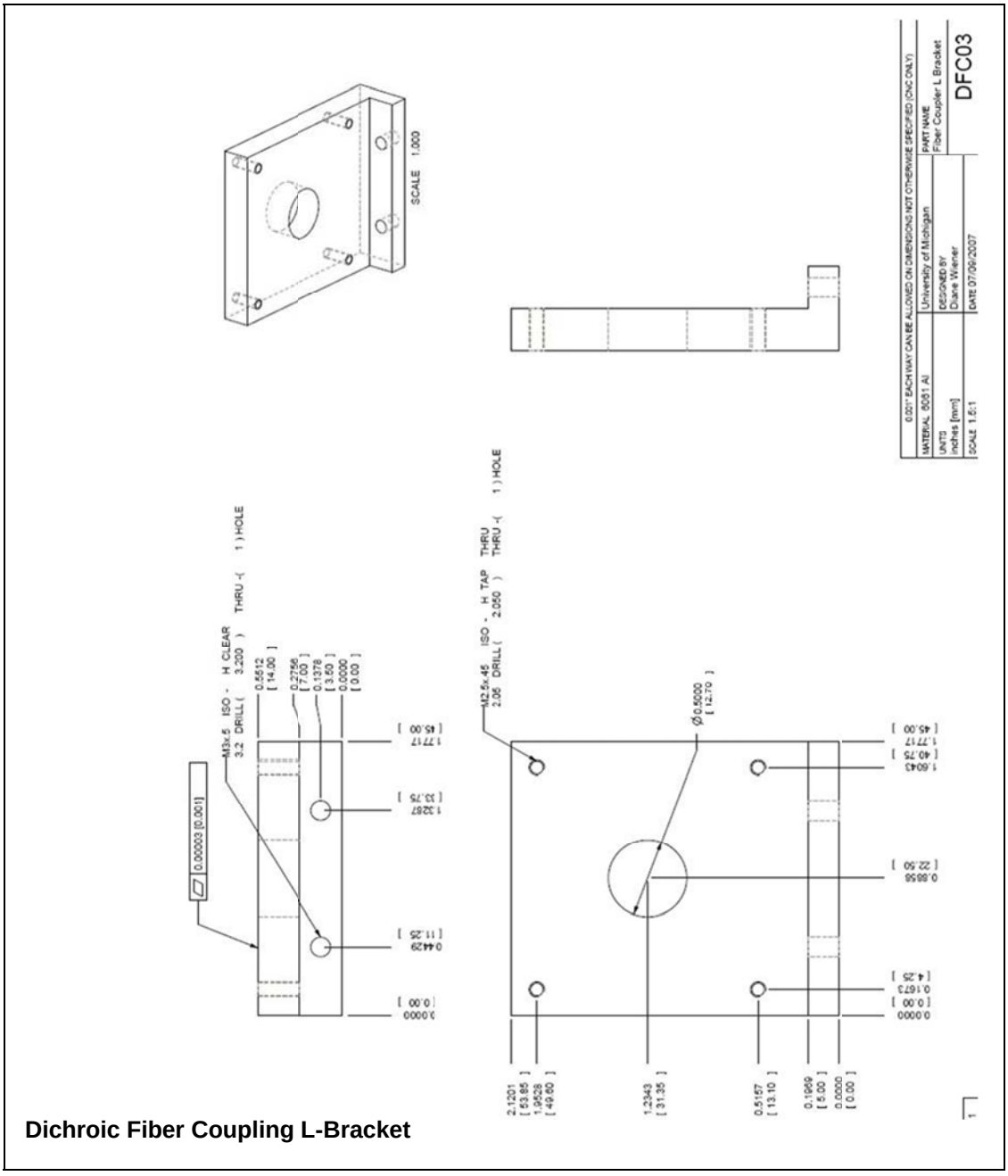


**Dichroic Fiber Coupling L-Bracket**

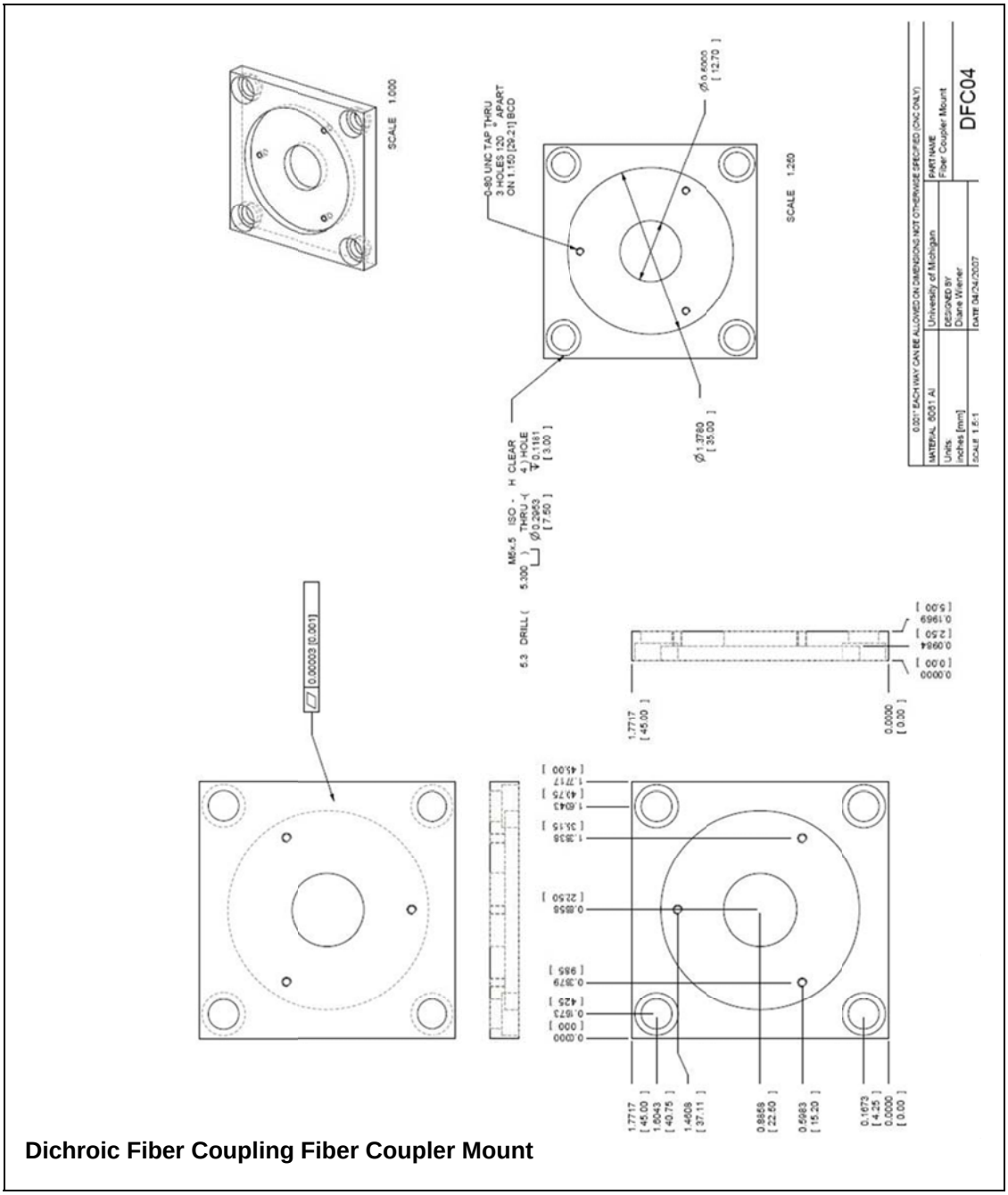


**Dichroic Fiber Coupling Fiber Coupler Mount**

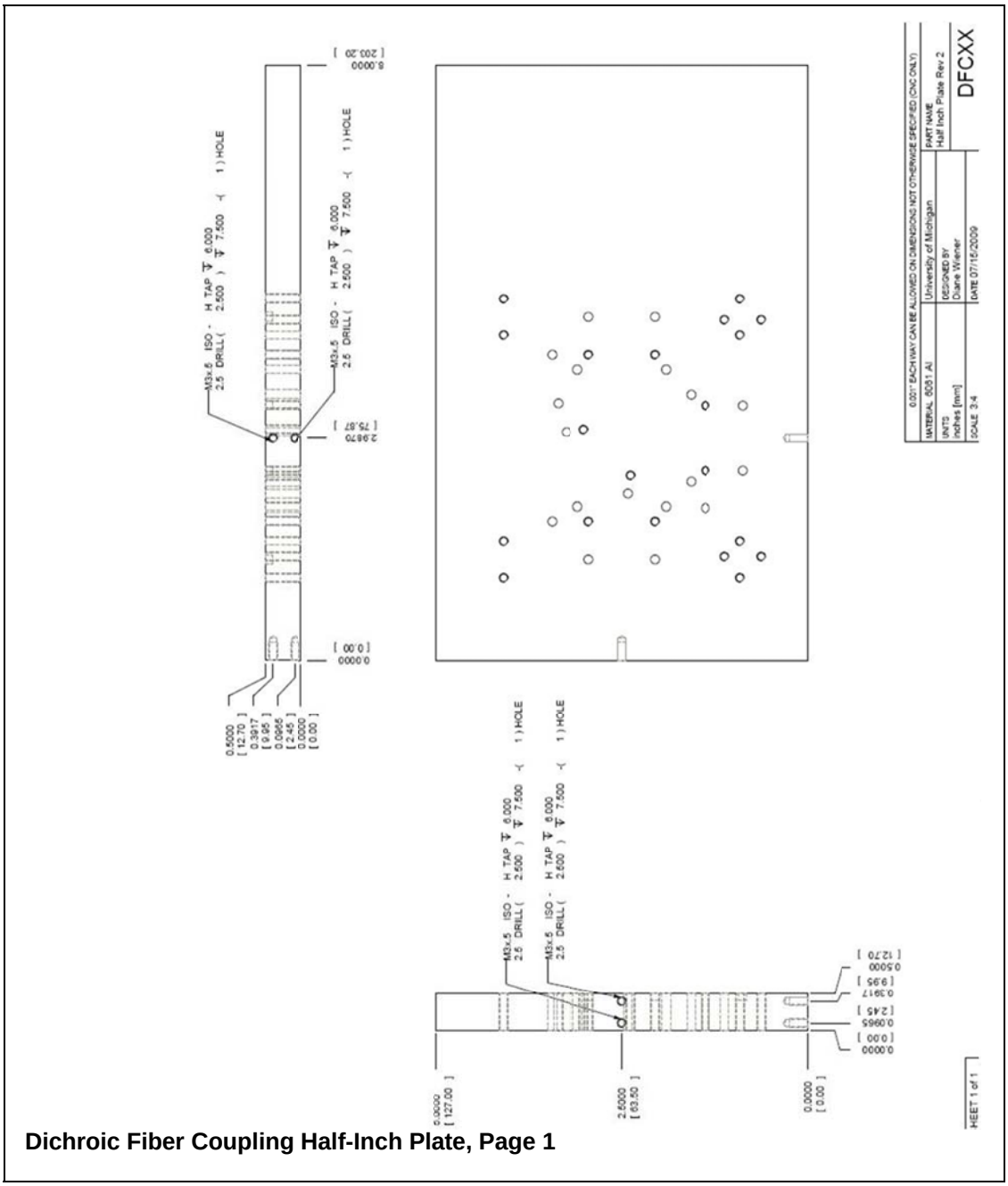


**Dichroic Fiber Coupling Half-Inch Plate, Page 1**

**Dichroic Fiber Coupling Half-Inch Plate, Page 2**

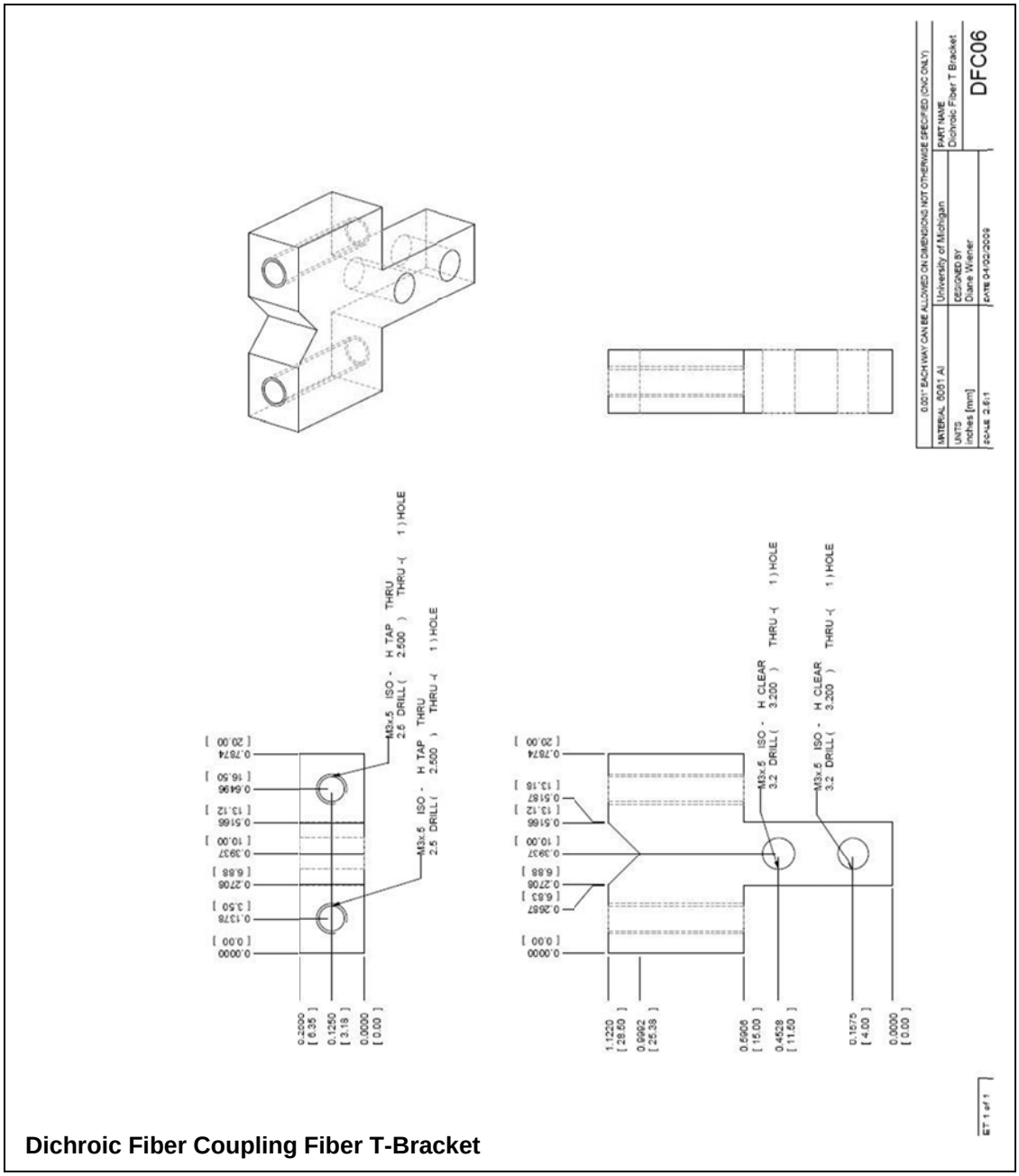


**Dichroic Fiber Coupling Fiber T-Bracket**

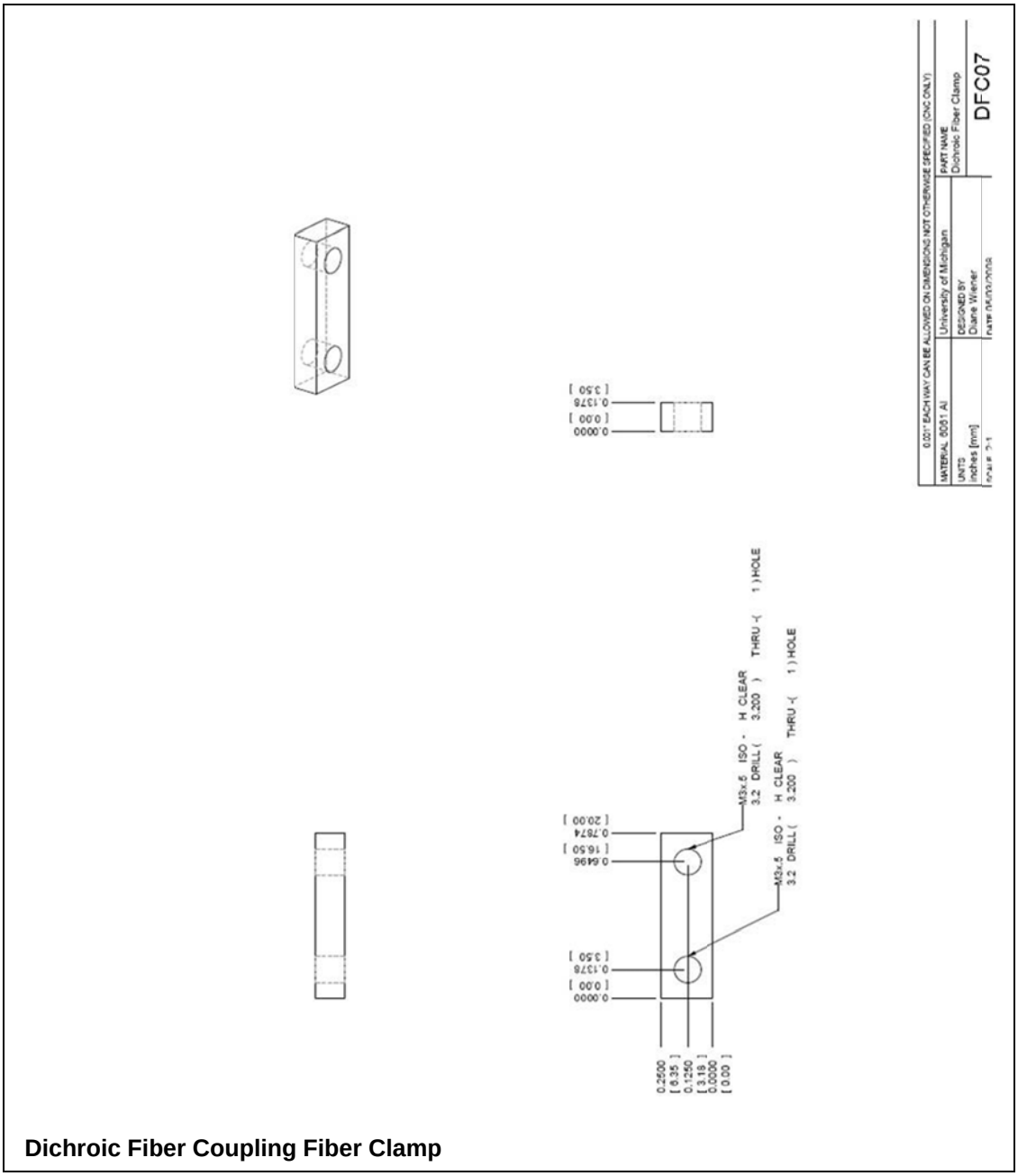


**Dichroic Fiber Coupling Fiber Clamp**

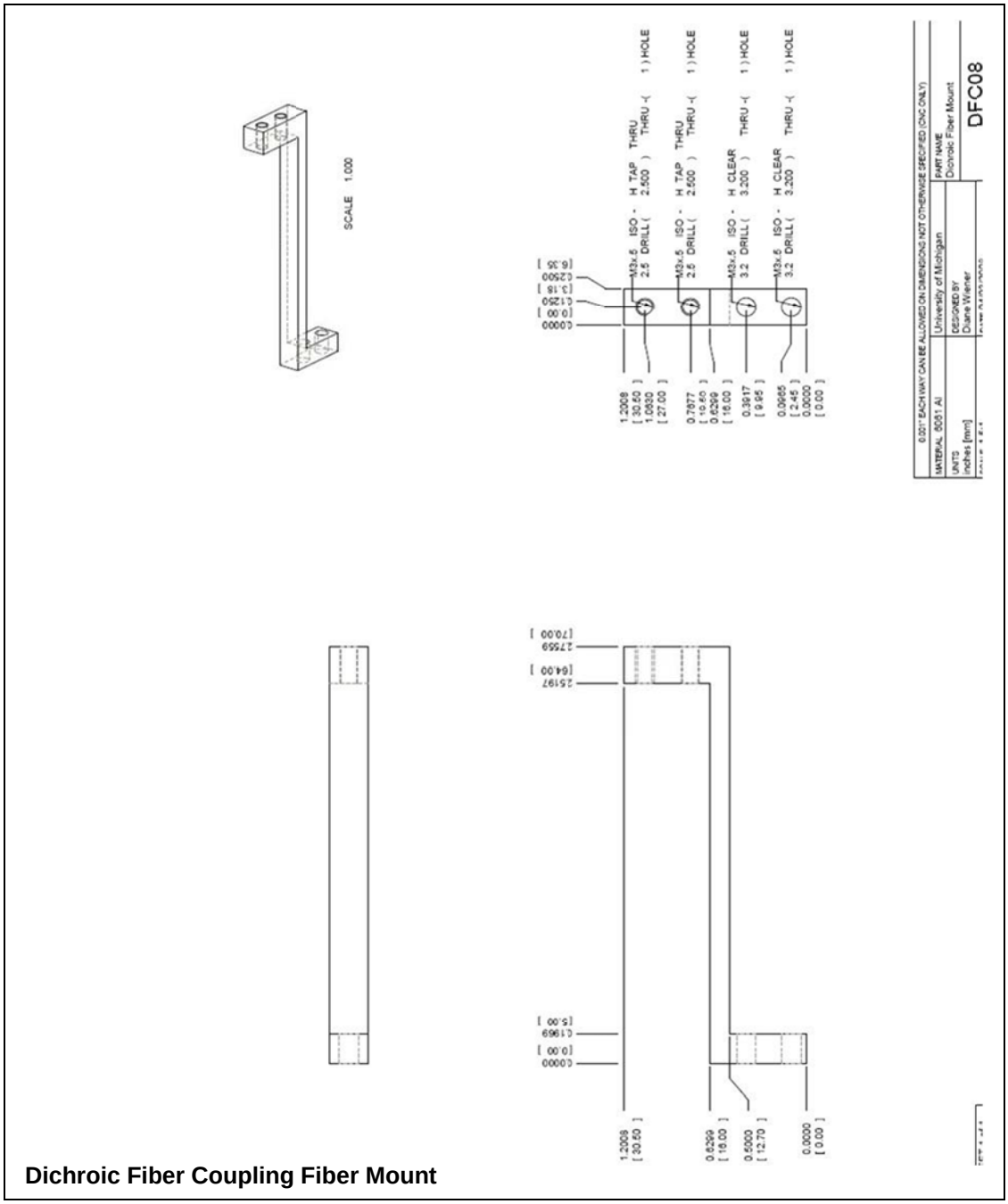


**Dichroic Fiber Coupling Fiber Mount**

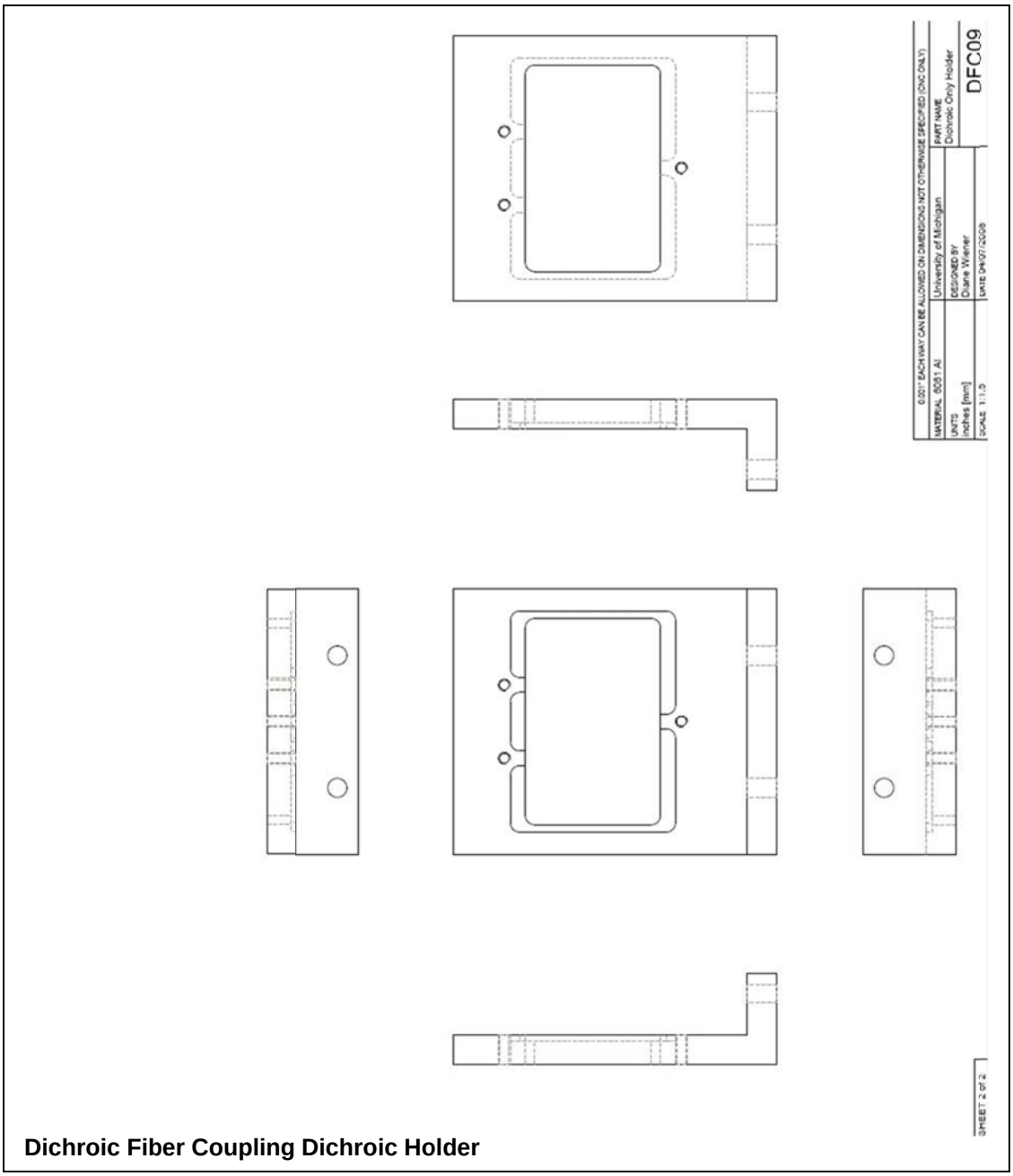


**Dichroic Fiber Coupling Dichroic Holder**

*3. T7 RNA Polymerase Binding Assay*

T7 RNA Polymerase assays were performed in two parallel steps: (1) incubating streptavidin gold nanoparticles with biotinylated T7 RNA polymerase (T7 RNAP), and (2) preparing the glass assay chamber and sequentially building up the surface to attain surface-bound gold nanoparticles conjugated to DNA molecules. The two steps are performed as follows:

Preparation for biotinylated-T7 RNAP-streptavidin gold nanoparticle conjugates:

1.) Prepare 10 µl of a 10x dilution of the stock Ted Pella streptavidin gold nanoparticles:
    i. 9 µl of 2 mM Tris·HCl buffer
    ii. 1 µl of Ted Pella streptavidin gold nanoparticles
2.) Freely diffusing gold nanoparticle final concentration is 11 pM.
3.) Stock T7 RNAP is ~1 µM.
4.) The final concentration with 1 µl of biotinylated T7 RNAP in 12.5 µl final volume is 80 nM.
5.) Incubate 1.841 µl of 10x diluted Ted Pella streptavidin 40 nm gold nanoparticles with 1 µl of biotinylated T7 RNAP and 3.409 µl Tris·HCl buffer.
6.) Incubate the solution for 15 minutes.
7.) Add 0.625 µl of 10 mg/ml biotin-free casein (0.5 mg/ml final concentration) and 0.625 µl of 10 mg/ml BSA (0.5 mg/ml final concentration) to the T7 RNAP-gold nanoparticle solution.

8.) Incubate the solution for 15 minutes.

9.) Just prior to addition into the assay chamber add 2.5 µl of 25 mM $MgCl_2$ in 2 mM Tris·HCl buffer and 2.5 µl of Tris·HCl buffer. Mix the total solution well.

Assay chamber build-up preparation, surface passivation, and streptavidin gold nanoparticle build-up:

1.) Prepare 30 µl of a 5.98 pM solution of Ted Pella streptavidin gold nanoparticles in 10 mM Tris, pH 7.0-8.0 and 40 mM NaCl (T40 buffer):
    i. Use 2.4 µl from a 10x diluted stock in 30 µl total volume (27.6 µl of T40 buffer.
    ii. Flush the chamber with 30 µl of the solution into the assay chamber.
    iii. Incubate for 2 minutes.
2.) Flush the chamber with 200 µl T40 buffer.
3.) Passivate the chamber surface with 100 µl of 0.1 mg/ml biotin-free casein, incubating for 15 minutes.
    i. 99 µl of T40 buffer
    ii. 1 µl of 10 mg/ml biotin-free casein
4.) Passivate the chamber surface with 100 µl of 0.1 mg/ml BSA (supplemented with 0.1 mg/ml biotin-free casein), incubating for 15 minutes.
    i. Prepare 128.8 µl of 0.1 mg/ml BSA and 0.1 mg/ml biotin-free casein solution. 28.8 µl of the solution will be used for the dsDNA dilution.

ii. 126.22 µl of T40 buffer

iii. 1.29 µl of 10 mg/ml BSA

iv. 1.29 µl of 10 mg/ml biotin-free casein

5.) Add the biotinylated dsDNA functionalized with biotin at a concentration of 40 nM in T40 buffer.

i. From the 1 µM working stock, dilute the DNA to the assay concentration of 40 nM.

ii. Use 1.2 µl from the 1 µM working DNA stock in 30 µl total.

iii. Dilute with 28.8 µl T40 buffer supplemented with 0.1 mg/ml BSA and 0.1 mg/ml biotin-free casein.

iv. Flush 30 µl of the working stock biotinylated dsDNA into the assay chamber.

v. Incubate for 20 minutes.

6.) Flush the chamber with 300 µl of 2 mM Tris·HCl buffer supplemented with 0.1 mg/ml biotin-free casein.

i. 294 µl of 2 mM Tris·HCl buffer

ii. 3 µl of 10 mg/ml stock biotin-free casein

iii. 3 µl of 10 mg/ml stock BSA

7.) Flush the chamber with the T7 RNAP-gold nanoparticle solution and seal.

8.) Visualize the chamber.

Biotinylated DNA sequences:

T7 Promoter sequence: includes the strong (class III) Φ10 bacteriophage T7 promoter sequence and 75 base pairs (non-template strand sequence):

5’-

AAGACTAATACGACTCACTATAGGGAGGAGGGAGAAGGACAAAGGAGACAA

GCCGACGGTGAACTTAACAGGATG-3’

UTP stalling sequence including the Φ10 bacteriophage T7 promoter sequence, UTP stall sites every 10 bases after the +14 stall site, and 75 base pairs (non-template strand sequence):

5’-

AAGACTAATACGACTCACTATAGGGAGCAGCGAGAATGACAAAGGATACAA

GCCGATGGAGAACAATACAGGCAG-3’

*4. Biotin-Neutravidin Gold Nanoparticle Binding Assays*

Biotin-neutravidin gold nanoparticle assays were performed in two parallel steps: (1) passivating the neutravidin gold nanoparticles, and (2) preparing the glass assay chamber and sequentially building up the surface to attain surface-bound biotin-gold nanoparticles. The two steps are performed as follows:

Preparation of NanoPartz neutravidin gold nanoparticle conjugates:

1.) The final neutravidin gold nanoparticle concentration is 55 pM.
2.) Incubate 3.54 µl of a 100x diluted NanoPartz neutravidin 40 nm gold nanoparticles with a premixed solution of 0.625 µl of 10 mg/ml biotin-free casein (0.5 mg/ml final concentration), 0.625 µl of 10 mg/ml BSA (0.5 mg/ml final concentration), and 7.71 µl of 10 mM Tris, pH 7.0-8.0 and 40 mM NaCl (T40 buffer).
3.) Incubate the solution for 30 minutes.

Assay chamber build-up preparation, surface passivation, and biotin gold nanoparticle build-up:

1.) Clean a standard glass slide.
2.) Spread a bead of vacuum grease along the width of the slide.
3.) Place 4x #0000 glass shards in the vacuum grease (nominal thickness 50 μm).
4.) Clean a 24 mm x 40 mm, #1 thickness glass cover slide.
5.) Place the long cover glass slide side perpendicular to the long glass slide side, creating a + -shaped, cross-flow assay chamber.
6.) Seal the two edges with nail polish.
7.) Prepare 30 μl of a 5.98 pM solution of NanoPartz biotin gold nanoparticles in 10 mM Tris, pH 7.0-8.0 and 40 mM NaCl (T40 buffer):
    i. Use 0.974 μl from a 100x diluted stock in 30 μl total volume (29.026 μl of T40 buffer.
    ii. Flush the chamber with 30 μl of the solution into the assay chamber.
    iii. Incubate for 2 minutes.
8.) Flush the chamber with 200 μl T40 buffer.
9.) Passivate the chamber surface with 100 μl of 0.1 mg/ml biotin-free casein, incubating for 15 minutes.
    i. 99 μl of T40 buffer
    ii. 1 μl of 10 mg/ml biotin-free casein

10.) Passivate the chamber surface with 100 µl of 0.1 mg/ml BSA (supplemented with 0.1 mg/ml biotin-free casein), incubating for 15 minutes.

i. 98 µl of T40 buffer

ii. 1 µl of 10 mg/ml BSA

iii. 1 µl of 10 mg/ml biotin-free casein

11.) Place the slide on the microscope.

12.) Record an image of the biotin gold nanoparticles on the surface.

13.) Place the droplet of the free neutravidin gold nanoparticles at the lip of the assay chamber.

14.) Visualize the chamber.

## REFERENCES


1. Selvin, P.R. and T. Ha, *Single-molecule techniques : a laboratory manual*. 2008, Cold Spring Harbor, N.Y.: Cold Spring Harbor Laboratory Press. vii, 507 p.
2. Weiss, S., *Fluorescence spectroscopy of single biomolecules.* Science, 1999. **283**(5408): p. 1676-83.
3. Weiss, S., *Measuring conformational dynamics of biomolecules by single molecule fluorescence spectroscopy.* Nature Structural Biology, 2000. **7**(9): p. 724-729.
4. Walter, N.G., et al., *Do-it-yourself guide: how to use the modern single-molecule toolkit.* Nature Methods, 2008. **5**(6): p. 475-489.
5. Bustamante, C., Z. Bryant, and S.B. Smith, *Ten years of tension: single-molecule DNA mechanics.* Nature, 2003. **421**(6921): p. 423-7.
6. Bustamante, C., et al., *Single-molecule studies of DNA mechanics.* Curr Opin Struct Biol, 2000. **10**(3): p. 279-85.
7. Mehta, A.D., et al., *Single-molecule biomechanics with optical methods.* Science, 1999. **283**(5408): p. 1689-95.
8. Greenleaf, W.J., M.T. Woodside, and S.M. Block, *High-resolution, single-molecule measurements of biomolecular motion.* Annu Rev Biophys Biomol Struct, 2007. **36**: p. 171-90.
9. Xie, X.S. and H.P. Lu, *Single-molecule enzymology.* Journal of Biological Chemistry, 1999. **274**(23): p. 15967-15970.
10. Lewin, B., *Genes IX*. 9th ed. 2008, Sudbury, Mass.: Jones and Bartlett Publishers. xvii, 892 p.
11. Alberts, B., J.H. Wilson, and T. Hunt, *Molecular biology of the cell*. 5th ed. 2008, New York: Garland Science. xxxiii, 1601, [90] p.
12. Calladine, C.R., et al., *Understanding DNA : the molecule & how it works*. 3rd ed. 2004, San Diego, CA: Elsevier Academic Press. 352.
13. Perez, A., et al., *Towards a molecular dynamics consensus view of B-DNA flexibility.* Nucleic Acids Res, 2008. **36**(7): p. 2379-94.
14. Perez, A., F.J. Luque, and M. Orozco, *Dynamics of B-DNA on the microsecond time scale.* J Am Chem Soc, 2007. **129**(47): p. 14739-45.
15. Spies, M.A. and R.L. Schowen, *The trapping of a spontaneously "flipped-out" base from double helical nucleic acids by host-guest complexation with beta-cyclodextrin: the intrinsic base-flipping rate constant for DNA and RNA.* J Am Chem Soc, 2002. **124**(47): p. 14049-53.
16. Pardi, A., et al., *Kinetics for exchange of imino protons in the d(C-G-C-G-A-A-T-T-C-G-C-G) double helix and in two similar helices that contain a G . T base pair, d(C-G-T-G-A-A-T-T-C-G-C-G), and an extra adenine, d(C-G-C-A-G-A-A-T-T-C-G-C-G).* Biochemistry, 1982. **21**(25): p. 6567-74.

17. Reinhard, B.M., et al., *Calibration of dynamic molecular rulers based on plasmon coupling between gold nanoparticles.* Nano Lett, 2005. **5**(11): p. 2246-52.
18. Sonnichsen, C., et al., *A molecular ruler based on plasmon coupling of single gold and silver nanoparticles.* Nat Biotechnol, 2005. **23**(6): p. 741-5.
19. Spencer, M., *Fundamentals of light microscopy*. IUPAB biophysics series. 1982, Cambridge [Cambridgeshire] ; New York: Cambridge University Press. x, 93 p.
20. Hecht, E., *Optics*. 4th ed. 2002, Reading, Mass.: Addison-Wesley. vi, 698 p.
21. Yildiz, A., et al., *Myosin V walks hand-over-hand: single fluorophore imaging with 1.5-nm localization.* Science, 2003. **300**(5628): p. 2061-5.
22. Churchman, L.S., et al., *Single molecule high-resolution colocalization of Cy3 and Cy5 attached to macromolecules measures intramolecular distances through time.* Proc Natl Acad Sci U S A, 2005. **102**(5): p. 1419-23.
23. Gelles, J., B.J. Schnapp, and M.P. Sheetz, *Tracking kinesin-driven movements with nanometre-scale precision.* Nature, 1988. **331**(6155): p. 450-3.
24. Schafer, D.A., et al., *Transcription by Single Molecules of Rna-Polymerase Observed by Light-Microscopy.* Nature, 1991. **352**(6334): p. 444-448.
25. Lakowicz, J.R., *Principles of fluorescence spectroscopy*. 3rd ed. 2006, New York: Springer. xxvi, 954 p.
26. Roy, R., S. Hohng, and T. Ha, *A practical guide to single-molecule FRET.* Nat Methods, 2008. **5**(6): p. 507-16.
27. Jares-Erijman, E.A. and T.M. Jovin, *FRET imaging.* Nat Biotechnol, 2003. **21**(11): p. 1387-95.
28. Ha, T., et al., *Probing the interaction between two single molecules: fluorescence resonance energy transfer between a single donor and a single acceptor.* Proc Natl Acad Sci U S A, 1996. **93**(13): p. 6264-8.
29. Verbrugge, S., et al., *Alternating-site mechanism of kinesin-1 characterized by single-molecule FRET using fluorescent ATP analogues.* Biophys J, 2009. **97**(1): p. 173-82.
30. Zhuang, X., et al., *Correlating structural dynamics and function in single ribozyme molecules.* Science, 2002. **296**(5572): p. 1473-6.
31. Mori, T., R.D. Vale, and M. Tomishige, *How kinesin waits between steps.* Nature, 2007. **450**(7170): p. 750-4.
32. Kuznetsov, S.V., et al., *Direct observation of DNA bending/unbending kinetics in complex with DNA-bending protein IHF.* Proc Natl Acad Sci U S A, 2006. **103**(49): p. 18515-20.
33. Yuan, C., et al., *Spontaneous sharp bending of DNA: role of melting bubbles.* Nucleic Acids Res, 2006. **34**(16): p. 4554-60.
34. Shroff, H., et al., *Biocompatible force sensor with optical readout and dimensions of 6 nm3.* Nano Lett, 2005. **5**(7): p. 1509-14.

35. Shroff, H., et al., *Optical measurement of mechanical forces inside short DNA loops.* Biophys J, 2008. **94**(6): p. 2179-86.
36. Ross, J., et al., *Multicolor single-molecule spectroscopy with alternating laser excitation for the investigation of interactions and dynamics.* J Phys Chem B, 2007. **111**(2): p. 321-6.
37. Edelman, L.M., R. Cheong, and J.D. Kahn, *Fluorescence resonance energy transfer over approximately 130 basepairs in hyperstable lac repressor-DNA loops.* Biophys J, 2003. **84**(2 Pt 1): p. 1131-45.
38. Myong, S., et al., *Repetitive shuttling of a motor protein on DNA.* Nature, 2005. **437**(7063): p. 1321-5.
39. Katiliene, Z., E. Katilius, and N.W. Woodbury, *Single molecule detection of DNA looping by NgoMIV restriction endonuclease.* Biophys J, 2003. **84**(6): p. 4053-61.
40. Coban, O., et al., *Conformational heterogeneity in RNA polymerase observed by single-pair FRET microscopy.* Biophys J, 2006. **90**(12): p. 4605-17.
41. Donnert, G., C. Eggeling, and S.W. Hell, *Major signal increase in fluorescence microscopy through dark-state relaxation.* Nat Methods, 2007. **4**(1): p. 81-86.
42. Smith, S.B., L. Finzi, and C. Bustamante, *Direct mechanical measurements of the elasticity of single DNA molecules by using magnetic beads.* Science, 1992. **258**(5085): p. 1122-6.
43. Strick, T.R., et al., *The elasticity of a single supercoiled DNA molecule.* Science, 1996. **271**(5257): p. 1835-7.
44. Sacconi, L., et al., *Three-dimensional magneto-optic trap for micro-object manipulation.* Opt Lett, 2001. **26**(17): p. 1359-61.
45. Ashkin, A., *Applications of Laser Radiation Pressure.* Science, 1980. **210**(4474): p. 1081-1088.
46. Abbondanzieri, E.A., et al., *Direct observation of base-pair stepping by RNA polymerase.* Nature, 2005. **438**(7067): p. 460-5.
47. Vologodskii, A., *Determining protein-induced DNA bending in force-extension experiments: theoretical analysis.* Biophys J, 2009. **96**(9): p. 3591-9.
48. Vanzi, F., et al., *Lac repressor hinge flexibility and DNA looping: single molecule kinetics by tethered particle motion.* Nucleic Acids Res, 2006. **34**(12): p. 3409-20.
49. Pouget, N., et al., *Single-particle tracking for DNA tether length monitoring.* Nucleic Acids Res, 2004. **32**(9): p. e73.
50. Brinkers, S., et al., *The persistence length of double stranded DNA determined using dark field tethered particle motion.* J Chem Phys, 2009. **130**(21): p. 215105.
51. Yuan, C., et al., *DNA bending stiffness on small length scales.* Phys Rev Lett, 2008. **100**(1): p. 018102.
52. Mathew-Fenn, R.S., R. Das, and P.A. Harbury, *Remeasuring the double helix.* Science, 2008. **322**(5900): p. 446-9.

53. Mathew-Fenn, R.S., et al., *A molecular ruler for measuring quantitative distance distributions.* PLoS ONE, 2008. **3**(10): p. e3229.
54. Okonogi, T.M., et al., *Sequence-dependent dynamics of duplex DNA: the applicability of a dinucleotide model.* Biophys J, 2002. **83**(6): p. 3446-59.
55. Okonogi, T.M., et al., *Flexibility of duplex DNA on the submicrosecond timescale.* Biophys J, 1999. **77**(6): p. 3256-76.
56. Rice, S., et al., *A structural change in the kinesin motor protein that drives motility.* Nature, 1999. **402**(6763): p. 778-84.
57. Homola, J., S.S. Yee, and G. Gauglitz, *Surface plasmon resonance sensors: review.* Sensors and Actuators B-Chemical, 1999. **54**(1-2): p. 3-15.
58. Dunn, A.R. and J.A. Spudich, *Dynamics of the unbound head during myosin V processive translocation.* Nat Struct Mol Biol, 2007. **14**(3): p. 246-8.
59. Nan, X., P.A. Sims, and X.S. Xie, *Organelle tracking in a living cell with microsecond time resolution and nanometer spatial precision.* Chemphyschem, 2008. **9**(5): p. 707-12.
60. Yasuda, R., et al., *Resolution of distinct rotational substeps by submillisecond kinetic analysis of F1-ATPase.* Nature, 2001. **410**(6831): p. 898-904.
61. Yang, Y.H. and J.M. Nam, *Single nanoparticle tracking-based detection of membrane receptor-ligand interactions.* Anal Chem, 2009. **81**(7): p. 2564-8.
62. Spetzler, D., et al., *Single molecule measurements of F1-ATPase reveal an interdependence between the power stroke and the dwell duration.* Biochemistry, 2009. **48**(33): p. 7979-85.
63. Ueno, H., et al., *Simple dark-field microscopy with nanometer spatial precision and microsecond temporal resolution.* Biophys J, 2010. **98**(9): p. 2014-23.
64. Yguerabide, J. and E.E. Yguerabide, *Light-scattering submicroscopic particles as highly fluorescent analogs and their use as tracer labels in clinical and biological applications.* Anal Biochem, 1998. **262**(2): p. 137-56.
65. Baciu, C.L., et al., *Protein-membrane interaction probed by single plasmonic nanoparticles.* Nano Lett, 2008. **8**(6): p. 1724-8.
66. Elghanian, R., et al., *Selective colorimetric detection of polynucleotides based on the distance-dependent optical properties of gold nanoparticles.* Science, 1997. **277**(5329): p. 1078-81.
67. El-Sayed, I.H., X.H. Huang, and M.A. El-Sayed, *Surface plasmon resonance scattering and absorption of anti-EGFR antibody conjugated gold nanoparticles in cancer diagnostics: Applications in oral cancer.* Nano Letters, 2005. **5**(5): p. 829-834.
68. Haes, A.J. and R.P. Van Duyne, *A nanoscale optical biosensor: sensitivity and selectivity of an approach based on the localized surface plasmon resonance spectroscopy of triangular silver nanoparticles.* J Am Chem Soc, 2002. **124**(35): p. 10596-604.

69. Malicka, J., et al., *DNA hybridization using surface plasmon-coupled emission.* Anal Chem, 2003. **75**(23): p. 6629-33.
70. Maxwell, D.J., J.R. Taylor, and S. Nie, *Self-assembled nanoparticle probes for recognition and detection of biomolecules.* J Am Chem Soc, 2002. **124**(32): p. 9606-12.
71. McFarland, A.D. and R.P. Van Duyne, *Single silver nanoparticles as real-time optical sensors with zeptomole sensitivity.* Nano Letters, 2003. **3**(8): p. 1057-1062.
72. Nam, J.M., C.S. Thaxton, and C.A. Mirkin, *Nanoparticle-based bio-bar codes for the ultrasensitive detection of proteins.* Science, 2003. **301**(5641): p. 1884-6.
73. Prigodich, A.E., et al., *Nano-flares for mRNA regulation and detection.* ACS Nano, 2009. **3**(8): p. 2147-52.
74. Raschke, G., et al., *Biomolecular recognition based on single gold nanoparticle light scattering.* Nano Letters, 2003. **3**(7): p. 935-938.
75. Nusz, G.J., et al., *Label-free plasmonic detection of biomolecular binding by a single gold nanorod.* Analytical Chemistry, 2008. **80**(4): p. 984-9.
76. Aslan, K., C.C. Luhrs, and V.H. Perez-Luna, *Controlled and reversible aggregation of biotinylated gold nanoparticles with streptavidin.* Journal of Physical Chemistry B, 2004. **108**(40): p. 15631-15639.
77. Kreibig, U. and M. Vollmer, *Optical properties of metal clusters*. 1995, Berlin ; New York: Springer. xx, 532 p.
78. Mulvaney, P., *Not all that's gold does glitter.* Mrs Bulletin, 2001. **26**(12): p. 1009-1014.
79. Sepulveda, B., et al., *LSPR-based nanobiosensors.* Nano Today, 2009. **4**(3): p. 244-251.
80. Yguerabide, J. and E.E. Yguerabide, *Light-scattering submicroscopic particles as highly fluorescent analogs and their use as tracer labels in clinical and biological applications.* Anal Biochem, 1998. **262**(2): p. 157-76.
81. Jain, P.K., et al., *Noble metals on the nanoscale: optical and photothermal properties and some applications in imaging, sensing, biology, and medicine.* Acc Chem Res, 2008. **41**(12): p. 1578-86.
82. Jain, P.K., et al., *Calculated absorption and scattering properties of gold nanoparticles of different size, shape, and composition: Applications in biological imaging and biomedicine.* Journal of Physical Chemistry B, 2006. **110**(14): p. 7238-7248.
83. Kelly, K.L., et al., *The optical properties of metal nanoparticles: The influence of size, shape, and dielectric environment.* Journal of Physical Chemistry B, 2003. **107**(3): p. 668-677.
84. El-Sayed, M.A., *Some interesting properties of metals confined in time and nanometer space of different shapes.* Acc Chem Res, 2001. **34**(4): p. 257-64.
85. Mulvaney, P., *Surface plasmon spectroscopy of nanosized metal particles.* Langmuir, 1996. **12**(3): p. 788-800.
86. Myroshnychenko, V., et al., *Modelling the optical response of gold nanoparticles.* Chemical Society Reviews, 2008. **37**(9): p. 1792-1805.

87. Oldenburg, S.J., et al., *Nanoengineering of optical resonances.* Chemical Physics Letters, 1998. **288**(2-4): p. 243-247.
88. Rong, G., H. Wang, and B.M. Reinhard, *Insights from a nanoparticle minuet: two-dimensional membrane profiling through silver plasmon ruler tracking.* Nano Lett, 2010. **10**(1): p. 230-8.
89. Liz-Marzan, L.M., *Tailoring surface plasmons through the morphology and assembly of metal nanoparticles.* Langmuir, 2006. **22**(1): p. 32-41.
90. Tan, S.J., et al., *Building plasmonic nanostructures with DNA.* Nat Nanotechnol, 2011. **6**(5): p. 268-276.
91. Link, S., M.B. Mohamed, and M.A. El-Sayed, *Simulation of the optical absorption spectra of gold nanorods as a function of their aspect ratio and the effect of the medium dielectric constant.* Journal of Physical Chemistry B, 1999. **103**(16): p. 3073-3077.
92. Schmucker, A.L., et al., *Correlating Nanorod Structure with Experimentally Measured and Theoretically Predicted Surface Plasmon Resonance.* Acs Nano, 2010. **4**(9): p. 5453-5463.
93. Slaughter, L.S., et al., *Single-Particle Spectroscopy of Gold Nanorods beyond the Quasi-Static Limit: Varying the Width at Constant Aspect Ratio.* Journal of Physical Chemistry C, 2010. **114**(11): p. 4934-4938.
94. Brioude, A., X.C. Jiang, and M.P. Pileni, *Optical properties of gold nanorods: DDA simulations supported by experiments.* Journal of Physical Chemistry B, 2005. **109**(27): p. 13138-13142.
95. Yu, Y.Y., et al., *Gold nanorods: Electrochemical synthesis and optical properties.* Journal of Physical Chemistry B, 1997. **101**(34): p. 6661-6664.
96. Jain, P.K. and M.A. El-Sayed, *Noble Metal Nanoparticle Pairs: Effect of Medium for Enhanced Nanosensing.* Nano Letters, 2008. **8**(12): p. 4347-4352.
97. Rechberger, W., et al., *Optical properties of two interacting gold nanoparticles.* Optics Communications, 2003. **220**(1-3): p. 137-141.
98. Su, K.H., et al., *Interparticle coupling effects on plasmon resonances of nanogold particles.* Nano Letters, 2003. **3**(8): p. 1087-1090.
99. Frens, G., *Particle-Size and Sol Stability in Metal Colloids.* Kolloid-Zeitschrift and Zeitschrift Fur Polymere, 1972. **250**(7): p. 736-&.
100. Frens, G., *Controlled Nucleation for Regulation of Particle-Size in Monodisperse Gold Suspensions.* Nature-Physical Science, 1973. **241**(105): p. 20-22.
101. Hansen, P.M., et al., *Expanding the optical trapping range of gold nanoparticles.* Nano Letters, 2005. **5**(10): p. 1937-1942.
102. Loweth, C.J., et al., *DNA-based assembly of gold nanocrystals.* Angewandte Chemie-International Edition, 1999. **38**(12): p. 1808-1812.
103. Mirkin, C.A., et al., *A DNA-based method for rationally assembling nanoparticles into macroscopic materials.* Nature, 1996. **382**(6592): p. 607-609.
104. Slaughter, L., W.S. Chang, and S. Link, *Characterizing Plasmons in Nanoparticles and Their Assemblies with Single Particle Spectroscopy.* Journal of Physical Chemistry Letters, 2011. **2**(16): p. 2015-2023.

105. Busson, M.P., et al., *Optical and topological characterization of gold nanoparticle dimers linked by a single DNA double strand.* Nano Lett, 2011. **11**(11): p. 5060-5.
106. Braslavsky, I., et al., *Objective-type dark-field illumination for scattering from microbeads.* Applied Optics, 2001. **40**(31): p. 5650-5657.
107. Mock, J.J., et al., *Distance-dependent plasmon resonant coupling between a gold nanoparticle and gold film.* Nano Letters, 2008. **8**(8): p. 2245-2252.
108. Sonnichsen, C., et al., *Spectroscopy of single metallic nanoparticles using total internal reflection microscopy.* Applied Physics Letters, 2000. **77**(19): p. 2949-2951.
109. Wei, Q.H., et al., *Plasmon resonance of finite one-dimensional Au nanoparticle chains.* Nano Letters, 2004. **4**(6): p. 1067-1071.
110. Liu, G.L., et al., *A nanoplasmonic molecular ruler for measuring nuclease activity and DNA footprinting.* Nature Nanotechnology, 2006. **1**(1): p. 47-52.
111. Smith, S.B., Y. Cui, and C. Bustamante, *Overstretching B-DNA: the elastic response of individual double-stranded and single-stranded DNA molecules.* Science, 1996. **271**(5250): p. 795-9.
112. Wang, M.D., et al., *Stretching DNA with optical tweezers.* Biophys J, 1997. **72**(3): p. 1335-46.
113. Baumann, C.G., et al., *Ionic effects on the elasticity of single DNA molecules.* Proc Natl Acad Sci U S A, 1997. **94**(12): p. 6185-90.
114. Bouchiat, C., et al., *Estimating the persistence length of a worm-like chain molecule from force-extension measurements.* Biophys J, 1999. **76**(1 Pt 1): p. 409-13.
115. Bustamante, C., et al., *Entropic elasticity of lambda-phage DNA.* Science, 1994. **265**(5178): p. 1599-600.
116. Cluzel, P., et al., *DNA: an extensible molecule.* Science, 1996. **271**(5250): p. 792-4.
117. Marko, J.F. and E.D. Siggia, *Stretching DNA.* Macromolecules, 1995. **28**(26): p. 8759-8770.
118. Seol, Y., et al., *Elasticity of Short DNA Molecules: Theory and Experiment for Contour Lengths of 0.6 7 {micro}m.* Biophys J, 2007. **93**(12): p. 4360-73.
119. Williams, M.C., et al., *Effect of pH on the overstretching transition of double-stranded DNA: evidence of force-induced DNA melting.* Biophys J, 2001. **80**(2): p. 874-81.
120. Reinhard, B.M., et al., *Use of plasmon coupling to reveal the dynamics of DNA bending and cleavage by single EcoRV restriction enzymes.* Proc Natl Acad Sci U S A, 2007. **104**(8): p. 2667-72.
121. Rong, G., et al., *Resolving sub-diffraction limit encounters in nanoparticle tracking using live cell plasmon coupling microscopy.* Nano Lett, 2008. **8**(10): p. 3386-93.
122. Wang, H.Y. and B.M. Reinhard, *Monitoring Simultaneous Distance and Orientation Changes in Discrete Dimers of DNA Linked Gold*

*Nanoparticles.* Journal of Physical Chemistry C, 2009. **113**(26): p. 11215-11222.
123. Grecco, H.E. and O.E. Martínez, *Experimental determination of distance and orientation of metallic nanodimers by polarization dependent plasmon coupling*. 2011. 2011.
124. Kapoor, V., et al., *New lasers for flow cytometry: filling the gaps.* Nat Methods, 2007. **4**(9): p. 678-679.
125. Skewis, L.R. and B.M. Reinhard, *Spermidine Modulated Ribonuclease Activity Probed by RNA Plasmon Rulers.* Nano Lett, 2007.
126. Axelrod, D., E. Hellen, and R. Fulbright, *Total Internal Reflection Fluorescence*
*Topics in Fluorescence Spectroscopy*, J. Lakowicz, Editor. 2002, Springer US. p. 289-343.
127. Sund, S.E., J.A. Swanson, and D. Axelrod, *Cell membrane orientation visualized by polarized total internal reflection fluorescence.* Biophysical Journal, 1999. **77**(4): p. 2266-2283.
128. Novotny, L. and B. Hecht, *Principles of nano-optics*. 2006, Cambridge ; New York: Cambridge University Press. xvii, 539 p.
129. Xiao, L.H., et al., *Imaging Translational and Rotational Diffusion of Single Anisotropic Nanoparticles with Planar Illumination Microscopy.* J Am Chem Soc, 2011. **133**(27): p. 10638-10645.
130. Cai, D., K.J. Verhey, and E. Meyhofer, *Tracking single Kinesin molecules in the cytoplasm of mammalian cells.* Biophys J, 2007. **92**(12): p. 4137-44.
131. Jain, P.K., et al., *Review of some interesting surface plasmon resonance-enhanced properties of noble metal nanoparticles and their applications to biosystems.* Plasmonics, 2007. **2**(3): p. 107-118.
132. Parak, W.J., et al., *Biological applications of colloidal nanocrystals.* Nanotechnology, 2003. **14**(7): p. R15-R27.
133. Lee, J.S., et al., *Silver nanoparticle-oligonucleotide conjugates based on DNA with triple cyclic disulfide moieties.* Nano Letters, 2007. **7**(7): p. 2112-2115.
134. Doty, R.C., et al., *Extremely stable water-soluble Ag nanoparticles.* Chemistry of Materials, 2005. **17**(18): p. 4630-4635.
135. Skewis, L.R. and B.M. Reinhard, *Control of Colloid Surface Chemistry through Matrix Confinement: Facile Preparation of Stable Antibody Functionalized Silver Nanoparticles.* Acs Applied Materials & Interfaces, 2010. **2**(1): p. 35-40.
136. Jain, P.K., W.Y. Huang, and M.A. El-Sayed, *On the universal scaling behavior of the distance decay of plasmon coupling in metal nanoparticle pairs: A plasmon ruler equation.* Nano Letters, 2007. **7**(7): p. 2080-2088.
137. Mock, J.J., et al., *Shape effects in plasmon resonance of individual colloidal silver nanoparticles.* Journal of Chemical Physics, 2002. **116**(15): p. 6755-6759.
138. Grecco, H.E. and O.E. Martinez, *Distance and orientation measurement in the nanometric scale based on polarization anisotropy of metallic dimers.* Opt Express, 2006. **14**(19): p. 8716-8721.

139. Hurst, S.J., A.K. Lytton-Jean, and C.A. Mirkin, *Maximizing DNA loading on a range of gold nanoparticle sizes.* Anal Chem, 2006. **78**(24): p. 8313-8.
140. Claridge, S.A., et al., *Directed assembly of discrete gold nanoparticle groupings using branched DNA scaffolds.* Chemistry of Materials, 2005. **17**(7): p. 1628-1635.
141. Claridge, S.A., et al., *Isolation of discrete nanoparticle-DNA conjugates for plasmonic applications.* Nano Lett, 2008. **8**(4): p. 1202-6.
142. Zanchet, D., et al., *Electrophoretic isolation of discrete Au nanocrystal/DNA conjugates.* Nano Letters, 2001. **1**(1): p. 32-35.
143. Li, Z., et al., *Multiple thiol-anchor capped DNA-gold nanoparticle conjugates.* Nucleic Acids Res, 2002. **30**(7): p. 1558-62.
144. Zheng, M., F. Davidson, and X. Huang, *Ethylene glycol monolayer protected nanoparticles for eliminating nonspecific binding with biological molecules.* J Am Chem Soc, 2003. **125**(26): p. 7790-1.
145. Robinson, D.B., et al., *Stabilization of Nanoparticles Under Biological Assembly Conditions Using Peptoids.* Biopolymers, 2011. **96**(5): p. 669-678.
146. Stakenborg, T., et al., *Increasing the stability of DNA-functionalized gold nanoparticles using mercaptoalkanes.* Journal of Nanoparticle Research, 2008. **10**: p. 143-152.
147. Muhlpfordt, H., *The Preparation of Colloidal Gold Particles Using Tannic-Acid as an Additional Reducing Agent.* Experientia, 1982. **38**(9): p. 1127-1128.
148. Park, S.Y., et al., *DNA-programmable nanoparticle crystallization.* Nature, 2008. **451**(7178): p. 553-6.
149. Claridge, S.A., et al., *Enzymatic ligation creates discrete multinanoparticle building blocks for self-assembly.* J Am Chem Soc, 2008. **130**(29): p. 9598-9605.
150. Marhaba, S., et al., *Surface Plasmon Resonance of Single Gold Nanodimers near the Conductive Contact Limit.* Journal of Physical Chemistry C, 2009. **113**(11): p. 4349-4356.
151. Reinhard, B.M., et al., *Plasmon Rulers as Dynamic Molecular Rulers in Enzymology.* Methods in Enzymology, Vol 475: Single Molecule Tools, Pt B, 2010. **474**: p. 175-198.
152. Yang, J., J.Y. Lee, and H.P. Too, *Size sorting of Au and Pt nanoparticles from arbitrary particle size distributions.* Analytica Chimica Acta, 2005. **546**(2): p. 133-138.
153. Parak, W.J., et al., *Conformation of oligonucleotides attached to gold nanocrystals probed by gel electrophoresis.* Nano Letters, 2003. **3**(1): p. 33-36.
154. Skewis, L.R. and B.M. Reinhard, *Spermidine modulated ribonuclease activity probed by RNA plasmon rulers.* Nano Lett, 2008. **8**(1): p. 214-20.
155. Chen, Y., et al., *Enhanced stability and bioconjugation of photo-cross-linked polystyrene-shell, au-core nanoparticles.* Langmuir, 2007. **23**(14): p. 7491-7497.

156. Kang, Y.J. and T.A. Taton, *Controlling shell thickness in core-shell gold nanoparticles via surface-templated adsorption of block copolymer surfactants.* Macromolecules, 2005. **38**(14): p. 6115-6121.
157. Bryant, Z., et al., *Structural transitions and elasticity from torque measurements on DNA.* Nature, 2003. **424**(6946): p. 338-41.
158. Koster, D.A., et al., *Friction and torque govern the relaxation of DNA supercoils by eukaryotic topoisomerase IB.* Nature, 2005. **434**(7033): p. 671-4.
159. Forth, S., et al., *Abrupt Buckling Transition Observed during the Plectoneme Formation of Individual DNA Molecules.* Phys Rev Lett, 2008. **100**(14): p. 148301.
160. Guydosh, N.R. and S.M. Block, *Backsteps induced by nucleotide analogs suggest the front head of kinesin is gated by strain.* Proc Natl Acad Sci U S A, 2006. **103**(21): p. 8054-9.
161. Green, N.M., *Avidin.* Adv Protein Chem, 1975. **29**: p. 85-133.
162. Green, N.M., *Avidin. 1. the Use of (14-C)Biotin for Kinetic Studies and for Assay.* Biochem J, 1963. **89**: p. 585-91.
163. Green, N.M. and E.J. Toms, *The properties of subunits of avidin coupled to sepharose.* Biochem J, 1973. **133**(4): p. 687-700.
164. Jung, L.S., et al., *Binding and dissociation kinetics of wild-type and mutant streptavidins on mixed biotin-containing alkylthiolate monolayers.* Langmuir, 2000. **16**(24): p. 9421-9432.
165. Hermanson, G.T., *Bioconjugate techniques*. 1996, San Diego: Academic Press. xxv, 785 p.
166. Daniel, M.C. and D. Astruc, *Gold nanoparticles: Assembly, supramolecular chemistry, quantum-size-related properties, and applications toward biology, catalysis, and nanotechnology.* Chemical Reviews, 2004. **104**(1): p. 293-346.
167. Jadzinsky, P.D., et al., *Structure of a thiol monolayer-protected gold nanoparticle at 1.1 angstrom resolution.* Science, 2007. **318**(5849): p. 430-433.
168. Whitesides, G.M. and P.E. Laibinis, *Wet Chemical Approaches to the Characterization of Organic-Surfaces - Self-Assembled Monolayers, Wetting, and the Physical Organic-Chemistry of the Solid Liquid Interface.* Langmuir, 1990. **6**(1): p. 87-96.
169. Manning, G.S., *The molecular theory of polyelectrolyte solutions with applications to the electrostatic properties of polynucleotides.* Q Rev Biophys, 1978. **11**(2): p. 179-246.
170. Schmid, G. and A. Lehnert, *The Complexation of Gold Colloids.* Angewandte Chemie-International Edition in English, 1989. **28**(6): p. 780-781.
171. Zanchet, D., et al., *Electrophoretic and structural studies of DNA-directed Au nanoparticle groupings.* Journal of Physical Chemistry B, 2002. **106**(45): p. 11758-11763.

172. Lee, C.Y., et al., *Evidence of impurities in thiolated single-stranded DNA oligomers and their effect on DNA self-assembly on gold.* Langmuir, 2005. **21**(11): p. 5134-5141.
173. Burns, J.A., et al., *Selective Reduction of Disulfides by Tris(2-Carboxyethyl)Phosphine.* Journal of Organic Chemistry, 1991. **56**(8): p. 2648-2650.
174. Ruegg, U.T. and J. Rudinger, *Reductive cleavage of cystine disulfides with tributylphosphine.* Methods Enzymol, 1977. **47**: p. 111-6.
175. Mastroianni, A.J., et al., *Probing the conformational distributions of subpersistence length DNA.* Biophys J, 2009. **97**(5): p. 1408-17.
176. Yang, L.L., et al., *Calibration of Silver Plasmon Rulers in the 1-25 nm Separation Range: Experimental Indications of Distinct Plasmon Coupling Regimes.* Journal of Physical Chemistry C, 2010. **114**(11): p. 4901-4908.
177. Chapman-Smith, A. and J.E. Cronan, *In vivo enzymatic protein biotinylation.* Biomolecular Engineering, 1999. **16**(1-4): p. 119-125.
178. Choi-Rhee, E. and J.E. Cronan, *The biotin carboxylase-biotin carboxyl carrier protein complex of Escherichia coli acetyl-CoA carboxylase.* Journal of Biological Chemistry, 2003. **278**(33): p. 30806-30812.
179. Schatz, P.J., *Use of Peptide Libraries to Map the Substrate-Specificity of a Peptide-Modifying Enzyme - a 13 Residue Consensus Peptide Specifies Biotinylation in Escherichia-Coli.* Bio-Technology, 1993. **11**(10): p. 1138-1143.
180. Thomen, P., et al., *T7 RNA polymerase studied by force measurements varying cofactor concentration.* Biophys J, 2008. **95**(5): p. 2423-33.
181. Thomen, P., P.J. Lopez, and F. Heslot, *Unravelling the mechanism of RNA-polymerase forward motion by using mechanical force.* Phys Rev Lett, 2005. **94**(12): p. 128102.
182. de Boer, H.A., L.J. Comstock, and M. Vasser, *The tac promoter: a functional hybrid derived from the trp and lac promoters.* Proc Natl Acad Sci U S A, 1983. **80**(1): p. 21-5.
183. Lionberger, T.A. and E. Meyhofer, *Bending the Rules of Transcriptional Repression: Tightly Looped DNA Directly Represses T7 RNA Polymerase.* Biophysical Journal, 2010. **99**(4): p. 1139-1148.
184. Mentesana, P.E., et al., *Characterization of halted T7 RNA polymerase elongation complexes reveals multiple factors that contribute to stability.* Journal of Molecular Biology, 2000. **302**(5): p. 1049-1062.
185. Steitz, T.A., *The structural changes of T7 RNA polymerase from transcription initiation to elongation.* Current Opinion in Structural Biology, 2009. **19**(6): p. 683-690.
186. Xia, Y.N., et al., *Shape-Controlled Synthesis of Metal Nanocrystals: Simple Chemistry Meets Complex Physics?* Angewandte Chemie-International Edition, 2009. **48**(1): p. 60-103.
187. Wiley, B., et al., *Shape-controlled synthesis of silver and gold nanostructures.* Mrs Bulletin, 2005. **30**(5): p. 356-361.

188. Romo-Herrera, J.M., R.A. Alvarez-Puebla, and L.M. Liz-Marzan, *Controlled assembly of plasmonic colloidal nanoparticle clusters.* Nanoscale, 2011. **3**(4): p. 1304-1315.
189. Rodriguez-Fernandez, J., et al., *Seeded growth of submicron Au colloids with quadrupole plasmon resonance modes.* Langmuir, 2006. **22**(16): p. 7007-10.
190. Pastoriza-Santos, I. and L.M. Liz-Marzan, *N,N-Dimethylformamide as a Reaction Medium for Metal Nanoparticle Synthesis.* Advanced Functional Materials, 2009. **19**(5): p. 679-688.
191. Oh, E., et al., *One-Phase Synthesis of Water-Soluble Gold Nanoparticles with Control over Size and Surface Functionalities.* Langmuir, 2010. **26**(10): p. 7604-7613.
192. Zhang, T., Z.Q. Yang, and D.S. Liu, *DNA discrete modified gold nanoparticles.* Nanoscale, 2011. **3**(10): p. 4015-4021.
193. Olk, P., et al., *Distance dependent spectral tuning of two coupled metal nanoparticles.* Nano Letters, 2008. **8**(4): p. 1174-1178.
194. Liu, G.L., et al., *A nanoplasmonic molecular ruler for measuring nuclease activity and DNA footprinting.* Nat Nanotechnol, 2006. **1**(1): p. 47-52.
195. Jain, P.K. and M.A. El-Sayed, *Noble metal nanoparticle pairs: effect of medium for enhanced nanosensing.* Nano Lett, 2008. **8**(12): p. 4347-52.
196. Novo, C., et al., *Influence of the medium refractive index on the optical properties of single gold triangular prisms on a substrate.* Journal of Physical Chemistry C, 2008. **112**(1): p. 3-7.
197. Armstrong, S.H., et al., *Preparation and Properties of Serum and Plasma Proteins .12. The Refractive Properties of the Proteins of Human Plasma and Certain Purified Fractions.* J Am Chem Soc, 1947. **69**(7): p. 1747-1753.
198. Jung, L.S., et al., *Quantitative interpretation of the response of surface plasmon resonance sensors to adsorbed films.* Langmuir, 1998. **14**(19): p. 5636-5648.
199. Darst, S.A., et al., *Two-dimensional crystals of streptavidin on biotinylated lipid layers and their interactions with biotinylated macromolecules.* Biophys J, 1991. **59**(2): p. 387-96.
200. Weber, P.C., et al., *Structural origins of high-affinity biotin binding to streptavidin.* Science, 1989. **243**(4887): p. 85-8.
201. Wallin, A.E., A. Salmi, and R. Tumay, *Step length measurement - Theory and simulation for tethered bead constant-force single molecule assay.* Biophysical Journal, 2007. **93**(3): p. 795-805.
202. Moffitt, J.R., et al., *Recent advances in optical tweezers.* Annual Review of Biochemistry, 2008. **77**: p. 205-228.
203. Jain, P.K., S. Eustis, and M.A. El-Sayed, *Plasmon coupling in nanorod assemblies: Optical absorption, discrete dipole approximation simulation, and exciton-coupling model.* Journal of Physical Chemistry B, 2006. **110**(37): p. 18243-18253.

204. Gluodenis, M. and C.A. Foss, *The effect of mutual orientation on the spectra of metal nanoparticle rod-rod and rod-sphere pairs.* Journal of Physical Chemistry B, 2002. **106**(37): p. 9484-9489.
205. Link, S. and M.A. El-Sayed, *Spectral properties and relaxation dynamics of surface plasmon electronic oscillations in gold and silver nanodots and nanorods.* Journal of Physical Chemistry B, 1999. **103**(40): p. 8410-8426.
206. Gunnarsson, L., et al., *Confined plasmons in nanofabricated single silver particle pairs: experimental observations of strong interparticle interactions.* J Phys Chem B, 2005. **109**(3): p. 1079-87.
207. Dunn, J.J. and F.W. Studier, *Complete Nucleotide-Sequence of Bacteriophage-T7 DNA and the Locations of T7 Genetic Elements.* Journal of Molecular Biology, 1983. **166**(4): p. 477-535.
208. Kassavetis, G.A. and M.J. Chamberlin, *Pausing and Termination of Transcription within the Early Region of Bacteriophage-T7 DNA Invitro.* Journal of Biological Chemistry, 1981. **256**(6): p. 2777-2786.
209. Levin, J.R. and M.J. Chamberlin, *Mapping and Characterization of Transcriptional Pause Sites in the Early Genetic Region of Bacteriophage-T7.* Journal of Molecular Biology, 1987. **196**(1): p. 61-84.
210. Bath, J. and A.J. Turberfield, *DNA nanomachines.* Nat Nanotechnol, 2007. **2**(5): p. 275-84.